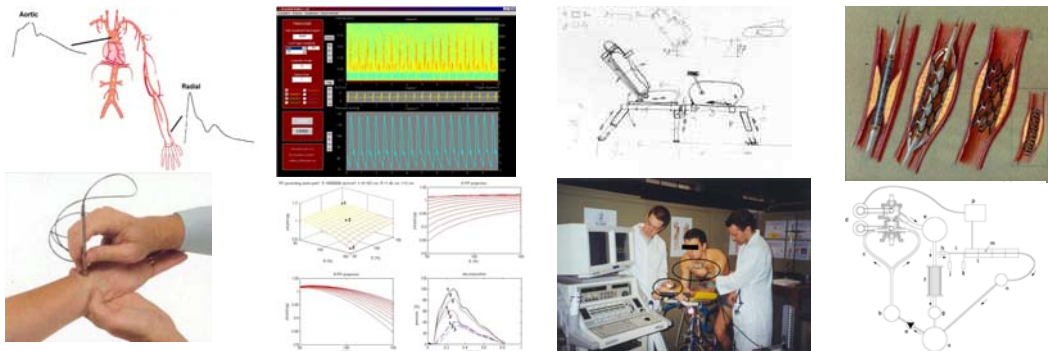


Assessment of Vascular Haemodynamics

**Investigation of non-invasive and minimally invasive
methods for assessment of vascular function at rest and
during cardiovascular challenge**



Koen S. Matthys, MSc EME

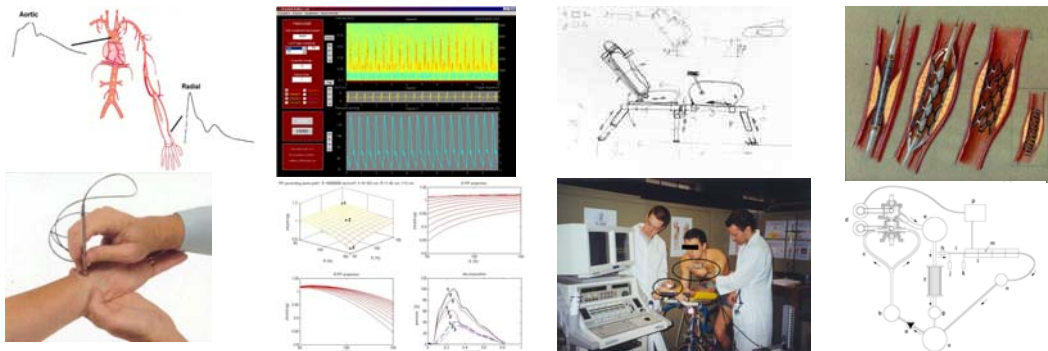
Academic Year 2003-2004

Thesis supervisors: Prof. P. R. Verdonck, PhD & Prof. P. Segers, PhD

"From now on, I'm not doing anything I don't want to do! The world owes me happiness, fulfillment and success.... I'm just here to cash in."

Assessment of Vascular Haemodynamics

**Investigation of non-invasive and minimally invasive
methods for assessment of vascular function at rest and
during cardiovascular challenge**



Koen S. Matthys, MSc EME

Academic Year 2003-2004

Thesis supervisors: Prof. P. R. Verdonck, PhD & Prof. P. Segers, PhD

ISBN 9080885711

© Koen S. Matthys, 2004.

Cover illustration shows a drawing by Marcel Anteunis of a supine bicycle.

Contact author at: matthys_k@hotmail.com

Thesis supervisors: Prof. P. R. Verdonck, PhD & Prof. P. Segers, PhD

Hydraulics Laboratory

Department of Civil Engineering (TW15V)

Faculty of Applied Sciences

Ghent University (UG)

St-Pietersnieuwstraat 41 B-9000 Ghent

Members of the exam committee:

Prof. Ronny Verhoeven, PhD (chairman, Faculty of Applied Sciences, UG)

Yves D'Asseler, PhD (secretary, Faculty of Applied Sciences, UG)

Prof. Alberto Avolio, PhD (Graduate School Biomedical Engineering, UNSW, Sydney)

Stéphane Carlier, MD, PhD (Cardiovascular Research Foundation, New York)

Stefaan De Mey, PhD (European Space Research and Technology Centre, Noordwijk)

Prof. Patrick Segers, PhD (supervisor, Faculty of Applied Sciences, UG)

Prof. Luc Van Bortel, MD, PhD (Faculty of Medicine, UG)

Prof. Pascal Verdonck, PhD (supervisor, Faculty of Applied Sciences, UG)

Prof. Henri Verhaaren, MD, PhD (Faculty of Medicine, UG)

This research has been made possible by a specialization grant of the Institute for the Promotion of Innovation by Science and Technology in Flanders (IWT993175) and a practicum student scholarship of the University of New South Wales, Sydney, Australia.

Table of Contents

Table of Contents	1
I Introduction	3
1 The Heart and the Circulation	5
2 Rationale for this Thesis	35
II Methodology I: Biomechanics, Identification and Modelling	41
1 Background: Vascular Biomechanics.....	43
2 Transfer Function Estimation Methods for the Aorta-Radial Path	93
3 An Arterial Network Model to Assess Pulse Pressure Reduction	115
III Methodology II: Measuring Devices and Signal Acquisition	127
1 Background: Pressure and Flow	129
2 Development and modelling of arterial tonometry.....	155
3 Arterial tonometry as an alternative for long-term intra-arterial pressure monitoring.....	171
4 An acquisition tool for synchronized monitoring of a Doppler spectrogram, an electrocardiogram and arterial tonometry.....	191
IV Vascular haemodynamics during physical exercise and drug-induced stress	203
1 Background: Exercise and Dobutamine.....	205
2 Haemodynamic assessment in adolescents during a standing and supine bicycle stress test.....	215
3 Haemodynamic assessment in adults during dobutamine stress or a treadmill exercise test	229
V Vascular haemodynamics during coronary intervention	241
1 Background: Stents, QCA, IVUS & FFR	243
2 Evaluation of the FFR Index for the Assessment of Stent Deployment	261
3 A Corrected FFR Index to Account for the Myocardial Waterfall Effect.....	279
General Discussion and Conclusion	297
Appendix	307
Nomenclature	317
References	335
Acknowledgements	371

I Introduction

In the first chapter, some basics concerning the anatomy and physiology of the heart and the circulatory system are explained. The second chapter clarifies the rationale and outline of this thesis. In these two chapters of this introductory part an attempt was made to avoid any reference to mathematical equations or models, as this will be dealt with in more detail in the following part elaborating on vascular biomechanics.

A decorative vertical bar on the left side of the page, consisting of a thin grey line and a thicker black line.

1 The Heart and the Circulation

History

The heart and the circulation, or the circulation and the heart, it is the story of the ball and chain: they are complementary in every way and to discuss one without mentioning the other is therefore pointless. Although this thesis will mainly focus on the arterial circulation -the vessel network that provides muscles and organs with the necessary elements to function in a healthy way- a brief description on the function and the working of the heart could not be omitted.

The investigation of heart and vessels goes back to ancient times. The Egyptians, Chinese and Greeks independently described the importance of palpation of the pulse in their medical literature. A characteristic of those times is the mystique that surrounds them and the peculiar way in which physiological phenomena were described. For example, in the Chinese manuscript 'Huang Ti Nei Ching Wen. The Yellow Emperor's Classic of Internal Medicine' by the emperor Huang Ti, one can read that: 'the pulse of a healthy heart should feel like continuous hammer blows...like the notes of a string instrument...like wood floating on water or like fish gliding through waves'! Huang Ti is thought to have lived c. 2697-2597 BC, but some believe that he was only a legendary figure and the book was actually written by a large number of people, composed to one manuscript by the 2nd century BC.(Naqvi and Blaufox 1998)

It was the ancient civilization of Greece that established the relationship of the heart with the blood vessels, when the pulse was recognized as a function of the heart. Gradually through time, the knowledge about the cardiovascular system improved, but this journey was also full of misconceptions. The fact that arteries contract and relax was known since the time of Aristotle. Following this, the Alexandrian Erasistratus (310-250BC), also called 'the father of physiology', believed that the arteries were filled with air, or 'pneuma', which was released as soon as the artery was severed, and that the blood from the neighbouring veins quickly filled in to take its place. Claudius Galenus, or Galen (131-199) wrote more on the subject of the pulse than anyone before or since. Interesting is his experimental approach where he used a hollow reed to simulate an artery. However, though his teachings prevailed for at least five centuries, a lot of mistakes were also passed on in this way. He wrongfully described the ebb and flow of blood in arteries and the passing of blood from the right side of the heart to the

left side through pores, thinking of the circulation as an open-circuit. Only much later, Galileo Galilei (1564-1642) countered these findings and considered the circulation of blood to be in a closed system.(Allbutt 1921; Dobson 1927)

Despite the fact that the history of the investigation of heart and circulation dates back so far in time, the modern perception of the cardiovascular system is derived from the ideas stipulated only in 1616 by a contemporary of Galileo, named William Harvey (1578-1657). He described the circulation of the blood in the following way: ‘the movement of the blood in a circle is caused by the beat of the heart.’ and ‘the pulsation of the arteries is nothing else than the impulse of the blood within them.’ Later, in 1628, Harvey wrote his famous book in Latin called: ‘*Exercitatio Anatomica de Motu Cordis et Sanguinis in Animalibus*’ about the anatomical treatise on the movement of the heart and blood in animals.(Bettman 1979)

Since then, the evolution in the field of cardiovascular research has again expanded greatly, but it would be beyond the scope of this introduction to elaborate on that. In the next paragraphs some basic understandings of the heart and the circulation are given to the extent that they are necessary for the rest of this thesis. I leave it to the interested reader to search for more extensive information in the huge database on cardiovascular literature available today.

1 The heart

1.1 Anatomical aspects

The human heart acts like a pump, which provides for the blood circulation in the human body. The blood circulation in its turn takes care of the transportation of oxygen, nutrients and humoral agents necessary for a healthy functioning of muscles and organs. To fulfill this logistic task, the cardiovascular system has two circulatory blood flows at its disposal. On one hand, there is the small or pulmonary circulation, in which blood is pumped to the lungs, oxygenated and then taken back to the heart. On the other hand, there is the large or systemic circulation. The arterial part of the systemic circulation brings oxygenated blood to the muscles and organs where the exchange occurs after which the veins carry the oxygen deficient blood back to the heart. For this reason, oxygenated blood is commonly referred to as ‘arterial blood’, and oxygen deficient blood as ‘venous blood’. Note that this is only correct when speaking of the systemic circulation, as in the pulmonary circulation oxygen deficient blood is transported by the lung *arteries* and oxygenated blood by the pulmonary *veins*.

1.1.1 General nomenclature

The heart is divided into four cavities or ‘chambers’. The ‘upper’ chambers of the heart, the atria, are anatomically separated from the ‘lower’ chambers or ventricles by a fibrous ring. In order to maintain appropriate direction of flow in the chambers and to allow adequate pressure management during the heart cycle, four cardiac valves are situated within this ring. One can say that the heart is divided into a right- and a left-sided pump, which propel oxygen deficient blood into the pulmonary circulation and oxygenated blood into the systemic circulation, respectively. Left and right side of the heart are separated by the septum.

A schematic overview is given in Figure 1–1. The upper and lower venae cavae (11,12) collect venous blood into the right atrium (1) from where it passes through a tricuspid valve (3) - the valve has three valve cusps or leaflets - into the right ventricle (2). Contraction of ventricle wall fibres pushes the blood through the pulmonic valve (4) via the pulmonic artery (5) towards the lungs where the oxygenation takes place. Via the pulmonic veins (6), the

blood reaches the left atrium (7), passes through the mitral valve (8) - a bicuspid valve with two cusps - during the relaxation or filling phase and fills the left ventricle. With the following contraction, the blood is pushed through the aortic valve (9) into the aorta (10) and the rest of the arterial circulation.

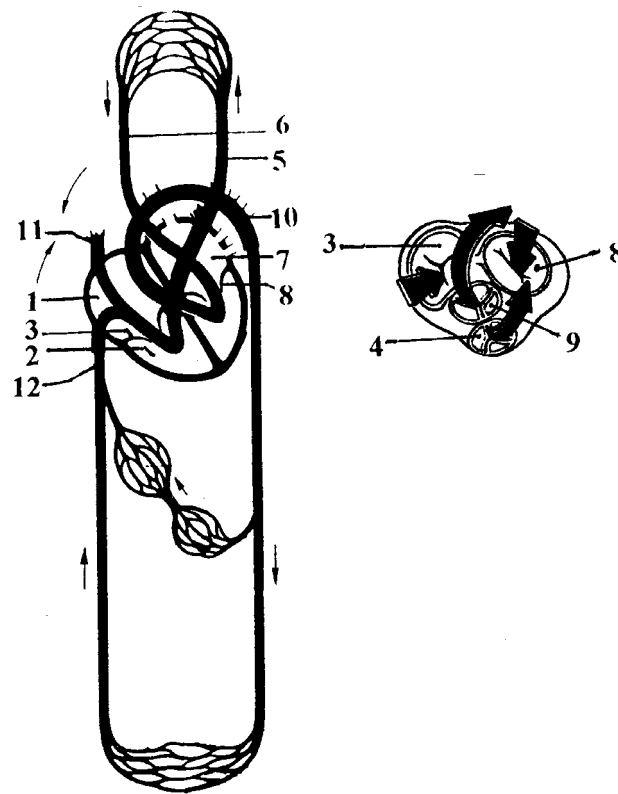


Figure 1–1 Schematically representation of the circulation, together with a cross-section of the heart at base showing the four valves.(Kahle, Leonhardt et al. 1992)

1.1.2 Heart wall structure

The heart is situated in the thoracic cavity in between the lungs. The pericardium, composed of two layers (visceral and parietal pericardium), encloses the heart. A small amount of lubricating fluid separates the two pericardial layers and reduces friction created by the pumping heart. The heart wall itself is composed of three layers (Figure 1–2). The myocardium is the middle, muscular layer. The outer epicardium and the inner endothelial layer (or endocardium) surround the muscular layer as thin, smooth protective tissues. Muscle development of the myocardium is dependent on location and function. The atrial walls are the thinnest since the atria are low-pressure chambers mainly serving as blood reservoirs. The

walls of the ventricles must endure higher pressures and are therefore more developed. The left ventricle wall is thicker than the right ventricle wall since the pressure build-up in the left ventricle is several times higher than the pressure build-up in the right ventricle.

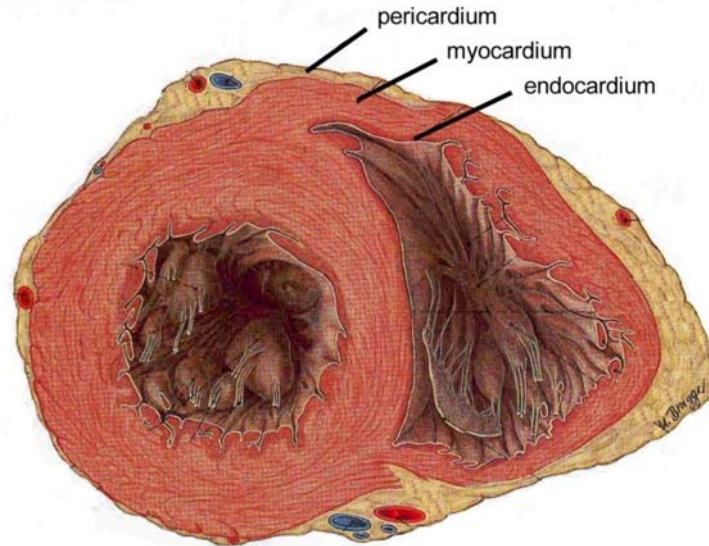


Figure 1–2 The different layers of the heart wall.(Putz and Pabst 1994b)

1.2 Physiological aspects

1.2.1 Electrical aspects

The myocardium of the heart consists of cardiac muscle cells or myocytes. When an electric excitation wave (a depolarization wave) stimulates the cardiac muscle, the subsequent calcium release in the cellular mechanisms induces a mechanical response of muscular contraction. It is followed by electrical recovery or repolarization, corresponding to muscular relaxation. A specialized conduction pathway exists in the myocardium to ensure rhythmic and synchronized excitation and contraction of the heart muscle (Figure 1–3, left). A cardiac impulse starting from the sinoatrial node (SA) spreads to the interatrial pathway and provokes contraction of the atria. The electric impulse then reaches the atrioventricular node (AV), which is positioned at the top of the intraventricular septum. Finally, the wave of electric excitation spreads from the AV node to the ventricles via the bundle of His, which branches into the Purkinje fibers.

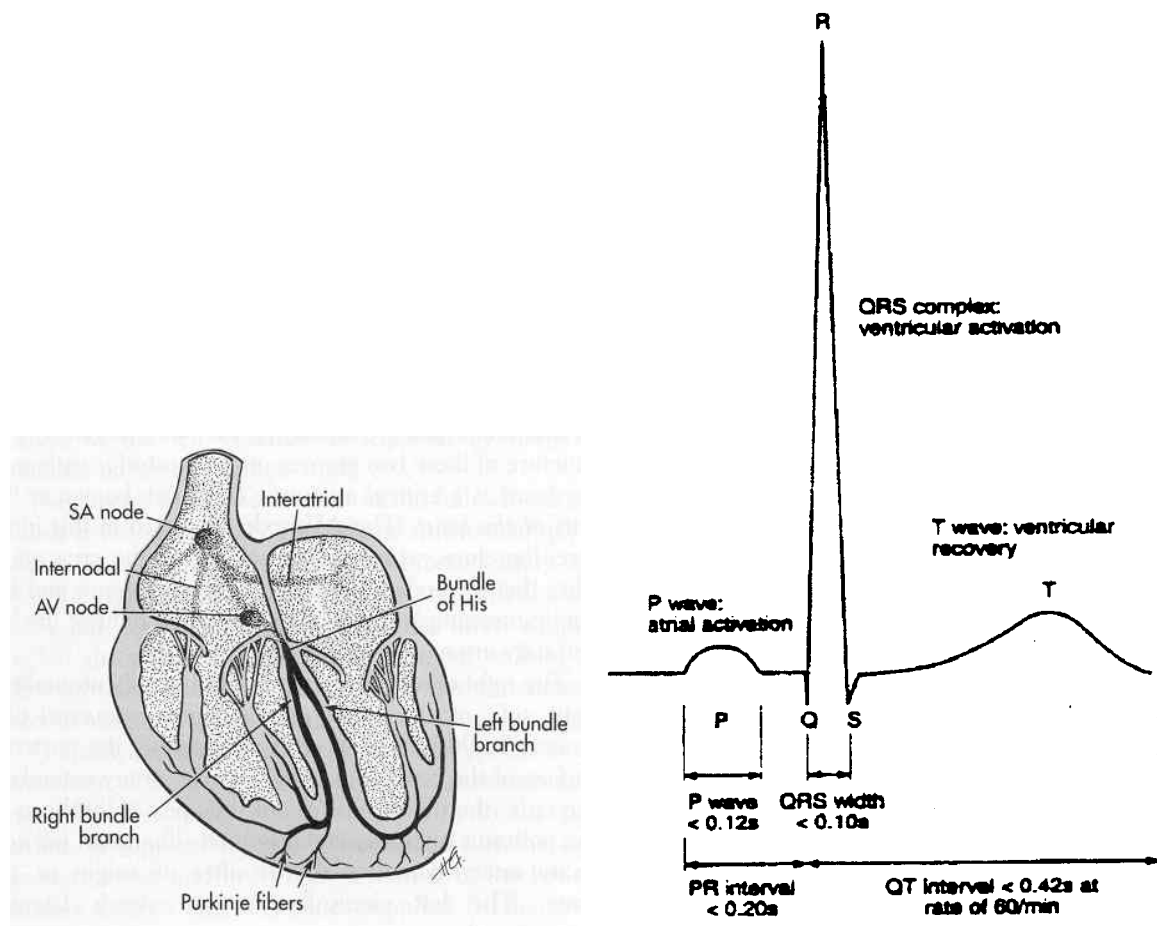


Figure 1–3 The cardiac conduction system and the electrocardiogram.(Price and Wilson 1992)

The electrocardiogram (ECG) reflects the summated electrical activity of all the myocardial cells recorded from the body surface (Figure 1–3, right). Characteristic wave complexes on the ECG are P, QRS, and T-waves. The P-wave corresponds to atrial depolarization, originating from an impulse from the SA node. The QRS complex represents ventricular depolarization. The amplitude of this wave is large as a result of the large muscle mass traversed by the electric impulse. The PR interval includes the transmission time through the atria and the delay of the impulse at the AV node. Ventricular repolarization generates the T wave.

1.2.2 Mechanical aspects

The heart can be looked upon as a mechanical pump generating the appropriate output that meets the needs of the metabolism. Pressure and flow signals during a cardiac cycle of an

adult in rest are depicted in Figure 1–4. The ECG is shown to give an indication about the timing within the cardiac cycle.

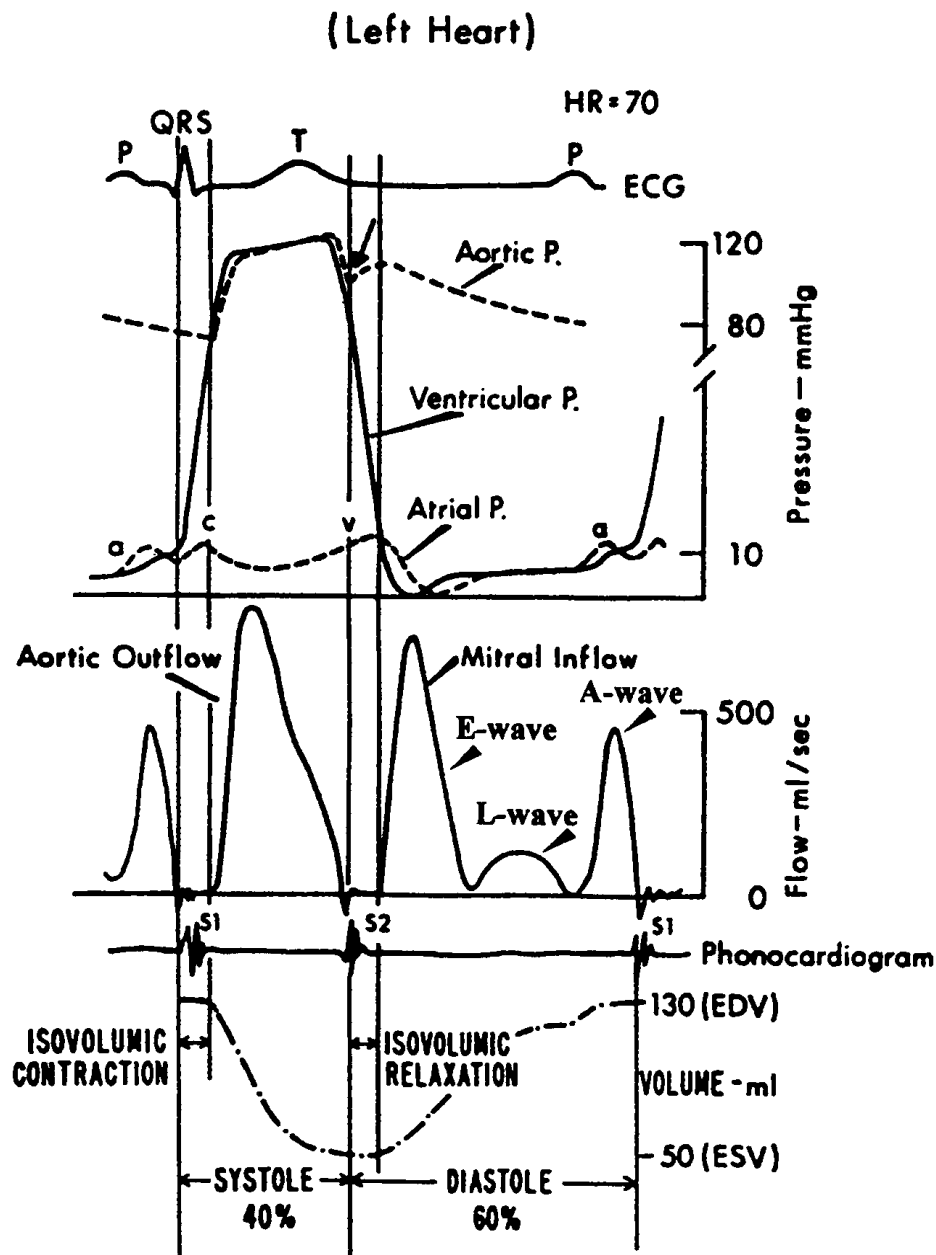


Figure 1–4 Pressure and flow during one cardiac cycle.(Yellin 1995)

During the systolic part of the heart cycle, left ventricular (LV) pressure rises from 0 to 120 mmHg. When LV pressure rises above aortic pressure, the aortic valve opens and blood is ejected from the LV into the arterial circulation. Approximately two thirds of the bloodvolume in the ventricle at the end of diastole (end-diastolic volume, EDV) is ejected

during systole. This portion of ejected blood is called the ejection fraction (EF). The residual ventricular volume at the end of systole is referred to as the end-systolic volume (ESV).

The diastolic portion of the heart cycle can be subdivided into four phases: (1) isovolumic relaxation, (2) rapid or early filling (E-wave), (3) diastasis (L-wave) and (4) atrial contraction (A-wave). In the first phase, between the time of aortic valve closure and mitral valve opening, LV pressure relaxes exponentially from the aortic pressure level to the pressure level existing in the left atrium (LA). The next phase, i.e. early filling (E-wave), begins when pressure in the LV falls below that in the LA, causing the mitral valve to open and the LV to begin filling. The early filling phase coincides with and is dependent on continued LV relaxation. This phase ends when pressure in the two chambers is equalized. Although this rapid filling comprises only about 30% of diastole, it accounts for up to 80% of LV filling volume. The third phase is the diastasis. Little filling, if any, comes from pulmonary vein flow (L-wave). With increased heart rate this phase shortens more than the other three. The fourth phase, atrial contraction (A-wave), contributes for 15% to 25% of LV filling volume under normal conditions but can contribute as much as 40% if LV relaxation is diminished. (Guyton and Hall 2000)

Heart rate (HR) is defined as the amount of cardiac cycles or beats per minute (bpm). Stroke volume (SV) is the volume of blood ejected by the ventricles per heartbeat. The volume ejected by the ventricles per minute is called the cardiac output (CO). Cardiac output depends on the relationship between the two variables HR and SV and is defined as:

$$CO = HR \times SV \qquad \text{Eqn. 1.1}$$

As an example, average CO in rest for a ‘normal’ adult person is about 5-6 l/min. For an average HR of 72 bpm, SV would then be around 70-80 ml. However, these values are strongly influenced by the definition of a ‘normal adult’. CO also adapts to the demands of the peripheral tissues for oxygen and nutrients, and will go up for example during physical exercise.

	<i>Before training</i>	<i>After 6 month training</i>	<i>Top Runner</i>
<i>HR at rest (bpm)</i>	75	60	36
<i>HR max (bpm)</i>	195	192	174
<i>SV rest (ml)</i>	60	75	125
<i>SV max (ml)</i>	100	125	200
<i>CO rest (l/min)</i>	4.5	4.5	4.5
<i>CO max (l/min)</i>	19.5	24.0	34.8

Table 1–1 Values for HR, SV and CO for a 15 year old adolescent before and after a 6 months endurance training schedule, compared with the values for a top athlete.(Wilmore and Costill 1999)

Table 1–1 demonstrates how training can influence the HR, SV and CO values. Despite the fact that HR_{rest} and SV_{rest} for each subject are significantly different, the CO_{rest} (4.5 l/min , $HR_{rest} \times SV_{rest}$) is the same for the 3 subjects in rest. At exercise however, CO_{max} values rise the more the person is trained (from 19.5 l/min to 34.8 l/min), and this while HR drops compared to a less-trained person under the same load conditions (from 195 to 174 bpm). A trained person has more economical energy consumption: he develops a larger CO with a lower HR, because of his trained heart that can deliver a bigger SV.

2 The coronary arteries

2.1 Anatomical aspects

In order to deliver a continuous amount of power, the heart muscle needs to have its own blood supply. An inadequate irrigation of the heart muscle is referred to as a state of 'ischaemia', which can lead to 'myocardial infarction' (tissue necrosis). The latter is one of the most common causes of mortality in all industrialized countries. The important task of providing the heart with oxygenated blood is taken care of by the coronary arterial network.

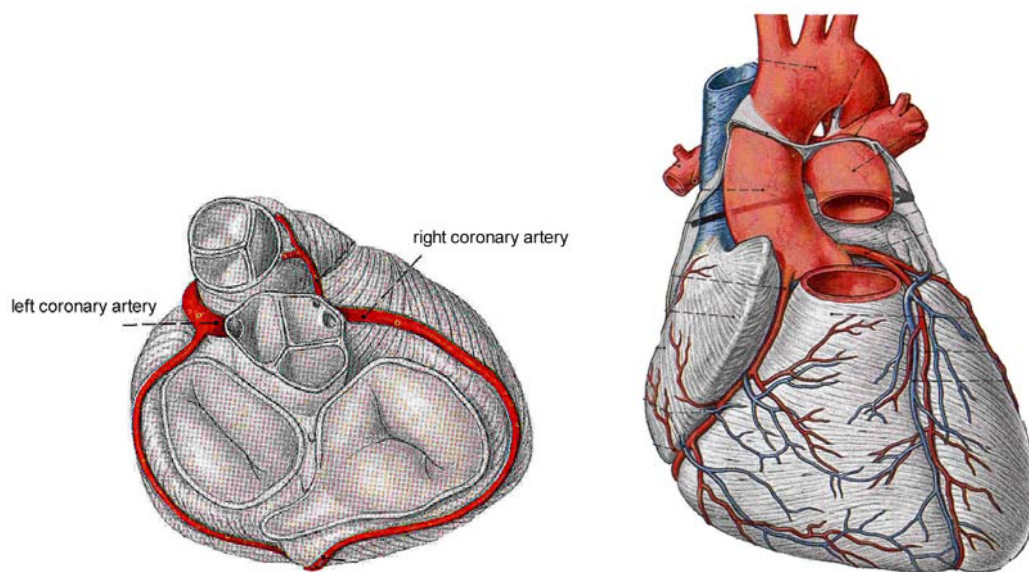


Figure 1–5 The coronary arterial network.(Putz and Pabst 1994b)

The branching of the coronary arterial network is different for every individual. Variations in anatomical structure are inherent to arteries and the coronaries make no exception to that rule. The most common situation is the one where 2 coronaries are branching from the aorta at the sinus aorta, slightly distal from the aortic valve (Figure 1–5, left). However, it happens (38%) that multiple (more than 2) coronaries branch from the aorta, and in seldom cases (less than 1%), the heart is fed by only one coronary artery.(Kahle, Leonhardt et al. 1992)

The area of irrigation can also vary. The following classification can be made using the blood supply to the posterior wall of the ventricles as a criterion: a 'balanced' type of supply is present when the posterior interventricular coronary branch originates from the right coronary artery (70%); a situation of 'left dominance' occurs when the posterior interventricular branch

comes from the left coronary artery (20%), and a 'right dominance' occurs when the posterior ventricle walls are mainly supplied by several branches descending from the right coronary artery (10%).(Putz and Pabst 1994b)

Since the coronary network can have multiple individual variations, it is not easy to determine anatomical positioning and branching in a unique way. In general however, the nomenclature of epicardial and myocardial coronaries, capillaries and finally the collateral network is applied.(Brandenburg, Fuster et al. 1987; Kapoor 1989; Pijls and De Bruyne 1997)

2.1.1 *Epicardial coronaries*

Epicardial coronaries have a diameter ranging from a few millimeter down to 400 μm and are the beginning of the coronary network: arising from the aortic sinus above the aortic valve, they are positioned along the epicardial surface of the heart wall (Figure 1–6). The left main coronary artery (LCA) is split up into the left anterior descending coronary artery (LAD) and the left circumflex coronary artery (LCX). Occlusion of the LAD can reduce the pump capacity of the left ventricle by 2/3.(Van Nooten 1998) The right coronary artery (RCA) splits into a posterior descending (RPD) and marginal branch (RMB). The origin of the posterior descending artery determines the coronary dominance.(Brandenburg, Fuster et al. 1987)

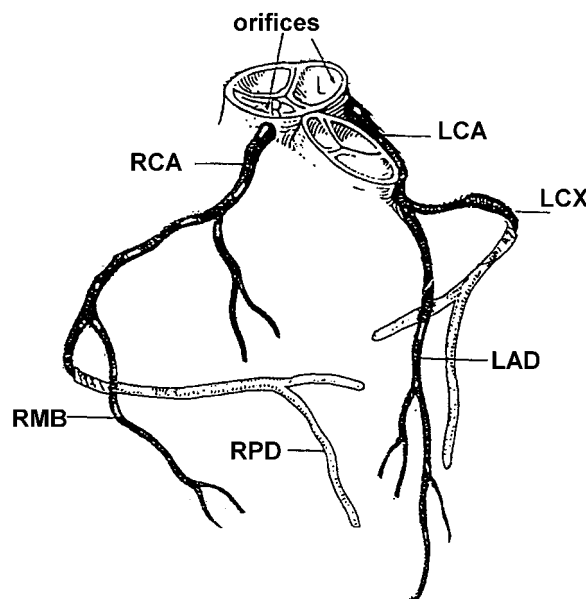


Figure 1–6 Nomenclature of the epicardial branches of the coronary arterial network.

Epicardial coronaries are clearly visible on a coronary angiogram (a diagnosis technique based on X-ray techniques which will be discussed further). Stenoses due to arteriosclerosis (degenerative changes in the artery wall) mainly occur in the epicardial part of the coronary tree. The occurrence of such a stenosis is the prevalent cause of myocardial ischaemia and can lead to thrombosis and myocardial infarction.

2.1.2 Myocardial coronaries

Myocardial coronaries are the prolongation of the epicardial coronaries, enter the myocardium and have diameters of 400 μm and less. The myocardial coronaries are no longer clearly visible on an angiogram and it is no longer possible to execute a mechanical revascularization in case lesions are present. Myocardial vessels are also called resistance vessels because of their significant resistance effect for the myocardial perfusion.

2.1.3 Capillaries

The capillaries compose a network of tiny blood vessels (diameters of 5 μm) with a density of 3500 vessels/ mm^2 . Small muscle cells are woven in between the capillaries, allowing the capillary bed to expand under the influence of internal pressure and the tone of these attached muscle cells.

2.1.4 Collateral network

The collateral bed or ‘anastomoses’ are the ‘bridging vessels’ between all other arteries in the coronary network. It is nowadays accepted that these rudimentary connection vessels are present in each heart from birth.(Pijls and De Bruyne 1997) They are not visible on arteriography because of their low flow range, but when a stenosis develops, this network expands and forms bridges or collateral pathways that deviate the blood alongside of the occlusion to irrigate the more distal locations together with the ischaemic area.

2.2 Physiological aspects

2.2.1 Myocardial resistance

Blood supply to peripheral tissues in the human body is done during the whole cardiac cycle but mainly in systole, the contracting phase of the heart. However, since this contraction of the heart muscles forces the myocardial coronary arteries to occlude, the heart itself is mainly irrigated during relaxation or diastole. (Khoury and Gregg 1963) Figure 1–7 shows the correlation between aortic blood pressure and blood flow in left and right coronary artery.

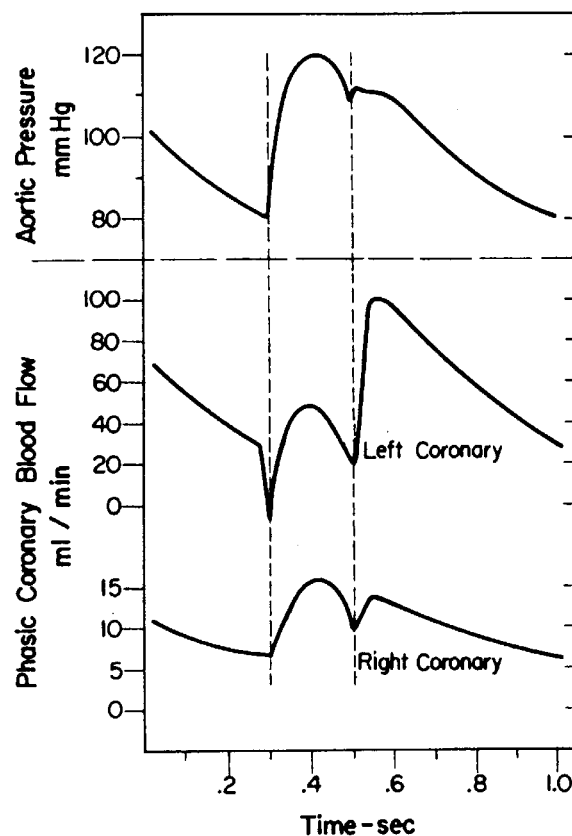


Figure 1–7 Effect of myocardial resistance: coronary perfusion occurs mainly during diastole. (Berne, Sperelakis et al. 1979)

2.2.2 Autoregulation

The coronary circulation has some regulatory properties that provide several blood flow responses to specific conditions. One is the ‘autoregulation’ mechanism. It is an intrinsic response that allows maintaining the coronary blood flow at a fairly constant level over a

wide range of perfusion pressures. This phenomenon is illustrated in Figure 1–8 where the relationship is shown between autoregulation (A) and maximal vasodilatation (D). The difference between the two curves represents coronary reserve or flow reserve at a specific perfusion pressure, with constant aortic pressure and HR. Since the slope of curve (A) is much less steep than the slope of (D), one can understand that the autoregulation mechanism protects the coronary perfusion in this way from large fluctuations, which would already occur at moderate arterial pressure changes.

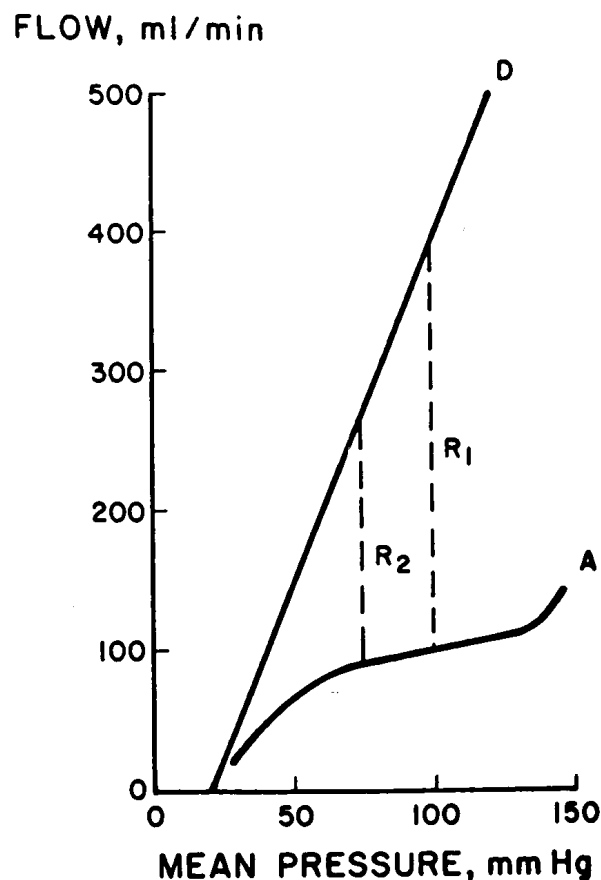


Figure 1–8 Relationship between coronary artery perfusion pressure and blood flow during autoregulation (A) and maximal vasodilatation (D). The difference between the two curves represents the flow reserve at a given pressure. (Hoffman 1984)

2.2.3 Metabolic regulation

Myocardial perfusion takes up 5 to 10% of the total SV. Oxygen demand in rest for the myocardium is up to 20 times higher than for the skeletal muscles. (Pijls and De Bruyne 1997)

As a consequence, the extraction of oxygen within the myocardium between coronaries and muscle cells is close to the maximum efficiency rate, meaning that a higher demand for oxygen leads to a higher demand in blood flow to be supplied by the coronaries. The myocardial oxygen consumption and the coronary flow thus have a strong linear relation. The regulation of the volume of coronary blood flow in proportion of the myocardial workload, or metabolic demands, is referred to as the 'metabolic regulation'.(Gregg and Shipley 1944)

As to the underlying mechanisms of this second intrinsic response, a lot of discussion is involved. Over the years, adenosine has been under attention as one of the most probable metabolic factors playing a principal role. The contribution of the endothelium cells of the inner vessel wall layer to blood flow regulation has also been acknowledged.(Ku 1982; Stewart, Pohl et al. 1988) However, most likely several factors instead of just a single one play their respective parts.(Olson and Bungert 1987) Given the fact that responses to stimuli or pharmaceutical agents can differ widely in larger or smaller arteries (Foreman and Kirk 1980), the net coronary flow response to an intervention is often not readily predictable.

2.2.4 *Reactive hyperaemia*

'Hyperaemia' is defined as a state of maximal flow. 'Reactive hyperaemia' is an intrinsic response of the coronary circulation occurring after release of an occlusion, when a coronary flow is suddenly delivered of typically 3 to 5 times the blood flow present before the occlusion. The peak level of this augmented flow during the reactive hyperaemic response is directly proportional to the duration of the occlusion, but attains the highest values with occlusions lasting about 20 s.(Olson and Gregg 1965; Pijls and De Bruyne 1997) This is a very useful condition during clinical measurements. Since longer occlusions do not produce a higher peak flow, one can assume a maximal vessel dilatation (and thus minimal resistance to flow) at that moment.

Pharmaceutical drugs such as adenosine, dipyridamole or papaverine also induce reactive hyperaemia.(Canty, Klocke et al. 1985) Figure 1–9 (lower signal) shows the effect of adenosine injections (ADO IC) and a temporary balloon occlusion (coronary interventions will be discussed further in detail) on a mean coronary flow velocity profile. The balloon occlusion makes coronary flow drop completely to zero. After removing the occlusion, flow

velocity maximizes to more than 3 times the level it had before the balloon was put in place. This is the state of reactive hyperaemia, where blood flow becomes primarily function of the coronary cross-sectional area at any given perfusion pressure.

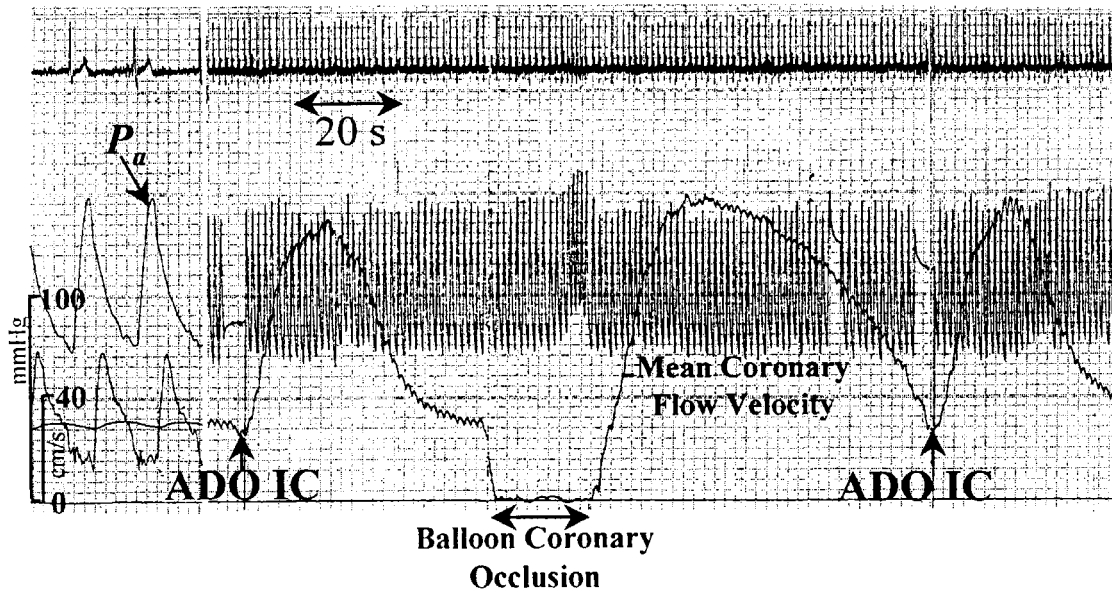


Figure 1-9 ECG, aortic pressure (mmHg) and mean coronary flow velocity (cm/s) during 3 events of induced reactive hyperaemia (ADO IC, balloon occlusion, ADO IC). (Pijls and De Bruyne 1997)

3 The large arteries

3.1 Anatomical aspects

The large arteries are the main branches of a well-designed and complex vessel network that has to provide for oxygen, nutrients and humoral agents to the whole human body. The anatomical highlights of the whole arterial tree are shown in Figure 1–11. The relevant arteries, for topics described in this thesis, are depicted in Figure 1–10 on the left. They involve the vessels of the ‘aorta-radial’ path: aortic arch (1), carotid artery (2), subclavian artery (3), axillary artery (4), brachial artery (5) and the radial artery (6).

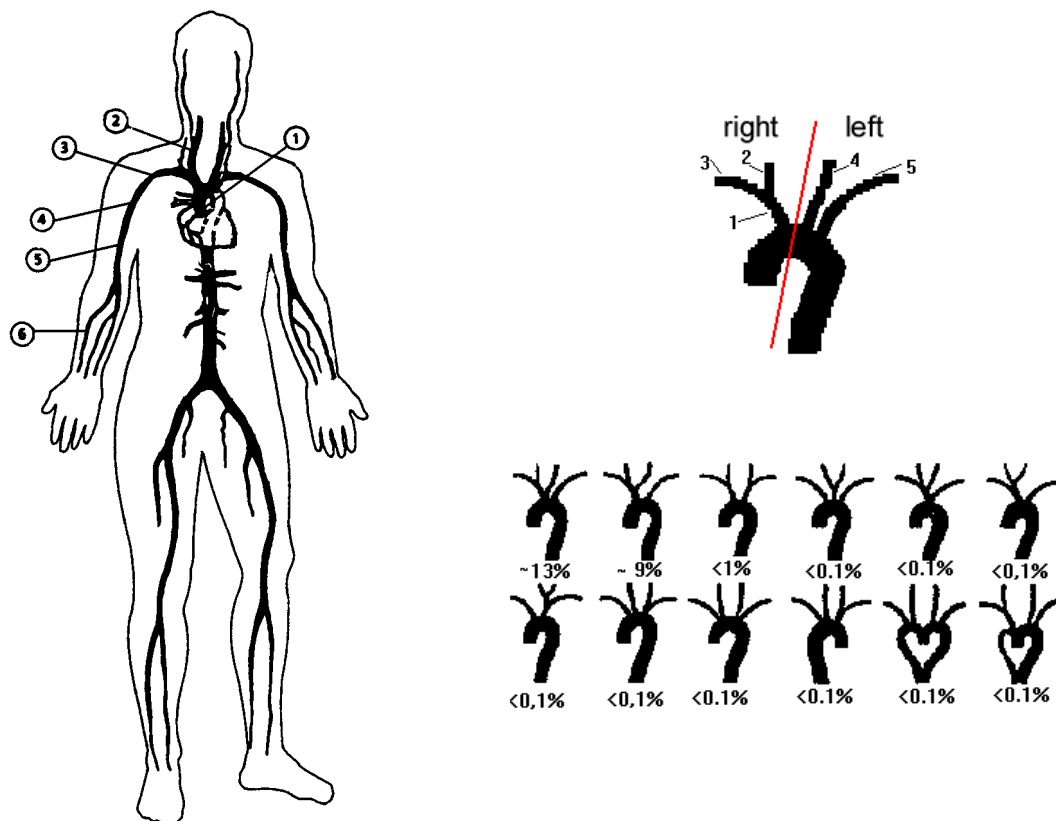


Figure 1–10 Left: The aorta-radial path.(Stergiopoulos, Young et al. 1992) Right: Variations on the offspring of carotid and subclavian arteries from the aortic arch.

3.1.1 Central arteries

Central arteries include the aorta, the coronaries, the carotid arteries and the direct branches of the aorta descendens. All arterial vessels are - directly or indirectly - branches from the aorta. The aorta is the biggest artery in the body and is connected to the heart, communicating with the LV through the aortic valve. The aorta ascendens is the rising part of the aorta, from the heart towards the aortic arch. Further distal, the term aorta descendens is applied, which is the descending part of the aorta going down through the thorax.

Towards the upper limbs, direct branches of the aortic arch can have different configurations (Figure 1–10, upper right). Most common configuration (77%) is the one where the most right branch, the brachiocephalic artery (1), splits into the right carotid (2) and subclavian (3) artery, while on the left side the carotid (4) and subclavian (5) artery are directly branching from the aorta. Other configurations (23%) do occur sometimes (Figure 1–10). These anatomical variations develop during the embryonic phase and do not cause severe negative implications in terms of functionality.

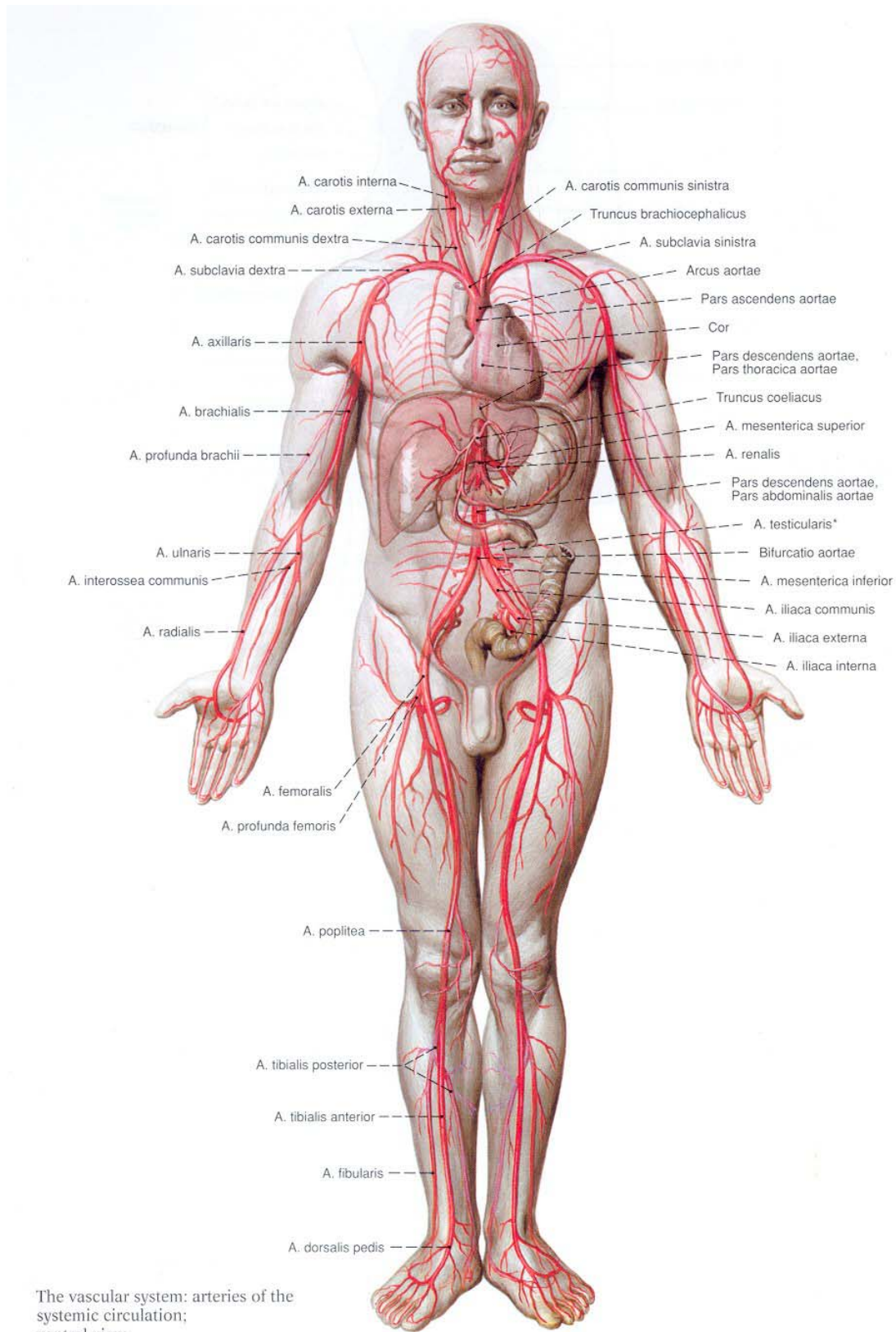
Towards the lower limbs, direct branches of the aorta descendens supply internal organs such as liver and kidneys. Further down, the abdominal aorta (part of the aorta below the diaphragm) splits into the right and left iliac artery, both having an internal branch towards the inner pelvis, and an external branch towards the legs.

3.1.2 Peripheral arteries

Peripheral arteries comprise the head and neck arteries, the brain arteries, and the arteries of upper and lower limbs. The carotid artery goes straight up the neck and splits into an external and internal branch. The latter enters the skull to supply blood to the eye cavities, hypophysis and the brains (vertebral arteries), while the external branch serves the region of the neck, face and skull (superficial temporal artery).

Shoulder and upper arm are being supplied with blood via the subclavian artery, evolving into axillary and brachial artery and splitting at the height of the elbow into the radial and ulnar artery, which irrigate the lower arm. The radial artery runs towards the thumb side and evolves into smaller, deeper lying hand arteries. The ulnar artery runs towards the pink side

and evolves into smaller, superficial hand arteries. For the legs, the external iliac artery evolves into the femoral and tibial artery to finally reach the smaller foot arteries.



The vascular system: arteries of the systemic circulation; ventral view.

* in the female: A. ovarica

Figure 1–11 The systemic circulation.(Putz and Pabst 1994a)

3.1.3 Vessel wall structure and tapering

The vessels in the arterial tree do not have a constant diameter from beginning to end. The cross-sectional area of an artery becomes gradually smaller when moving further away from the heart. This is called ‘geometric tapering’. Figure 1–12 (upper panel) shows the decrease of the mean external radius at various sites along the aorta, measured at physiological pressure in dogs.(Fry, Griggs et al. 1963) A lot of similarities exist between mammalian circulatory properties, and earlier experimental data is often derived from canine measurements.(Li 1996) Figure 1–12 (lower panel) gives an indication of values for a human aorta.(Latham, Westerhof et al. 1985)

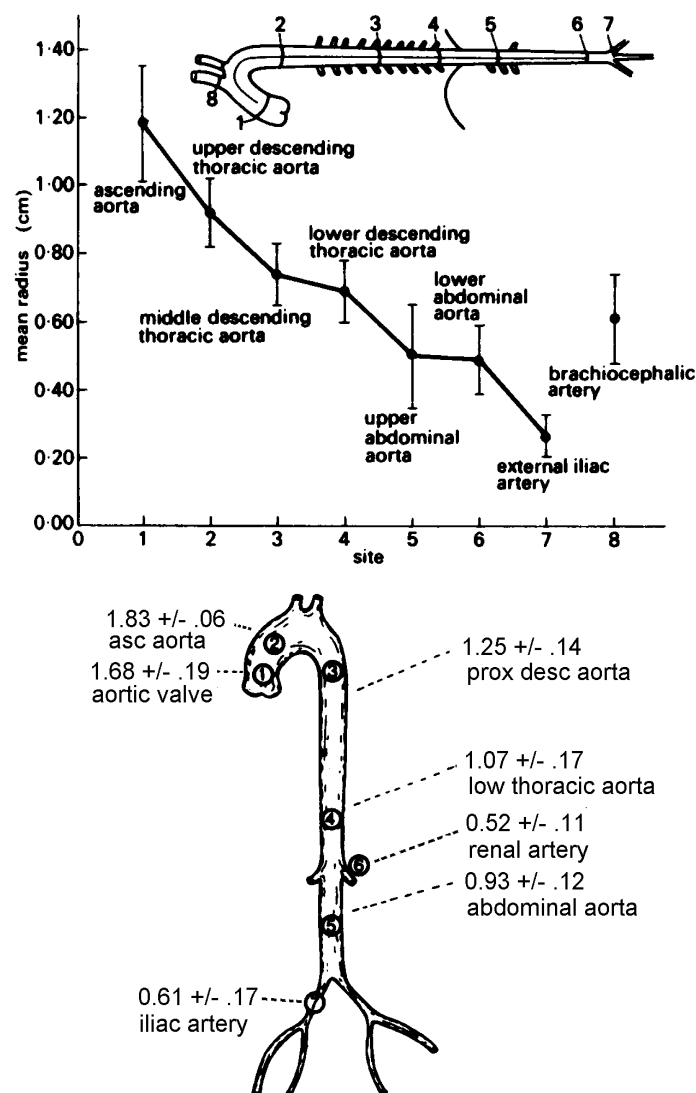


Figure 1–12 Up: Aortic tapering in dogs.(Fry, Griggs et al. 1963) Down: Radius values in a human aorta.(Latham, Westerhof et al. 1985)

A daughter branch always has a smaller diameter than the mother branch. However, although the lumen area of each daughter branch at a junction is smaller than the mother branch lumen area, the combined cross-sectional area of the daughter branches is always slightly bigger than the offspring cross-sectional area. For example, the area ratio at the aortic arch was calculated to be about 1.08 by Li et al. (Li, Melbin et al. 1984), thus slightly bigger than 1. The consequence of this is discussed further in this chapter.

The arterial wall is not an inert and stiff hydraulic tube. It consists of non-homogeneous, organic tissue in which complex exchange and control mechanisms take place. The vessel wall consists of highly extensible elastin material, of very stiff collagen with a high tensile strength, and of smooth muscle cells that, as opposed to skeletal and cardiac muscle, mainly invaginate their cell walls rather than exerting a longitudinal shortening. (Cooke and Fay 1972) Three concentric regions can be distinguished: the tunica intima, media and adventitia (Figure 1–13). The intima layer (1) is the innermost layer and mainly takes care of exchange mechanisms through the vessel wall. This very thin layer (0.5-1 μm) is made of endothelium cells, which in general have a longitudinal direction compared to the vessel axis. The middle layer or tunica media (3) is thicker, built mainly of smooth muscle cells distributed in a more or less concentric way, which play an important role in the mechanical properties of the vessel. For example, the arterial wall actively contracts and relaxes and can control and adapt its 'vascular tone' when influenced by vasoactive agents or by changing perfusion pressure. Intima and media layer are separated by an elastic tissue, the internal laminae (2). The tunica adventitia (5) consists primarily of connective tissue that merges with the artery surrounding tissue. In some vessels, a (somewhat thinner) elastic membrane (4) between media and adventitia is present.

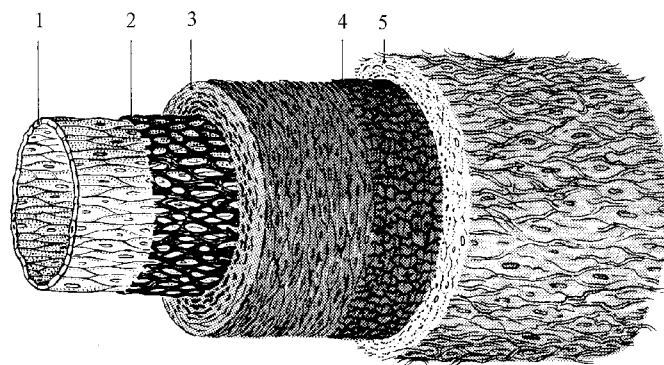


Figure 1–13 Different layers of the artery vessel wall. (Kahle, Leonhardt et al. 1992)

The relative amount of components forming the arterial wall changes from site to site along the arterial tree (Figure 1–14). The mechanical properties depend as much on the connections between elastin, collagen and muscle than on the size and orientation of the muscular layer (Kenner 1967) but in general terms, the amount of elastin diminishes when more distal from the heart, and the muscular layer increases in size, hereby also increasing the relative wall thickness. Vessels become gradually stiffer towards the periphery, hence also the terms ‘elastic’ (aorta and proximal portions of its major branches) and ‘muscular’ arteries (distal portions of major branches and their descendants). This effect is sometimes referred to as ‘elastic tapering’.

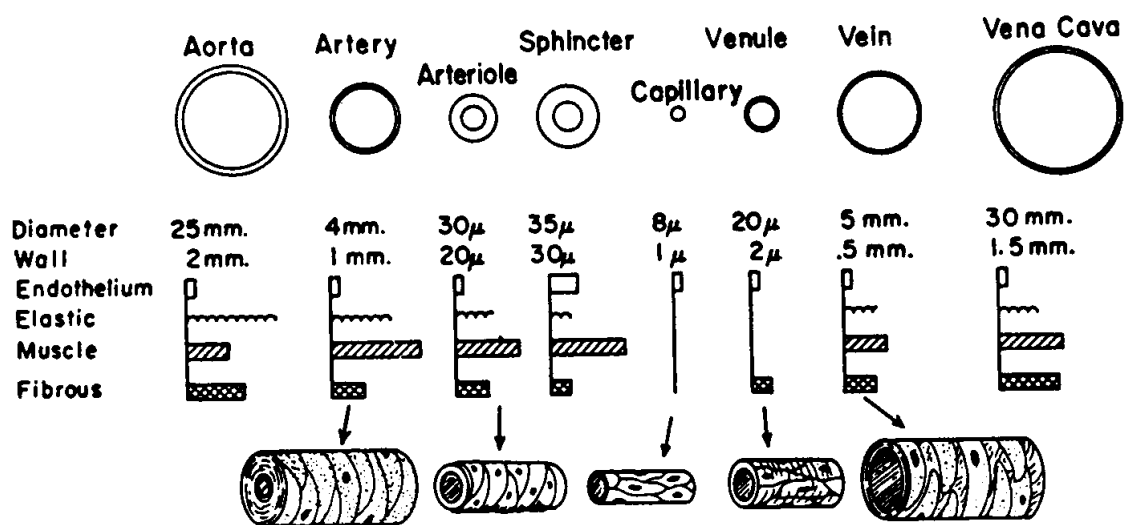


Figure 1–14 Composition of the arterial and venous wall in the systemic circulation.(Rushmer 1972)

3.2 Physiological aspects

3.2.1 Pressure and flow

The heart is a pulsatile pump, generating pressure and flow waves travelling throughout the circulatory system. A typical aortic pressure and flow waveform for one cardiac cycle is depicted in Figure 1–15.

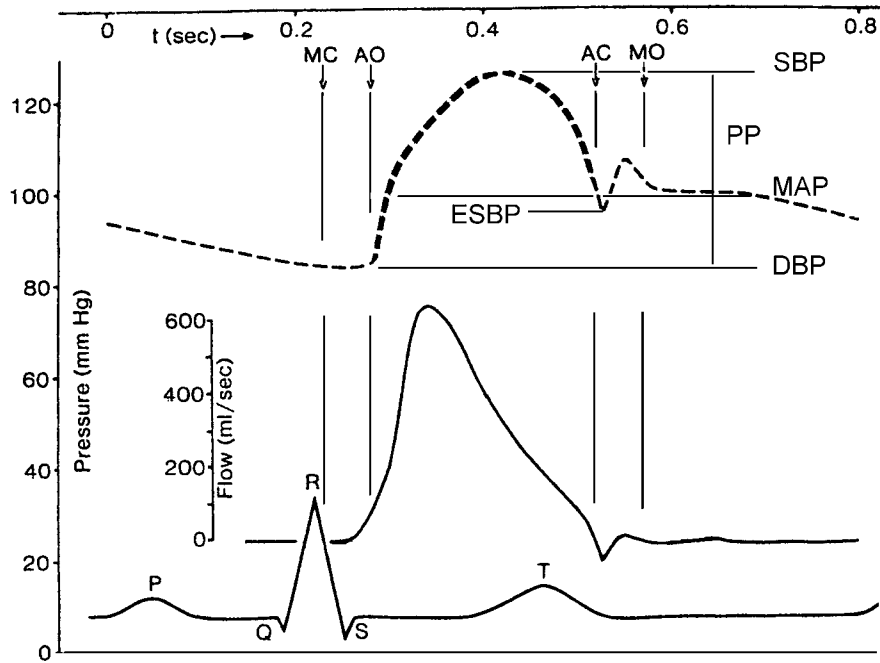


Figure 1–15 Aortic pressure and flow wave for one cardiac cycle at the aortic valve.

The timing of these arterial pressure and flow waveforms with respect to the contraction and relaxation of the heart can be read from the ECG. Important characteristics of the pressure waveform are: the peak of the pressure curve, called ‘systolic blood pressure’ (SBP, normal value typically around 120 mmHg), the mean arterial pressure (MAP), and the minimum of the pressure curve or ‘diastolic blood pressure’ (DBP, normal value typically around 80 mmHg). The difference between SBP and DBP is called pulse pressure (PP). The minimum corresponding to the closing of the aortic valve (AC), called the ‘dicrotic notch’, has a pressure value referred to as ‘end systolic blood pressure’ (ESBP).

When the pumping characteristics of the heart change (e.g. increased HR or SV during exercise), the shape of pressure and flow waves varies as well. In stationary heart conditions, the waveforms at one location can be regarded as steady-state oscillations. For example, the pressure and flow waveforms at the aortic valve depicted in Figure 1–15 will look exactly the same for every cardiac cycle provided that no metabolic changes occur. However, the waves do change shape as they travel along the arterial tree, as shown in Figure 1–16, and the reasons for this lie in the geometric and elastic characteristics of the vascular tree.

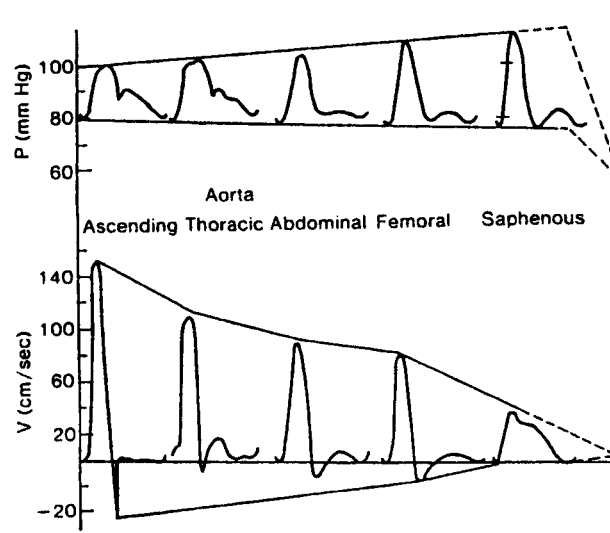


Figure 1-16 Evolution of pressure and flow wave along the arterial tree.(McDonald 1960)

3.2.2 Compliance

Figure 1-17 shows an illustration of the famous Windkessel theory by Stephen Hales (1733), who made an analogy with the buffer reservoir or compression chamber (Windkessel in German) from fire engines and the elastic recoil of vessel walls. Otto Frank (1899) transformed this analogy later on in a quantitative model.(Hales 1733; Frank 1899) Similar to how the compression chamber from the fire-engine induces dampening on the pulsatile output to provide a more continuous flow, the compliance of the arterial wall allows to store a certain blood volume during ejection that is subsequently released during the filling phase when the aortic valve is closed.

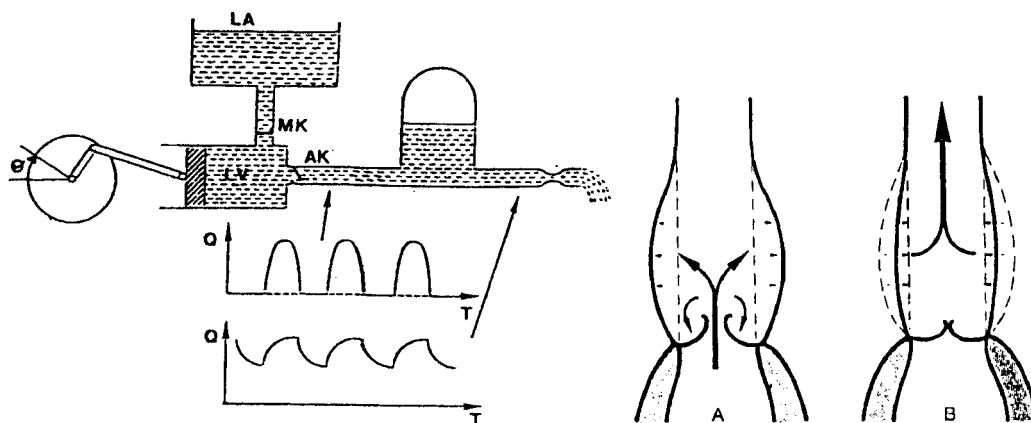


Figure 1-17 The Windkessel effect: a fire engine compression chamber (left) and ejection of blood from the ventricle into the aorta (right).(Verdonck 1993)

Since elastic properties of the vessel wall change from compliant to stiff when moving distal from the heart, the arteries lose their buffer capacity to dampen out the waves, which together with wave reflections results in steeper waveforms towards the periphery.

3.2.3 Resistance

Due to geometric tapering, arterial branches get smaller and smaller, and the resistance of an artery against perfusion increases towards the periphery. However, because of the phenomenon that the combined cross-sectional area of the daughter branches is always slightly bigger than the offspring cross-sectional area, there is in fact perfusion redistribution at every junction as shown in Figure 1–18. One can notice that as the vascular tree expands, mean pressure drops slowly until the arterioles and capillaries are reached where the largest pressure drop occurs. The mean velocity curve is slightly descending along the aorta, goes down more rapidly in the peripheral arteries and takes a steep fall at the height of the vascular beds, where the total cross-sectional area has enlarged greatly compared to central aortic site.

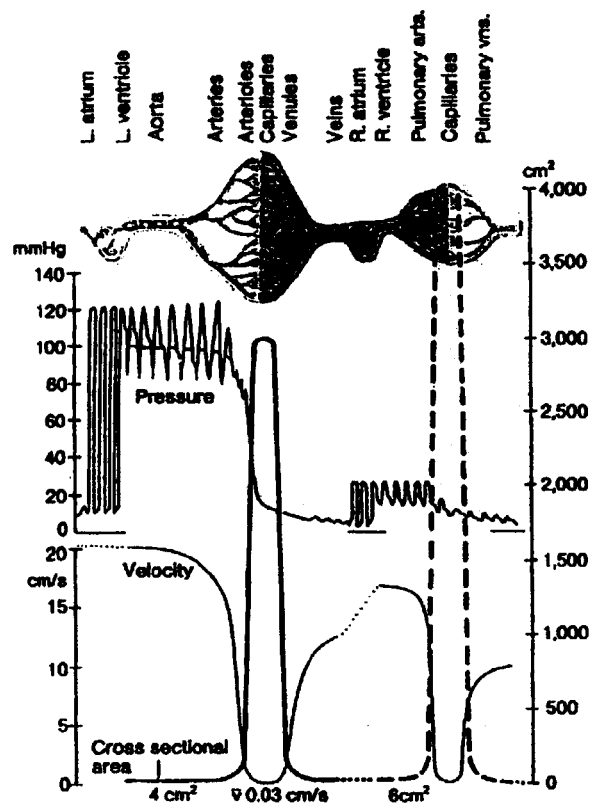


Figure 1–18 Mean pressure and velocity curves in the systemic circulation.(Schmidt and Thews 1989)

3.2.4 Wave reflections

Due to the non-uniformities in the vascular tree in terms of geometry and elasticity, reflection points are induced in this branched closed loop system and backward travelling pressure and flow waves develop. The reflection of waves is in fact the prominent factor determining their final shape. As shown in Figure 1–19, a pressure wave is actually built up by a forward wave, added with the backward travelling reflections, while the flow wave is built up by the forward wave subtracted with reflected components. (Westerhof, Sipkema et al. 1972; Li 1986; Nichols, O'Rourke et al. 1987)

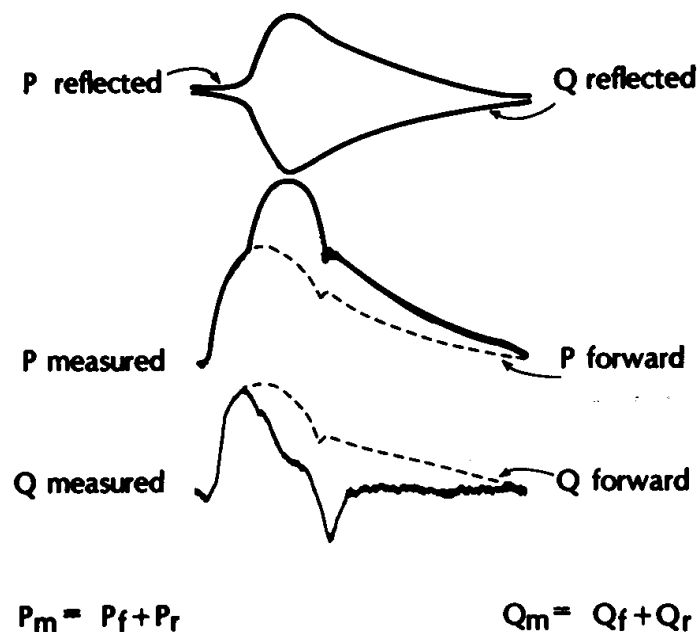


Figure 1–19 Decomposition of arterial pressure and flow in forward and reflected waves. (Nichols, O'Rourke et al. 1987)

3.2.5 Aging and pathological conditions

Under the influence of aging or pathological conditions such as 'hypertension' (high blood pressure) and 'atherosclerosis' (narrowing of the vessel lumen due to deposits of several substances, generally called 'plaque'), the waveforms change shape as well but this will not be discussed further. As an illustration, the aortic pressure and flow waveforms of an old and young subject are shown in Figure 1–20. The augmentation index (Aix), introduced in the 1980s as a simplified interpretation of the effect of wave reflections (Murgu, Westerhof et al.

1980), is defined as the ratio of ΔP and PP , with ΔP being the difference between SBP and the pressure P_i at the inflection point:

$$Aix = \pm \frac{\Delta P}{PP} \quad \text{Eqn. 1.2}$$

Type A waveforms (old subject) have an inflection point before the point of SBP, and result in a positive Aix , while for type C waveforms (young subjects) the inflection point occurs later than the point of SBP, and the Aix has a negative value.

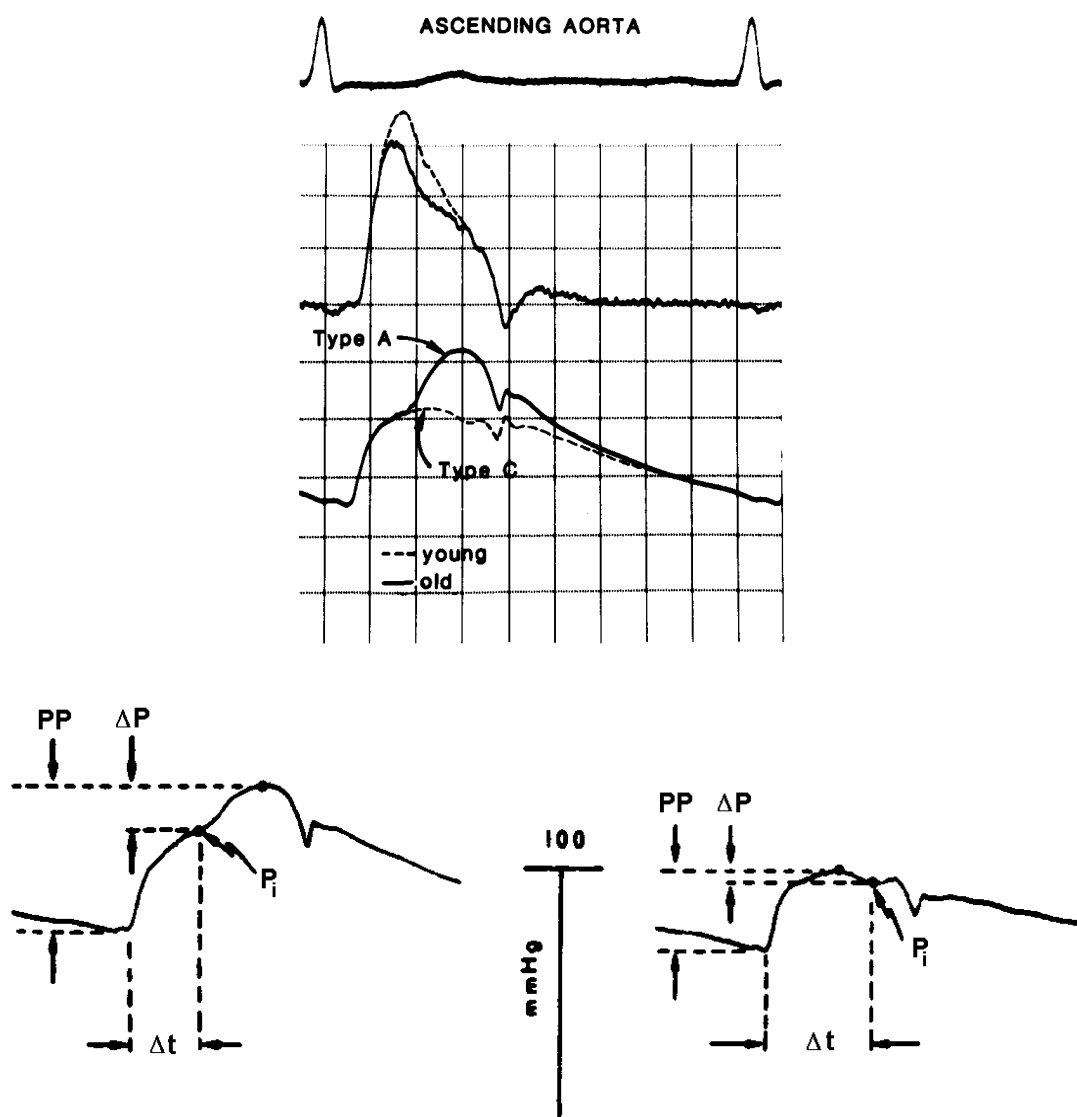


Figure 1-20 Type A and type C waveforms characterizing an older and younger person, respectively. Type A waveforms induce positive Aix indices, type C waveforms correspond to negative Aix indices. (Murgo, Westerhof et al. 1980; Nichols, O'Rourke et al. 1985)

Summary

Starting with a brief historical introduction, the relevant anatomical and physiological aspects of the heart and the circulation have been discussed. The electrical stimulation of the heart as well as the different pressure and flow events during one cardiac cycle have been explained. The heart wall composition was described. Cardiac haemodynamic parameters such as cardiac output (CO), heart rate (HR), stroke volume (SV) and the relation among them were defined, together with the influence of training or exercise.

The arterial circulation can be divided into coronaries, supplying blood to the heart itself, and large arteries, which irrigate the rest of the body. Nomenclature for the coronaries has been addressed as well as the myocardial resistance effect and some important regulatory mechanisms such as autoregulation, metabolic regulation and reactive hyperaemia.

The large arteries can be divided in central and peripheral arteries. The arterial wall structure and the effects of geometric and elastic tapering were discussed. Arterial compliance and the Windkessel effect, together with resistance properties and the influence of vascular branching, wave reflections and aging have been described in an intuitive way, holding back strict mathematics for the second part on vascular biomechanics.



2 Rationale for this Thesis

1 Background

In recent years, the study of the cardiovascular system of an individual at early age has been given an increasing social importance. It has been demonstrated that most heart and vessel diseases have either a genetic base or have been induced by lifestyle.(Guillaume, Lapidus et al. 1996; Vogel and Benitez 2000; Hanevold, Waller et al. 2004) Such risk factors for degeneration of the blood vessels ('atheromatosis') have already been clearly delineated and comprise the lack of physical activity (Cameron and Dart 1994), smoking (Caro, Lever et al. 1987), overweight (Balkestein, van Aggel-Leijssen et al. 1999), high blood pressure (Tice, Peterson et al. 1996), disturbed sugar metabolism ('diabetes') (McVeigh 1996), and disturbed cholesterol and lipid metabolism (Wilkinson, Prasad et al. 2002; Millen, Quatromoni et al. 2004). Methods that can identify people at risk in a stage before the pathological process causes irreversible damage are important from prevention point of view, especially since therapeutic measures are getting more and more efficient. Where applicable, the studies in this thesis were focused towards a juvenile population as an early risk detection requires a specific approach towards children and young adults.(McCarthy 2001; Berenson 2002)

The key to all this lies within an adequate haemodynamic description and understanding of the pump function of the heart and the properties of the vascular bed. Today the heart pump characteristics are being assessed with satisfying accuracy. The properties of the vascular tree are still not investigated to the same depth however. The fluid dynamic phenomena and regulation mechanisms occurring in a non-uniform visco-elastic tube network (the blood circulation) are still complex and current-day topics in haemodynamic research. Several epidemiological studies have shown the importance of variations in pulse pressure (Benetos, Safar et al. 1997; Franklin, Khan et al. 1999; Asmar, Rudnichi et al. 2001), vascular resistance (James, Watt et al. 1995; Matthys, Craen et al. 1996) and especially arterial stiffness and elasticity (Hirai, Sasayama et al. 1989; London, Pannier et al. 1994; Blacher, Pannier et al. 1998; McVeigh, Bratteli et al. 1999; Kingwell, Waddell et al. 2002). In this thesis, these topics will fulfill a prominent role and they will be addressed via indices and parameters which are based on pressure and flow measurements.

A fast, simple and non-invasive haemodynamic analysis of the vascular tree remains a difficult task for several reasons. A first requirement for the (real-time) calculation of the

desired parameters and indices is the simultaneous and synchronized acquisition of heart rate together with blood pressure and blood flow waveforms at the height of the aortic valve (i.e. at the inlet of the vascular tree). Although basic as this may sound, that kind of combined data acquisition is non-existent in current commercially available equipment used in clinical practice.

A reason for this is that, as opposed to ultrasound technology for continuous non-invasive blood *flow* assessment, non-invasive technology for continuous blood *pressure* registration still has many shortcomings and is not established in routine clinical practice. Moreover, there is the necessity of using a mathematical model ('transfer function') to derive central pressure from peripheral non-invasively measured pressures. Note that this is not required for velocity or flow as ultrasound allows a direct non-invasive measurement at the site of the aortic valve.

Finally, apart from an ever-growing and necessary theoretical knowledge (vascular biomechanics) together with the above mentioned practical issues (simultaneous and synchronized acquisition, limitations of current pressure sensor technology and additional mathematical analysis), there is also a dynamic aspect to be considered. Different loading conditions such as physical exercise tests, but also interventional procedures, have a thorough impact on the haemodynamic state. Up to now, the bigger part of studies involving assessment of vascular haemodynamic parameters have been looking at adult subjects at rest in supine position, while the effects of early age and stress conditions induced by either drugs or by physical exercise have been lacking the appropriate attention.

2 Outline of this thesis

This introductory Part I provided the basic and necessary understanding of the heart and the circulation (Chapter 1), together with the rationale of this thesis (Chapter 2). The problems stated in the above paragraph will now be addressed further and are organized in two sections: methodological aspects (Part II and Part III) and (clinical) applications (Part IV and Part V).

Part II, the first part of the methodology section, goes deeper into theoretical aspects of vascular biomechanics (Chapter 1), focusing on the problem of vessel wall properties, system identification (transfer function) and modelling (arterial network). More specific, a comparison of two transfer function models for the aorta-radial pathway is presented (Chapter 2) and an existing arterial network model is expanded and optimized to investigate the effects of variations in aortic elasticity and diameter on pulse pressure (Chapter 3).

Part III, the second part of the methodology section, looks at practical aspects. It gives an introduction to the measurement techniques for pressure and flow (Chapter 1), focuses then on continuous blood pressure registration via the method of arterial tonometry (Chapter 2), looks at the potential of tonometry as a long-term monitoring tool (Chapter 3) and describes the development of an in-house acquisition program for ECG, pressure and flow (Chapter 4).

Part IV, the first part of the applications section, presents non-invasive haemodynamic analysis during rest and stress conditions with a specific interest for determining large artery compliance. Several preliminary experiments are being described (Chapter 1), together with a first in vivo (feasibility) study during a supine and standing bicycle test (Chapter 2) and a second in vivo (clinical) study during a drug-induced or treadmill stress test (Chapter 3).

Part V, the second part of the applications section, presents minimally invasive haemodynamic analysis during an interventional procedure (coronary stenting). First, an introduction on applied cathlab visualization techniques is given (Chapter 1). Then, the optimal deployment of a stent is quantified by means of a pressure-derived index (FFR) (Chapter 2). Finally, the impact of the myocardial ‘waterfall’ effect is being looked upon from which a corrected FFR index (FFR_C) is derived (Chapter 3).

II Methodology I: Biomechanics, Identification and Modelling

This second part serves to give insights in biomechanics, system identification and system modelling for the vascular tree. Considering the first, blood and vessel properties as well as fluid dynamic principles are addressed, and some mathematical tools are looked upon briefly (Chapter 1). Next, system identification theory is applied by means of transfer function analysis. In Chapter 2 different transfer function approaches are implemented and discussed for the aorta-radial path. Finally, a numerical model of the arterial tree is considered (Chapter 3), in which the influence of wall stiffness and diameter changes on pulse pressure are investigated.



1 Background: Vascular Biomechanics

History

William Harvey's book *De Motu Cordis* in 1628 had finally put science on the right track in terms of anatomical knowledge and physiological understanding of the cardiovascular system. However vital his work has been, applying the language of mathematics on the observed phenomena had the potential of bringing cardiovascular research to another new level. This was an observation made by some of the greatest minds in the history of science, at a time when the theoretical treatment of fluid dynamics was starting to flourish. And although a few milestones in mathematics and physics were only much later applied onto cardiovascular topics, such as the fluid viscosity concept of Isaac Newton (1642-1727), a considerable amount of the ground-breaking endeavors were interdisciplinary from the very start.

Great researchers were crossing borders in terms of ideas, such as Stephen Hales (1733) comparing properties of the circulation with those of a fire-engine, as well as in terms of expertise, such as Daniel Bernoulli (1700-1782), a friend and contemporary of Leonhart Euler, relating pressure changes in a fluidum in motion to the balance of potential and kinetic energy. Bernoulli had a position as Professor of Anatomy at the University of Basel; he merely combined it with a personal interest in mathematics. It is now his biggest contribution to science.(Speiser 1982)

Arterial haemodynamics advanced further in the nineteenth century, principally in Germany, England and France. J.L.M. Poiseuille (1797-1869), another well-known achiever in the field of fluid dynamics, had training in physics but was a physician with an interest in cardiovascular research. And the same goes for Thomas Young (1773-1829), again both a physicist and physician.(Laird 1980) His work on human vision and color perception, and especially his theories on elasticity (Young's E modulus) are famous.

Some of the original ideas were merely simple, however brilliant, analogies or basic concepts and were only much later described in a strict, theoretical way by others, such as the Windkessel theory of Hales treated by Otto Frank (1865-1944).(Frank 1899) Other theories were forgotten and reinvented at a later time. The work on pulse wave velocity in arteries is most often attributed to Moens and Korteweg (1878), hence the formula which carries their

names, but this was in fact already derived by Young (1808) many years earlier.(Young 1808; Young 1809; Korteweg 1878; Moens 1878)

Finally, some theories just took a very long time to be introduced into the field of cardiovascular research. Up to the 1950s, arterial pressure and flow wave analysis was performed and explored only in the time-domain. In need for more advanced techniques enabling to dig deeper than the obvious information given by analysing wave contours (foot, peak, inflection points, etc.), the theory of Fourier (1768-1830) on decomposing a wave into its harmonic content was first applied on the arterial circulation by people such as John Womersley around 1955 and Michael Taylor a few years later.(Womersley 1955b; Womersley 1957a; Taylor 1966)

From then on, the mathematical analysis of haemodynamics again took a new turn and evolved profoundly. Many people have made many more contributions, and this introduction was not at all intended as an exhaustive list. In the same way, the topics discussed in the rest of this chapter are merely selected on their relevance to the applications mentioned in this thesis. Some standard reference works on the field of haemodynamics have been written by William R. Milnor and Donald A. McDonald and their co-workers.(McDonald 1960; Milnor 1989; Nichols and O'Rourke 1990)

1 Blood composition and viscosity

So far, the properties of the fluidum at hand have not been addressed. Blood is not a homogeneous substance: it is a suspension of cells in plasma, a yellowish fluid mainly consisting of water (90%) and proteins (8%). The suspended particles comprise the red blood cells or ‘erythrocytes’, white blood cells or ‘leucocytes’, and blood platelets or ‘thrombocytes’ (Figure 1–1).

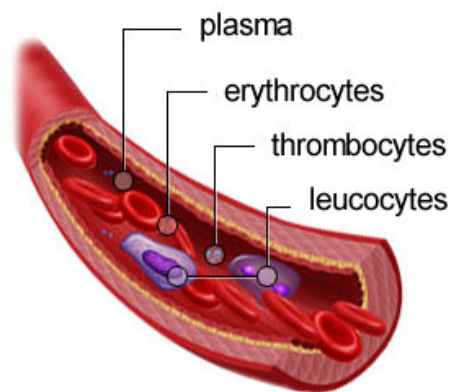


Figure 1–1 Composition of blood: a suspension of red blood cells (erythrocytes), white blood cells (leucocytes) and platelets (thrombocytes) in plasma.

Red blood cells are bi-concave shaped. They have an average diameter of 7-8 μm , contain the protein called ‘haemoglobin’ (Hb), giving the red color, and carry around the oxygen from the lungs through the body. Red blood cells are highly elastic and can form aggregates, called ‘rouleaux’. White blood cells are in charge of the body’s defense and immune system against infections and foreign particles, such as bacteria. They are colourless and have an irregular shape, and are bigger than red blood cells. The ratio of the red to white blood cell amount is about 500 to 1. Blood platelets are cell fragments important for proper blood clotting. They can secrete a hormone called ‘serotonin’ which constricts torn blood vessels. The concentration of cells in the blood is expressed as the ‘haematocrit’ value, the percentage volume of the blood in which the cells have sediment by centrifugation. Normal values in healthy human subjects lie between 40% and 50%.

Looking at a fluidum in motion as infinitely thin layers sliding over each other with different velocity (laminar flow), one can define the internal friction between adjacent layers as the fluid ‘viscosity’. The theoretical treatment of the viscosity concept dates back to Isaac

Newton, and is illustrated in Figure 1–2. The stress σ (force F per unit area A) required to move the laminae against the friction between the layers will be proportional to the velocity gradient dv/dr , called the ‘shear rate’, or:

$$\sigma = \mu \frac{dv}{dr} \quad \text{Eqn. 1.1}$$

with μ being the coefficient of dynamic fluid viscosity (Pa.s).

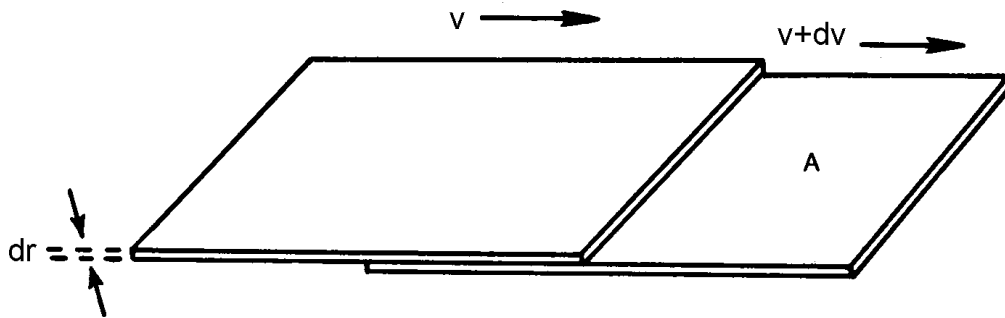


Figure 1–2 Concept of internal friction or ‘viscosity’ between sliding fluidum layers.

Newtonian liquids by definition have a constant viscosity coefficient at all rates of shear (Figure 1–3). This applies for many homogeneous liquids (e.g. water), but suspension fluids like blood deviate from this. Blood has a small yield stress σ_{ys} (around 15 mPa) which is to be overcome before deformation occurs.(Kim 2002) Further, at low shear rates the apparent viscosity of blood increases markedly (shear thinning effect) and in small tubes the apparent viscosity at higher rates of shear is smaller than it is in larger tubes (Fahraeus-Lindqvist effect). The latter starts to be detectable with tubes less than 1mm internal diameter (i.e. about 100 times the diameter of a red blood cell).(Fahraeus and Lindqvist 1931; Haynes 1961; Morris, Smith 2d et al. 1987)

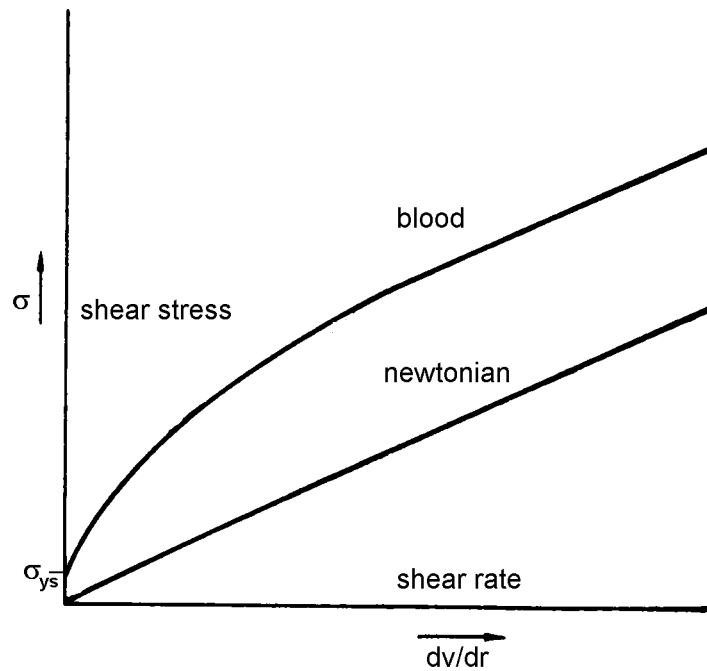


Figure 1–3 Viscosity behaviour for a Newtonian fluid and for blood.

It has been acknowledged that plasma behaves like a Newtonian fluid.(Merril, Benis et al. 1965) Progressively adding red cells to the plasma will increase the viscosity. With a cell concentration or haematocrit (Hct) under 10%, no non-Newtonian characteristics are noticed, and for Hct up to 45% fluid viscosity μ can be said to vary linearly with cell concentration, thus covering most clinical conditions (Figure 1–4).

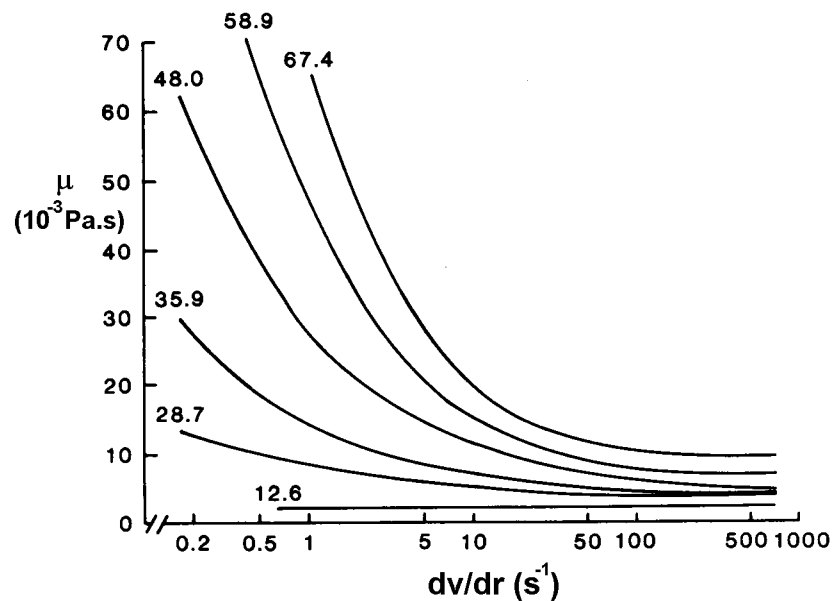


Figure 1–4 Influence of viscosity by haematocrit for increasing shear rate.(Brooks, Goodwin et al. 1970)

Aerobic training is known to increase total blood volume by 20% to 25%. Plasma volume and Hb both increase, but since plasma volume increases more, the Hct values of athletes or persons performing regular physical exercise is slightly lower than their sedentary counterparts.(Nieman 1995) Apart from exercise, Hct is also correlated with other previously mentioned cardiovascular risk factors such as smoking, obesity, etc. and a series of prospective studies have tried to investigate Hct (as well as plasma viscosity, red cell aggregation or whole blood viscosity in general) as a predictor of cardiovascular mortality.(Danesh, Collins et al. 2000) Although there is some association between the determinants of blood rheology and the risk of coronary heart disease (Gagnon, Zhang et al. 1994), the impact of rheological parameters still needs further investigation.(Danesh, Collins et al. 2000; De Backer, De Buyzere et al. 2002) The above rheological issues are mentioned here for completion but the study of their influence on vascular function goes beyond the scope of this thesis.

In this thesis the complex fluid dynamics on the capillary level will be stayed clear of, and only tubes with diameters around 500 μm and upward (epicardial and myocardial coronaries and large arteries) will be addressed, so that the ‘high shear’ or ‘small tube’ viscosity effect is negligible. Further, since no phenomena of fluid-wall interaction will be discussed, and normal haematocrit values (around 45%) are assumed, it is a fair approximation to use the ‘asymptotic’ viscosity value (constant value reached at shear rates above 200 s^{-1} , see Figure 1–4) for the remainder of this thesis, thus attributing a Newtonian behaviour to blood. In following chapters mostly $\mu = 0.0035 \text{ Pa.s}$ at 37 °C was used for calculations.

2 Arterial wall properties and pulse wave velocity

As described in the previous chapter, the arterial wall is an anisotropic, active tissue, composed of several distinct materials occurring in different ratios along the arterial tree. In order to somehow quantify the geometric and mechanical properties, one can turn to mathematical modelling. For example, the area change due to geometric tapering is most often modelled with a simple exponential function, of the form:

$$A(z) = A_0 e^{-\left(\frac{k_t z}{R_0}\right)} \quad \text{Eqn. 1.2}$$

with A_0 the area and R_0 the radius of the upstream section, and taperfactor k_t varying along the arterial tree, ranging from 0.02 to 0.05 (Figure 1–5). (Caro, Pedley et al. 1978; Li 1987)

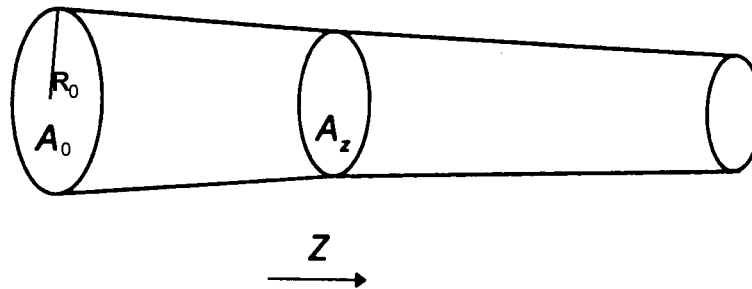


Figure 1–5 A simple exponential model for the geometric tapering in arteries.

However, the complexity of a phenomenon is not seldom proportional to the amount of models, equations and approximations derived for it. This is particularly true for the assessment of the visco-elastic properties of the vascular wall and the associated pulse wave velocity. Since all of these theoretical derivations are built upon a number of simplifying assumptions, it is not an easy question to value one over the other and in fact all contribute to some extent to a better understanding of the problem.

More specific and in the light of what is needed in further chapters, only the elastic behaviour of a uniform, incompressible bulk material will be discussed and that of an isotropic, thin-walled, cylindrical tube model. Visco-elastic effects are regarded only when a sinusoidal pressure waveform is applied. Formulae for thick-walled models are more elaborated derivations of the thin-walled formulae, and any repetitive natural pulsation can be

decomposed in its sinusoidal components (see section 3 of this chapter), so these are acceptable simplifications.

2.1 Stress-strain for elastic behaviour

The elastic properties of a material can be described by its Young's modulus of elasticity E , defined by the ratio of tensile stress σ to tensile strain ε . Elongation in one direction by a tensile stress implies a contraction in the two other directions. The transverse strains are proportional with the elongating strain and the proportionality constant is defined as Poisson's ratio ν_p . A positive ν_p is related to a decrease in transverse direction due to a longitudinal extension, hence the negative signs in the formulae. Looking at stress along the longitudinal axe (Figure 1–6), one finds:

$$E_{zz} = \frac{\sigma_{zz}}{\varepsilon_{zz}} \quad \text{Eqn. 1.3}$$

$$\nu_{p\,xz} = -\frac{\varepsilon_{xx}}{\varepsilon_{zz}} \quad \text{Eqn. 1.4}$$

$$\nu_{p\,yz} = -\frac{\varepsilon_{yy}}{\varepsilon_{zz}} \quad \text{Eqn. 1.5}$$

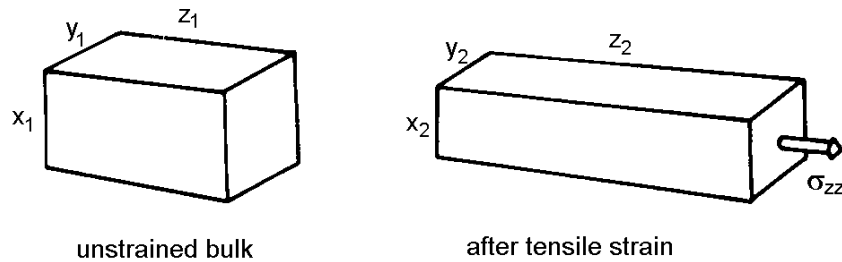


Figure 1–6 Effect of elongating tensile stress σ_{zz} on uniform bulk material. Hereby is $x_2 < x_1$, $y_2 < y_1$, $z_2 \gg z_1$. Longitudinal strain in z : $\varepsilon_{zz} = (z_2 - z_1)/z_1 > 0$. Transverse strain in x : $\varepsilon_{xx} = (x_2 - x_1)/x_1 < 0$. Transverse strain in y : $\varepsilon_{yy} = (y_2 - y_1)/y_1 < 0$.

For an isotropic material, E and ν_p are the same in all directions. E has the dimension of a stress (Pa), ν_p is dimensionless. From the above formulae it can be derived that a value of 0.5

for Poisson's ratio implies that the volume of the material does not change with the elongation. Assuming small radial and longitudinal deformations with respect to the lumen diameter and vessel length, the stress and strain relation is linear, the material obeys Hooke's law of elasticity and the slope of the curve is the (constant) E-modulus.

Since the non-homogeneous walls of blood vessels exhibit a curvilinear stress-strain relationship instead of a linear Hookean, it is better to define an incremental elastic modulus E_{inc} (Krafka 1939; Bergel 1961b) at a particular length L_m as the tangent to the stress-strain curve at that point (Figure 1–7):

$$E_{inc} = \frac{\Delta\sigma L_m}{\Delta L} \quad \text{Eqn. 1.6}$$

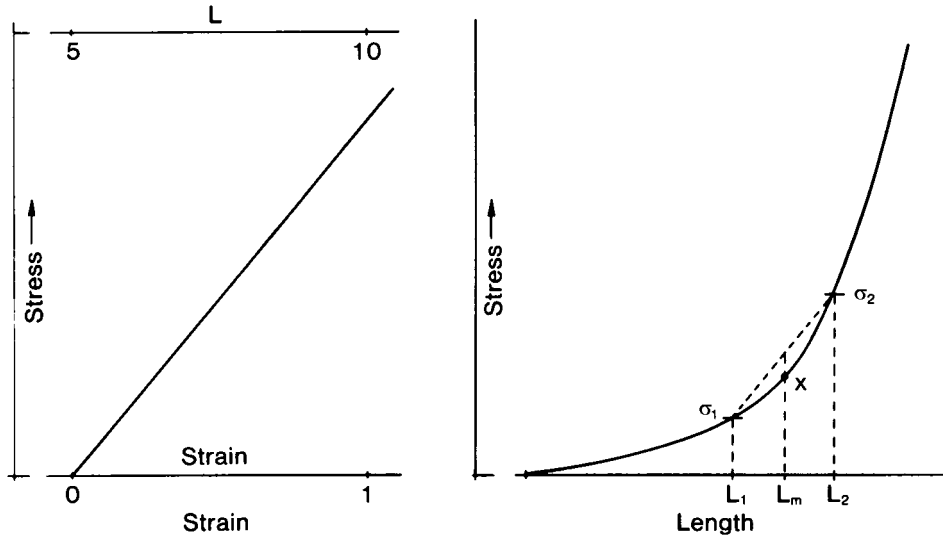


Figure 1–7 Left: Linear stress-strain relation with a constant slope (E-modulus). Right: Non-linear stress-strain relation with E-modulus as a function of the length. E_{inc} for the length L_m is then defined as $\Delta\sigma L_m / \Delta L$ with $\Delta\sigma = \sigma_2 - \sigma_1$, $\Delta L = L_2 - L_1$ and $L_m = (L_1 + L_2)/2$. (Milnor 1989)

For a linear elastic material, Eqn. 1.3 and Eqn. 1.6 produce the same results.

Dealing with blood vessels, it is more appropriate to use cylindrical rather than rectangular coordinates. Radial, circumferential and longitudinal directions are symbolized by r , θ and z . An approximation of the transmural pressure (intravascular minus extravascular pressure) distending the vessel wall can be quantified by the law of Laplace, who derived a relation between the circumferentially directed forces per unit length, referred to as the wall tension

T_w , the transmural pressure p_t and the radius R (Eqn. 1.7). Stress is force per unit area and thus the formula for circumferential stress $\sigma_{\theta\theta}$ in a thin-walled cylindrical shell (Figure 1–8), with h being the wall thickness, p the internal pressure and the external pressure assumed to be zero, is expressed in (Eqn. 1.8). (Peterson, Jensen et al. 1960) These formulae will return when dealing with radial applanation tonometry.

$$T_w = p_t R \quad \text{Eqn. 1.7}$$

$$\sigma_{\theta\theta} = \frac{pR}{h} \quad \text{Eqn. 1.8}$$

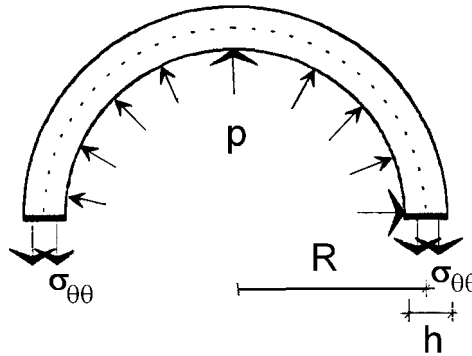


Figure 1–8 Illustration of the law of Laplace for a thin-walled cylindrical shell.

It was mainly the work of Bergel in the early 1960s to replace the above equations for stress and strain with appropriate expressions for thick-walled tubes. For example, the E_{inc} expression for a thick-walled, isotropic elastic tube of uniform diameter and wall thickness becomes:

$$E_{inc} = \frac{R_i^2(1 + \nu_p)}{(R_o^2 - R_i^2)} \left\{ r(1 - 2\nu_p) + \frac{R_o^2}{r} \right\} \frac{\Delta p}{\Delta r} \quad \text{Eqn. 1.9}$$

with R_o the outer and R_i the inner radius, r the radial coordinate of any point in the wall, and Δr the radial displacement of the point by a change in pressure Δp . (Bergel 1961b; Bergel 1961a) Other researchers continued elaborating this work on appropriately defining the modulus of elasticity. (Peterson, Jensen et al. 1960; Gow and Taylor 1968)

2.2 Stress-strain for visco-elastic behaviour

Blood vessels are not purely elastic. This would mean that an applied stress produces an instantaneous strain, which disappears immediately after stress removal. When the transmural pressure is increased stepwise, the vessel only gradually dilates to a new value ('creep' phenomenon). Inversely, the sudden increase of vessel diameter invokes an increase in tension that declines over time to a lower level ('relaxation' phenomenon). This is called 'visco-elastic' behaviour (Figure 1–9). The elastic modulus measured when the steady state has settled in for stress and strain is referred to as the static E-modulus (E_{stat}).

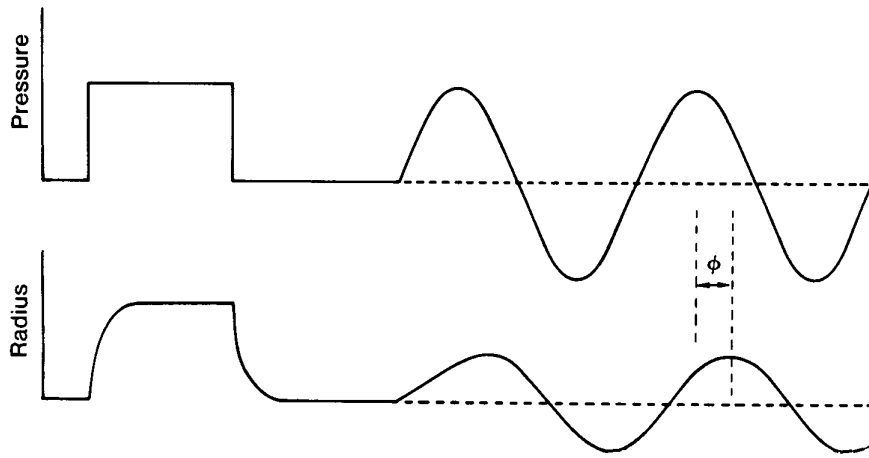


Figure 1–9 Left: Visco-elastic vessel response (bottom) on a pressure step increase (top): creep. Right: Visco-elastic vessel response (bottom) on a pressure oscillation (top): phase delay.(Milnor 1989)

E_{stat} is lacking the information on the viscous, time-dependent behaviour. Since the visco-elastic property mainly causes a phase difference between applied force and resulting displacement, a complex visco-elastic modulus E_c can be defined. When applying a sinusoidal pressure oscillation, there will be a phase lag between this stress and the resulting strain oscillations, which can be regarded as a measure of wall viscosity. The ratio of the amplitude of the imposed sinusoidal pressure to the amplitude of the radial oscillations is the amplitude of the complex E-modulus, denoted by $|E_c|$, while the phase angle between the two waves is denoted by ϕ (positive values indicating that pressure leads radial distension):

$$E_c = |E_c| \cos \phi + j |E_c| \sin \phi \quad \text{Eqn. 1.10}$$

This is a frequency dependent E-modulus. By applying sinusoidal stresses at various frequencies or by decomposing a natural pressure oscillation into its harmonic content (see section 3 of this chapter), discrete values for E_c can be determined.(Milnor 1989; Li 2000)

Hardung was the first to describe the visco-elasticity effect by a complex term E' :

$$E' = E_{dyn} + j\eta\omega \quad \text{Eqn. 1.11}$$

with E_{dyn} a real E-modulus term added with a complex part $j\eta\omega$, consisting of η the wall viscosity, and ω the angular frequency of the oscillating stress.(Hardung 1952) This terminology was adapted by other researchers later on.(Bergel 1961a; Gow and Taylor 1968) Womersley used a different set of symbols (Womersley 1957a), as this was more convenient for his treatments of flow through visco-elastic tubing:

$$E_c = E(1 + j\omega\Delta E) \quad \text{Eqn. 1.12}$$

so that, if compared with Eqn. 1.11:

$$\omega\Delta E = \frac{\eta\omega}{E_{dyn}} = \tan\phi \quad \text{Eqn. 1.13}$$

Also for the complex E-modulus, thick walled analogues are available:

$$E_c = \frac{2(1-\nu_p^2)R_i^2 R_o \Delta p}{(R_o^2 - R_i^2)\Delta R_o} e^{j\phi} \quad \text{Eqn. 1.14}$$

with Δp the amplitude of the sinusoidal pressure and ΔR_o the amplitude of the outer wall displacements.(Bergel 1961a)

The formulae for the complex E-moduli can be confusing sometimes in their physiological meaning. Attempts to regard the separate terms in the expressions as being the representatives for the elastic and the viscous effect have not yet lead to satisfying results for blood vessels. Comparing the behaviour with that of mechanical spring-dashpots models have only led to

conclusion that a high number of elements and time constants is necessary, again getting further and further from any physiological counterpart.(Westerhof and Noordergraaf 1970; Wesseling, Weber et al. 1973) In the first place, one should regard the complex E-moduli merely as mathematical expressions of empiric stress-strain relationships observed from experiments.

2.3 Pulse wave velocity

The relationship between the speed of a travelling pulse wave in an artery and the blood vessel elasticity, has been the subject of scientific endeavours from the 19th century on.(Young 1808) Again the resulting formulae are bounded in accuracy by the underlying assumptions made for their derivation. It is sufficient here to state the most well known expression by Moens and Korteweg that relates the E-modulus to pulse wave velocity c_0 (PWV). This equation assumes a fluid with density ρ (kg/m³) in a cylindrical, elastic tube with inner radius R_i (Korteweg 1878; Moens 1878):

$$c_0 = \sqrt{\frac{Eh}{2\rho R_i}} \quad \text{Eqn. 1.15}$$

As an example for an aorta ascendens segment, one can suppose the following values for a young individual (derived from the arterial network model presented in chapter 3): $E = 6.58 \times 10^5$ Pa; $h = 0.163$ cm and $R_i = 1.45$ cm. Together with blood density $\rho = 1050$ kg/m³, the pulse wave velocity in the aorta ascendens becomes $c_0 = 5.9$ m/s (see also Figure 1–10, bottom).

The formula for thick-walled tubes as derived by Bergel (following the Bramwell-Hill derivation) is expressed as:

$$c_0^2 = \frac{Eh}{2\rho R_o} \left\{ \frac{2 - \lambda}{2 - 2\lambda(1 - \nu_p - 2\nu_p^2) + \lambda^2(1 - \nu_p - 2\nu_p^2) - 2\nu_p^2} \right\} \quad \text{Eqn. 1.16}$$

with $\lambda = h/R_o$ (Bramwell and Hill 1922; Bergel 1961b; Bergel 1961a) For $\nu_p = 0.5$, this becomes:

$$c_0^2 = \frac{Eh}{2\rho R_o} \frac{2}{3} \left(2 - \frac{h}{R_o} \right) \quad \text{Eqn. 1.17}$$

The latter formula gives an indication about the error involved when assuming a thin wall, although the term $Eh/2\rho R_o$ differs from the Moens-Korteweg equation (Eqn. 1.15) by using the *outer* radius R_o instead of the *inner* radius R_i . A way of quantifying c_0 in vivo is by measuring the delay between the foot of a travelling wave at two different locations, separated by a known distance (Figure 1–10). This measurement can be done non-invasive by use of ultrasound or arterial tonometry techniques (see Part III).

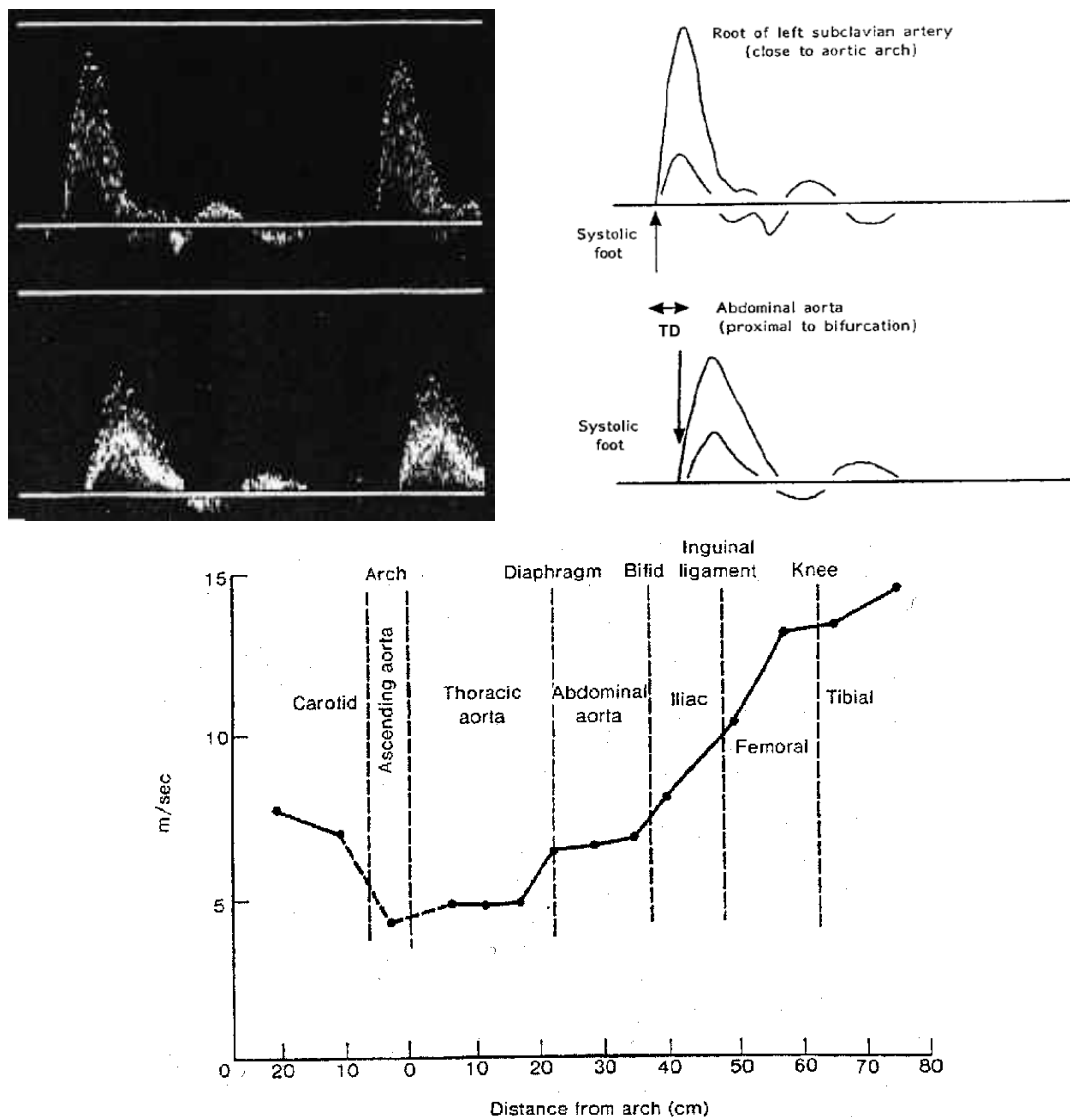


Figure 1–10 Upper panels: Measured velocities at the subclavian (top) and abdominal aorta (bottom). TD is the measured time delay.(Lehmann, Gosling et al. 1992) Lower panel: Variation of the pulse wave velocity when moving further distal from the heart.(Nichols and McDonald 1972)

3 Harmonic content of periodic waveforms

Any repetitive waveform can be decomposed into a series of sinusoidal terms. This important feature often used in waveform contour analysis today, was derived by J.B.J. Fourier (1768-1830) some 200 years ago, hence also the term ‘Fourier decomposition’.

Sinusoidal waves have some interesting properties that allow a compact way of expressing information. A sinusoidal wave with amplitude M (often also termed ‘modulus’ M , but to avoid confusion with e.g. ‘E-modulus’ it was replaced by the term ‘amplitude’ throughout this thesis), phase ϕ , and frequency f (i.e. periodic cycles of the wave per seconds, expressed in Hz), can always be decomposed in the sum of a cosine and a sine wave, having the same angular frequency ω ($\omega = 2\pi f$), but no phase angle:

$$M \cos(\omega t - \phi) = A \cos \omega t + B \sin \omega t \quad \text{Eqn. 1.18}$$

$$\tan \phi = \frac{B}{A} \quad \text{Eqn. 1.19}$$

$$M \cos \phi = A \quad \text{Eqn. 1.20}$$

$$M \sin \phi = B \quad \text{Eqn. 1.21}$$

$$M^2 = A^2 + B^2 \quad \text{Eqn. 1.22}$$

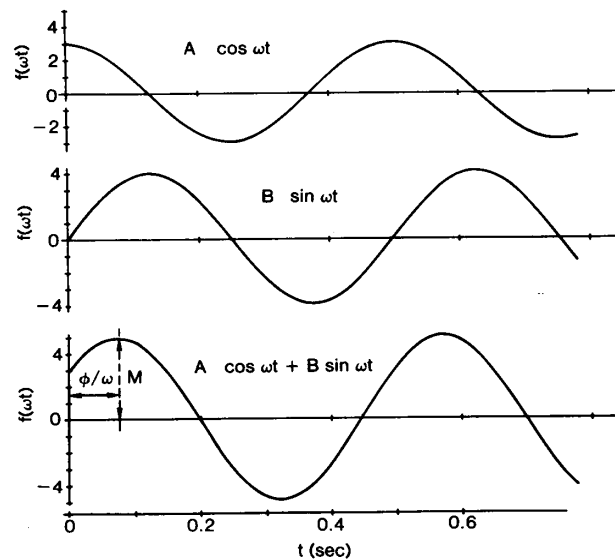


Figure 1–11 A sinusoidal wave with amplitude M , phase ϕ , and frequency f decomposed in a cosine and a sine wave, having the same angular frequency ω , but no phase angle.(Milnor 1989)

Further, sinusoidal waves can be expressed as the real part of a complex number:

$$M \cos(\omega t - \phi) = \text{Re}\{M e^{j(\omega t - \phi)}\} \quad \text{Eqn. 1.23}$$

since:

$$e^{jx} = \cos x + j \sin x \quad \text{Eqn. 1.24}$$

Fourier's theorem states that any periodic function $f(t)$ can be decomposed into an infinite sum of cosine and sine waves, by means of the following formulae (Franklin 1949):

$$f(t) = \frac{A_0}{2} + \sum_{k=1}^{\infty} (A_k \cos k\omega t + B_k \sin k\omega t) \quad \text{Eqn. 1.25}$$

$$A_k = \frac{2}{T} \int_{-T/2}^{T/2} f(t) \cos k\omega t \cdot dt \quad \text{Eqn. 1.26}$$

$$B_k = \frac{2}{T} \int_{-T/2}^{T/2} f(t) \sin k\omega t \cdot dt \quad \text{Eqn. 1.27}$$

for $k = 0, 1, 2, \dots, \infty$, and $A_0/2$ being the mean value of $f(t)$.

Or, one can prefer the more compact exponential notation, derived from Eqn. 1.24 and Eqn. 1.25:

$$f(t) = \frac{A_0}{2} + \frac{1}{2} \sum_{K=1}^{\infty} (A_K - jB_K) e^{jK\omega t} + \frac{1}{2} \sum_{K=1}^{\infty} (A_K + jB_K) e^{-jK\omega t} \quad \text{Eqn. 1.28}$$

what can be simplified to:

$$f(t) = \sum_{K=-\infty}^{\infty} F(K) e^{jK\omega t} \quad \text{Eqn. 1.29}$$

with $F(K)$ being:

$$F(K) = \frac{(A_K - jB_K)}{2} \quad \text{Eqn. 1.30}$$

for $K = 0, \pm 1, \pm 2, \dots, \pm\infty$

Inversely, $F(K)$ can be derived from Eqn. 1.26, Eqn. 1.27 and Eqn. 1.30:

$$F(K) = \frac{1}{T} \int_{-T/2}^{T/2} f(t) e^{-jK\omega t} \cdot dt \quad \text{Eqn. 1.31}$$

Eqn. 1.31 allows for a time function $f(t)$ to be transformed into the ‘frequency-domain’, while Eqn. 1.29 is the inverse transformation of $F(K)$ into a ‘time-domain’ visualization.

Of course, this is a rather theoretical derivation. In practice, one can approximate $f(t)$ by a *finite* sum of sine and cosine waves, and moreover, the equations can be simplified, though some extra conditions have to be taken care of. Below, the methodology for calculating a practical example is described (Milnor 1989):

Consider one pulsation selected from an acquisition. The period is T , the number of registered samples y_s for this pulsation is N , and the time interval between each sample is Δt , so that the real time becomes $t_s = s\Delta t$ with index $s = 0, 1, \dots, N-1$. The Fourier coefficients can then be calculated from:

$$A_K = \frac{2}{N} \sum_{s=0}^N y_s \cos K\omega t_s \quad \text{Eqn. 1.32}$$

$$B_K = \frac{2}{N} \sum_{s=0}^N y_s \sin K\omega t_s \quad \text{Eqn. 1.33}$$

for $K = 0, 1, 2, \dots, N/2$.

The decomposition for every y_s becomes:

$$y_s = \frac{A_0}{2} + \left\{ \sum_{K=1}^{N/2} A_K \cos K\omega t_s + \sum_{K=1}^{N/2} B_K \sin K\omega t_s \right\} \quad \text{Eqn. 1.34}$$

from which the properties of every harmonic can be calculated by using:

$$M = (A^2 + B^2)^{1/2} \quad \text{Eqn. 1.35}$$

$$\phi = \arctan \frac{B}{A} \quad \text{Eqn. 1.36}$$

For Eqn. 1.36, the phase angle must be placed in the correct quadrant, in accordance with the signs of A and B (e.g. $A < 0$, then $\phi > \pm 90^\circ$). The above equations can be computed with software (usually with an optimized algorithm called the ‘Fast Fourier Transform’ (FFT)) and can then be represented in a discrete line spectrum as illustrated in Figure 1–12.

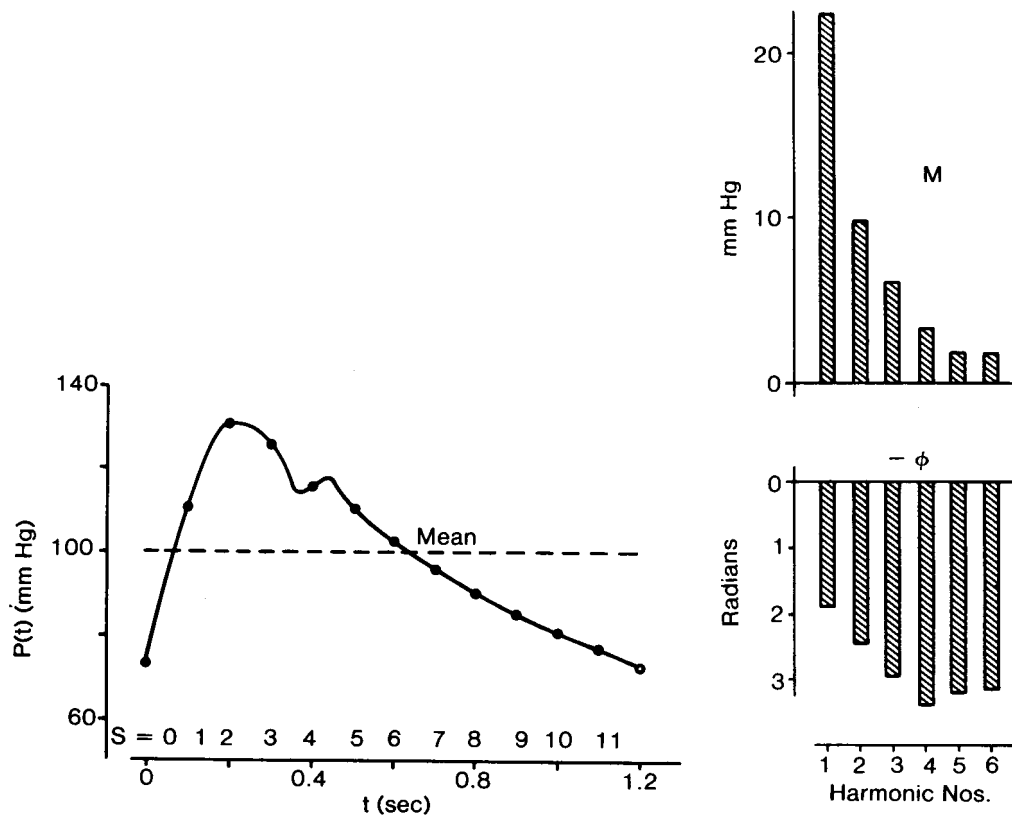


Figure 1–12 Left: Arterial pressure pulsation with $T=1.2$ s, sampled by $N=12$ values. Right: Amplitudes M and phase angles ϕ for the first six harmonics.(Milnor 1989)

When working with a set of N discrete sample values per period T , the total number of harmonics is limited to $N/2$. Otherwise, so-called ‘aliasing’ artefacts will occur. This is caused by the fact that one needs at least two points on a sinusoidal wave with a specific frequency in order to determine it completely. The frequency of the highest determinable harmonic is defined as the ‘folding’ (or ‘Nyquist’) frequency:

$$f_{Nyq} = \frac{1}{2\Delta t} \quad \text{Eqn. 1.37}$$

The fundamental frequency is $1/T$, or:

$$f_{fund} = \frac{1}{N\Delta t} \quad \text{Eqn. 1.38}$$

This implies that the sampling interval time Δt should be chosen with respect to the desired frequency output. Physiological pressure and flow waves in humans and large mammals have their largest components below 10 Hz, and above 30 Hz the remaining frequency content is almost nil (Figure 1–13).(Nichols and O'Rourke 1990)

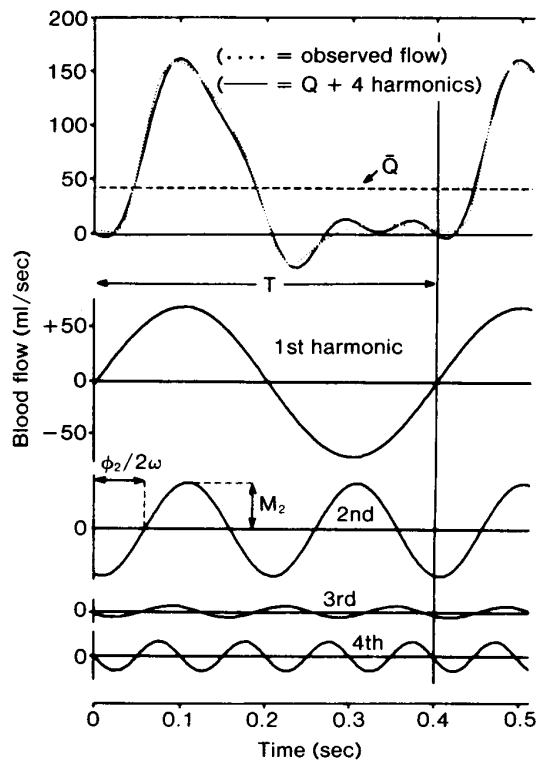


Figure 1–13 Reconstruction (dotted line) of a flow pulsation (full line) with the mean and only 4 harmonics.(Milnor 1972)

4 Pressure - flow relations

4.1 Steady flow

A ‘steady’ or ‘stationary’ flow condition is the situation where the flow rate is constant and no acceleration or deceleration occurs. The state when a fluidum moves in adjacent layers (as already used to derive the equations of fluid viscosity) is referred to as ‘laminar’ or ‘streamline’ flow. When the flow rate is increased more and more, a point is reached where the flow particles no longer move in a regular way along a streamline but sway randomly across the tube’s cross section. This is called ‘turbulent’ flow. The transition from laminar to turbulent can be quantified by the dimensionless Reynolds number, which is defined as:

$$\text{Re} = \frac{\rho V D}{\mu} \quad \text{Eqn. 1.39}$$

with dynamic fluid viscosity μ (Pa.s), density ρ (kg/m³), a ‘characteristic’ length D (m), usually a tubediameter, and a ‘characteristic’ fluid velocity V (m/s), being the average cross-sectional velocity for steady flow.

For a cylindrical tube model, Hagen (1839) and Poiseuille (1846) independently showed that under steady laminar conditions, flow should be proportional to the fourth power of the tube radius, to the pressure drop over the tube and inversely proportional to the length.(Poiseuille 1840) These were all experimental derivations, and the actual value of the proportional factor, being $\pi/8\mu$, was only determined yet another 20 years later by Wiedemann (1856) and Hagenbach (1860). Consider a thin-walled cylindrical tube with radius R and pressure drop P_1 - P_2 over the length L . The velocity v at a point on a cylindrical fluid shell with radius r is given by:

$$v = \frac{(P_1 - P_2)}{4\mu L} (R^2 - r^2) \quad \text{Eqn. 1.40}$$

so that volume flow Q can be calculated from:

$$Q = \int_0^R 2\pi r v_r \cdot dr \quad \text{Eqn. 1.41}$$

thus becoming:

$$Q = \frac{\pi R^4 (P_1 - P_2)}{8\mu L} \quad \text{Eqn. 1.42}$$

The velocity profile has a parabolic shape, with an average velocity being half of the axial velocity (Figure 1–14).

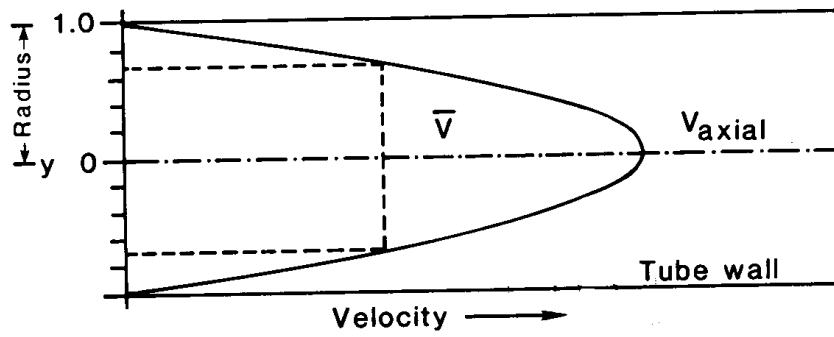


Figure 1–14 Parabolic profile of a laminar Poiseuille flow in a cylindrical tube, with average velocity being half of the axial velocity.

The theoretical derivation of the formula implied some assumptions, and it is relevant to see whether these conditions are met in blood vessels. First of all, the fluid is supposed to be homogeneous with a viscosity independent of shear rate. The liquid does not slip at the wall. The tube is rigid and long compared to the inlet. The flow should be laminar and there is a steady flow rate. (Milnor 1989)

It was already discussed that a constant viscosity can be assumed for blood with normal haematocrit values in arteries with an internal radius bigger than 0.5 mm. The fact that the liquid does not slip at the wall has been found to be universally true. (Fung 1981) The mentioned geometric and elastic conditions for the vessels can only apply for small, thick-walled vessels, but in too small vessels the viscosity condition will be violated. The laminar flow condition is almost certainly present in all vessels where flow is sufficiently steady to apply Poiseuille's equation. (Nichols and O'Rourke 1990) Finally, the steady flow rate is certainly not obtained in the large arteries where flow is clearly pulsatile.

As a conclusion, the Poiseuille flow model can be used as a good approximation in relatively small arteries under certain conditions. In large arteries, it is of an educational value due to its simplicity and can be used to provide insights in mean values, but it should not be applied when the pulsatile character of flow is also to be accounted for.

4.2 Pulsatile flow

Quite a lot of models for pulsatile flow have been derived and reviews on these matters are available by Noordergraaf et al. and Cox et al. (Cox 1969; Noordergraaf 1969). Nevertheless, many subsequent researchers have followed John Womersley's work on pulsatile flow. Although he was not the first at it, he linearized the general Navier-Stokes equations, by showing that the non-linear terms were negligible in the application to blood flow. After a first rigid cylindrical model, he introduced the alterations necessary in the case of an elastic and viscoelastic vessel wall. The equations were later revised and one of the first and most important changes was the adaptation for thick-walled tube models. (Cox 1968)

Extensive derivations of formulae are not relevant here and can be found in literature. (Womersley 1955b; Womersley 1955c; Womersley 1955a; Womersley 1957a; Womersley 1957b) However, a brief overview is suitable. The general form of the equation for the motion of a viscous, incompressible liquid in a cylindrical tube with radius R can be described as:

$$\frac{\partial^2 v}{\partial r^2} + \frac{1}{r} \frac{\partial v}{\partial r} - \frac{1}{v} \frac{\partial v}{\partial t} = - \frac{1}{\mu} \frac{\partial p}{\partial z} \quad \text{Eqn. 1.43}$$

with kinematic viscosity $\nu = \mu/\rho$ (m^2/s). Pressure drop over a distance L , is defined as a sinusoidal motion:

$$\frac{p_1 - p_2}{L} = \frac{\partial p}{\partial z} = A^* e^{j\omega t} \quad \text{Eqn. 1.44}$$

The solution for longitudinal velocity component v of the lamina at a position $y = r/R$ from the axis becomes:

$$v = \frac{A^*}{j\omega\rho} \left(1 - \frac{J_0(\alpha j^{3/2})}{J_0(\alpha j^{3/2})} \right) e^{j\omega t} \quad \text{Eqn. 1.45}$$

with Womersley parameter α defined as:

$$\alpha^2 = \frac{R^2 \omega \rho}{\mu} = \frac{R^2 \omega}{\nu} \quad \text{Eqn. 1.46}$$

and J_0 and J_1 Bessel functions of order zero and one. (Pipes 1958; Dwight 1961)

Integration of the velocity v over the cross-sectional area gives an expression for flow q :

$$q = \frac{\pi R^2 A^*}{j\omega\rho} \left(1 - \frac{2J_1(\alpha j^{3/2})}{\alpha j^{3/2} J_0(\alpha j^{3/2})} \right) e^{j\omega t} \quad \text{Eqn. 1.47}$$

With $M \cos(\omega t - \phi)$ being the real part of the pressure gradient and the bracketed part of Eqn. 1.47 renamed as $[1 - F_{10}]$, the equation for q can be written as:

$$q = \frac{\pi R^2}{\omega\rho} M [1 - F_{10}] \sin(\omega t - \phi) \quad \text{Eqn. 1.48}$$

or with:

$$[1 - F_{10}] = M'_{10} e^{j\varepsilon'_{10}} \quad \text{Eqn. 1.49}$$

and substituting Eqn. 1.46:

$$q = \frac{\pi R^4 M}{\mu} \frac{M'_{10}}{\alpha^2} \sin(\omega t - \phi + \varepsilon'_{10}) \quad \text{Eqn. 1.50}$$

In the latter equation $M'_{10}/\alpha^2 \rightarrow 1/8$ as $\alpha \rightarrow 0$ and $\epsilon'_{10} \rightarrow 90^\circ$ (Figure 1–15), so that $M \sin(\omega t - \phi + 90^\circ)$ becomes $M \cos(\omega t - \phi)$, which equals $\partial p / \partial z$, thus finding the equation of Poiseuille (Eqn. 1.42).

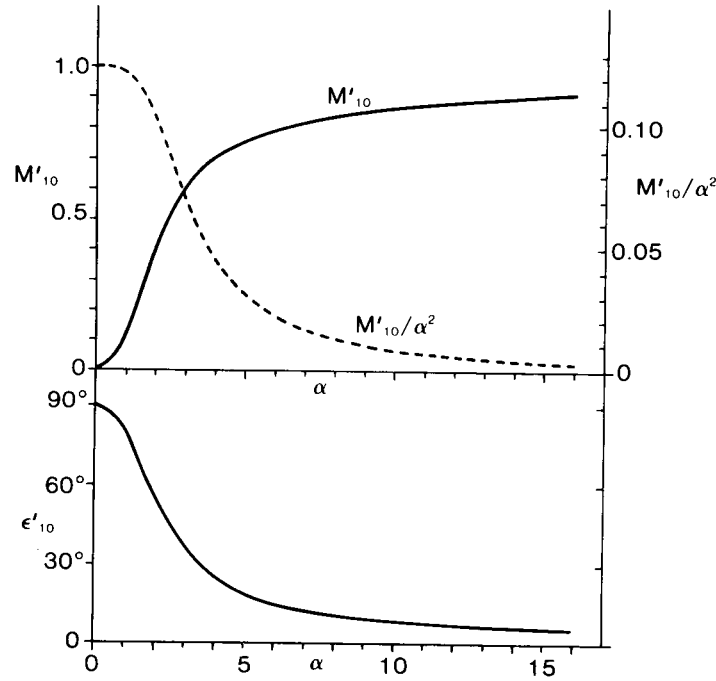


Figure 1–15 The parameters M'_{10} , M'_{10}/α^2 and ϵ'_{10} in function of α . For lower α , the parameters reach values that suit Poiseuille flow. (Womersley 1955c)

Analogue assumptions as in the case of steady flow have been made with respect to viscosity, tube length etc., and the errors introduced by them are found negligible. Looking specifically at the condition of laminar flow, the streamline flow is interrupted the more proximal to the heart and at least during systole, but these disturbances are very short in time and are not likely to have a large impact on the predicted flow. Further, the Womersley equations have been tested experimentally for different values of α . In general, the agreement between the measured and theoretical flow was very close. (Linford and Ryan 1965) The Womersley equation for pulsatile flow and the Poiseuille equation for steady flow can not be applied to arteries from a strict mathematical point of view, but they both provide a very close approximation to what is measured in vivo and it is most certainly acceptable for further practical use and derivations.

5 Resistance and impedance

5.1 Steady flow

A lot of the terminology for vascular haemodynamic parameters has been taken from electric circuit theory. Looking at steady flow, a vascular ‘resistance’ R_s can be defined as:

$$P_1 - P_2 = R_s Q \quad \text{Eqn. 1.51}$$

This is clearly an analogy of Ohm’s law ($V = RI$) with pressure drop $P_1 - P_2$ as voltage difference V and volume flow Q as (direct) current I . From Poiseuille’s law (Eqn. 1.42), it can be seen that resistance R_s can be written as:

$$R_s = \frac{8\mu L}{\pi R^4} \quad \text{Eqn. 1.52}$$

In case of pulsatile flow conditions this method can still be found applicable to the mean terms as mentioned before.

The vessel radius largely determines the vascular resistance, since length and viscosity can be assumed constant. Looking at the complete vascular network, the ‘total vascular resistance’ (TVR) can be seen as the resistance of large arteries, small arteries (‘arterioles’), capillaries, and veins. The resistance of the arterioles will be the most significant one, considering that the parameter is proportional to the pressure drop, hence also the term ‘peripheral’ resistance. As the pressure in the veins can be assumed to be almost zero, TVR can also be written as:

$$TVR = \frac{MAP}{CO} \quad \text{Eqn. 1.53}$$

5.2 Pulsatile flow

Considering pulsatile flow, the electrical terminology used for alternating current can be used. The vascular ‘impedance’ describes the relation between sinusoidal components of pressure and flow. Thus, to use the theory of impedances it is always necessary to decompose a natural (pressure and/or flow) pulsation into its harmonic content. Impedance values are complex numbers and are represented for every harmonic frequency with an amplitude and phase (Figure 1–16). Impedances are both defined in terms of volume blood flow as in terms of (average) blood velocity. In essence this is just a matter of approach, as the velocity impedances only differ from volume flow impedances by the term πR^2 . The following definitions apply (McDonald 1955; Womersley 1955a; Milnor 1989; Nichols and O'Rourke 1990):

‘Longitudinal’ impedance:

$$Z_L = \frac{-\frac{dp}{dz}}{q} \quad \text{Eqn. 1.54}$$

The longitudinal impedance is the ratio of the pressure *gradient* to flow, thus being the pulsatile analogon of vascular resistance.

‘Input’ impedance:

$$Z_i = \frac{p}{q} \quad \text{Eqn. 1.55}$$

Input impedance is the ratio of pressure to flow at a specific cross-section and is influenced by everything distal in the arterial tree from that location. The input impedance at the end of a vessel is called the ‘terminal’ impedance Z_T .

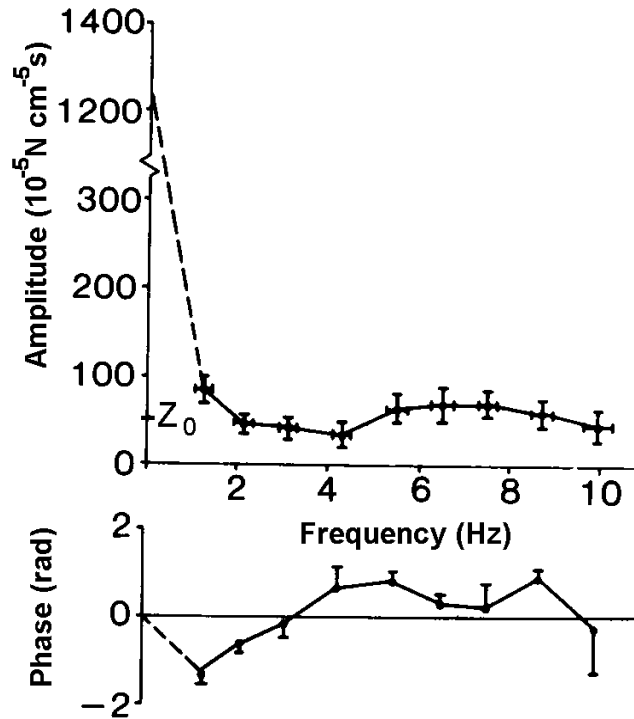


Figure 1–16 Input impedance Z_i in the ascending aorta in man, averaged from five adult subjects, calculated by Fourier series. Estimation for the characteristic impedance Z_0 is indicated (Nichols, Conti et al. 1977)

‘Characteristic’ impedance:

$$Z_0 = \frac{p}{q} = Z_i \quad \text{Eqn. 1.56}$$

For the abstract case of an endless tube with uniform properties along the whole tube, input impedance would become ‘characteristic’ impedance. In practice, this case doesn’t occur (the tube is not terminated by a ‘matching’ impedance, as the vessel properties do change distal from the measuring location) and characteristic impedance cannot be calculated in a direct way in the vascular system. Z_0 can however be derived indirectly e.g. by averaging from the Z_i (high) frequency spectrum (Figure 1–16). In Womersley terminology, the formula for Z_0 becomes:

$$Z_0 = \frac{\rho c_0}{\sqrt{1 - V_p^2}} (1 - F_{10})^{-1/2} \quad \text{Eqn. 1.57}$$

The resulting reflecting waves due to the mismatched impedance, can however be determined by the characteristic impedance as the forward and backward components of pressure and flow waves still behave according to the characteristic impedance.(Westerhof, Sipkema et al. 1972) With the complex reflection coefficient Γ^* defined as:

$$\Gamma^* = \frac{p_b}{p_f} = -\frac{q_b}{q_f} \quad \text{Eqn. 1.58}$$

and propagation constant γ defined as:

$$\gamma = \frac{j\omega}{c_0}(1 - F_{10})^{-1/2} \quad \text{Eqn. 1.59}$$

it can be shown that pressure p and flow q can both be decomposed in a forward (p_f, q_f) and backward (p_b, q_b) travelling wave, as follows:

$$Z_0 = \frac{p_f}{q_f} = -\frac{p_b}{q_b} \quad \text{Eqn. 1.60}$$

$$p = p_f e^{-\gamma z} + p_b e^{\gamma z} \quad \text{Eqn. 1.61}$$

$$q = q_f e^{-\gamma z} + q_b e^{\gamma z} = \frac{p_f}{Z_0} e^{-\gamma z} - \frac{p_b}{Z_0} e^{\gamma z} \quad \text{Eqn. 1.62}$$

A 180° phase shift occurs between the reflection of a pressure and corresponding flow wave. The pressure wave is augmented by a positive reflection, while the flow is decreased with a negative reflection (Figure 1–17).(Westerhof, Sipkema et al. 1972; Mohan and Melvin 1982; Li 1986; Nichols, O'Rourke et al. 1987; Jeremy, Huang et al. 1994)

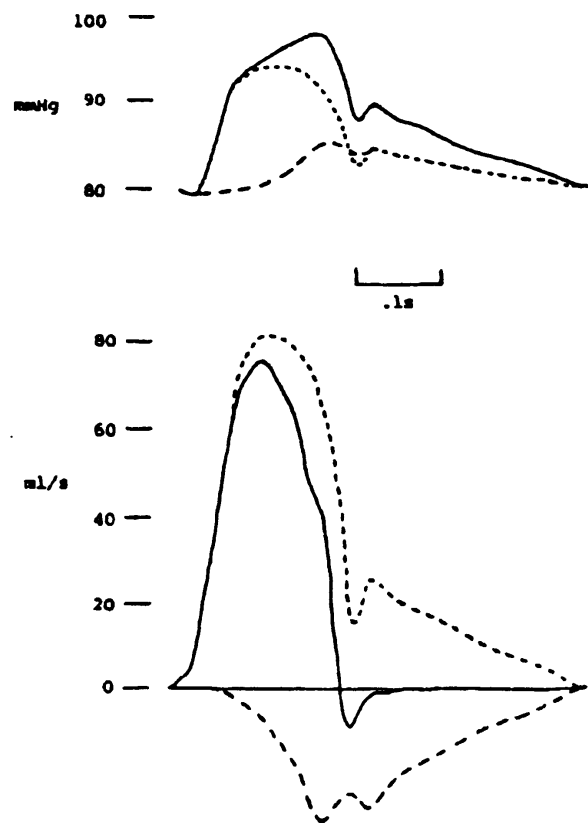


Figure 1-17 Decomposition of pressure (up) and flow (bottom) into a forward (dotted line) and reflected (striped line) component.(Li 1986)

6 Arterial compliance

6.1 Definition

The buffer capacity of the visco-elastic vessels to store a volume of blood was referred to already as the ‘arterial compliance’ effect (Figure 1–18, left). This passive response of a blood vessel (there is also an active smooth muscle response due to hormonal or neural stimulation) on a pressure variation can be mathematically defined as:

$$C = \frac{\Delta V_l}{\Delta P} \quad \text{Eqn. 1.63}$$

with ΔV_l being the corresponding volume variation to a pressure variation ΔP .

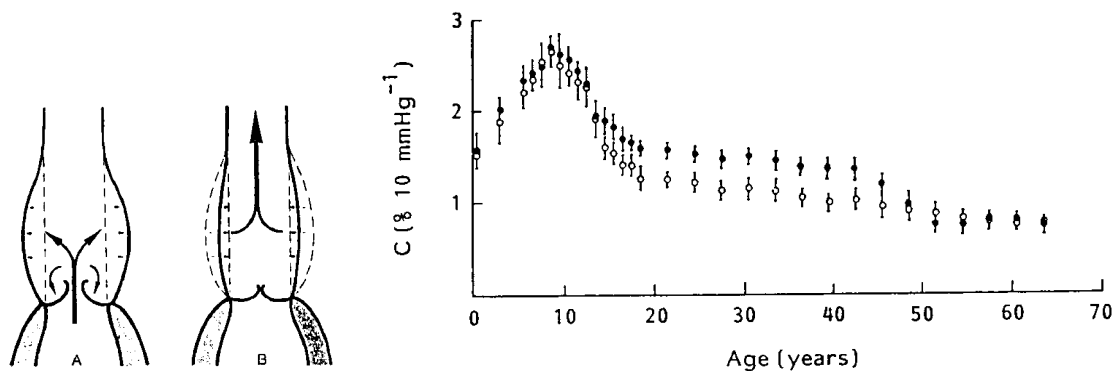


Figure 1–18 Left: Compliance effect of aorta.(Verdonck 1993) Right: Compliance variation in the aorta with age and gender (open circles: male; closed circles: female. In fact, in this picture C is represented by the compliance coefficient CC expressed per 10 mmHg of PP).(Lehmann, Gosling et al. 1992)

Loss of arterial compliance is noted by an increase in PP, mostly due to an increase in SBP, but also because of a decrease of DBP (Randall, Van Den Bos et al. 1984), which results in a decreased coronary perfusion pressure.(Kass, Saeki et al. 1996) Pulse wave velocity c_0 will increase, resulting in faster travelling backward waves that increase SBP as well.(Segers 1997) Finally the cardiac load will increase, which can lead to left ventricle hypertrophy.(Rajkumar, Cameron et al. 1997) Arterial compliance is clinically correlated with age and gender, as shown on Figure 1–18. Compliance gradually diminishes to reach a more constant value only at higher age. Compliance in females is consistently higher than in

males.(Lehmann, Gosling et al. 1992) Further, compliance is subject to pathological changes such as atherosclerosis (plaque deposits and thickening of the intimal layers will diminish compliance), diabetes mellitus (disturbed sugar-metabolism induces abnormal high consumption of lipids and proteins which affects vascular compliance) and hypertension (high working pressures cause vascular remodelling and increased wall thickness results in lower compliance).(Segers 1997) Finally compliance changes are also induced by lifestyle factors as was e.g. shown by Avolio et al. (Avolio, Fa-Quan et al. 1985; Avolio 1995), e.g. by looking at a comparison between urban and rural communities in China. In most cases unfortunately the above mentioned impact factors do not occur in an isolated way (e.g. aging, remodelling, pathological changes are often coupled) and it is not easy to attribute compliance changes to one unique factor. Nevertheless, arterial compliance stays an important haemodynamic parameter for cardiovascular diagnosis and as with resistance/impedance, compliance can be looked upon locally (compliance-coefficient CC) or can be defined for the whole arterial system, referred to as ‘total arterial compliance’ (TAC).

6.2 Local arterial compliance

6.2.1 Definitions

Supposing that a volume variation (diameter D , area A , length L) only occurs in radial direction of the cylindrical vessel (a longitudinal change is impeded by branching and surrounding tissue), a compliance coefficient CC (mm^2/mmHg) can be defined as (Segers 1997):

$$CC = \frac{\frac{\Delta V_l}{L}}{\Delta P} = \frac{\Delta A}{\Delta P} = \frac{\pi \frac{(D + \Delta D)^2}{4} - \pi \frac{D^2}{4}}{\Delta P} \approx \frac{\pi D}{2} \frac{\Delta D}{\Delta P} \quad \text{Eqn. 1.64}$$

when supposing that ΔD is small. CC describes the functional behaviour of the artery and expresses the relation between pressure variation and corresponding diameter variation. For matters of completeness, the distensibility coefficient or relative compliance coefficient DC (mmHg^{-1}) is also mentioned here and can be defined as (Segers 1997):

$$DC = \frac{\frac{\Delta V_l}{V_l}}{\frac{\Delta P}{\Delta P}} = \frac{\frac{\Delta A}{A}}{\frac{\Delta P}{\Delta P}} = \frac{2}{D} \frac{\Delta D}{\Delta P} = CC \frac{4}{\pi D^2} \quad \text{Eqn. 1.65}$$

The CC parameter can be linked with the elasticity modulus E (and thus also with pulse wave velocity by the Moens-Korteweg equation Eqn. 1.15) by the formula of Laplace Eqn. 1.8 ($\sigma = \Delta P D / 2h$) :

$$E = \frac{\sigma}{\varepsilon} = \frac{\Delta P}{\Delta D} \frac{D^2}{2h} = \frac{\pi D^3}{4hCC} \quad \text{Eqn. 1.66}$$

Formulae for thick-walled tubes are available (D_i representing inner diameter) (Segers 1997) :

$$E = \frac{3}{8} \frac{D_i (D_i + 2h)^2}{h(D_i + h)} \frac{\Delta P}{\Delta D} \quad \text{Eqn. 1.67}$$

6.2.2 Pressure dependency

Determination of local CC requires knowledge of pressure variation ΔP in an arterial segment and the movement of vessel wall ΔD . Pressure can be determined by arterial tonometry and wall movement by ultrasound technology (see Part III). Derivation of carotid diameter variation is illustrated in Figure 1–19.

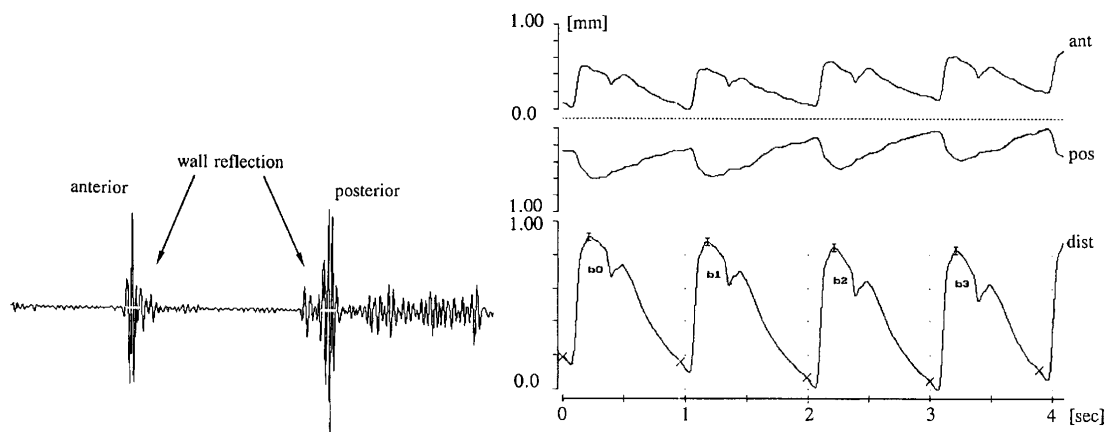


Figure 1–19 Left: Echoes coming from the carotid artery wall. First reflection is from the most superficial wallside (anterior), second reflection shows the more distal wallside (posterior). (Reneman, Hoeks et al. 1996) Right: Variation over time of anterior and posterior wall (up), which allows to calculate diameter variation (bottom). Initial diameter was 5.78 mm. (Reneman, Hoeks et al. 1996)

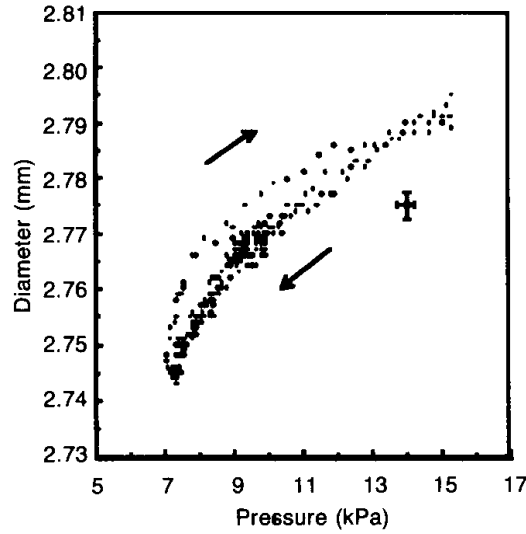


Figure 1–20 Variaton of the diameter (mm) with pressure (1 kPa \approx 7.5 mmHg) of the radial artery. Note the hysteresis. (Tardy, Meister et al. 1991)

When combining the wall displacement with pressure registration, pressure-diameter curves as illustrated in Figure 1–20 can be derived. These measurements allow to fit theoretical pressure-diameter or pressure-area relations, such as the following model of Langewouters which was one of the most elaborate studies of the mechanical behaviour of arterial vessel walls. (Langewouters, Wesseling et al. 1984; Langewouters, Wesseling et al. 1985) He investigated in vitro the pressure-area relation of segments from 45 thoracic (segmentlength 10 cm) and 20 human abdominal aortae (segmentlength 6 cm). From these measurements he derived the so-called ‘arc-tangent’ model of Langewouters (Figure 1–21), in which a relation between cross-sectional area and pressure was defined as:

$$A(P) = A_m \left\{ \frac{1}{2} + \frac{1}{\pi} \arctan \left(\frac{P - P_0}{P_1} \right) \right\} \quad \text{Eqn. 1.68}$$

in which A_m , P_0 and P_1 are three independent parameters to be derived for each segment. The CC for this segment is then given by:

$$CC = \frac{\Delta A}{\Delta P} = \frac{\frac{A_m}{\pi P_1}}{1 + \left(\frac{P - P_0}{P_1} \right)^2} \quad \text{Eqn. 1.69}$$

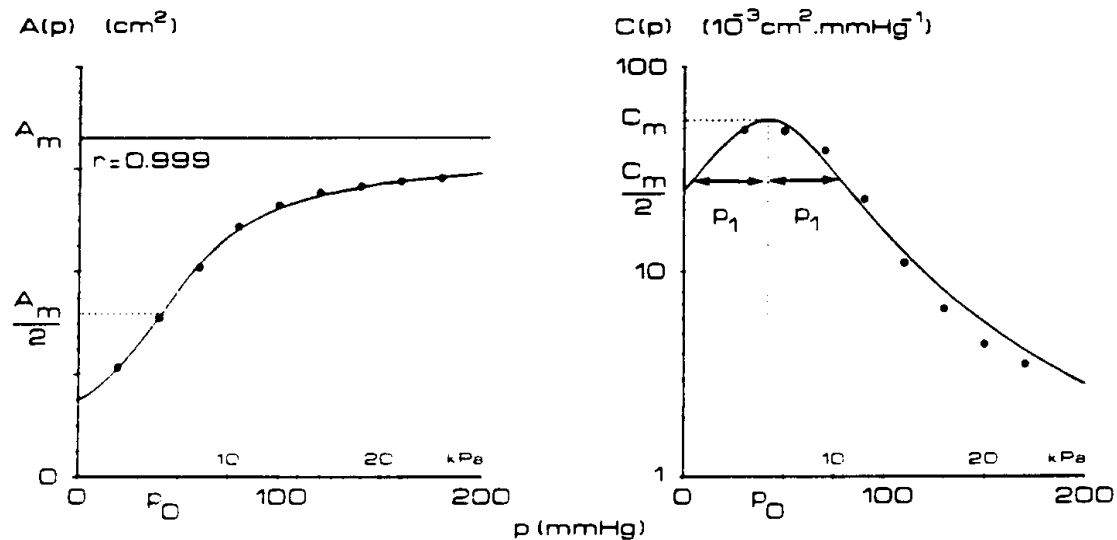


Figure 1–21 Left: Area $A(P)$ in function of pressure. Right: $CC(P)$ for pressure from 0 to 200 mmHg.(Langewouters, Wesseling et al. 1984)

Figure 1–21 reveals the physical meaning of the model parameters. A_m is the maximal area of the aorta at high pressures. P_0 is the pressure corresponding with the inflection point of curve $A(P)$, while P_1 represents a measure for the steepness of the curve, and thus compliance. For pressure P_0 is compliance-coefficient CC maximal; for a pressure $P_0 \pm P_1$ compliance becomes half of its maximal value.

The artery wall clearly shows a non-linear pressure dependent behaviour.(Langewouters, Wesseling et al. 1984, Hayashi, 1993 #746) At low pressures, stress is absorbed by the elastin. At increasing strain, also the collagen becomes active which induces a rapid increase in wall stiffness. When comparing elastic properties of different vessels, it is thus important to do comparisons at the same pressure level. Pathophysiological changes of local compliance (expressed as CC or DC) occur in a non-homogenous manner, and the conduit of muscular arteries (e.g. radial artery) is different from elastic arteries (e.g. carotid artery). Reneman et al. (Reneman, Hoeks et al. 1996) suggest that treatment of hypertension should not be focused on lowering blood pressure but on an amelioration of the vessel compliance.

6.3 Total arterial compliance

Deriving TAC properties in vivo or in vitro is difficult, as it requires isolating the vessel(s) and performing experiments with increasing static pressure load to derive pressure-volume relations.

When SV and PP are known, a rough estimation for maximal arterial compliance can already be made by using:

$$C_{\max} = \frac{SV}{PP} \quad \text{Eqn. 1.70}$$

In the previous sections electrical theory has been used to describe quantities of resistance and impedance. Besides mere terminology, an electric circuit analogon can be used as a real mathematical model for the arterial tree. Each arterial property that is regarded is then represented by one electric component. This is called discrete or ‘lumped’ parameter modelling, and the models are named ‘Windkessel’ models, referring to theory of Hales (1733) who already then discretized (or lumped) the arterial properties. Arterial models will be further addressed in the next section, but to estimate the compliance property the most simple 2-element Windkessel model (2WK) will already be used here. In this case, a distinct physiological function can still be attributed to the components: in the 2WK, resistance is simply represented by the resistor and compliance by the capacitance.

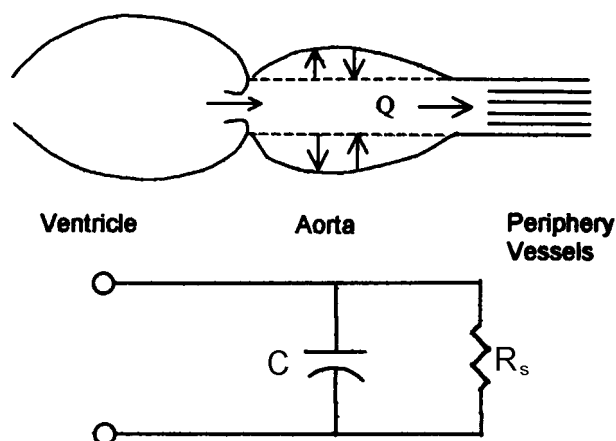


Figure 1–22 Top: Schematic 2WK with compliance properties modelled in 1 chamber (aorta), and resistance in the peripheral vessels. Bottom: Electrical analogon for the 2WK.(Li 2000)

6.3.1 Time decay method (TDM)

Consider the simplified model as shown in Figure 1–22. Due to the law on conservation of mass, the inflow q_i into the elastic chamber is the sum of the outflow q_o to the peripheral vessels and the stored amount of blood q_c :

$$q_i = q_c + q_o \quad \text{Eqn. 1.71}$$

From Eqn. 1.63 it can be seen that q_c is related to the rate of pressure change by:

$$q_c = \frac{dv_l}{dt} = C \frac{dp}{dt} \quad \text{Eqn. 1.72}$$

From Eqn. 1.51 one can describe q_o by means of the arterial to venous pressure drop $p - p_v$ and the vascular resistance R_s :

$$q_o = \frac{p - p_v}{R_s} \quad \text{Eqn. 1.73}$$

Assuming the venous pressure p_v to be zero, and substituting Eqn. 1.72 and Eqn. 1.73 into Eqn. 1.71, an expression for pressure p and flow $q_i = q$ with parameters C and R_s is obtained:

$$q = C \frac{dp}{dt} + \frac{p}{R_s} \quad \text{Eqn. 1.74}$$

Considering only the diastolic part of the heart cycle, then $q = 0$, which gives:

$$\frac{dp}{p} = - \frac{dt}{R_s C} \quad \text{Eqn. 1.75}$$

so that integration of both sides leads to an expression for the variation of pressure during diastole over time:

$$p = P_{es} e^{-\frac{(t-t_d)}{\tau}} \quad \text{Eqn. 1.76}$$

with $\tau = R_s C$ and P_{es} being the end-systolic pressure occurring at time t_d , the onset of diastole. When estimating R_s from MAP and CO (Eqn. 1.53), C can then be obtained by fitting an exponential function to Eqn. 1.76.(Li 2000)

To apply the TDM, knowledge about the CO and MAP is necessary. Further, the assumed condition that q equals zero is strictly speaking only valid for the aortic root, since q not necessarily becomes zero at other locations during diastole. Finally, since the discrete modelling is only valid when looking at waves with low-frequency components, the time t_d should not be taken at the dicrotic notch (sharp inflection, thus high-frequencies). A possibility is to do the fitting on the last 2/3 of diastole.(Simon, Safar et al. 1979)

6.3.2 Area method (AM)

When integrating Eqn. 1.74 over a time period $t_2 - t_1$ during diastole, one obtains:

$$\int_{t_1}^{t_2} \frac{dp}{dt} dt + \frac{1}{R_s C} \int_{t_1}^{t_2} p dt = 0 \quad \text{Eqn. 1.77}$$

so that:

$$\tau = R_s C = - \frac{\int_{t_1}^{t_2} p dt}{P_{t_2} - P_{t_1}} \quad \text{Eqn. 1.78}$$

The integral in Eqn. 1.78 is the area underneath the pressure curve in time period $t_2 - t_1$, hence the name ‘area method’ (AM).

Again knowledge about the CO and MAP is necessary, but this time there is no need to exponential curve fitting and the method is applicable even when diastolic pressure is not following an exponential decay.(Liu, Brin et al. 1986) Further, the time period $t_2 - t_1$ is not fixed but this can also be seen as a disadvantage since the choice of the time interval influences the results. The suggested method by Liu et al. is using the time interval $t_d - t_s$ (dicrotic notch-end of diastole).

The double area method uses a time interval that can span the whole heart cycle (thus also assuming that R_s and C are constant in that timeframe):

$$\int_{t_1}^{t_2} q dt = C(P_{t_2} - P_{t_1}) + \frac{1}{R_s} \int_{t_1}^{t_2} p dt \quad \text{Eqn. 1.79}$$

Since the method is being applied in both systole and diastole, two equations can be derived, which allows to consider R_s as a second unknown variable (besides C), thus not requiring information on CO and MAP.(Segers 1997)

6.3.3 Pulse pressure method (PPM)

The pulse pressure method (PPM) is an iterative procedure based on the 2WK and the measurement of an aortic pressure and flow to determine compliance of the arterial tree (Figure 1–23). From pressure and flow, one determines vascular resistance R_s , while an initial value for C is chosen.(Stergiopoulos, Meister et al. 1994) With these parameters, the equations for the 2WK model are being solved and corresponding pulse pressure (PP) is calculated. Comparison with the measured PP allows adjusting the value for C and doing a second, third, etc. iteration. The PPM method is a stable and simple method, independent of time intervals or pressure curve fitting and applicable in normal and pathological circumstances. However, information on both aortic pressure and flow is required.

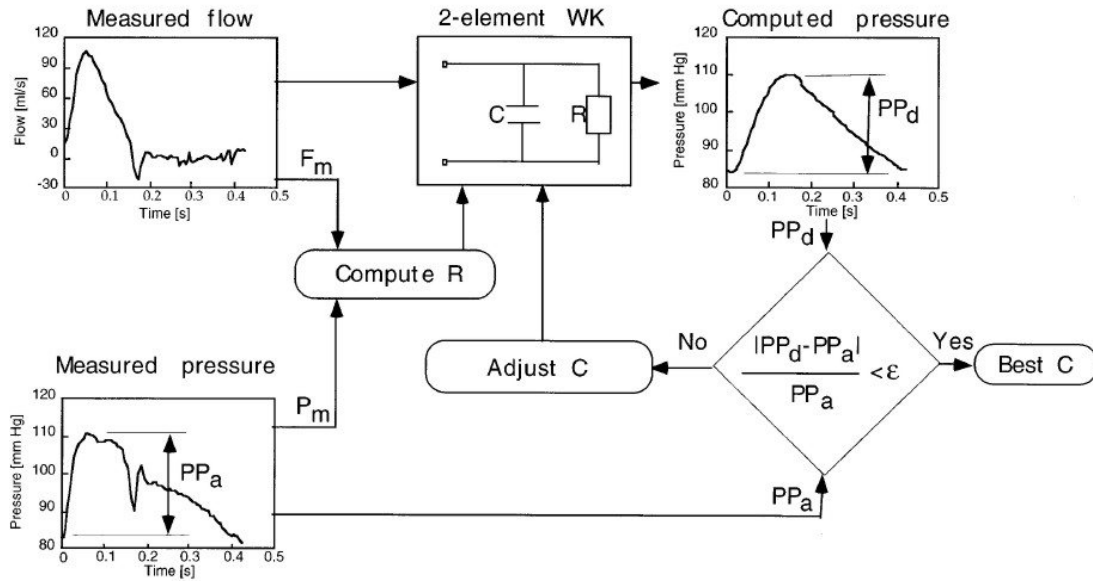


Figure 1–23 Schematic diagram of pulse pressure method (PPM). Mean pressure (P_m) over mean flow yields value of total peripheral resistance (R). PP_a , measured pulse pressure; PP_d , pulse pressure predicted by two-element Windkessel (2WK) model using measured flow as input. 2WK is formed by the known R and an assumed compliance value (C). Iterative scheme searches for value of C that yields the closest agreement between PP_a and PP_d . This is the best estimate of total arterial compliance. (with permission from (Stergiopoulos, Segers et al. 1999))

6.3.4 Higher order WK methods

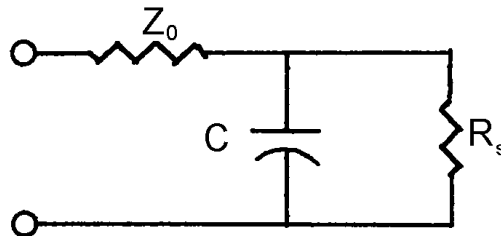


Figure 1–24 3WK model with compliance C , resistance R_s and characteristic impedance Z_0 .

Making use of higher order models, the concept of impedance (pulsatile flow) can be introduced into the electrical analogon. An estimation for the input impedance Z_i can be calculated from a 3WK when the aortic pressure and flow is known, by the following equation (Milnor 1989):

$$Z_i = \frac{(R_s + Z_0) + j\omega R_s Z_0 C}{1 + j\omega R_s C} \quad \text{Eqn. 1.80}$$

The differential equation for the 3WK becomes:

$$\frac{dp}{dt} = \frac{Z_0 + R_s}{R_s C} q + Z_0 \frac{dq}{dt} - \frac{p}{R_s C} \quad \text{Eqn. 1.81}$$

From mean pressure and flow, peripheral resistance can be calculated and it can be considered to quantify this solely as R_s or as $R_s + Z_0$. Stergiopoulos et al. use the latter, and calculate R_s , C and Z_0 by introducing measured flow into the 3-element WK and minimizing the difference between measured and theoretical pressure. (Stergiopoulos, Meister et al. 1995) Another approach would be to fit the theoretical and measured input impedance. (Laskey, Parker et al. 1990) Other derivations of the compliance parameter with higher order WK models are available in literature, but are less intuitive and not imperative for this thesis. (Goldwyn and Watt 1967; Deswysen, Charlier et al. 1980)

6.3.5 *Pressure dependency*

Some pressure-dependent methods have been constructed for the TAC parameter. As an illustration, the method of Li et al. (Li, Cui et al. 1990) is explained here, where the constant compliance in the classical 3WK model (Figure 1–24) has been replaced by a pressure-dependent function $C(p) = a \cdot e^{bp}$. Total aortic flow q_a is divided over the branch with resistance R_s (q_R) and the branch with compliance (q_C):

$$q_a = q_R + q_C \quad \text{Eqn. 1.82}$$

Pressure $p(t)$ proximal to R_s and C is given by:

$$p(t) = p_a(t) - Z_0 q_a \quad \text{Eqn. 1.83}$$

Flow through resistance R_s and compliance C is given by:

$$q_R = \frac{p(t)}{R_s} \quad \text{Eqn. 1.84}$$

$$q_c = q_a - \frac{p(t)}{R_s} \quad \text{Eqn. 1.85}$$

Using the definition of compliance C (Eqn. 1.63), flow q_c also equals:

$$q_c = \frac{dV_l}{dt} = C \frac{dp}{dt} \quad \text{Eqn. 1.86}$$

From Eqn. 1.85 and Eqn. 1.86 one obtains:

$$\frac{dp}{dt} = \frac{q_a - \frac{p(t)}{R_s}}{C} \quad \text{Eqn. 1.87}$$

After discretization (iteration index i), the model equations become:

$$p(t_{i+1}) = p(t_i) + \Delta t \frac{q_a(t_i) - \frac{p(t_i)}{R_s}}{C(p(t_i))} \quad \text{Eqn. 1.88}$$

$$p(t_i) = p_a(t_i) - q_a(t_i)Z_0 \quad \text{Eqn. 1.89}$$

Application of the method requires knowledge (measurements) about aortic flow q_a and aortic pressure p_a , from which the TVR R_s and the characteristic impedance Z_0 are determined. Iteration starts with initial values of the parameters a and b for the relation $C(p) = a \cdot e^{bp}$. Aortic flow q_a is administered to the model, aortic pressure p_a is calculated and compared with the measured value. Parameters a and b are optimized through the iteration process by reducing the error between model calculations and measurements of p_a . With this model, compliance is maximal in early systole and minimal at peak-systole, after which compliance increases exponentially up to the maximal value.

7 Arterial modelling

The principles, definitions and theories discussed in the previous sections were not always easy to derive or to validate in vivo. For this reason, numerical models play an important role in gaining insights in vascular biomechanics. It is however important to stay conscious of the fact that models are always based on initial hypotheses and simplifications, and the results are the mere implications of that. Quoting William R. Milnor, who has rightfully been referred to several times in this chapter, one must bear in mind the following: ‘Models are a kind of temporary working assumptions, and their purpose should be to provoke, not take the place of, new experimental observations.’

7.1 Tube model

Obvious hydraulic models for the arterial tree are simple cylindrical tubes (or a network of tubes) to which common fluid dynamic equations are applied, though this time with blood as the test fluidum for which viscosity and other properties have to be accounted for. These models have been used frequently in this chapter.

7.2 Electrical analogon

There is a parallel to be drawn between electric circuit theory and haemodynamic quantities in the cardiovascular system (Table 1–1). Electrical analoga are discrete or lumped parameter models where each haemodynamic property is modelled/lumped by one component in the electrical model. These so-called Windkessel models (WK) have already been used in the previous section for the estimation of arterial compliance. Low order models (order = number of elements) can address physiological meaning to the electric components, but with higher order models the haemodynamic interpretation of each component tends to get lost in the complexity of the model.

When many electric networks are strung together to form a ‘transmission line’ model, the haemodynamic properties can be regarded as spread out over the different segments of the line, and finite propagation time in blood vessels can be simulated.

<i>Electric</i>		<i>Hydraulic</i>	
<i>Quantity</i>	<i>Dimension</i>	<i>Quantity</i>	<i>Dimension</i>
Voltage	V(olt)	Pressure	mmHg
Current	A(mphère)	Flow	ml/s
Resistor	$\Omega = V/A$	Resistance	mmHg/(ml/s)
Capacitance	$F(\text{arad}) = A.s/V$	Compliance	ml/mmHg
Inductance	$H(\text{enry}) = V.s/A$	Inertance	mmHg/(ml/s ²)
Conductance	$1/\Omega = A/V$	Leakage	(ml/s)/mmHg

Table 1–1 Comparison of electric and hydraulic components.

7.3 Arterial network

A combination of both tube models and electrical analogs allows constructing so-called ‘arterial networks’, where an attempt is made to respect both the geometrical as the haemodynamic properties of the circulation. A model is typically divided into several ‘branches’, connected with each other via a number of ‘nodes’. Every branch has its own properties in terms of diameter, wall-thickness, length, E-modulus, etc. At the nodes (especially the end or ‘terminal’ node) appropriate electrical analogs are used to define matching properties in terms of input and terminal impedances. This kind of network model will be explained and used further in Chapter 3 of this part.

7.4 System identification

System identification techniques provide mathematical modelling of dynamic systems based on the measurements of input and output signals. This can be done in several ways. First, the system can schematically be divided into subsystems (deductive approach) of which the properties can be found by using the laws of physics (mass, energy, momentum, etc.). This leads to a set of algebraic equations for every subsystem, which can be merged together to form a so-called ‘White Box’ model for the whole system, in which model parameters have a physical meaning. The method is restricted to simple systems, or to systems on which no measurements can be performed, and is in fact a ‘modelling’ technique in its true sense.

A second (inductive) approach is to measure input and output signals without information on the working of the investigated system and merely analyze these signals to construct a 'Black Box' model for the system at hand. This method depends on experimental conditions (normal working signals, or specific test signals) and is more an 'identification' technique. It can be used for complex systems, but the internal structure of the system is usually lost, as system parameters have no physical meaning. Of course, a combination of both approaches is possible and combining both theoretical insights from modelling with experimental knowledge from identification is often the preferred way to obtain a solid 'Gray Box' system model.

Classifications of models are done in various ways. In this thesis, the terminology of parametric and non-parametric models, and time-domain and frequency-domain models will be used. They can also be described as graphical (e.g. frequency-response plots) and analytical models (differential equations). In brief and oversimplified, parametric models make use of the information at time t , to calculate output values at time $t + 1$. Non-parametric models are divided into 'transient analysis' where a step input or impulse is given (step/impulse response methods) and the corresponding output is registered (time-domain), and 'frequency analysis' where a sinusoidal input is used (sine response) and the corresponding amplitude and phase shift of the sinusoidal output is acquired (frequency-domain). In the following chapter a parametric and non-parametric method will be compared when looking at the transfer function of the aorta-radial path.

7.5 In vitro modelling

Apart from the above numerical modelling approaches, one can of course also turn to the 'in vitro' experiments, where real vessels are isolated and used in an extracorporeal, experimental setting or where vessels are simulated by physical visco-elastic tube models. The latter choice was made in this thesis to look at stenosed coronary vessels, which is explained further in part V. Since in vitro experiments can never simulate the total complexity of the human body and all interacting elements, they remain of course as much an approximation as their numerical counterparts. In the end, an adequate combination of in vivo, in vitro and in numero techniques still leads to the best possible description and understanding of the investigated problem.

8 About the use of a transfer function

In the last decade, arterial transfer function (TFF) models have been introduced and promoted into the field of non-invasive haemodynamics. Indeed it seems a promising thought to solve the persistent lack of non-invasive central aortic pressure measurements with a little touch of mathematics. By using a non-invasive peripheral pressure measurement and a mathematical TFF model, central aortic pressure waveforms can be synthesized. Several theoretical derivations on transfer functions came about in the 1990s, combined with clinical validation studies.(Karamanoglu, Gallagher et al. 1995; Karamanoglu and Fenely 1996; Takazawa, O'Rourke et al. 1996; Chen, Nevo et al. 1997; Cameron, McGrath et al. 1998; Stergiopulos, Westerhof et al. 1998; Fetics, Nevo et al. 1999) A practical implementation of a TFF model even found its way into a commercially available pressure device (Sphygmocor™, AtCor Medical Pty Ltd, West Ryde, NSW, Australia). However, recently several concerns have led to a debate in literature about the use(fulness) of arterial TFF models.(Hope, Meredith et al. 2003; Hope, Tay et al. 2003; Millasseau, Ritter et al. 2003; O'Rourke, Avolio et al. 2003; O'Rourke, Kim et al. 2004)

In the end, there are three issues to be dealt with: the input of the TFF, the TFF itself, and the output. As for the TFF input or the non-invasive peripheral pressure measurement, one of the frequently used techniques is radial tonometry (as also used by the mentioned Sphygmocor™ system). It will be shown in the next part of this thesis that arterial tonometry has a lot of potential but also some strong inherent limitations, especially concerning calibration, which have a substantial impact on accuracy of tonometry readings in certain situations (e.g. during long-term monitoring). Thus the registration of the peripheral pressure has to be carried out with care and precision as it will reflect on the accuracy of an estimated central pressure with a TFF.

Second, the TFF itself. There are different theoretical derivations and some are better than others. As an example, two different methods of TFF modelling (Chen, Nevo et al. 1997; Fetics, Nevo et al. 1999) will be addressed in the next chapter to look at the different qualities and drawbacks. Further, theoretical derivations are still such that they present a generalized transformation for a group of patients and/or conditions.(Takazawa, O'Rourke et al. 1996; Chen, Nevo et al. 1997; Cameron, McGrath et al. 1998) Thus the applicability on individual

patients remains a valid concern. It is true that one of the most frequently used models (Chen, Nevo et al. 1997) has only been validated on a small number of adults in rest. Whether the TFF holds in women, children or different load and pathological conditions deserves further investigation.(Hope, Tay et al. 2002; Hope, Tay et al. 2004)

Up to now, attempts to individualize the TFF modelling still have not been very successful.(Segers, Carlier et al. 2000) Which leads to the third issue: the output. It is established that the peripheral measurement has limitations, and the mathematical TFF is a generalization. But how much do these current drawbacks affect the potential benefits of a TFF model in a clinical setting?

One derived parameter that is clearly under discussion is the previously defined augmentation index (Aix), as a measure of wave reflection. Millasseau et al. recently reported in their study (Millasseau, Patel et al. 2003) that the Aix from the radial pulse without use of a transfer function showed a close linear correlation with the aortic Aix (estimated by using the transfer function), suggesting a limited value of the TFF in the study of wave reflection as the information is readily available at the radial pulse.(Millasseau, Ritter et al. 2003) O'Rourke et al. (O'Rourke, Avolio et al. 2003) commented the study of Millasseau by stating that the introduction of the Sphygmocor™ was not only done to study central haemodynamics but also because they couldn't reliably identify evidence of wave reflection on the falling systolic limb of the radial waveform. O'Rourke et al. also stressed that even though radial waveforms may contain effects of wave reflection, the process of central pressure estimation remains more clinically useful for automated feature extraction and ventricular load determination than the radial pulse analysis alone.

Hope et al. (Hope, Tay et al. 2003) focused more on the general clinical benefit and reliability. In their study, a scaled but untransformed radial artery waveform was evaluated as an alternative to a TFF estimated aortic waveform. They compared not only Aix, but also other parameters such as SBP, DBP, and time intervals to peak or inflection. Their conclusion was that since they didn't find reliable parameter data from the TFF estimation that they couldn't already derive directly from the (scaled) radial waveform, the use of a complex TFF analysis might not offer additional clinical benefit to the simple analysis of radial artery waveforms. However, also the findings in this study and the followed methodology have been countered with valid questions and concerns.(O'Rourke, Kim et al. 2004)

In conclusion, the last word on TFF modelling has definitely not been written. TFF techniques have had both believers and adversaries from the very start, and still today several prominent research groups cannot find a mutual agreement as far as the real clinical value of a TFF approach is concerned. It was decided to focus in this thesis on some methodological aspects of TFF modelling but to stay clear from the recent on-going discussion about additional clinical benefit from a TFF approach. The TFF will be regarded as an appealing technique for non-invasive haemodynamics that still has limitations to overcome but can already be used in clinical practice provided that an appropriate mathematical method is applied and the peripheral measurement is carried out with the necessary accuracy.

Summary

This chapter has given an introduction to the principles of vascular biomechanics, signal analysis and system modelling. After a brief historical overview, blood composition and viscosity aspects have been explained. Further, the arterial wall properties have been addressed, with a specific attention paid to the visco-elastic wall properties and the corresponding derivations for the elastic modulus E .

Pressure and flow waveforms were looked at in the frequency-domain and the principles of decomposing a wave into its harmonic content by means of Fourier analysis was explained. From a fluid dynamic point of view, the interaction between pressure and flow was also investigated and described in terms of steady and pulsatile flow, by means of theories by Poiseuille and Navier-Stokes, adapted by Womersley.

Important haemodynamic properties such as resistance, impedance and compliance have been derived and elaborated on. Finally, the arterial models necessary for this thesis such as the Windkessel models or electrical analogs, arterial networks, system identification and in vitro models were pointed out and their principle working has been clarified. All of them will be used in following chapters in this thesis. A discussion about the additional clinical benefits of a transfer function model was also presented.



2 Transfer Function Estimation Methods for the Aorta-Radial Path

Abstract

Knowledge on the morphology of the central aortic waveform is important for haemodynamic calculations but up to now non-invasive techniques measure pressure only at peripheral locations. Therefore, it is necessary to perform a mathematical transformation ('transfer function', TFF) from the measurement site to the central aortic site. These mathematical derivations have advantages and limitations that are fairly unknown to the clinical or non-specialized end-user, though the outcome (in the form of Bode plots) is nevertheless being used more and more in haemodynamic studies. As more information on the underlying system identification process can contribute to avoid the erroneous application of TFF methods, approaches for the TFF estimation of the aorta-radial path have been described and compared in this study. Analysis of the theoretical background, assumptions and boundary conditions, together with Bode plots derived from an invasive patient dataset, show that the parametrically derived, radial-to-aorta TFF with time-shift approach has substantial benefits over a non-parametric method or a parametric method with inversion approach, because of its time-domain mathematical expression between input and output signal, easier optimization of model characteristics, ability to perform on smaller data sequences and lesser noise amplification.

1 Introduction

In current haemodynamic research, the aorta-radial path has been under a lot of attention. Non-invasive measurement techniques for arterial pressure waveforms are introduced into clinical practice. However, since in most cases the central aortic waveform is the desired output (for further haemodynamic calculations) and non-invasive devices up to now are only applied on peripheral (superficial) arteries, a mathematical transformation from the measurement site to the central aortic site has to be performed. (Pauca, O'Rourke et al. 2001) This mathematical transformation is called the 'transfer function' (TFF) for the arterial pathway under investigation, in this case being the aorta-radial path.

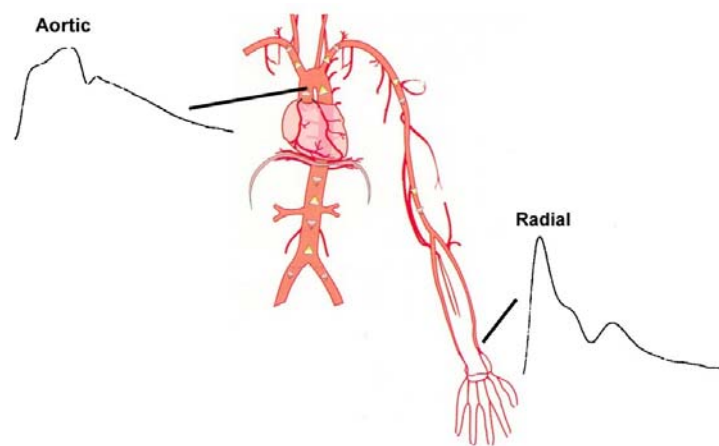


Figure 2–1 The aorta-radial path in the vascular system needs to be described by means of a transfer function (TFF).

Although in some advanced non-invasive pressure measuring devices a TFF model is already implemented (Söderström, Nyberg et al. 2002; Wilkinson, Prasad et al. 2002), a detailed analysis of the output still deserves a lot of attention for two reasons. First of all, the output is obviously influenced by the vessel wall properties of the arterial pathway, thus very dependent on individual characteristics of every examined subject. Second, external parameters such as different loading conditions (e.g. rest or exercise) will also have an impact. Since a TFF is very patient dependent, a generalized TFF has been described and used in literature (Chen, Nevo et al. 1997), and up to now attempts to individualize the transformation have not been very successful. (Segers, Carlier et al. 2000) However, in this study, the methodology of estimating a TFF model was the primary focus, and problems of patient dependency and loading conditions were addressed but not investigated in depth.

A subject's TFF can be derived from an invasive dataset of central aortic pressure and peripheral radial pressure. After that, the TFF can be used to transform all future (non-invasive) peripheral measurements to a central aortic equivalent. Several techniques are available for TFF estimation. These mathematical derivations have advantages and limitations that are fairly unknown to the clinical end-user, though the outcome (in the form of Bode plots) is nevertheless being used more and more in haemodynamic studies. As more information on the underlying system identification process can contribute to avoid the erroneous application of TFF methods, some important approaches for the estimation of the radial-aortic TFF have been described and compared in this study by implementing different parametric identification methods (autoregressive exogenous model, ARX/IV4) and a non-parametric method (spectral analysis, SPA) in a graphical user-friendly interface (GUI).

2 Methods

The investigated identification methods for TFF estimation in this study are described below and implemented in a GUI (TFFInvestigator, ©K Matthys) written in Matlab 6® environment (The Mathworks Inc., Natick, MA). The deeper background of applied models should be found in specialized literature.(Ljung 1987; Stearns and Hush 1990; Burrus, McClellan et al. 1994; Stearns and Ruth 1996; Nelles 2001) In order to compare the outcome of all these methods, Bode plots were constructed by means of an invasive dataset of central aortic and peripheral radial pressure waveforms, together with a non-invasive radial pressure measured via arterial tonometry (see Part III), recorded in an anaesthetized patient (male, 78 years) recovering from a bypass graft intervention (cardiology department, Ghent University Hospital). Written informed consent and institutional approval was obtained. Invasive data was used to derive the TFF, while tonometric data was used with this TFF to estimate an aortic pressure waveform that could then be compared with the invasively measured aortic pressure.

2.1 Parametric identification using the linear ARX/IV4-model

The principle of this approach is to look at the aorta-radial system in the time-domain without any information (Black Box), to assume a model structure for it (in this case the **AutoRegressive EXogenous** model, ARX), and to estimate the parameters defining this model by an algorithm, which is based on minimizing a cost-function $V(e)$. Although the vascular tree is not a linear system, linear modelling can still form a good approximation. The ARX model is the most widely applied linear dynamic model for system identification purposes because of the easy-to-compute model parameters, as they can be estimated by a linear least squares (LS) technique.(Ljung 1987; Nelles 2001)

Suppose that the real process has a structure of the form :

$$y(t) = \frac{B(q^{-1})}{A(q^{-1})}u(t-d) + \frac{1}{A(q^{-1})}n(t) \quad \text{Eqn. 2.1}$$

Hereby is $y(t)$ the output signal, $u(t)$ the input signal and $n(t)$ the noise acting on the system. Further is q^{-1} the shift-operator (the time-domain counterpart of $e^{j\omega}$ in the frequency-domain), t the discrete time index and d the time-shift between input and output.

The structure of this process can be identified/estimated by the ARX model as described by:

$$\hat{A}(q^{-1})y(t) = \hat{B}(q^{-1})u(t-d) + e(t) \quad \text{Eqn. 2.2}$$

with polynomials $\hat{A}(q^{-1})$ and $\hat{B}(q^{-1})$:

$$\hat{A}(q^{-1}) = 1 + \hat{a}_1 q^{-1} + \dots + \hat{a}_{n_a} q^{-n_a} \quad \text{Eqn. 2.3}$$

$$\hat{B}(q^{-1}) = \hat{b}_1 q^{-1} + \dots + \hat{b}_{n_b} q^{-n_b} \quad \text{Eqn. 2.4}$$

Hereby is $e(t)$ the residual error between the real and the estimated output (comprising the effect of parameter estimation errors and noise introduction). Finally, n_a and n_b are the orders of parameter estimation for the ARX model, and \hat{a}_i , \hat{b}_i the parameters to be estimated. In this study, the system structure (determined by n_a , n_b and d) was supposed to be known a priori. The parameter orders were empirically defined as $n_a = n_b = 10$, and the time-shift parameter d was used to fine-tune and stabilize the TFF. Estimated orders have to be high enough to respect system dynamics, but a too high order will increase noise-sensitivity. (Ljung 1987; Stearns and Hush 1990; Burrus, McClellan et al. 1994; Stearns and Ruth 1996) However, there are advanced methods available to identify system structure as well (such as cross-validation techniques or the Akaike Information Criterion). (Ljung 1987; Nelles 2001)

When one writes Eqn. 2.1 as a regressive model, this becomes:

$$y(t) = -a_1 y(t-1) - \dots - a_{n_a} y(t-n_a) + b_1 u(t-d-1) + \dots + b_{n_b} u(t-d-n_b) + n(t) \quad \text{Eqn. 2.5}$$

In order to minimize the residual error $e(t)$, a cost-function $V(e)$ can be defined as:

$$V(e) = \sum e^2(t) \quad \text{Eqn. 2.6}$$

The LS method minimizes the cost-function $V(e)$ in function of the parameters a_i and b_i to be estimated. Consider a column vector of sampling points $X(t) = [-y(t-1) \dots -y(t-n_a) u(t-d-1) \dots u(t-d-n_b)]^T$ and a column vector of estimated parameters $\hat{\theta} = [\hat{a}_1 \dots \hat{a}_{n_a} \hat{b}_1 \dots \hat{b}_{n_b}]^T$ containing all a_i and b_i . The linear regression in Eqn. 2.5 then states that:

$$y(t) = X(t)^T \theta + n(t) \quad \text{Eqn. 2.7}$$

The residual error can be derived from:

$$e(t) = X(t)^T (\theta - \hat{\theta}) + n(t) \quad \text{Eqn. 2.8}$$

In case that $n(t)$ is white noise (random noise with zero mean value), minimizing $V(e)$ allows to determine the optimal parameters for the ARX model as:

$$\hat{\theta} = \left[\sum X(t) X(t)^T \right]^{-1} \sum X(t) y(t) \quad \text{Eqn. 2.9}$$

In case that $n(t)$ is not random (not white but coloured noise), the parameters from the ARX method will be estimated in a ‘biased’ (systematical deviation from the optimal value) and ‘non-consistent’ way (bias does not approach zero when number of samples goes to infinity). Therefore, the method of instrumental variables (IV4) was implemented instead of the original ARX, which avoids correlations between noise and the data samples, thus allowing the LS estimator to find the optimal $\hat{\theta} = \theta$. After minimizing the residual error $e(t)$ while estimating parameters a_i and b_i , Eqn. 2.2 to Eqn. 2.4 allows to find the transfer function TFF_{ARX} of the process as a time-domain formula:

$$TFF_{ARX} = q^{-d} \frac{b_1 q^{-1} + \dots + b_{n_b} q^{-n_b}}{1 + a_1 q^{-1} + \dots + a_{n_a} q^{-n_a}} \quad \text{Eqn. 2.10}$$

In order to compare this technique with the non-parametric method described next, Bode plots were derived for this TFF by replacing the time-domain shift-operator q^{-1} with its frequency-domain counterpart $e^{j\omega}$ and by subsequently deriving the amplitude $|TFF_{ARX}|$ and phase $\angle TFF_{ARX}$ of this complex function in terms of frequency.

2.2 Non-parametric identification using correlation and spectral analysis

Another approach is making use of the harmonic content of pressure waves (frequency-domain) and applying correlation and spectral analysis (SPA). The concept of correlation was originally intended as a means to detect periodic signals immersed in ‘noise’ (e.g. radar transmission), but the idea was introduced by Randall (Randall 1958) and Taylor (Taylor 1966) into circulatory physiology and effectively applied to the (almost) periodic natural pulsations and low noise of the cardiovascular system. The idea of the method is that a point on a harmonic wave is highly correlated with the corresponding point in a later cycle, while this does not occur in random (noise) oscillations. An ‘auto-correlation’ function R_{uu} looks at the correlation of a function with itself and forms a real power spectrum, while ‘cross-correlation’ R_{uy} looks at the correlation between two different functions and forms a complex power spectrum. :

$$R_{uu}(\tau) = \lim_{N \rightarrow \infty} \frac{1}{N} \sum_{t=0}^{N-1} u(t)u(t+\tau) \quad \text{Eqn. 2.11}$$

$$R_{uy}(\tau) = \lim_{N \rightarrow \infty} \frac{1}{N} \sum_{t=0}^{N-1} u(t)y(t+\tau) \quad \text{Eqn. 2.12}$$

with time-shift $\tau = 0, \pm 1, \pm 2, \dots$ and N the number of samples.

Spectral analysis theory learns that the (real) auto-spectrum $S_{uu}(\omega)$ of the input signal is defined as:

$$S_{uu}(\omega) = \sum_{\tau=-\infty}^{\infty} R_{uu}(\tau) e^{-j\omega\tau} \quad \text{Eqn. 2.13}$$

and the (complex) cross-spectrum $S_{uy}(j\omega)$ between input and output signal as:

$$S_{uy}(j\omega) = \sum_{\tau=-\infty}^{\infty} R_{uy}(\tau) e^{-j\omega\tau} \quad \text{Eqn. 2.14}$$

Since $S_{uy}(j\omega)$ is a complex number, one can also write:

$$S_{uy}(j\omega) = C_{uy}(\omega) + jQ_{uy}(\omega) \quad \text{Eqn. 2.15}$$

with $C_{uy}(\omega)$ the (real) co-spectrum and $Q_{uy}(\omega)$ the (real) quad-spectrum.

It can be proven that the (complex) frequency-response function $H(e^{j\omega})$, which is in fact the transfer function TFF_{SPA} of the process in a frequency-domain representation, can be found from the auto- and cross-spectrum of input $u(t)$ and output $y(t)$ by the following property:

$$S_{uy}(j\omega) = H(e^{j\omega})S_{uu}(\omega) \quad \text{Eqn. 2.16}$$

There is no formula in the time-domain, but only a graphical representation of the frequency-response function by means of a pair of Bode plots, showing the amplitude of the TFF_{SPA} or $|H(e^{j\omega})|$ and phase of the TFF_{SPA} or $\angle H(e^{j\omega})$ in terms of frequency ω :

$$|TFF_{SPA}| = |H(e^{j\omega})| = \frac{\sqrt{C_{uy}^2(\omega) + Q_{uy}^2(\omega)}}{S_{uu}(\omega)} \quad \text{Eqn. 2.17}$$

$$\angle TFF_{SPA} = \angle H(e^{j\omega}) = \arctan \frac{Q_{uy}(\omega)}{C_{uy}(\omega)} \quad \text{Eqn. 2.18}$$

The practical implementation of the spectra $S_{uy}(j\omega)$ and $S_{uu}(\omega)$ can be done by means of the Discrete Fourier Transform (DFT). The signals $u(t)$ and $y(t)$ can be written in a discrete way as:

$$DFT(u) = U(k) = \sum_{t=0}^{N-1} u(t)e^{-j2\pi t k / N} \quad \text{Eqn. 2.19}$$

$$DFT(y) = Y(k) = \sum_{t=0}^{N-1} y(t)e^{-j2\pi t k / N} \quad \text{Eqn. 2.20}$$

with k the sample index from 0 to $N/2$ ($k = \omega N/2\pi$). A discrete approximation of the ‘Wiener-Khinchin integral’ for the calculation of the power spectra (or periodograms) (Ljung 1987), gives the following:

$$\hat{S}_{uu}(k) = \frac{T}{N} U^*(k)U(k) \quad \text{Eqn. 2.21}$$

$$\hat{S}_{uy}(k) = \frac{T}{N} U^*(k)Y(k) \quad \text{Eqn. 2.22}$$

Hereby is T the sampling period, N the length (number of samples) of the finite time-window used, $U(k)$ the DFT of the windowed input $u(t)$ and $Y(k)$ the DFT of the windowed output $y(t)$, symbol $*$ denoting the complex conjugate and symbol $\hat{}$ denoting an approximated or estimated value.

From Eqn. 2.16 and the above Eqn. 2.21 and Eqn. 2.22 it follows that:

$$TFF_{SPA} = H(k) = \frac{Y(k)}{U(k)} \quad \text{Eqn. 2.23}$$

with k the sample index from 0 to $N/2$ ($k = \omega N/2\pi$).

When the length of the finite time-window is a power of two, the fast FFT algorithm can be used as a good approximation of the DFT algorithm for the calculation of $Y(k)$ and $U(k)$. A Hanning window (with relatively small main lobe and limited frequency leak, making it appropriate for stochastic signals) was chosen, which can be described by:

$$w(t) = 0.5 - 0.5 \cos \frac{2\pi t}{N-1} \quad \text{Eqn. 2.24}$$

with $0 \leq t \leq N-1$. Stochastic signals without specific temporal structure are hard to analyze by means of only one periodogram. Therefore, an averaging is necessary for the calculation of the desired power spectra to reduce the variance. An averaging can be done in the time-domain (averaging of multiple periodograms determined on relatively short analysis

windows) or in the frequency-domain (smearing of one periodogram determined with one long analysis window, by averaging a certain number of frequency components). The time-domain approach is the most beneficial from a computational point of view and has been implemented in this study. The method used is called the ‘Averaging Modified Periodograms Method’. (Welch 1967) Concluding one obtains:

$$TFF_{SPA} = \frac{\sum FFT(y_H).FFT(u_H)^*}{\sum |FFT(u_H)|^2} \quad \text{Eqn. 2.25}$$

with y_H and u_H the output $y(t)$ and input $u(t)$ after a Hanning time-window.

2.3 Implementation of system identification methods

Both the ARX/IV4 and SPA technique have been implemented in a GUI in the Matlab 6[®] environment (The Mathworks Inc., Natick, MA). An illustration is shown in Figure 2–2. Options for filtering and different methods of calibration of signals are implemented (upper left). Measured signals are shown (upper right), together with the estimated aortic signals (lower left), which are compared with the invasively measured aortic data, and finally the Bode plots for both parametric and non-parametric techniques (bottom right).

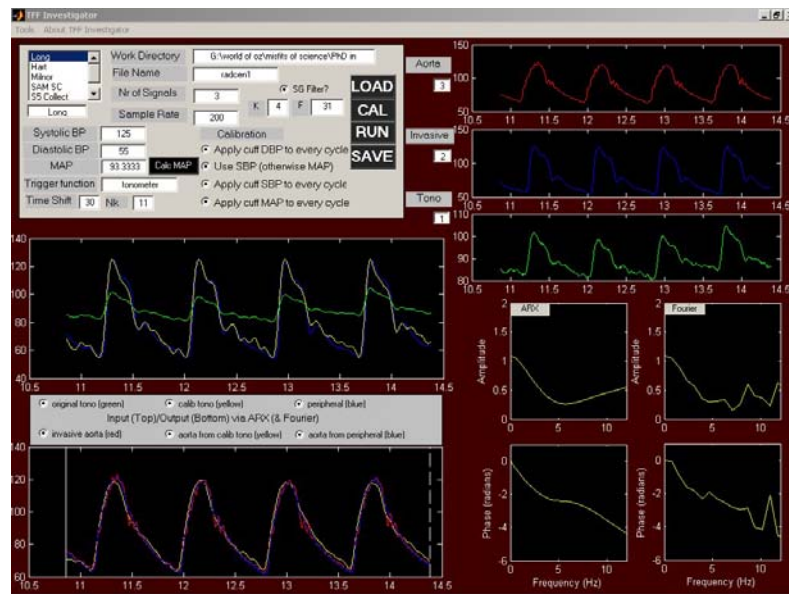


Figure 2–2 GUI front panel, allowing to estimate aortic pressures from peripheral measurements by means of a TFF.

3 Results

3.1 Comparison between parametric and non-parametric identification

In Figure 2–3 the comparison is shown between the parametric and the non-parametric identification method for the TFF determination from aorta to radial artery (Ao-R TFF), which is the physiological direction of the vascular system. Thus, for the Ao-R TFF the input is the invasive aortic signal (AoI) and the output is the invasive radial signal (RO).

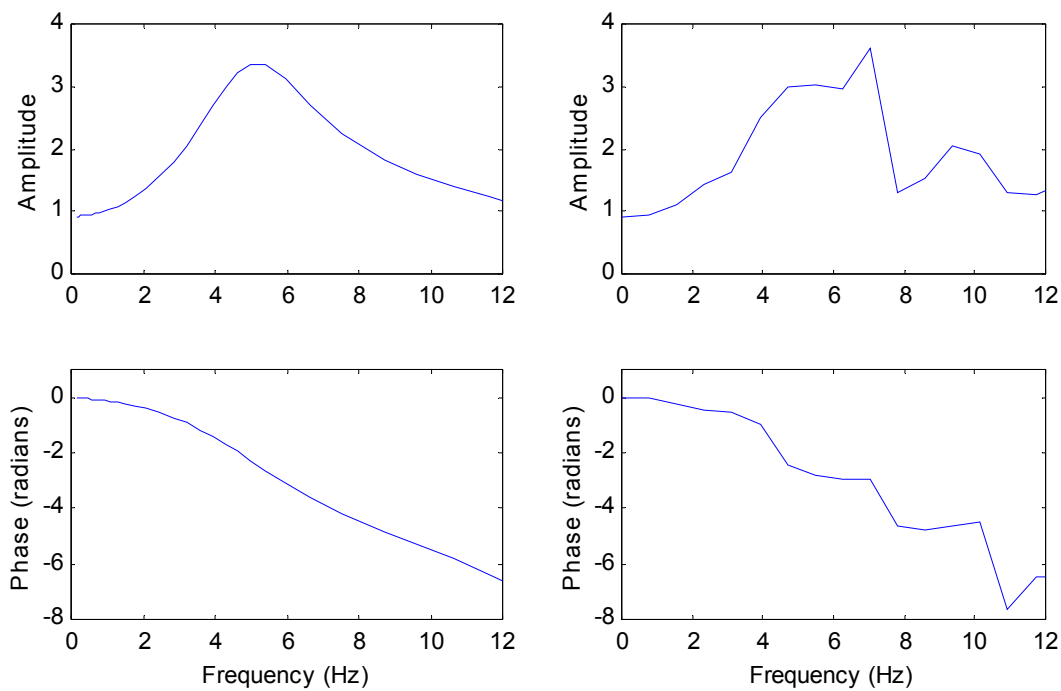


Figure 2–3 Comparison between the parametric and the non-parametric identification method for the TFF determination from aorta to radial artery (Ao-R TFF).

In Figure 2–4 the comparison is shown between the parametric and the non-parametric identification method for the TFF determination from radial artery to aorta (R-Ao TFF), which is the practical direction when transforming measured peripheral data to central pressure data. For determination of the R-Ao TFF, the input is the invasive radial signal (RI) and the output is the invasive aortic signal (AoO). To maintain a causality relation, it is necessary to artificially shift the RI a number of samples, so that it occurs in time before the AoO, which is of course the inverse of the physiological reality. A time-shift of $d = 30$ samples was used, resulting in $30/200 = 0.15$ s of delay, when using a sample rate of 200 S/s,

which is a typical time value for a travelling wave to go from central aortic to the radial site in the arterial tree.

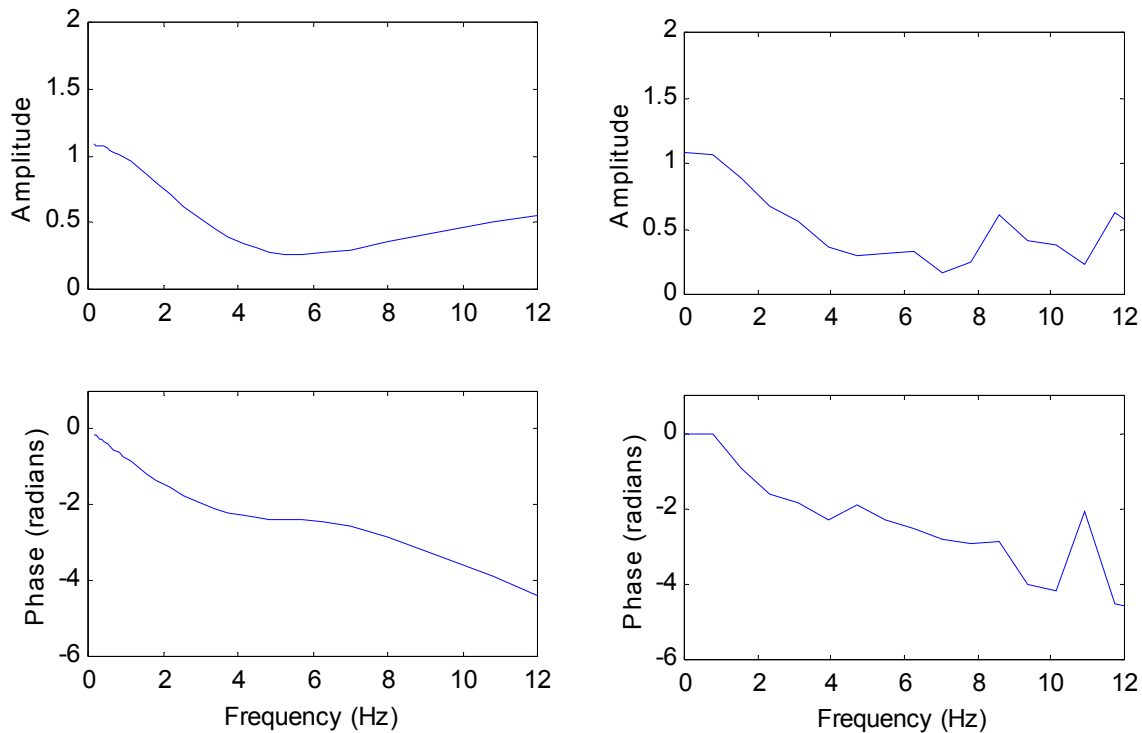


Figure 2-4 Comparison is shown between the parametric and the non-parametric identification method for the TFF determination from radial artery to aorta (R-Ao TFF).

The more recent technique of the parametric identification had the preference over the non-parametric method. First, the smoother curves of the parametric method were clearly visible in both the Ao-R TFF and the R-Ao TFF. This is a result of the fact that the spectral window length for the non-parametric method represents a trade-off one has to make between amount of sample windows (more windows means better averaging and smoother curves) and length of one window (more windows means small amount of sample points per windows, thus less accurate FFT). This trade-off is a trial-and-error issue and cannot be strictly defined. A second advantage of the parametric method was the fact that a time-domain TFF formula is available that links input and output signal, whereas the non-parametric method only gives direct information per frequency component (derived from the Bode plots), but not on the original input signal. Finally, the parametric method required less data sequences than the non-parametric method, which will be advantageous when investigating transient effects (Valsalva manoeuvre, abdominal compression) besides steady state waveforms.

3.2 Comparison between two different parametric approaches

Focusing on parametric identification, again two different approaches to derive a TFF were compared. One could use the inverse of the physiological Ao-R TFF (Figure 2–5, right), denoted further as the ‘inversion’ approach or Ao-R TFF^{-1} , or one could use the non-physiological R-Ao TFF (Figure 2–5, left), denoted further as the ‘time-shift’ approach since the radial input signal is shifted for causality reasons as explained higher.

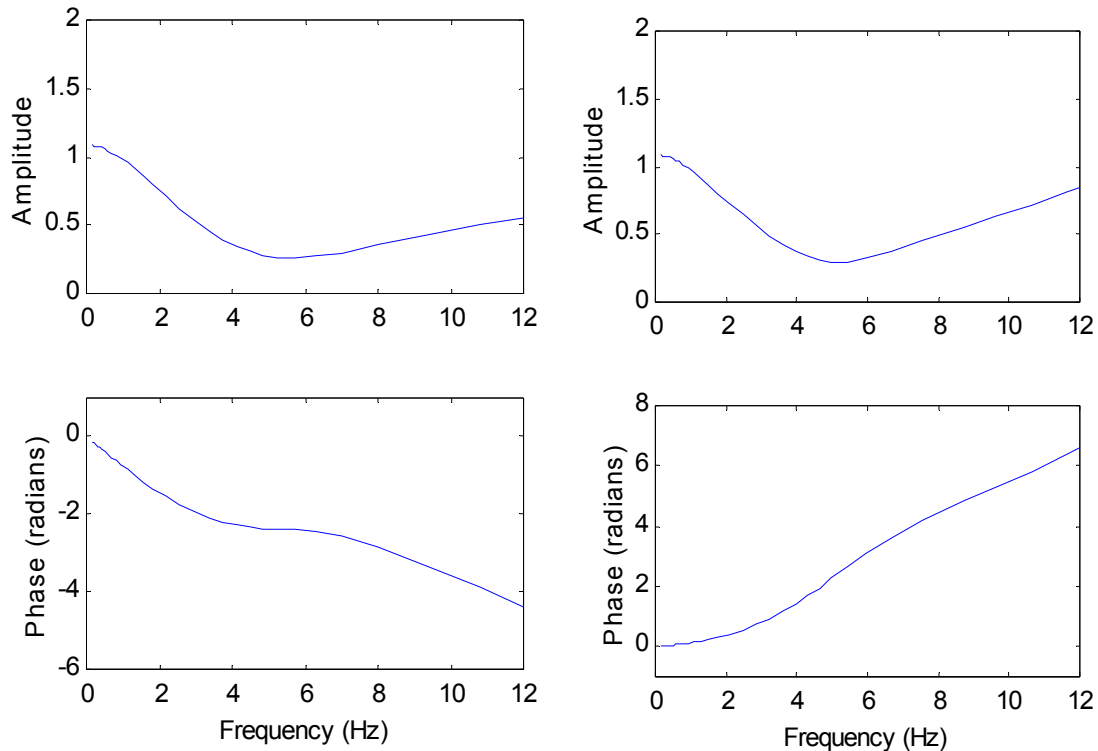


Figure 2–5 Comparison of two different parametric approaches. Left: The ‘time-shift approach’ or R-Ao TFF. Right: The ‘inversion approach’ or Ao-R TFF^{-1} .

Notice that for Ao-R TFF^{-1} , phase was rising with frequency which is a logical consequence of the inversion. Further, the inversion approach required additional treatment in case of instable poles in the TFF and a filter to reduce signal instability (noise). More noise was introduced due to the fact that higher frequencies are more amplified than with the R-Ao TFF as shown in Figure 2–6.

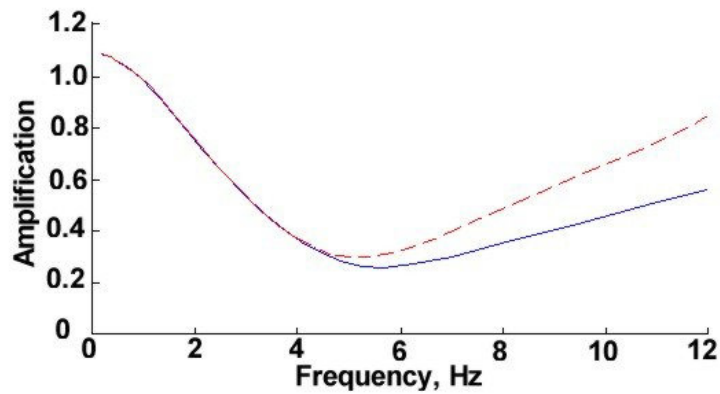


Figure 2–6 Comparison of the amplitude Bode plots of the Ao-R TFF⁻¹ (striped line) and the R-Ao TFF (full line).

The noise level difference is illustrated in Figure 2–7 showing estimated aortic signal (full line) and the measured invasive aortic signal (striped line). Notice the noise-sensitivity and time delay between real and estimated signal in case of the inversion approach Ao-R TFF⁻¹ (bottom) and the good agreement for time-shift approach R-Ao TFF (top).

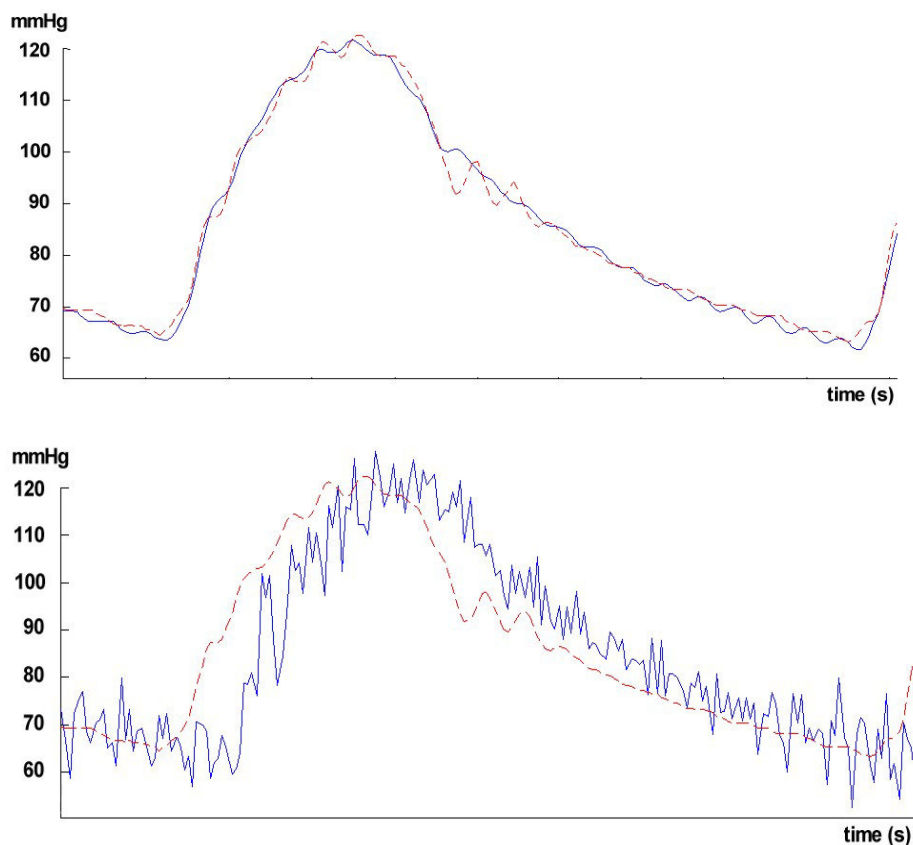


Figure 2–7 The noise level difference between the inversion and time-shift approach. Full line is the estimated aortic signal, striped line is the measured invasive aortic signal. Top: The time-shift approach R-Ao TFF. Bottom: The inversion approach Ao-R TFF⁻¹.

4 Discussion

Karamanoglu et al. (Karamanoglu, Avolio et al. 1990) and later Segers et al. (Segers, Carlier et al. 2000) started from a model for the vessel path that is simplified (tapering from aorta to radial artery modeled by a three-step cylindrical tube with no side branches) with parameters that have a physiological meaning (such as compliance and impedance). Making use of Fourier harmonic decomposition, the model is subsequently fitted to measured input (central aortic waveform) and output data (radial artery waveform) to estimate the remaining unknowns of the model. This could be referred to as a gray-box approach. Looking at the system as a black box as was done in this study, where estimated parameters for the identified model have no physiological meaning, allowed to maintain a more general model structure that still created the link between central aortic and radial artery waveform, but without having to worry about the real physiological vessel structure. A disadvantage was that insight in the vessel path structure was lost.

In this study, different approaches for the estimation of the radial-aortic transfer function (TFF) were described and compared. The theoretical background of a parametric (ARX/IV4) and non-parametric identification method (SPA) was explained and implemented in a user-friendly software interface (GUI). Although the methods may be quite standard system identification techniques for automation and control applications in engineering industry, in the field of (clinical) haemodynamic analysis mostly only the outcome in the form of Bode plots (often only the amplitude plot) is recognized as a more or less familiar tool. However, the knowledge on for instance parameter order, window length or reversing the physiological direction and the impact on the Bode plots is important and can contribute to a more adequate use of TFF methods in clinical practice.

Such a more clinically oriented study by Chen et al. (Chen, Nevo et al. 1997) used a parametric ARX model for the estimation of central aortic pressure waveforms from radial tonometry. No elaborate description of the mathematical background is given (only some general principles are briefly addressed in appendix), nor is the time-domain formula given from which the spectra are derived for visualization, and also the Bode plots of the TFF that allow the reconstruction of the aortic waveform (see Figure 2–4 in this study) are not shown, but only the illustrative plots in the physiological direction from aorta to radial artery (see

Figure 2–3 in this study). It is however mentioned by Chen et al. that an inversion approach was used (see Figure 2–5, right in this study) for the parametric ARX model and that the noise amplification was resolved by convolving the TFF with a low-pass filter of which the cut-off frequency was dependent on the magnitude of the TFF in the physiological direction. In this study a time-shift approach was presented that avoids beforehand the extra noise amplification, which is a better approach than filtering afterwards in the inversion approach as was done by Chen et al.

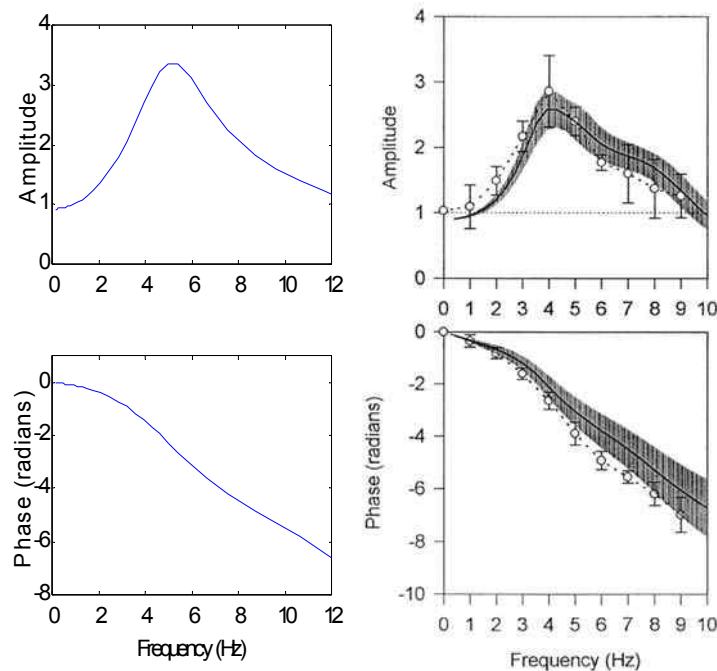


Figure 2–8 Parametric method with inversion approach. Patient dataset used in this study (left) shows a good correspondence with the generalized TFF of Chen et al. (right, shaded area defining 95% confidence interval) (Chen, Nevo et al. 1997) and even better with the TFF of Karamanoglu et al. (right, striped line and circles (mean) with error bars) (Karamanoglu, O'Rourke et al. 1993).

These Ao-R Bode plots (physiological direction) from the generalized TFF derived in the manuscript of Chen et al. are nevertheless frequently used in haemodynamic analysis (Figure 2–8, right). Its validity in specific situations (young or female subjects, exercise load,...) is rightfully questioned since this generalized TFF is averaged from only 20 patients (16 male, mean age 59, range 36-78 years) in supine resting position, but as mentioned earlier, up to now attempts to individualize the TFF have not been successful (see also section 8 of the previous chapter). Therefore, it was interesting to verify whether the Bode plots Figure 2–5 (right) from the patient dataset used in this study (male, 78 years) show a good correspondence with this generalized TFF, which is the case as shown in Figure 2–8. Looking

at the TFF derived in an older work on 14 patients (13 male, mean age 53.7, range 36-70 years) by relating amplitude and phase of corresponding input and output harmonic components (thus a non-parametric approach) (Karamanoglu, O'Rourke et al. 1993), shows that the mean values (Figure 2–8, circles on the right) really correspond well with the Bode plots from the presented study, also for the high frequencies.

Despite the high variance on the generalized TFF by Chen et al., there seems to be a slight second uprising on the Bode plot around 7-8 Hz which is not shown on the TFF from Karamanoglu et al. or the plots from this study. Since the manometer system used in this study was accurate enough in terms of frequency response and in fact was even slightly underdamped (natural frequency 15.2 Hz, damping coefficient 0.15 as derived from a fast flush test (Kleinman, Powell et al. 1992)), two other reasons for the slight difference in amplitude at higher frequencies might be the following. First of all, Chen et al. used the simple ARX model, while in this study the ARX/IV4 method was implemented. As described in the theoretical derivation in the methods section, the simple ARX model might not find optimized parameters when the noise on the system is not entirely random and leave more noise (high frequencies) in the model. Second, Chen et al. estimated a TFF with the invasive aortic signal and the radial tonometric (thus non-invasive) signal while in this study as well as in the study of Karamanoglu et al. the TFF was composed by means of two invasive signals. It can be argued that it is interesting to already include the wrist-tonometer system in the aorta-radial TFF, but this TFF is then only valid for the specific tonometer model applied in a specific patient acquisition session. The approach using two invasive signals provides a more noise-free TFF and a separation of the aorta-radial system from the radial-tonometer system. As such, this approach is more generally applicable.

This study focused on methodology aspects and their impact on the Bode plots, but did not investigate the patient dependent aspects and their impact on the plots. Two manuscripts in literature report of such patient findings: an appendix to the higher mentioned paper by Chen et al. (Chen, Nevo et al. 1997) and a more recent, more elaborate study by Fetters et al. (Fetters, Nevo et al. 1999) However, they in turn did not make a comparison between all different estimation approaches addressed in the presented study.

In the appendix of Chen et al. about the parametric inversion approach (Chen, Nevo et al. 1997), an illustration (reprinted in Figure 2–9) was given of the variance difference between a

parametric and non-parametric Ao-R TFF (again only the physiological direction of the vascular system). Panel A shows ARX Bode plots based on six individual heart cycles, 1024 data points, panel B shows Fourier derived TFF using the same data points, divided in 2 segments of 512 points and panel C shows Fourier derived TFF using 6144 data points, divided in 12 segments of 512 points each. From this it was found that the parametric method had a lower variance for the TFF estimation than the non-parametric method when the same amount of points are used. Only with the larger dataset the variance was similar between ARX and SPA. Note that the amplitude from the parametric method constructed from 6 heart cycles shows a second peak at higher frequencies, while this was clearly reduced already in the averaged or generalized ARX plots from the same manuscript by Chen et al. for which all data points from 20 patients were used (Figure 2–8, right). This again underlines the strong patient dependency of TFF estimation.

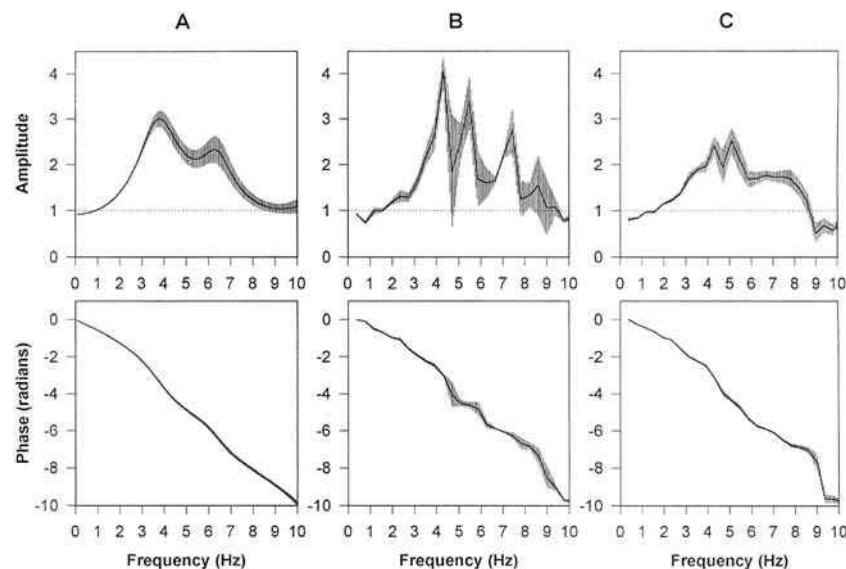


Figure 2–9 Reprinted from Chen et al.(Chen, Nevo et al. 1997) A: ARX Bode plots based on six individual heart cycles, 1024 data points. B: Fourier derived TFF using the same data points, divided in 2 segments of 512 points. C: Fourier derived TFF using similar but 6144 data points, divided in 12 segments of 512 points each. From this it was found that the parametric method has a lower variance for the TFF estimation when the same amount of points are used. Only with the larger dataset the variance was similar between ARX and SPA.

Finally in Figure 2–10 (right) results from the more recent parametrical study on 19 subjects by Fetics et al. (Fetics, Nevo et al. 1999) are displayed (14 male, age 51 ± 16 years), in which a more elaborate theoretical review is given (for the parametric but not for the non-parametric method however), as well as the R-Ao TFF (thus not in the physiological way, but in the direction needed to reconstruct the central waveform) and also a time-shift approach is

presented. However, Fetics et al. still used the simple ARX model not corrected for noise reduction with for instance an instrumental variables technique as done in this study, and TFF estimations were again derived not from two invasive signals, but from an invasive central and non-invasive radial signal. Figure 2–10 shows the differences found in this study (left) for the amplification of high frequencies with the time-shift and inversion approach, compared with results from the manuscript by Fetics et al. (right). A good correspondence was found. The amplification of the inversion approach found in this study (left panel, striped line) deviates from the mean on the right panel (thin full line) starting from 8 Hz and above, but remains within the (increasingly larger) SD intervals (thin dotted lines) shown in Figure 2–10 (right). This is clearly due to the instability of the inversion approach as was mentioned in the methods section.

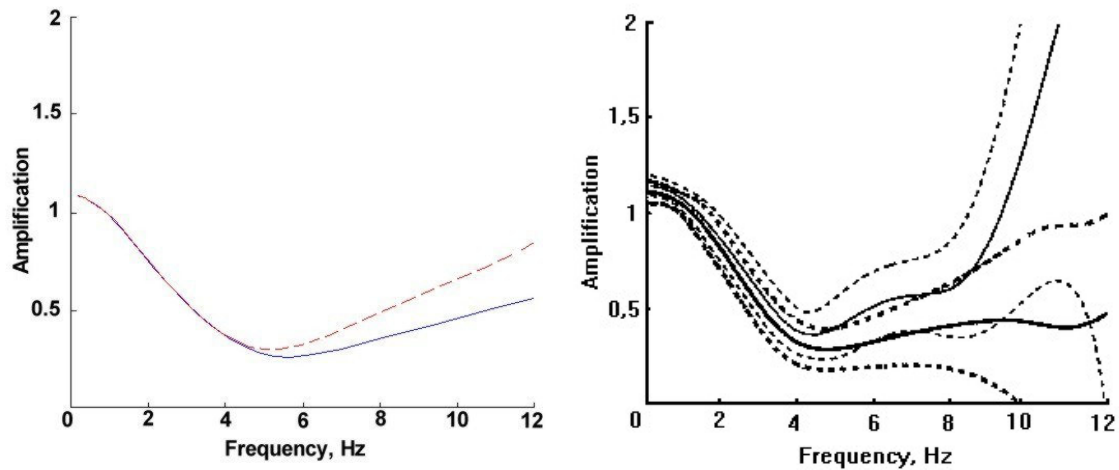


Figure 2–10 Comparison of the amplification realized by the parametric obtained R-Ao TFF with time-shift and inversion approach. Left: Results from this study. Striped line represents the inversion TFF, full line is the time-shift TFF. Right: Thin lines are the amplitude of the inversion TFF, bold lines of the time-shift TFF. Dotted lines represent SD intervals.(Fetics, Nevo et al. 1999)

5 Conclusion

In order to contribute to a better understanding of TFF estimation methods, this study provided a coherent overview of the theoretical background for some non-parametric and parametric system identification approaches. Techniques were explained and implemented, and Bode plots for an invasive patient dataset were constructed, described and compared. As opposed to (very limited) literature findings, an improved ARX/IV4 parametric model was used instead of the simple ARX model and for the TFF estimation two invasive signals were used, instead of an invasive central and a non-invasive peripheral signal.

It was already illustrated that the variance of a non-parametric method is bigger than for a parametric method when small datasets are used.(Chen, Nevo et al. 1997) It has been presented here that the parametrically derived TFF should be preferred not only for reasons of patient-dependent variance, which has to be further investigated on larger and more specific patient populations, but also for methodological reasons, as it immediately gives the relation of input and output signal in a mathematical formula (and not just per frequency component), and model characteristics are easier to optimize. It was further found that a time-shift parametric approach had a better accuracy and was not as sensitive to noise introduction as was the inversion parametric approach.



3 An Arterial Network Model to Assess Pulse Pressure Reduction

Abstract

A multi-branched model of the human arterial system that was constructed in earlier work, has been refined for the aorta and enhanced to allow automatic computation of the influence of changing vessel properties on haemodynamic parameters.

The original configuration containing 128 segments (10 for the aorta) and 68 nodes, was changed into 136 segments (18 for the aorta) and 76 nodes. This way, the aorta was divided from ascending to thoracic part in 14 segments with an averaged length of 1.8 ± 0.1 cm allowing to study the impact of specific and localized vessel wall changes. Seen the bottom-to-top approach of the compilation procedure, the old configuration could not just be expanded with extra segments but a new renumbered configuration of the whole arterial tree had to be implemented.

In particular the relation between variation of vessel diameter and elastic modulus E on pulse pressure at the aortic valve was investigated, as it is known that increased pulse pressure is a determinant of increased cardiac load which can lead to pathological conditions (e.g. ventricle wall hypertrophy). By calculating characteristic impedance, it was also possible to decompose pressure into forward and reflected waves. Finally, starting from the pathological state of a dilated aorta this model can predict the amount of vascular unloading necessary (by respective changes of diameter and elastic modulus E) to reduce increased pulse pressure to a desired normal value.

1 Introduction

The compliance of the aorta plays an important role in reducing the afterload for the left ventricle, as the buffer capacity (Windkessel effect) allows to dampen the generated pressure and flow pulsations. In certain pathological conditions such as Marfan syndrome (a genetic disorder that weakens connective tissue in the body) or due to aging, the aorta dilates and loses an amount of its compliant properties with repercussions on the wave travelling in the whole arterial tree as well as on the cardiac load.(Jeremy, Huang et al. 1994) Recent work by Okamoto et al. looked at the mechanical properties of a dilated human ascending aorta, providing information on elastic properties, strength and residual stress.(Okamoto, Wagenseil et al. 2002)

In the case of an aortic aneurysm, the wall dilation is such that a high risk of rupture is pertinent.(Mohan and Melvin 1982) Graft replacement then becomes imperative. A lot of work has currently been performed on the properties of both synthetic and tissue engineered grafts.(Ogle and Mooradian 2002) It has been shown that the compliance mismatch between the stiff graft and the highly compliant natural vessel wall leads to a significantly increased SBP, the loss of the natural Windkessel effect and an increased characteristic impedance.(Morita, Kuboyama et al. 1991) From animal experiments these events appear to correlate with the development of left ventricular hypertrophy after bypass-procedures with a non-compliant graft or an artificially induced coarctation in the proximal aorta.(Maeta and Hori 1985; Kobayashi, Yano et al. 1996; Morita, Asou et al. 2002)

The goal of this study was to adapt and enhance an arterial network model used in previous studies (Avolio 1980) in order to analyze the effects of dilation and compliance changes on arterial pressure and flow dynamics. More specific for this study, the relation was investigated between variation of radius R and elastic modulus E of the proximal aorta with the pulse pressure PP at the inlet of the ascending aorta. The mathematical model was also used to look at the relation between the pressure wave and its forward and backward components during the mentioned aortic wall changes. With the question in mind whether a *compliant* vascular graft could induce the necessary unloading, it was already investigated with the model how R - and E -changes could reduce an increased PP to a normal value.

2 Methods

In earlier work, a numerical network model (written in FORTRAN) of the human arterial system was constructed to analyze arterial blood pressure and flow dynamics. One can refer to the reporting of A. Avolio (Avolio 1980) for more mathematical details. In brief, the model has a multi-branching configuration consisting of 128 segments connected by 68 nodes, with each segment being a thin-walled uniform cylindrical tube having internal viscous, elastic and inertial properties (Figure 3–1, left and middle). It comprises central vessels and all principal peripheral arteries down to diameters of 2.0 mm. A terminating peripheral segment is formed by a resistance, determined by the characteristic impedance and the specified reflection coefficient for the segment. Navier-Stokes equations for pulsatile flow in elastic tubes (Womersley 1957a) and the Moens-Korteweg equation for wave velocity are used to obtain the solution of pulsatile blood pressure and flow in the modelled arterial system. As for the arterial wall, the visco-elastic properties are represented by a complex elastic modulus E (Bergel 1961a), and by the (tangent of the) angle ϕ representing the phase lead of pressure in relation to wall displacement (Westerhof and Noordergraaf 1970). Physiological data for the model segments (dimensions and elastic constants) are derived from literature manuscripts (Noordergraaf, Verdouw et al. 1963; Westerhof, Bosman et al. 1969) and anatomical atlases. By applying an input cardiac ejection waveform at the aortic root, pressure and flow waveforms can be determined at any node in the arterial model.

The original model has been enhanced by implementing a new expanded configuration together with additional features for visualization and wave decomposition (written in Matlab 6[®] environment (The Mathworks Inc., Natick, MA)). To refine the segmentation of the aorta, the model consisting of 128 segments (10 for the aorta) and 68 nodes was replaced with a model using 136 segments (18 for the aorta) and 76 nodes (Figure 3–1, right). This way, the aorta was divided from ascending to thoracic part in 14 segments (AS1-AS14) with an averaged length of 1.8 ± 0.1 cm allowing to look at localized aortic wall changes (Table 3–1). Seen the bottom-to-top approach of the compilation procedure of the original model (Avolio 1980), where impedance parameters are being assessed starting from the terminal branches up to the proximal segments, the old configuration could not merely be expanded with additional segments but a new renumbered configuration of the whole arterial tree had to be implemented. The feature of wave decomposition into forward and backward waves was

implemented by making use of the previously mentioned formulae Eqn. 1.58 to Eqn. 1.62 from Chapter 1. Physiological data for the model segments (dimensions and elastic constants) are available for an average young individual, an adult and an aged subject.

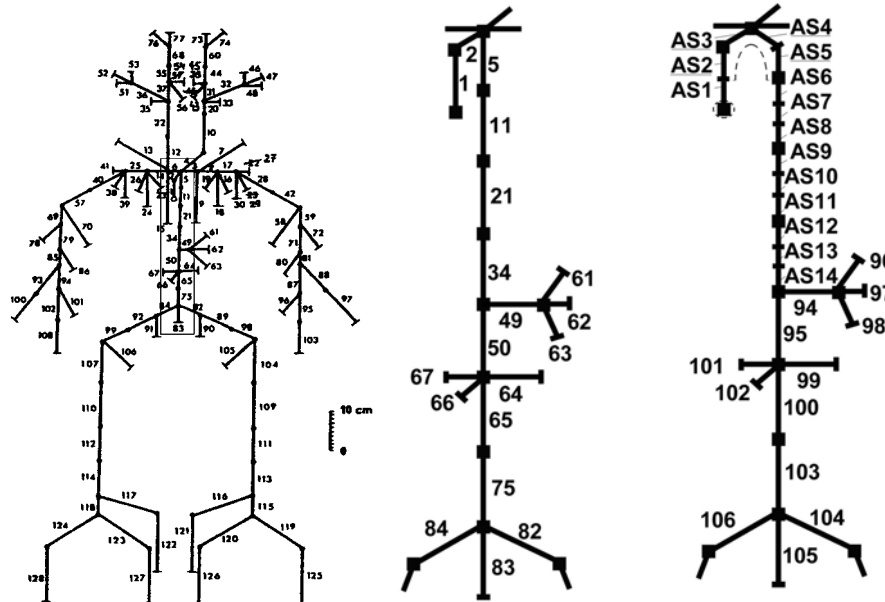


Figure 3–1 Left: Original arterial network model (128 segments, 68 nodes) as constructed in earlier work. (Avolio 1980) The rectangle denotes the aorta. Middle: Close-up of old aorta segments in original configuration. Right: Close-up of new aorta segments (AS1-AS14) in expanded arterial network model (136 segments, 76 nodes).

<i>Segment</i>	<i>Corresponding artery</i>	E_{100} (Pa)	h_{100} (cm)	R_{100} (cm)	L_{100} (cm)
AS1	ascending aorta part1	6.58E5	0.163	1.45	2.0
AS2	ascending aorta part2	6.58E5	0.163	1.45	2.0
AS3	aortic arch part1	6.98E5	0.132	1.12	2.0
AS4	aortic arch part2	7.41E5	0.127	1.07	1.95
AS5	aortic arch part3	7.41E5	0.127	1.07	1.95
AS6	thoracic aorta 1 part1	7.41E5	0.120	1.00	1.73
AS7	thoracic aorta 1 part2	7.41E5	0.120	1.00	1.73
AS8	thoracic aorta 1 part3	7.41E5	0.120	1.00	1.73
AS9	thoracic aorta 2 part1	7.54E5	0.116	0.95	1.73
AS10	thoracic aorta 2 part2	7.54E5	0.116	0.95	1.73
AS11	thoracic aorta 2 part3	7.54E5	0.116	0.95	1.73
AS12	thoracic aorta 3 part1	7.54E5	0.116	0.95	1.73
AS13	thoracic aorta 3 part2	7.54E5	0.116	0.95	1.73
AS14	thoracic aorta 3 part3	7.54E5	0.116	0.95	1.73

Table 3–1 Properties of the aortic segments for a young individual in the expanded network configuration for the control situation (X_{100}): elastic modulus E_{100} (Pa), wall thickness h_{100} (cm), radius R_{100} (cm) and length L_{100} (cm).

3 Results

An example of an output of the arterial model is illustrated in Figure 3–2 (control situation parameters and values are denoted by subscript ‘100’). The PP data of a young individual was examined at the height of the aortic valve (at the beginning of the first aorta ascendens part AS1, Figure 3–1, right). The elasticity modulus E and radius R of the second aorta ascendens part AS2 together with the three aortic arch segments AS3-AS5 (total length 7.9 cm, Table 3–1 and Figure 3–1, right) are altered by $\pm 50\%$ in 10 incremental steps. The stepsize can be chosen, but a smaller step increases calculation time. For a specific value of E and R , the compilation of the whole arterial network takes 3 to 4 s on a recent laptop PC (AMD 2.2 GHz). Processing a $\pm 50\%$ variation in 10 steps of 5% for both E and R thus takes about 7 min of calculation time.

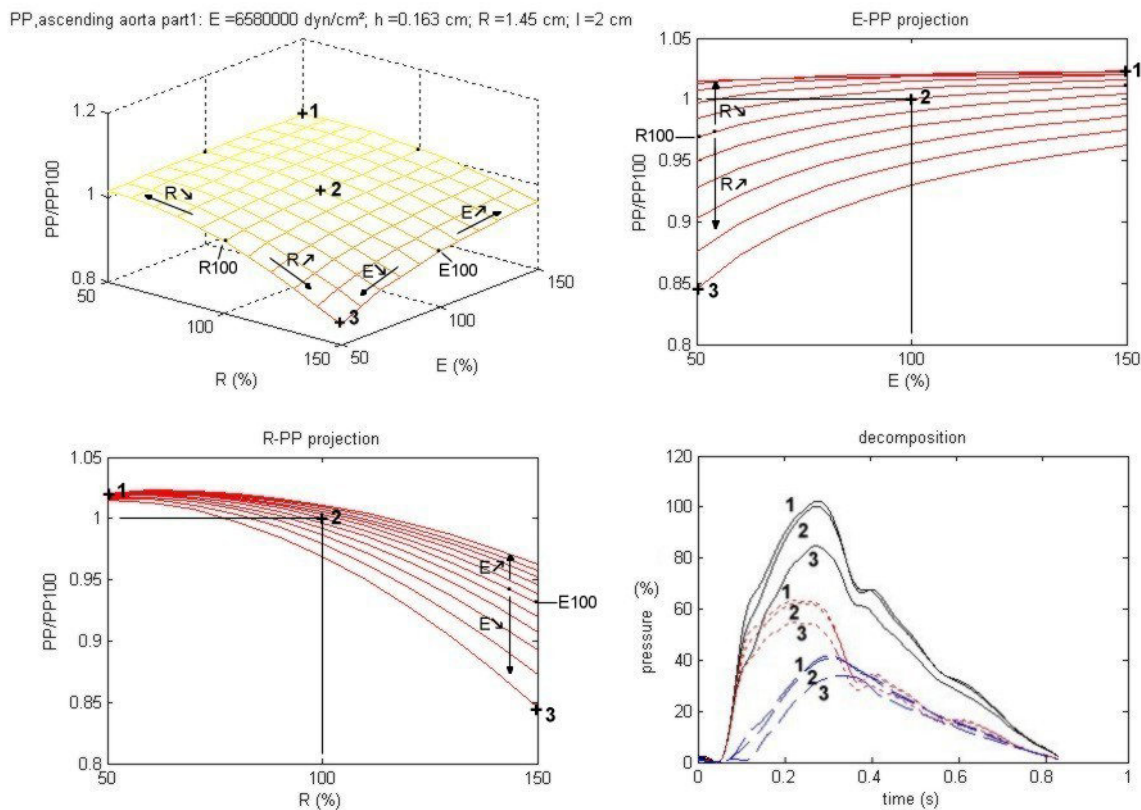


Figure 3–2 Upper left: PP for AS1 (normalized with PP₁₀₀) vs. E and R increments (percentages of E_{100} and R_{100}). Upper right: 2D projection showing PP vs. E . Bottom left: 2D projection showing PP vs. R . Bottom right: For a specific situation on the 3D mesh (examples designated with 1, 2 or 3), the pressure wave (full line) is presented together with its decomposition in forward (dotted line) and reflected wave (striped line). The pressure wave for situation 2 (control situation) is normalized (100%) while the other waves are quantified as percentages of that.

Results are presented as 3D mesh plots, in this case of PP for AS1 (normalized with PP_{100}) vs. E and R increments of AS2-AS5 (Figure 3–2, upper left). Also shown are 2D projections of PP vs. E (Figure 3–2, upper right), and PP vs. R (Figure 3–2, bottom left).

For three specific situations on the 3D plot (designated by 1, 2 and 3), the corresponding pressure wave is visualized together with the decomposition in forward and reflected waves (Figure 3–2, bottom right). Situation 1 is the case where the E-modulus of AS2-AS5 is augmented with 50% and R is reduced with 50%. Situation 1 thus represents a reduced and stiffened aortic arch. Situation 2 shows the control situation (X_{100}). Situation 3 is the case where the E-modulus of AS2-AS5 is reduced with 50% and R is augmented with 50%. Situation 3 thus represents a dilated, yet more compliant aortic arch.

4 Discussion and Conclusion

In this study, an existing arterial network model used in previous studies has been enhanced (i) in structure and (ii) in functionality. The model has received a more refined segmentation for the aorta (from ascending to thoracic part) and has been adapted such that the impact of variations in segment properties (E , R , h , l) can be investigated on pressure and flow characteristics. One and the same parameter can be altered in multiple segments at the same time, but so far the incremental step of variation has to be equal for all segments (e.g. E -variation with 10 steps of 5% for *all* designated segments). However, different parameters can be altered with different incremental changes (e.g. E -variation with 10 steps of 5%, together with R -variation in 6 steps of 3%). Further, it is possible to alter parameters of segments at non-neighbouring locations. In this way it would be possible, for instance, to investigate an increased peripheral resistance effect in all extremities and its impact on pressure and flow characteristics in the aorta. Finally, it should be noted that no ventricular-vascular interaction has been modelled, since a constant flow wave is used at the entrance of the arterial network. However, one could use the model in an iterative way and change the initial flow wave per time step with a newly calculated flow wave to solve this problem.

As an illustration in this study, PP in relation to E and R was investigated together with wave reflection and decomposition via 3D and 2D graphs. In the end, the arterial network model as presented here is merely a working tool, that does not take into account physiological boundaries. As such is the described situation 3 (a dilated and more compliant aortic arch) not a common realistic situation (dilatation normally induces stiffening). Thus, the resulting plots have to be analyzed with insight of the operator.

The validity of the original theoretical derivation has been assessed by comparison with human and animal data in different situations: impedance values, wave transmission, characteristics in the presence of an arterial stenosis etc. have been compared with literature findings or in vivo experiments.(Avolio 1980) Nevertheless, the arterial model has been constructed by means of mathematical formulae and as such is subject to error introduction due to linearization and approximation. For instance, this linear model disposes over a refined branching network (diameters down to 2.0 mm) but still every branch consists of a sequence of uniform cylindrical segments, and therefore doesn't dispose over smooth tapering

characteristics. Neither can a purely resistive terminal impedance, as used in the presented model, match the boundary conditions as well as more complex (e.g. 3WK model) impedance models from a later generation, as have been used in non-linear arterial networks.(Stergiopulos, Young et al. 1992) It has been shown that such restrictions of a linear model could have an erroneous effect on modelling of wave reflection, systolic pressure and pulse pressure.(Segers, Stergiopulos et al. 1997)

In a recent study by Ioannou et al. (Ioannou, Stergiopulos et al. 2003), the proximal aorta was wrapped with a stiff Teflon prosthesis to simulate an acute reduction of compliance and investigate the subsequent effects on vascular haemodynamics and left ventricle function. Wave decomposition and reflection were also analyzed. It was found that wrapping the aorta decreased total arterial compliance by $52 \pm 13\%$, while systolic blood pressure rised by $37 \pm 8\%$ and PP by $87 \pm 31\%$. The trends of their results (increase, decrease) on PP were corresponding with the results from this model, but the amplitude differed substantially. While Ioannou et al. found a drastic increase in PP after wrapping with a stiff material (E and R increase), only a limited PP increase was observed with this model (compare situation 2 and situation 1 on Figure 3–2). Their suggestion was that a more compliant prosthesis, matching the host artery compliance, could be expected to reduce haemodynamic changes after implantation, such as PP increase.

This seems to be confirmed by on-going in vitro experiments (A. Avolio, personal communication) whereby an ascending human aorta (age > 60 years, n = 9) connected to a constant flow pulsatile pump is wrapped with a *compliant* material. A small diameter reduction (4 % and 12 % for a wrapmaterial A and B respectively) due to the compliant wrapping caused a large reduction in effective E (almost 90%), which in turn reduced PP by 15-25% (Figure 3–3, circles). When similar changes of elastic modulus E were examined in the proximal aortic segments of the arterial network model presented here, it resulted in changes in PP that seemed to fit the experimental data (Figure 3–3, surface). The underestimation of the data produced by Ioannou et al. (Ioannou, Stergiopulos et al. 2003), might just be a matter of where the normal range is taken. The 3D mesh on Figure 3–2 shows a kind of plateau phase at largely increased E and reduced R. Maybe this plateau could be partly due to the mentioned linearization errors in the mathematical model, but most likely it will actually occur in vivo, though at a relatively much higher stiffness. Starting at a lower E-

value, an increase in E has a much larger impact on PP than the same increase started at a high E-value. Of course these findings still deserve further investigation.

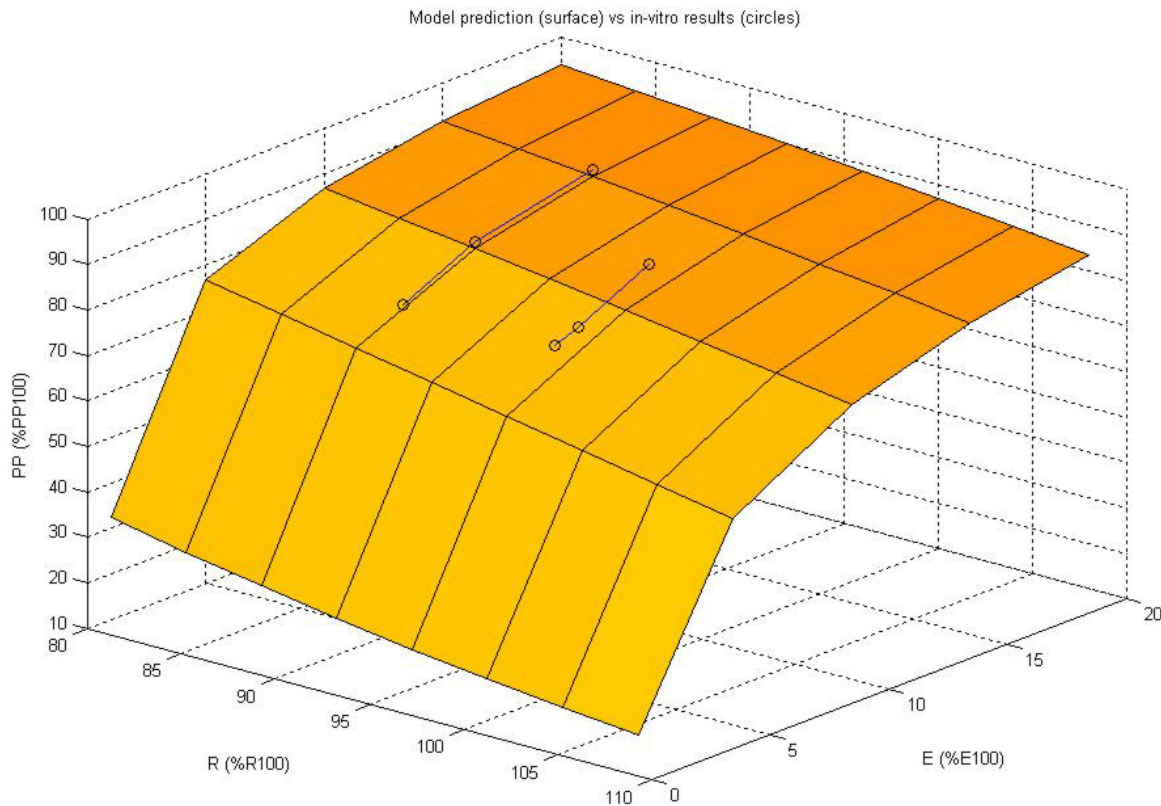


Figure 3–3 Model calculations (surface) of PP (normalized with PP_{100}) vs. E and R (percentages of E_{100} and R_{100}), together with 6 in vitro data points (circles). Connected circles represent 3 different variations of the same wrap material. Material A was supposed to induce a 12% reduction of R (the connecting line of material A circles indeed corresponds to $100 - 12 = 88\%$ on the R-axis), while material B was supposed to induce a 4% reduction of R (the connecting line of material B circles indeed corresponds to $100 - 4 = 96\%$ on the R-axis)

In clinical practice, reduction of pulse pressure is an important issue as it is known that increased pulse pressure is a determinant of increased cardiac load which can lead to pathological conditions (e.g. ventricle wall hypertrophy). (Madhavan, Ooi et al. 1994; Benetos, Safar et al. 1997) The presented arterial network model is a useful instrument to predict the amount of vascular unloading (by respective changes of diameter and elastic modulus E) necessary to, for instance, reduce an increased pulse pressure to a desired normal value in the case of a dilated aorta.

III Methodology II: Measuring Devices and Signal Acquisition

In this third part, invasive and non-invasive devices and methods for the registration of continuous pressure and flow waveforms are discussed and experimented with (Chapter 1). The method of arterial tonometry was elected for the pressure recordings in this thesis. Tonometry technology is being reviewed (Chapter 2) and looked upon as an alternative for long-term recording during surgery (Chapter 3). Finally, an in-house program was developed to meet the demands of simultaneous, synchronized and non-invasive ECG, pressure and flow acquisition (Chapter 4).

A decorative vertical bar on the left side of the page, consisting of a thin grey line and a thicker black line.

1 Background: Pressure and Flow

History

Initial theories of haemodynamics had been lacking the proper measurement instruments to validate the results. The research community had to await the creations of Marey (1860), Mahomed (1872) and others to get a non-invasive quantification of pressure pulsations with so-called 'sphygmograph' devices. Although very creative, they provided merely an estimation of mean pressure added with some pulse 'variations'. An accurate measuring device only came about with the work by Otto Frank (1865-1944) in 1903 on manometry.(Marey 1860; Mahomed 1872; Frank 1903)

The measurement of blood flow has always been behind on the measurement of blood pressure. Marey made some contribution on the direct measurement of flow. Carl Ludwig (1847) introduced the first continuously recording blood flow meter, and his student Adolph Fick (1829-1901) did important work on the calculation of cardiac output, which became a standard method following the first human catheterization done by Forssmann (on himself) in 1929 and popularized in the early 1940s by Cournand and others.(Forssmann 1929; Cournand and Ranges 1941)

Since the First World War, the domination of researchers from the USA cannot be denied. Pioneers in the field of cardiovascular physiology include people like Katz (1955), Wiggers (1950, 1952) and Hamilton (1962). In England there were Bramwell and Hill (1922) and on the mainland Wetterer in Germany who introduced the electromagnetic flowmeter (1937), independently from Kolin in the USA (1936). Gregg and colleagues started recording accurate flow waves in the coronaries (1940).(Kolin 1936; Gregg 1940)

In between wars there was little advance in cardiovascular medicine. After 1944, the sphygmomanometer focused too much attention on the systolic and diastolic values, introducing many myths on what is in fact nothing more than the maximum and minimum of the pressure wave. Technological advancement kept going, introducing micromanometers and diagnostic catheters around the 1970s.(Mills and Shillingford 1967; Murgo and Millar 1972)

Since then, also ultrasonic non-invasive flow recordings based on the Doppler principle have been introduced.(Hatle and Angelsen 1990) Many more developments became available in

recent years on the measuring and acquisition of pressure and flow waveforms, coinciding with advances in micro-electronics and silicon technology, but their description would be beyond the scope of this introduction. The techniques relevant to this thesis are described next.

1 Invasive pressure measurements

A lot has changed since Stephen Hales (1677-1761) made the first direct measurement of blood pressure by inserting a glass tube in a horse neck artery. But arterial cannulation with continuous pressure transduction and waveform display remains the accepted 'gold standard' for blood pressure monitoring today. Several peripheral arteries are available for percutaneous cannulation, but radial artery pressure monitoring is most common in anaesthesia and critical care.

The arterial cannulation using an integrated needle-guidewire-catheter assembly is commonly used (Figure 1–1). The wrist is positioned and the artery identified by palpation (A). The needle is then introduced through the skin and advanced towards the artery, generally at 30° to 45° (B). A flash of arterial blood into the collection reservoir identifies the artery as the needle tip enters the vessel. The guide wire is advanced through the needle into the vessel lumen (C). The catheter is advanced over the guide wire (D). After the catheter is fully advanced into the vessel lumen, the guide-wire is removed and a narrow bore, low compliance pressure tubing is fastened to the catheter (E). The apparatus is securely fixed to the wrist and connected to the pressure transducer. Large clinical investigations confirm a low incidence of long-term complications following radial artery cannulation.(Mandel and Dauchot 1977; Slogoff, Keats et al. 1983)

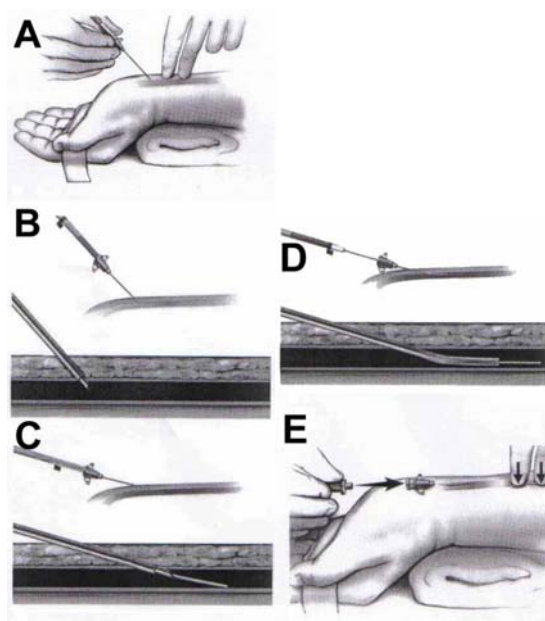


Figure 1–1 Subsequent steps of a radial arterial cannulation.

Apart from routine radial pressure monitoring, invasive pressure measurements are also performed during interventions, for example while treating stenosed coronaries. The cannulation procedure is analogue as described above but most often performed from the femoral artery. Nowadays, there are two kinds of pressure measuring guidewires. Hollow fluid-filled guidewires connected to an external transducer; and guidewires with a high fidelity micromanometer at the tip. The PressureWire[®] (Radi Medical Systems, Uppsala, Sweden) and WaveWire (Endosonics, Rancho Cordova, CA) are commercial examples of the latter. The Informer Wire (Scimed, Minneapolis, MN) on the other hand is a fluid filled catheter. Since fluid-filled lines need to be flushed, they take up more measuring time.(Pijls, Kern et al. 2000)

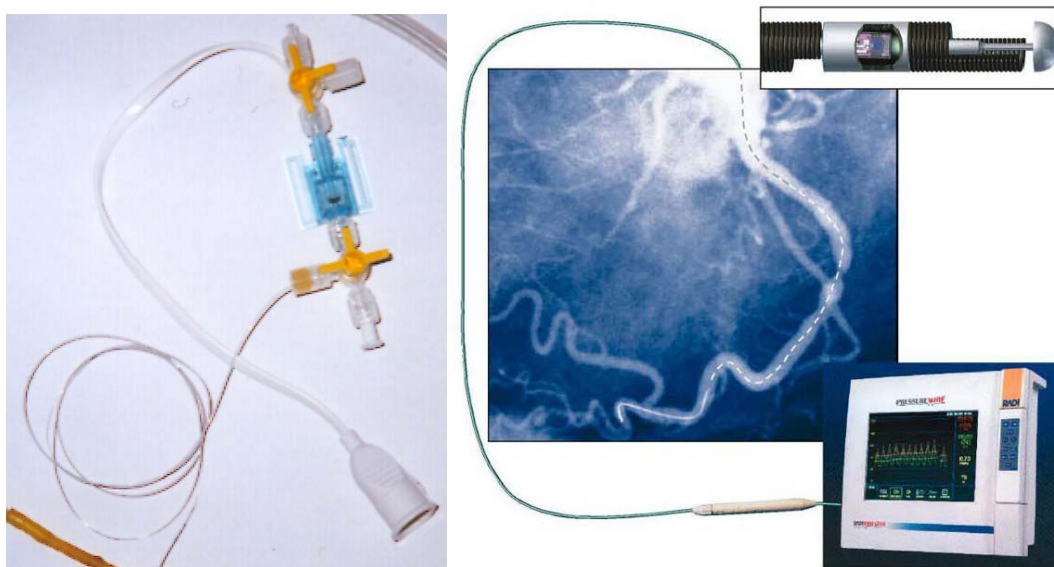


Figure 1–2 Left: Fluid-filled catheter with external transducer (Datex-Ohmeda, Helsinki, Finland). Right: Micromanometer at cathetertip (PressureWire[®], Radi Medical Systems, Uppsala, Sweden)

2 Non-invasive pressure measurements

2.1 Discrete measurements

Riva-Rocci¹ invented a device to measure cuff pressure in 1896, composed of a mercury manometer and an arm-encircling elastic cuff, inflatable with a rubber bulb. He described the measurement of systolic arterial blood pressure by determining the pressure at which the palpated radial arterial pulse disappeared as the cuff was inflated.(Riva-Rocci 1896)

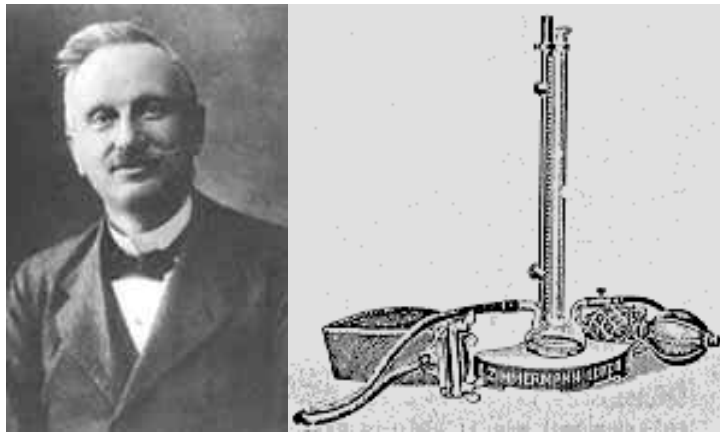


Figure 1–3 Scipione Riva-Rocci and his cuff pressure measuring device.

Undoubtedly, the most widely used manual discrete method for blood pressure determination is the auscultation of sounds originally described by Korotkoff in 1905.(Korotkoff 1905; Drzewiecki, Melbin et al. 1989) Using a Riva-Rocci sphygmomanometer and cuff, Korotkoff applied a stethoscope to the artery directly below the cuff to auscultate the sounds generated as the cuff was slowly deflated (Figure 1–4). These sounds are a complex series of audible frequencies produced by turbulent flow, instability of the arterial wall, and shock wave formation created as external occluding pressure on a major artery is reduced.

The pressure at which the first Korotkoff sound is auscultated is generally accepted as the systolic pressure (‘phase I’). The sound character progressively changes (‘phases II’ and ‘III’), becomes muffled (‘phase IV’), and finally absent (‘phase V’). Diastolic pressure is

¹ Scipione Riva-Rocci, 1863-1937. Italian internist and paediatrician.

recorded at phase IV or V. However, phase V may never occur in certain pathophysiologic states, such as aortic regurgitation.(Goldstein and Killip 1962)

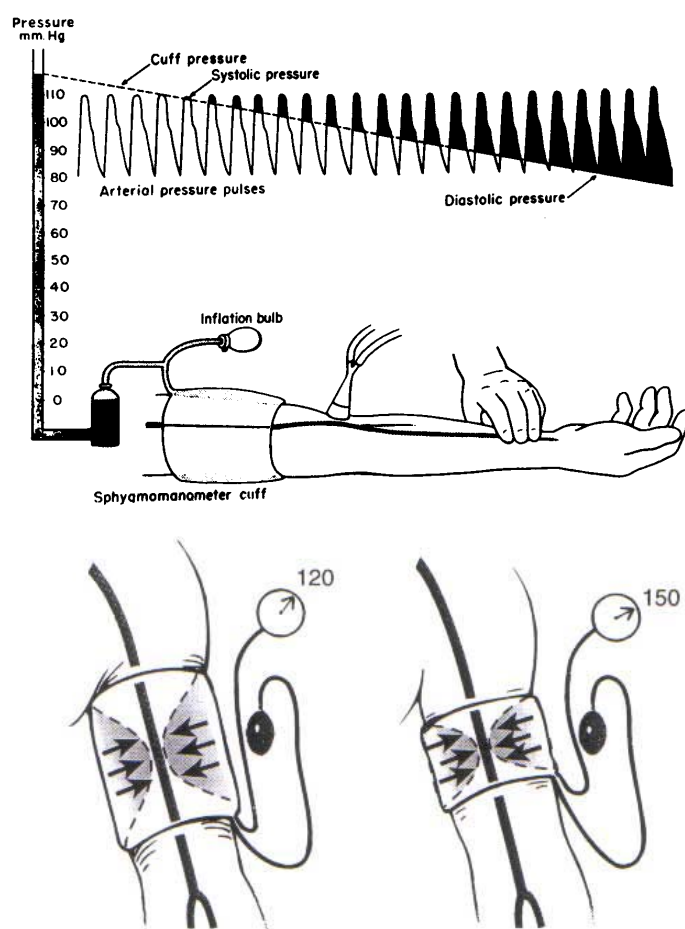


Figure 1–4 Up: Korotkoff auscultation method.(Li 2000) Bottom: Inappropriate cuff size (right) yields erroneous blood pressure values (overestimation with too small cuff).

Common sources of error during discrete manual blood pressure measurements include selection of an inappropriate cuff size or excessively rapid cuff deflation (Figure 1–4). Limitations of manual discrete blood pressure measurement have been overcome by automated non-invasive blood pressure devices (NIBP), which are now used widely in medical care. By applying a single algorithm or method of data interpretation, NIBP devices provide consistent, reliable values for systolic, diastolic, and mean arterial pressure (MAP). Most automated NIBP devices are based on the technique termed ‘oscillometry’, first described by von Recklinghausen in 1931.(von Recklinghausen 1931) With this method, oscillations in cuff pressure resulting from arterial pulsations during cuff deflation are sensed by the monitor and used to determine arterial blood pressure values. Peak amplitude of

arterial pulsations corresponds closely to true MAP.(Posey, Geddes et al. 1969) Values for systolic and diastolic pressure are derived using proprietary formulae that examine the rate of change of the pressure pulsations (Figure 1–5).(Geddes 1984) Systolic pressure is generally chosen as the pressure at which pulsations are increasing and are at 25 to 50 percent of maximum. Diastolic pressure is more difficult to determine but is commonly placed at the point where the pulse amplitude had declined by 80 percent.(Gorback 1988)

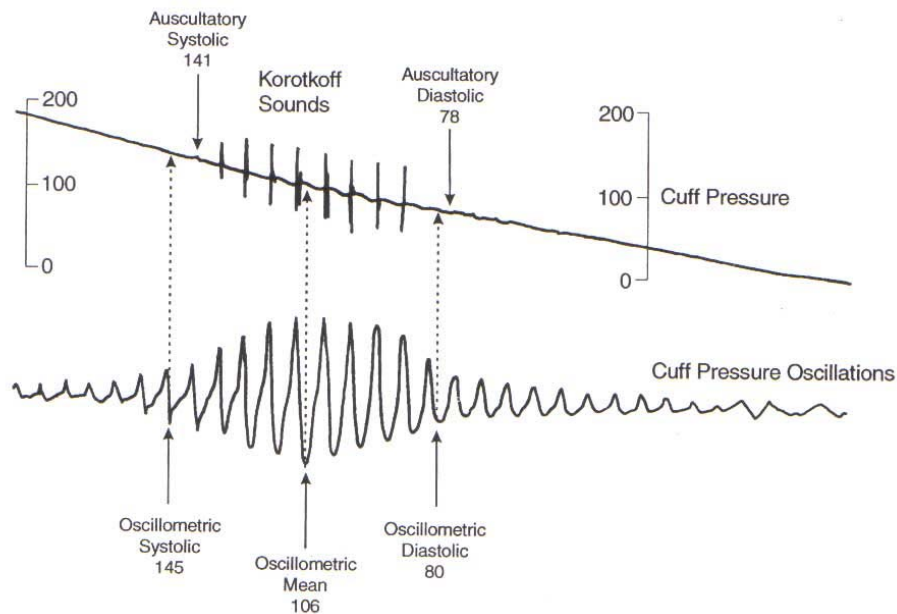


Figure 1–5 Comparison of blood pressure measurements using Korotkoff sounds and oscillometry. Oscillometric systolic blood pressure is recorded at the point where cuff pressure oscillations begin to increase, mean pressure corresponds to the point of maximal oscillations, and diastolic pressure is measured where the oscillations become attenuated.(Geddes 1984)

Under controlled clinical conditions, numerous investigators have demonstrated that automated NIBP measurements closely approximate directly (or invasively) measured arterial pressure.(Davis 1985; Ramsey 1991) However, other studies underscore the fact that marked disagreement occurs when direct and indirect (or non-invasive) pressure measurements are compared, particularly when the direct measurement is done at the radial artery or under changing clinical conditions.(Nystrom, Reid et al. 1985) When direct brachial artery pressures have been compared with indirect methods such as manual auscultation and automated oscillometry, the relation between the indirect and direct pressures varied between patients, within patients over time, and with changing haemodynamic conditions.(Gravlee and Brockschmidt 1990)

As noted, some authors have emphasized the lack of exact agreement between different measurements of blood pressure. Standards for performance of automated NIBP devices have been advanced by organizations such as the American Association for the Advancement of Medical Instrumentation (AAMI) and the British Hypertension Society. AAMI standards require a monitor to record blood pressure within 5 mmHg prediction error compared with the reference method, with 8 mmHg as largest standard deviation error for this comparison.(Association for the Advancement of Medical Instrumentation 1992) However, clinical performance of an NIBP monitor should be evaluated by other criteria as well. These include the number of outlier values, duration of discrepancies, magnitude of individual errors, and performance under variable clinical conditions.

The clinical conditions met in this thesis comprise usage during physical exercise tests as a calibration device for ‘applanation tonometry’ (see further in this chapter). Several commercially available automatic cuff-devices based on oscillometry were experimented with in this thesis, but none of them provided reliable output at *all* levels of exercise at *all* times. In fact, to this day there is no full-proof accurate discrete blood pressure device for use with exercise. Using the auscultation method during exercise is also not an easy task, due to the noise and movement. And last, these techniques require a finite time to produce the outcome which lies within the same order as the step-increment of an exercise protocol (about 3 min). This makes recalibration at the same exercise level impossible.

2.2 Continuous measurements

2.2.1 Penaz method

The Penaz method (1973) is based on unloading the arterial wall to measure a calibrated waveform in a finger.(Penaz 1973) A cuff is being placed around the middle phalanx of a finger or the base of the thumb finger (‘arterial volume clamp’ method, Figure 1–6), and blood pressure is determined by registering the cuff pressure needed to maintain a constant arterial volume (measured by light diodes or photoplethysmography). This method is commercialized in the Portapres[®] and Finapres[®] device (FMS Finapres Medical Systems, Arnhem, NL).



Figure 1–6 Measuring finger arterial waveforms with the Penaz method (Finapres® device, FMS Finapres Medical Systems, Arnhem, NL).

Continuous non-invasive finger blood pressure measurement devices have undergone clinical evaluations comparing their performance with direct arterial pressure measurements, which demonstrated small overall mean differences between finger and intra-arterial pressure measurements. (Smith, Wesseling et al. 1985) The potential for circulatory impairment of the distal finger caused by the constantly inflated cuff has been a cause for concern. Gravenstein et al. demonstrated mild hypoxemia in the capillary blood of the fingertip during finger blood pressure monitoring, but no adverse outcomes were noted in these study patients or in others in whom finger blood pressure measurement was performed for as long as 7 hours. (Gravenstein, Paulus et al. 1985)

Despite the positive comments above and its widespread use in ambulatory applications (especially related to aeronautical experiments), the Penaz method remains a peripheral monitoring technique which at the start of this thesis had not been investigated in literature as the input for a transfer function model that derives *central* aortic pressure (as opposed to radial arterial tonometry which is discussed further). In the work of Bos (Bos 1995), it was already shown that *brachial* pressure reconstruction from finger pressure measurements can only be achieved by using a digital filter/transfer function (Gizdulich and Wesseling 1990) for pulse wave distortion *and* additional corrections with newly derived formulae for the individual pressure gradient between brachial and digital artery pressure. But these proposed corrections still needed to be validated for young and healthy subjects and load conditions with changing blood pressure and wave amplification like standing up, head-up tilt, or vasoactive drugs. (Bos, van Goudoever et al. 1996)

One can also deduct that the shorter the pathway is between the peripheral site of pressure recording and the aortic valve, the less the error will be that is introduced (as more distal vessels get smaller, more tortuous and with more active muscular activity), which also is in favour of any device working more proximal to the heart. Seen the fact that at the start of this thesis radial arterial tonometry was also less widespread and fairly unknown, it was chosen to continue with the tonometric technology and investigate its potential in depth.

Concurrently with the tonometry based experiments in this thesis limited comparative studies with the Penaz method have been conducted in literature in recent years. In 2002, Nelesen et al. compared both the Finapres[®] with the Colin Pilot[®] radial tonometer measurement with an intermittent brachial blood pressure measurement device Dinamap[®] (Critikon, Tampa, FL) in cardiovascular reactivity studies.(Nelesen and Dimsdale 2002) They found that the Finapres[®] significantly overestimated systolic blood pressure and that the correlations between the Pilot[®] and Dinamap[®] were consistently higher than those between the Finapres[®] and Dinamap[®]. Also were there more artefacts (3.2%) with the Finapres[®] than with the Colin Pilot[®] (0.2%). In 2003, Birch et al. investigated whether the Finapres[®] and Colin[®] radial artery tonometer measure the same blood pressure changes following deflation of thigh cuffs.(Birch and Morris 2003) A significant difference was found between the blood pressure waveforms measured with the two devices, and especially the slower recovery time with the Finapres[®] was noted. They concluded that comparison with a direct arterial line should confirm which non-invasive measurement is more accurate, but this has not been performed as yet to our knowledge.

2.2.2 Volume pulse method

The volume pulse method can be used on any superficial artery. The method is based on the relationship between intravascular pressure distention and radial displacement, being:

$$\Delta r = \frac{dr}{dp} \Delta p \quad \text{Eqn. 1.1}$$

with:

$$\frac{dr}{dp} = \frac{3}{2} \frac{r(r+h)^2}{Eh(2r+h)} \quad \text{Eqn. 1.2}$$

when considering the simple model of a cylindrical uniform isotropic vessel (with intravascular pressure p , radius r , wall thickness h , and modulus of elasticity E). (Li 2000)

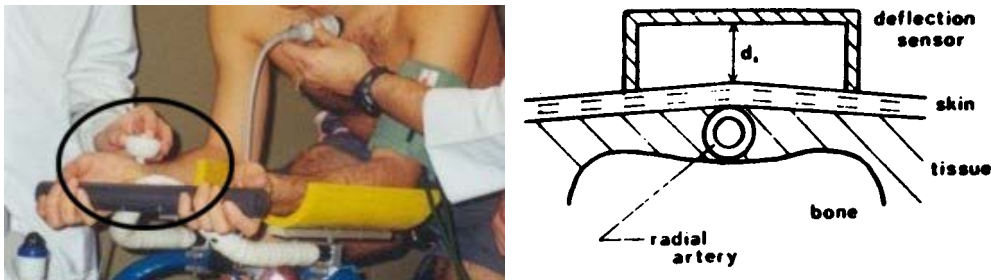


Figure 1–7 Left: The volume pulse method during an exercise test. Right: Schematical representation. (Li 2000)

The volume pulse method has been used in preliminary experiments in this thesis (Figure 1–7) and was fairly insensitive to motion artefacts, but turned out to be not accurate enough: the obtained waveforms were too dampened and only general characteristics of the shape of the wave could be assessed.

2.2.3 *Applanation tonometry*

Applanation tonometry can also be used on any superficial artery, but has a much higher resolution than the volume pulse method. In brief, a superficial artery, preferably supported by an underlying bone, is compressed and partially flattened (applanated) by the tonometric transducer. The balance of forces between the transducer ‘hold down pressure’ (HDP) and the internal pressure in the vessel allows to record the arterial waveform morphology. This signal must then be calibrated by e.g. cuff oscillometry from the upper arm. (Matthys and Verdonck 2002)

The technique, principles and drawbacks of arterial tonometry will be further explained in the following chapters as *hand-held* Millar® manual probes were chosen for the pressure measurements in this thesis. Kelly et al. reported an intraobserver variability of 4.5% and an interobserver variability of 11.6% to be achieved after 4 to 6 weeks’ use of the hand-held pen-

probe SPT-301 (Millar® Instruments Inc., Houston, TX).(Kelly, Hayward et al. 1989b) The principle of *automated* tonometry will be briefly explained here using the Colin® 7000 device as an example.

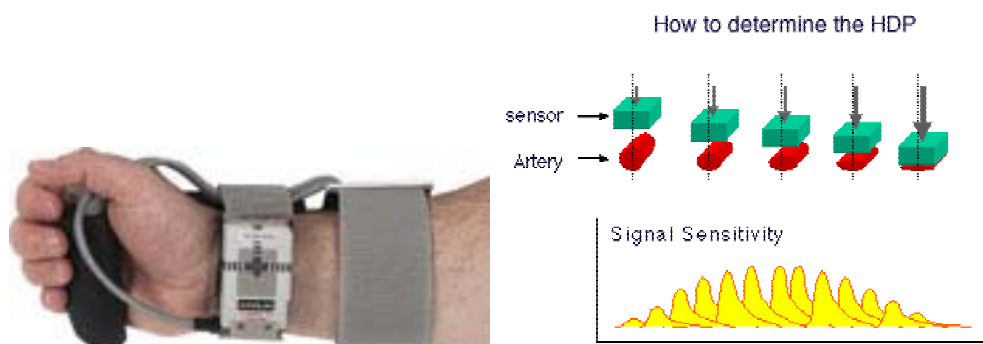


Figure 1–8 Automated tonometric device with determination of hold down pressure (HDP).(Colin® Medical Instruments Corp., San Antonio, TX)

The device consists of a sensor-array placed on the wrist over the radial artery. This sensor contains piezo-electric pressure transducers separated by 0.2 mm. A pneumatic pump presses the transducer array against the skin and tissue above the artery (HDP). To determine optimal HDP, the monitor searches through a range of pressure values until it measures a signal indicating of the form shown in Figure 1–8. When the artery is partially flattened, a graph, called a ‘tomogram’, is plotted to show sensor pulse amplitude versus sensor number in the array. The individual sensor elements whose pulse amplitudes are near the maximum pulse amplitude are calibrated to the systolic and diastolic values obtained in the oscillometric cuff measurement.(Sato, Nishinaga et al. 1993)

Apart from the common radial artery site, two alternative measuring sites have been looked at: the carotid and temporal artery. Of all superficial arteries, the carotid artery is the closest to the central aorta, with a pressure wave quite similar to the desired central pressure wave.(Karamanoglu and Fenely 1996) However, the fact that the artery is not supported by bone structure and the breathing pattern interferes with the registration, makes it a less appropriate site during exercise tests. In analogy with the work of the group around Yamakochi (Tanaka and Yamakoshi 1996; Nakagawara and Yamakoshi 2000), the temporal artery has been investigated. It is a branch of the carotid artery, thus still close to the central aorta, and supported by the skull. With an appropriate fixation mechanism this would be a handy site during exercise, but it was found that a successful palpation of the artery in order to position the tonometer was quite difficult and more patient dependent than the radial site.

3 Invasive flow measurements

The earliest method available for measuring cardiac output (CO) is based on the Fick² principle, stating that flow in a given period of time is equal to the amount of substance entering the stream of flow in the same period of time divided by the difference between the concentrations of the substance before and after the point of entry. (Nichols and O'Rourke 1990) The principle was never used by Fick himself to calculate cardiac output. By taking two blood samples at both sides of the heart, the formula for CO (l/min) using oxygen becomes (Guyton 1963):

$$CO = \frac{O_2 uptake}{arterial O_2 - venous O_2} \quad \text{Eqn. 1.3}$$

with arterial O₂ and venous O₂ in ml/l.

This method only provides for CO, thus a mean flow value. Pulsatile blood flow measurements came only later, and can be divided in 'electromagnetic' (Kolin 1936) or 'ultrasonic' (Franklin, Baker et al. 1962) devices. Both these devices usually measure velocity, which is then multiplied with the vessel's cross-sectional area to obtain volume flow.

Electromagnetic flowmeters use the property of blood that it conducts electricity. Based on Faraday³'s law of induction, blood velocity can be measured by registering the electromagnetic forces induced when aligning the blood vessel across a magnetic field. (Shercliff 1962) The ultrasonic or Doppler method is explained in more detail in the following section. Technological developments and miniaturization, combined with the introduction of catheterization advanced both the methods from cannulating or perivascular techniques to intravascular catheter-tip devices, so that they are now applied without exposing the vessel and can be used to directly measure velocity of red blood cells even in the small coronary arteries (Figure 1–9). (Mills and Shillingford 1967; Kern 2001)

² Adolph Fick, 1829-1901. German physiologist, with remarkable talent for mathematics and physics.

³ Michael Faraday, 1791-1867. English chemist and physicist, pioneer in electricity and magnetism.

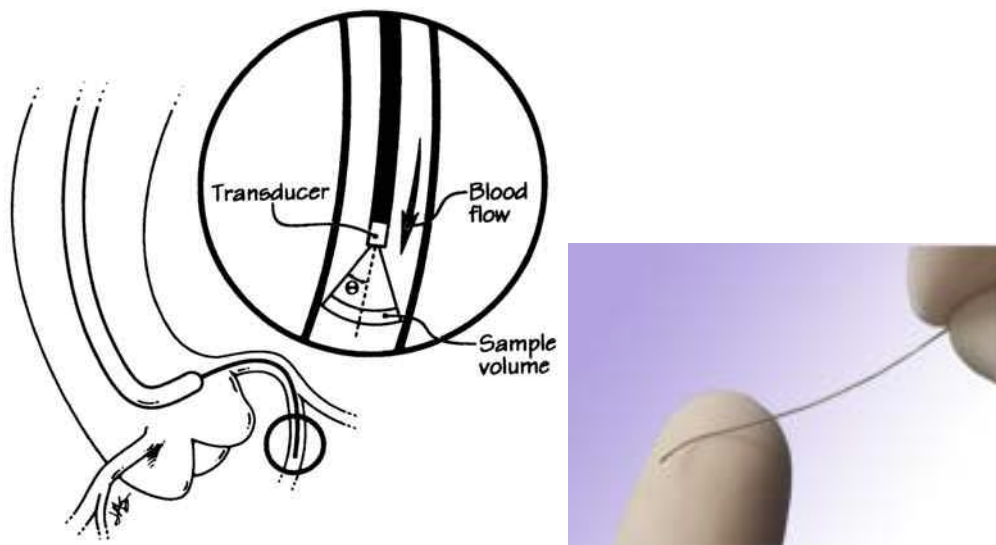


Figure 1–9 Doppler ultrasonic guidewire in the LAD coronary artery (FloWire®, Jomed, Helsingborg, Sweden).

4 Non-invasive flow measurements⁴

4.1 Medical ultrasound technology

Non-invasive assessment of blood flow information is nowadays obtained by an application of the Doppler principle to ultrasound technology. In medical ultrasound applications the employed frequencies usually comprise the range from about 1 to 20 Mhz.(Evans, McDicken et al. 1989) In 1880 Jacques and Pierre Curie discovered that applying a stress to a quartz crystal induces an electric potential across opposite faces of the material. This so-called piezo-electric effect is a most appropriate technique for medical ultrasound. The inverse piezo-electric effect is obtained by applying an electric field across the crystal to induce a mechanical deformation. In this manner, a piezo-electric transducer converts an oscillating electric signal into an acoustic wave, and vice versa. Figure 1–10 shows two examples of state of the art commercial echocardiography technology (Vivid 7 Vantage, GE Vingmed Ultrasound AS, Horten, Norway; Ultrasonic Cardiac Output monitor, Uscom, Sydney, Australia).



Figure 1–10 Left: Modern ultrasound device (Vivid 7 Vantage, GE Vingmed Ultrasound AS, Horten, Norway). Right: Research into portable ultrasound devices is growing (Ultrasonic Cardiac Output monitor, Uscom, Sydney, Australia).

⁴ Section 4.1, 4.2 and 4.3 modified with permission from De Mey, S. (2002). Diastology. Insights from model studies and clinical observations using color M-mode Doppler echocardiography. PhD Thesis. Faculty of Applied Sciences. Ghent, Ghent University.

Doppler and imaging techniques consist of illuminating the objects of interest by a beam of ultrasound and by analyzing the energy received from its interaction, i.e. reflection, absorption, or scattering with these objects. Objects much smaller than a wavelength cause Rayleigh scattering: a portion of the energy is scattered uniformly in all directions. If an object is much larger than a wavelength, it becomes a specular reflector: it acts much like a mirror. Specular reflections that return to the transducer may be a factor of 10^3 below the intensity of the transmitted signal. Backscattered ultrasound on red blood cells (Rayleigh scatter) is generally much weaker than the specular reflections from adjacent tissue interfaces.

Ultrasonic waves, applied to the chest wall and directed at the heart, are reflected back to the transducer whenever the beam crosses a boundary between tissues of different densities or acoustic impedances. The mechanical energy from these reflected sound waves, or cardiac “echoes”, is converted to electrical energy by the transducer and displayed in the form of a cardiac image (Figure 1–11).

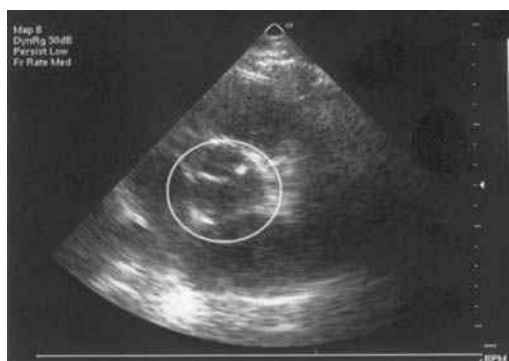


Figure 1–11 2D echocardiography suprasternal view of a closed aortic valve.

4.2 The Doppler principle

The principle that the perceived frequency of a traveling wave is altered by motion of the source, the receiver, or both, was first enunciated by Johann Doppler⁵ in 1842. Under the assumption of a stationary sound source of frequency f_0 , a receiver moving towards the sound source perceives a frequency f_R , which is given by:

$$f_R = f_0 + \frac{v}{c} f_0 \quad \text{Eqn. 1.4}$$

⁵ Johann Christian Doppler, 1803-1853. Austrian mathematician and physicist.

where v denotes the velocity at which the receiver moves and c the speed of sound. If the receiver moves away from the sound source, Eqn. 1.4 still holds, but this motion corresponds to a negative velocity.

On the other hand, if the receiver is stationary and the sound source moves towards the receiver, the latter experiences the frequency

$$f_R = \frac{c}{c - v} f_0 \quad \text{Eqn. 1.5}$$

In the case of a sound wave reflected by a moving object, the perceived frequency f_R with respect to the transmitted frequency f_0 is obtained by combining Eqn. 1.4 and Eqn. 1.5, since the reflector acts as both a receiver and a transmitter

$$f_R = \frac{c + v}{c - v} f_0 \quad \text{Eqn. 1.6}$$

The Doppler frequency f_D is defined as the difference between f_R and f_0 . Thus, the Doppler frequency caused by a moving reflector is given by:

$$f_D = f_R - f_0 = \frac{2v}{(c - v)} f_0 \quad \text{Eqn. 1.7}$$

In medical applications, the velocity v is much smaller than the sound speed ($|v| \approx 0\text{-}5$ m/s, $c \approx 1540$ m/s) and Eqn. 1.7 simplifies to:

$$f_D \approx \frac{2v}{c} f_0 \quad \text{Eqn. 1.8}$$

The Doppler frequency is not only proportional to the velocity, but also to the transmitted frequency, i.e., different Doppler frequencies are obtained, when the moving reflector is insonified with different frequencies f_0 .

It is also important to note that the receiver experiences only a Doppler frequency shift according to Eqn. 1.8, if the reflector is moving along the transmitted wave direction. For any other angle formed between the transmitter/receiver and the reflector's motion direction, the former perceives only the Doppler frequency shift corresponding to the vector component being parallel to the transmitted wave direction (Figure 1–12). Thus, Eqn. 1.8 must be scaled by $\cos\theta$:

$$f_D = \frac{2v}{c} \cos \theta \cdot f_0 \quad \text{Eqn. 1.9}$$

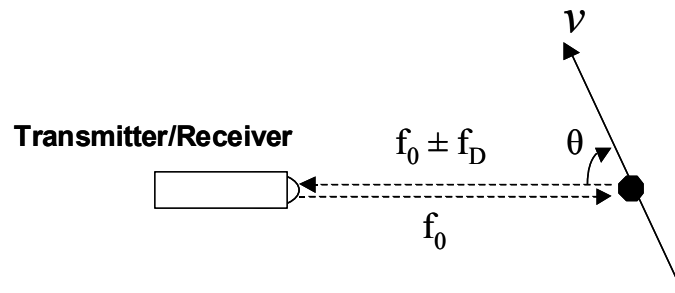


Figure 1–12 The Doppler frequency shift is proportional to the reflector's velocity component that is parallel to the transmitted wave direction.(De Mey 2002)

4.3 Doppler Modes

4.3.1 Continuous Wave Doppler

Continuous wave Doppler systems utilize a pair of piezo-electric elements to transmit and receive ultrasonic energy waves simultaneously. The transmitting transducer is continuously excited by the transmitting amplifier, which operates at a constant carrier-frequency f_0 . The receiving transducer captures the echoes from stationary, quasi-stationary, and moving objects. According to Eqn. 1.7, the desired Doppler information must be extracted from the received signal. The most common technique to achieve this is to pass the received signal through an IQ (in-phase and quadrature-phase) detector, as shown in Figure 1–13.

This demodulating scheme consists of multiplying the received echo $z(t) = \cos(\omega_0 + \omega_d)t$ by a pair of sinusoids at the transmit frequency ω_0 that are 90 degrees out of phase with each other ($\cos\omega_0 t$ and $\sin\omega_0 t$). The resulting signals are low-pass filtered to obtain $I(t) = \cos\omega_d t$ and

$Q(t) = \sin\omega_d t$. The magnitude and the phase of the Doppler shift can be determined from the quadrature components, $I(t)$ and $Q(t)$. The demodulated components can be combined to form a complex Doppler signal $z(t)$ as shown in :

$$z(t) = I(t) + jQ(t)$$

Eqn. 1.10

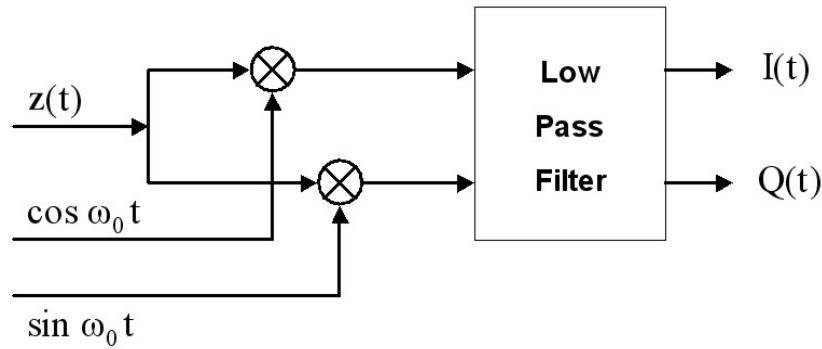


Figure 1–13 Quadrature demodulation diagram.(De Mey 2002)

A time-frequency analysis of the complex Doppler signal is performed to examine changes in the flow velocity as a function of time. A short-time Fourier transform (STFT) is generally employed to create a spectral Doppler image. The STFT first divides the signal into overlapping segments and performs a Fourier transform of each segment. The frequency (or velocity) and temporal resolution are controlled by the choice of the segment length and the overlap between the segments.

Doppler-shifted frequencies obtained from moving blood cells occur in the audible range. Normal blood flows causes Doppler frequencies in the 0-5 kHz range, whereas jets in stenotic vessel segments or from malfunctioning heart valves may cover the 5-20 kHz range. The result, however, does not only contain the desired Doppler information from blood, but also those from heart and vessel wall movements, typically in the 0-1200 Hz range. Those frequencies must be filtered out by a tunable high-pass filter, the so-called ‘Wall Motion Filter’, since their amplitudes are typically 40-100 dB higher than those from blood cells.(Isaaz, Thompson et al. 1989; Garcia, Thomas et al. 1998)

4.3.2 Pulsed Wave Doppler

While continuous wave Doppler has several strenghts, including the ability to examine high velocity flows and determine the maximum velocity along the ultrasonic beam, its major weakness is the inability to localize velocities along this same path. This weakness can be partially overcome by pulsed-wave systems as introduced in the late 1960s by Peronneau, Wells, and Baker.(Peronneau 1970; Wells 1977; Baker 1978) Transmission of a series of ultrasonic pulses, as opposed to a continuous wave, allow the user to define a range or depth of interrogation. The range specification allows the system to calculate the time required for each pulse to reach the desired depth and the reflected signal to return to the receiver. Analysis of the phase shift between transmitted and time-gated received signal, due to the movement of the ultrasound scatters, such as red blood cells, allows the estimation of blood velocity.

Ultrasound bursts are transmitted repeatedly with a pulse repetition frequency PRF. The maximum PRF is limited by the range of the target r_t and the speed of sound c :

$$\text{PRF}_{\max} = \frac{c}{2r_t} \quad \text{Eqn. 1.11}$$

For example, the examination of a target at 10 cm requires a time-of-flight equal to $2r_t/c$, or approximately 130 μs . The number of pulses that can be transmitted to make a velocity estimate from a single sample volume, or range gate, is limited by the duration in which the flow through the sample volume is considered stationary.

The time-of-flight for a burst to travel in parallel to the ultrasound beam towards a sample volume at distance l and back to the transducer is given by:

$$t_f = \frac{2l}{c} \quad \text{Eqn. 1.12}$$

Thus, the phase difference between the transmitted wave (reference wave) and the received echo is given by:

$$\phi = 2\pi \cdot f_0 \cdot t_f = 2\pi \cdot f_0 \frac{2l}{c} \quad \text{Eqn. 1.13}$$

By definition, the frequency of a signal is the derivation of its phase with respect to time:

$$\frac{1}{2\pi} \frac{d\phi}{dt} = 2f_0 \frac{1}{c} \frac{dl}{dt} \quad \text{Eqn. 1.14}$$

Since dl/dt corresponds to the projected velocity $v \cdot \cos\theta$, Eqn. 1.14 represents the Doppler frequency or:

$$f_D = 2f_0 \frac{v}{c} \cos\theta \quad \text{Eqn. 1.15}$$

From this equation it can be noticed that, although generally called a Doppler system, the pulsed wave system does not measure a frequency shift. The system detects the displacement in the reflected signal that is acquired for a set of transmitted pulses.

The returning echo, or backscattered signal, is analyzed for a specific interval following the time-of-flight for each pulse. The finite duration of the pulse, typically three to six cycles of the transmit frequency, results in a measurement derived from a range interval as opposed to an idealized point location. The duration of a three cycle pulse at $f_0 = 2$ MHz is $1.5 \mu s$ which corresponds to an axial measurement length of approximately 1.2 mm.

The trade-off between temporal and velocity resolution is similar to the case for continuous wave Doppler analysis. Continuing the earlier example of velocity estimation at 10 cm, a series of 64 pulses can be transmitted and received in approximately 8.8 ms. This results in a temporal resolution of approximately 10 ms and a frequency resolution of approximately 120 Hz. This frequency resolution is equivalent to a velocity resolution of approximately 4.7 cm/s. The temporal resolution can be increased to approximately 5 ms using a series of 32 pulses, however, the velocity resolution decreases to approximately 9.4 cm/s.

The gating of the echoes at a fixed time after the burst is transmitted implies the sampling of the received signal. Therefore, from Shannon's sampling theorem, the PRF must be twice as

much as the maximum frequency shift to be detected. Hence, the maximum unambiguously measurable velocity, the so-called Nyquist velocity, yields:

$$v_{\max} = v_{\text{Nyq}} = \frac{c}{2f_0 \cos \theta} \frac{\text{PRF}}{2} \quad \text{Eqn. 1.16}$$

Filling in Eqn. 1.11 in Eqn. 1.16 reveals an additional trade-off between velocity and spatial resolution imposed by the pulsed-wave system.

4.4 Practical example

As an example, the CO for patient John Doe is calculated by means of ultrasound. First a cardiac image as shown in Figure 1–11 was made by means of 2D echocardiography to measure the LVOT (left ventricular outflow tract or cross-sectional area of the aortic valve). The diameter of the LVOT was found to be 2.58 cm. Assuming a circular LVOT, one finds $\pi(2.58)^2 \text{ cm}^2$. Next, a Doppler spectogram was obtained by means of continuous wave Doppler, representing the blood flow velocity pattern of a few cardiac cycles (Figure 1–14, left). Following, the cardiac cycles are averaged and contour-traced (Figure 1–14, right). The maximum velocity (peak of the traced curve) appears to be 0.6797 m/s. Integrating the surface underneath the tracing, allows to calculate the mean flow velocity (0.1455 m/s). Multiplying the LVOT by the mean velocity and adjusting for the correct dimensions finally results in a CO of $\pi(2.58)^2 \times 0.1455 \times 10^{-2} \cdot 60 \text{ l/min} = 4.565 \text{ l/min}$.

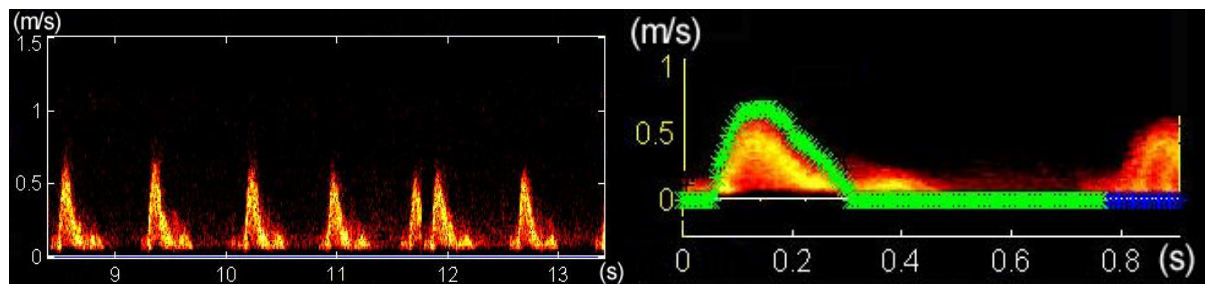


Figure 1–14 Left: A Doppler spectogram by means of continuous wave Doppler, representing the blood flow velocity pattern of a few cardiac cycles. Right: The cardiac cycles are averaged and contour-traced.

5 Combined pressure and flow measurements

In the previous sections various invasive and non-invasive devices have been looked upon. The most complete, quantitative description of the arterial system can be done by acquiring simultaneous pressure and flow waveforms at the site of the aorta ascendens, just above the aortic valve, which is the start of the arterial tree. In the past these measurements were only possible invasively, and stayed limited to animal experiments or exceptional small scale patient studies.(Mills, Gabe et al. 1970; Nichols, Conti et al. 1977; Murgo, Westerhof et al. 1980) Nowadays, several non-invasive methods are available but they are usually built for very specific investigations e.g. blood pressure measurement by means of a cuff manometer, heart rate and heart rate variability measurement with an electrocardiogram recorder, blood velocity through heart valves with ultrasound devices, etc. Although the information obtained from these signals separately is useful and important as such, using them in a combined way becomes a diagnosis tool that allows a more profound analysis of the cardiovascular system.

To provide for the specific requirements of combined pressure and flow analysis, at first, some tools for audio post-processing were looked upon as advanced programs in this field contain features to derive and visualize Doppler spectra, e.g. Adobe[®] Audition (Adobe Systems Inc., San Jose, CA) formerly known as Cool Edit Pro[®] (Syntrillium Software Corporation, Phoenix, AZ). In need of software that besides analysis also does acquisition, negotiations were setup with Notocord[®] (Notocord Systems, Croissy, FR) to add a new flow measurement module to the Notocord-Hem[™] package for biomedical signal processing, but these negotiations were discontinued by the company. Other products that received attention were the Handyscope[®] (Tie Pie Engineering, Sneek, NL) and the Advanced CODAS Analysis software (Dataq[®] Instruments, Akron, OH), but as they didn't completely fulfill the needs (e.g. no Doppler spectrum visualization), an attempt was made for an in-house acquisition program in Labview[™] environment (National Instruments Corporation, Austin, TX). Since in the end more knowledge and most importantly more post-processing analysis modules (e.g. SAM, [®]S Carrier) were already in-house available in Matlab 6[®] environment (The Mathworks, Inc., Natick, MA), the efforts for an acquisition instrument were redone in Matlab 6[®], which is presented in Chapter 4 of this part.


Summary

After a brief historical overview, the invasive techniques for blood pressure measurement were discussed. This included (radial) arterial cannulation for the direct measurement of blood pressure as well as coronary pressure guidewires to be used during interventions.

Several devices for non-invasive pressure measurement were considered. Discrete measurements are important for calibration purposes. They can be divided into the manual auscultatory method using a Riva-Rocci sphygomanometer and Korotkoff sounds on one hand, and the automated oscillometric devices on the other hand. Continuous pressure measurements can be done with the Penaz method, the volume pulse method or applanation tonometry. These three methods have been described and experimented with. Tonometry was chosen to be investigated further in this thesis.

Invasive measurements of pulsatile flow are either done with electromagnetic flowmeters or by ultrasonic devices. Measurement of cardiac output can make use of the Fick method. Non-invasive measurement of flow is being done by Doppler-echocardiography. The Doppler principle has been explained as well as its implementation in the ultrasound device. The different modes in which acquisitions can be performed were described (continuous wave Doppler and pulsed wave Doppler).

In the past, simultaneous pressure and flow measurements were invasive and difficult to obtain in clinical practice. Nowadays non-invasive measurement devices are available but they are not still not used in a combined, synchronized way, which would greatly enhance haemodynamic diagnostics. Attention has been given to commercial signal processing software, but the use and development of in-house acquisition and analysis technology seemed better suitable for further applications in this thesis.



2 Development and modelling of arterial tonometry*

* The content of this chapter has been published in Technology and Health Care 10:65-76 (2002)

Development and modelling of arterial applanation tonometry: a review
Koen Matthys and Pascal Verdonck

Abstract

Arterial tonometry allows non-invasive and continuous registration of the arterial pressure waveform, by applanating (flattening) a superficial artery supported by bone with an external transducer. Inspired by ocular tonometry used for eye disease diagnosis, G.L. Pressman and P.M. Newgard built the first arterial tonometer in 1963, and derived a discrete, linear mechanical model. Accuracy remained poor until new sensor production techniques (silicon technology) arrived. G.M. Drzewiecki et al. published a second, more elaborate theoretical model for tonometer positioning in 1983. Few years later, the first modern tonometers were commercialized. Although the problems of sensor positioning, motion artefacts and calibration still exist, the tonometer has proven its usefulness in arterial compliance and hypertension studies. Attention should now go to analysis of the arterial pressure waveforms, and the combination with other signals (e.g. flow wave morphology) to allow a complete non-invasive haemodynamic description of the heart and the arterial tree.

1 Introduction

Arterial applanation tonometry is a technique that allows continuous and non-invasive registration of the arterial pressure waveform. Such a continuous registration offers a pressure-time wave morphology that cannot be assessed by conventional cuff methods (Korotkoff/auscultation or oscillometry). Being non-invasive, it also means a fast and simple approach and above all, with only a small load for the patient compared to an interventional pressure measurement.

The principle of applanation tonometry is illustrated in Figure 2–1: a pressure transducer is placed upon a superficial artery, which is supported by bone structure so that adequate applanation of the vessel can be achieved to obtain the pressure waveform. As applanation tonometry can only provide for the *waveform*, this signal has to be calibrated by means of an external method, for example a cuff technique giving minimum and maximum blood pressure values, allowing the waveform to be rescaled to its correct offset and amplitude.

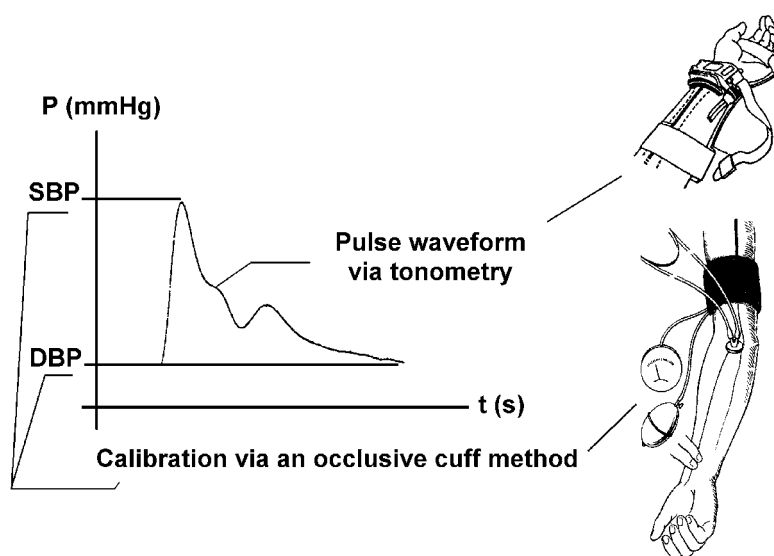


Figure 2–1 Arterial applanation tonometry provides a pressure-time wave morphology, which has to be calibrated by an external method, e.g. a conventional cuff technique. SBP: systolic blood pressure, DBP: diastolic blood pressure.

Arterial blood pressure measurement has evolved through history from ‘feeling or palpation of the pulse’, to the use of fully automatic pulse monitors. Pulse palpation has a very old and even somewhat mystic background. It can be traced back in literature as far as 2500 BC, when

the book ‘Huang Ti Nei Ching Su Wen. The Yellow Emperor’s Classic of Internal Medicine’ is believed to have been written by emperor Huang Ti.(Naqvi and Blaufox 1998) Some people claim that he was only a legendary figure and the book was actually written by a great many people, composed to one manuscript around the second century BC. Nevertheless, palpation of the pulse has been described by several ancient civilizations independently: the Egyptians, Greeks and Romans all left clues behind that are unmistakably proof of the importance they attached to diagnosing the arterial pulse in their medical practice.(Allbutt 1921; Dobson 1927; Bettman 1979)

The continuous registration of the pressure waveform, however, is from a much later period (midst of the nineteenth century) when Karl Vierordt, and especially Etienne Jules Marey invented and optimized the so-called ‘sphygmograph’.(Naqvi and Blaufox 1998) Somehow, the interest in the pulse morphology faded rather quickly in favour of the measurement of only brachial systolic and diastolic blood pressure values, which at the end of the nineteenth century was made possible via the Riva-Rocci cuff method (1896).

Quantifying blood pressure through systolic and diastolic *values* became a simple and widespread diagnostic routine, but a lot of information hidden in the pressure *waveform* remained untouched by this method. It was only in the early 1960s that the importance of the pulse morphology was again brought under attention with the development of and advances in arterial applanation tonometry. Moreover, the clinical use of tonometry had its breakthrough only in the second half of the 1990s, so it has definitely taken some time to convince the medical world of the usefulness of such a device. Surely, the practical problems of calibration and positioning of the tonometer, contributed to the slow rise of its clinical application.

2 Techniques, devices and modelling

The basic concepts leading to arterial applanation tonometry were introduced from a very different angle. They can be traced down to the field of ophthalmology, where a technique called ‘ocular’ tonometry was already routinely used in the 1960s for the diagnosis of eye disease (and is still being used up to this day, but in a more modern version). It is a tool for measuring the internal pressure in the eye (normal value $\leq 20\text{mmHg}$), and is used to diagnose chronically elevated intraocular pressure (‘glaucoma’).

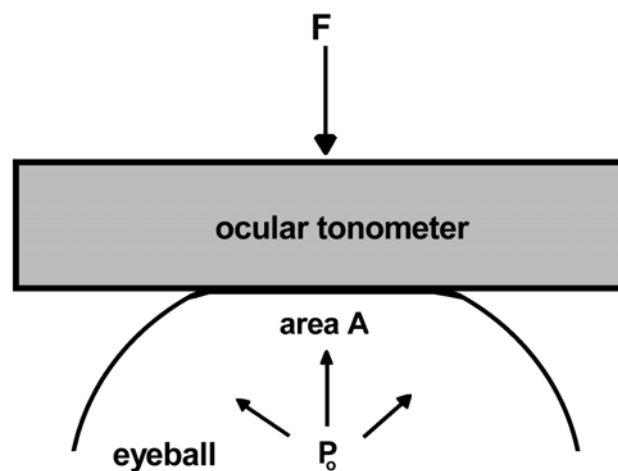


Figure 2–2 Illustration of the Imbert-Fick principle: internal pressure (P_o) in a spherical body with an infinitely thin, dry and elastic membrane wall, equals the force (F) exerted on this body, divided by the applanation surface (A). Due to applanation, initial intraocular pressure P_i rises to a value P_o . Hence Imbert-Fick law can be written as: $P_o = F/A$. (modified from (Duke-Elder and Gloster 1968))

For a better understanding of the importance of applanating the measuring site, whether it is an eye or an arterial vessel, the so-called Imbert-Fick principle (Figure 2–2) has to be addressed. Looking at the eye, the Imbert-Fick law states that internal pressure P_o in a spherical body with an infinitely thin, dry and elastic membrane wall, equals the force F exerted on this body, divided by the applanation surface A . (Duke-Elder and Gloster 1968) Of course the eye and cornea do not completely match the ideal conditions described above, but clinical practice has shown that the Imbert-Fick principle applies with sufficient approximation. Due to applanation with the ocular tonometer, original intraocular pressure (IOP) P_i rises to a value P_o . Hence the Imbert-Fick law can be written as: $P_o = F/A$, and if one can measure F and A , P_o can be derived.

On one hand, the exerted force F will be augmented with a small, unknown force because of the surface tension in the thin layer of tear fluid covering the cornea. On the other hand, the bending forces in the corneal tissue, which occur along the edge of the applanation surface A , will exert an additional force to be countered also by the force F , apart from the IOP. It was finally determined that a circular applanation surface with diameter of 3.06 mm is the most appropriate position for the tonometer, where tear capillarity and corneal bending forces balance each other and the Imbert-Fick law applies. (Goldmann and Schmidt 1957)

The gold standard in ocular tonometry is still the Goldmann tonometer from back in the 1950s (Scheie and Albert 1977), but the arterial tonometer found its origin in a more advanced but quite similar version namely the MacKay-Marg ocular applanation tonometer from the beginning of the 1960s (Figure 2–3). (Mackay, Marg et al. 1960) Apart from the improved (electronic) data-recording and visualization, this ocular tonometer had two qualities that were also present in the first arterial applanation tonometers: the introduction of an applanating surface on the tip of the tonometer in which the actual and smaller sensing area was embedded, and the use of the LVDT principle (Linear Variable Displacement Transducer) to measure the pressure. In the remainder of this chapter, the tonometer device will be referred to as ‘transducer’, while the actual sensing part of the transducer will be addressed as ‘sensor’.

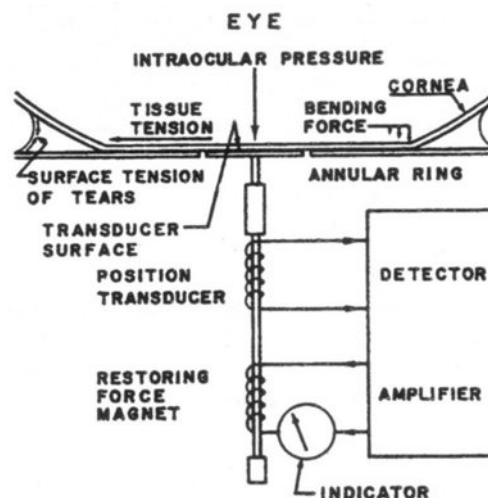


Figure 2–3 Schematic drawing of the MacKay-Marg ocular applanation tonometer from the beginning of the 1960s. Remark the applanating surface (‘annular ring’) and the use of the LVDT principle (two coils and protruding rod). (reprinted with permission from (Mackay, Marg et al. 1960))

In the early stage, mostly transducers with a membrane were used. A patent study by D.E. Bahr and K.R. Clark (Bahr and Petzke 1980) showed that H.R. Bierman in 1951 was already granted a patent for a device that can be seen as the forerunner of the current tonometer. The transducer consisted of a cylindrical, air filled metal chamber with a membrane on one end and closed on the other. A strain gauge sensor was mounted on the inner surface of the membrane. The diameter of the membrane was however many times greater than the diameter of the artery, which was the reason according to Bahr and Clark why only an approximation of the pulse waveform could be obtained. Moreover, this problem was aggravated by the relatively low sensitivity of the sensors applied in those days.

In 1963 G.L. Pressman and P.M. Newgard (Pressman and Newgard 1963) from Stanford Research Institute took on a radically new approach. Because of the later success, they are generally granted credit for building the first arterial tonometer. In the same period other attempts were made, for example by R. Bigliano (Smith and Bickley 1964) (Dupont de Nemours & Company, 1964) using a transducer with a small gas chamber but this never passed the research stage. Pressman and Newgard built a tonometer based on their theoretical model. The discrete and linear mechanical model they derived is depicted in Figure 2–4 (left). Compressible tissue is represented as linear springs, assuming that the deflections caused by applying the tonometer are so small that non-linearities are insignificant. The artery is assumed to rest on a firm base, to have elastic walls and to be surrounded by uniform tissue. (Pressman and Newgard 1963)

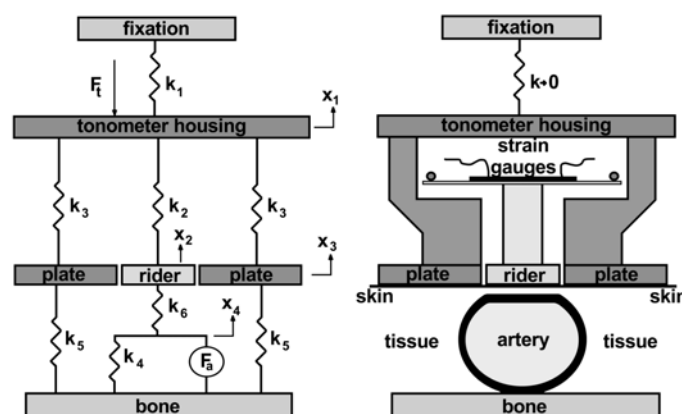


Figure 2–4 Linear spring model for arterial tonometry as derived by G.L. Pressman and P.M. Newgard in 1963 (left), and schematical drawing of a practical implementation (right). (modified with permission from (Pressman and Newgard 1963))

Their model distinguishes between parameters for the artery and surrounding tissue (F_a , k_4 - k_6) on one hand, and parameters for the transducer itself (F_t , k_1 - k_3) on the other, with F representing a force and k a linear spring constant. In this model the masses of transducer and artery system are ignored. For the artery and tissue, F_a represents the force exerted by the arterial pressure, while k_4 determines the arterial wall elasticity, and k_5 and k_6 the compressibility of the tissue adjacent and above the artery respectively. For the transducer, F_t stands for the HDP by which the transducer is pressed against the skin. The spring constant k_1 represents the transducer mounting, and k_3 is a parameter of the side plate or applanation surface, but which actually serves to model the relaxation of the underlying tissue.

Solving the corresponding equations of this model, it can be derived that the measured displacement $\delta = x_2 - x_3$ can be written as $\delta = F_a/k_2$ for $k_3 \rightarrow \infty$ (i.e. no relaxation of surrounding tissue), $k_4 \rightarrow 0$ (i.e. no normal wall tension) and $k_1 \rightarrow 0$. Although you would expect $k_1 \rightarrow \infty$ (i.e. infinitely stiff fixation of the tonometer) to firmly restrain the transducer, in practice this seems impossible to achieve, and that is why Pressman and Newgard used a pneumatic loading principle to maintain F_t constant and reduce k_1 nearly to zero. To reduce k_4 , they advise to press the transducer against the artery until a portion of the artery wall is flattened. Referring to MacKay's research on ocular tonometry (MacKay 1960), Pressman and Newgard used the Imbert-Fick principle to assume that arterial force F_a equals arterial pressure P_a multiplied by the applanated wall area A ($F_a = P_a \cdot A$). Under the conditions that transducer spring constant k_2 (i.e. stiffness of arterial rider) and applanated wall area A remain constant, the measured displacement δ will be directly proportional to arterial pressure P_a :

$$\delta = \frac{F_a}{k_2} = \frac{P_a \cdot A}{k_2} = \lambda \cdot P_a \quad \text{Eqn. 2.1}$$

with $\lambda = A/k_2$.

In the same article, Pressman and Newgard mention two versions of a tonometer transducer based on their theoretical model. The first observation is that the dimensions were already smaller and more comparable to those of the radial artery diameter. They also state that the sensing area should even be somewhat smaller than the artery, accurately positioned and centred over the artery. This sensing area formed the tip of a so-called 'arterial rider' which

was nothing more than a rod protruding through an aluminium applanating plate and fixed on a beam on which the strain-gauge sensors were applied (Figure 2–4, right). Arterial rider surface area of their most optimized transducer was ca. 2.5 mm². This concept of applanating plate and sensing rider is very similar with the concept of the mentioned Mackay-Marg ocular tonometer.

Some simple validation experiments (measurements during conversation, eye blinking, head movements...) were performed on the temporal artery (supported by the skull). (Pressman and Newgard 1965) In future vascular studies, usually the radial artery (pulse) or carotid artery (neck) was chosen. While the radial artery is a very appropriate and traditional measuring site, frequently used through history for palpation of the pulse, the carotid artery is not supported by bone, which makes it difficult to apply the tonometer. Furthermore there is always the danger of plaque rupture (going straight to the brains), especially with older people. On the other hand, the carotid artery waveform is very similar to the aortic waveform, explaining its popularity.

The results of the experiments of Pressman and Newgard were quite promising but the device was still hard to position and a strap alone was not sufficient. Manual positioning and correction were necessary because of the sensitivity to movement of the patient. (Pressman and Newgard 1963) Also the sensor was not yet of very high accuracy and the whole transducer still had relatively large dimensions, which is not favourable for accurate measurement, as will also be shown in the second theoretical model by G.M. Drzewiecki et al. (1983). (Drzewiecki, Melbin et al. 1983)

A contemporary named H. Okino published an in vitro study in 1964, in which he did some experiments on small pressurized chambers covered with a membrane and thin/thick walled elastic tubes loaded with membrane transducers as well as transducers based on a protruding rod. (Okino 1964) His conclusions were that an external sensor seemed likely to reliably obtain arterial pulse waveforms, but that an independent objective measurement e.g. sphygmomanometry was necessary for calibration of the pulse waveform. Although the findings of Okino were later overruled by the work of the aforementioned Drzewiecki, due to the use of too large sensors relative to the in vitro tubes, the fact remains that up to this day an absolute calibration still has not been accomplished and the traditional occlusive cuff methods are still used as an external calibration technique.

Anyhow, the Pressman and Newgard tonometer and their force-measuring concept was a huge step ahead and many different versions of this device came about shortly afterwards. J. Beneken and G.M.A. van der Hoeven (Van der Hoeven and Beneken 1970) built a transducer consisting of a piezo-resistive element placed on a small cantilevered beam. They also used the flat-plate concept of Pressman and Newgard in the sense that an O-ring surrounded the actual sensor.

A more important variation realized by P.D. Stein and E.F. Blick (Stein and Blick 1971) was based on the second principle already used by Mackay-Marg, namely the 'Linear Variable Displacement Transducer' (LVDT) that consisted of an electromagnetic core movement in a coil, but now placed on a superficial artery instead of the eyeball. According to Stein and Blick this was not only an appropriate method for the non-invasive continuous recording of the complete blood pressure waveform (e.g. during surgery), but also for observing transient effects of this pressure waveform, induced by drugs or physiological interventions (e.g. Valsalva manoeuvre).

Direct calibration, precise positioning and movement artefacts were still the major problems for Stein and Blick, although a mounting-bracelet for the sensor was already installed. Simultaneous intra-arterial (pressure catheter in the subclavian artery or aorta) and tonometrical pressure recordings were done in patients during cardiac catheterization and showed good agreement, even during transient effects. (Stein and Blick 1971) It is noteworthy that the intra-arterial pressure recording (aorta) was not done at the same locations as the tonometrical recordings (at the wrist/radial artery, and the foot/dorsal pedal artery) and that the observation was made that the radial pressure signal had better correlation with the aortic pressure signal than the dorsal pedal pressure signal, which perhaps today sounds logical seen the current knowledge on composition of blood pressure waveforms (propagated and reflected waves). (Nichols and O'Rourke 1990) The fact that the idea of wave propagation in the human vascular tree was not wide spread or fully understood at the time, is perhaps not surprising as basic *in vivo* (animal) experiments on this subject were being done in that very same period (O'Rourke 1971) (although the pulse propagation concept had already been described earlier (Hamilton and Dow 1939)).

The Bahr-Petzke tonometer (Bahr and Petzke 1973; Bahr, Dhupar et al. 1977) was a step in the right direction on the field of miniaturization and used a piezo-resistive sensor

($\varnothing = 1$ mm) made by the Kulite Company. It was a device comparable to the Pressman-Newgard tonometer and also used an applanation surface.

Apart from sensor quality, the movement of the hand and the forearm and especially of the thumb, caused motion artefacts due to the changing of the cross sectional area of the pulse during measurement. A solution is of course to measure at other locations than the radial artery. To obtain a good signal, a supporting bone structure is however required, and this condition limits the possible measuring sites. As mentioned the temporal artery (on the skull, near the temple) is also suitable, but could not find many support. The idea of the temporal artery was however recently rediscovered by the research group of K. Yamakochi (Tanaka and Yamakoshi 1996; Nakagawara and Yamakoshi 2000), although they use a different technique than tonometry for the continuous blood pressure measurement (so-called ‘volume compensation method’).

The reproduction of the pulse remained from an intermediate quality, and it wasn’t until the end of the 1970s that things really changed when sensors with appropriate limited dimensions and high accuracy appeared, because of the upcoming new sensor production techniques and especially the silicon technology.

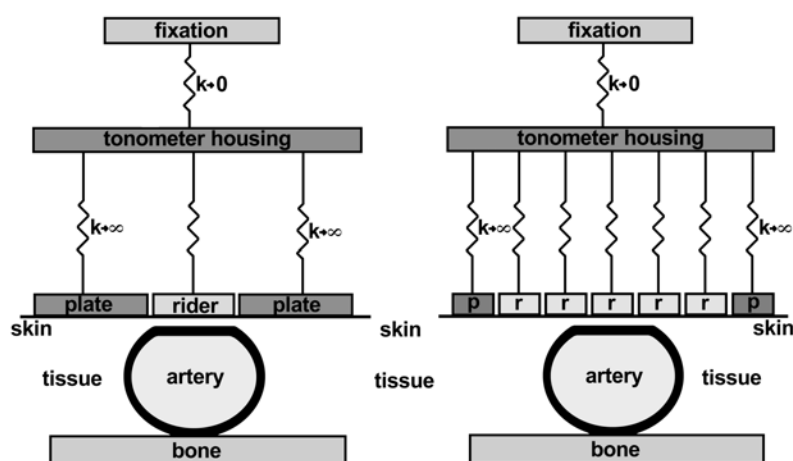


Figure 2–5 Linear spring model of a tonometer with one arterial rider (left) vs. a transducer with an array of sensors (right). (modified from (Weaver, Eckerle et al. 1978))

In 1978 the tonometer of Pressman and Newgard was optimized at SRI International (formerly: Stanford Research Institute) by C.S. Weaver, J.S. Eckerle and P.M.

Newgard.(Weaver, Eckerle et al. 1978) They developed a transducer with multiple sensors to resolve most of the positioning problem (Figure 2–5, right). The basic idea was that there would always be one of the sensors picking up a good signal. This reasoning could of course only be put to practice through the far-going miniaturization of the sensors (the whole transducer has to be small compared to the artery, so the individual sensors have to be even smaller). This was realized with an array of sensors (setup in line) on a silicon substrate via integrated circuit (IC) technology.(Eckerle and Newgard 1976) They also developed an algorithm to select the sensor that picks up the best signal (a so-called ‘artery finding algorithm’).

Since then tonometry was refined more and more, and a second and more elaborate theoretical model concerning positioning of the tonometer was published by G.M. Drzewiecki et al. in 1983.(Drzewiecki 1979; Drzewiecki and Noordergraaf 1979; Drzewiecki, Melbin et al. 1983)

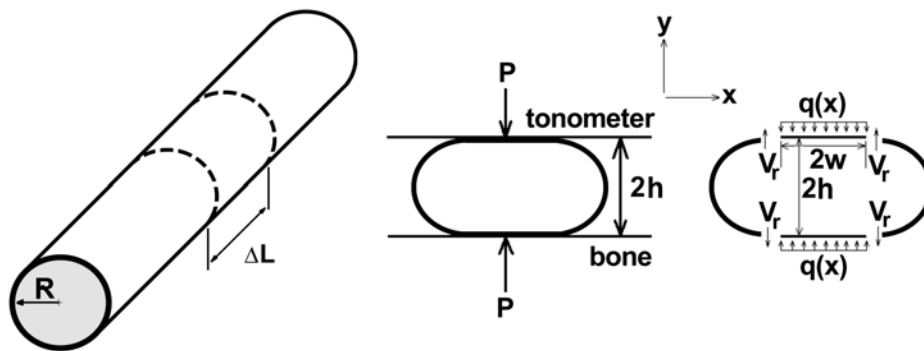


Figure 2–6 Representation of the theoretical model for arterial tonometry derived by G. M. Drzewiecki et al. in the early 1980s. (modified with permission from (Drzewiecki, Melbin et al. 1983))

An artery is now represented by a cylindrical tube, instead of a spring model (Figure 2–6). In this model the skin layer is neglected and a homogeneous and isotropic artery wall with a small thickness is assumed. In reality the Young’s modulus of the wall tissue is not a constant, and the wall thickness can actually be up to 20% of the artery radius, but including this would have strongly increased the complexity of the model.

Assuming also a uniform deformation of the artery along its length, every cross-section will have an identical stress and strain except near the ends (‘de St. Venant’s principle’), allowing to analyze only one artery segment with length ΔL . In Figure 2–6 (middle) the cross-sectional

area is clamped between two parallel plates: on one hand the supporting bone, and the tonometer on the other. The radius of the undeformed artery is named R and the distance between the two plates is $2h$. When the tonometer is applied, the segment is distorted along the vertical axis, hence shortening the distance between the plates. The applied HDP and the contact length can be written as a function of the distance $2h$. From this, Drzewiecki derived the contact stress distribution curve by means of curved beam mechanics. The derived contact stress $\sigma_c(x)$ is depicted in Figure 2–7 as a function of x (artery centre is considered $x = 0$), and this for different degrees of deflection in the y direction. (Frisch-Fay 1962)

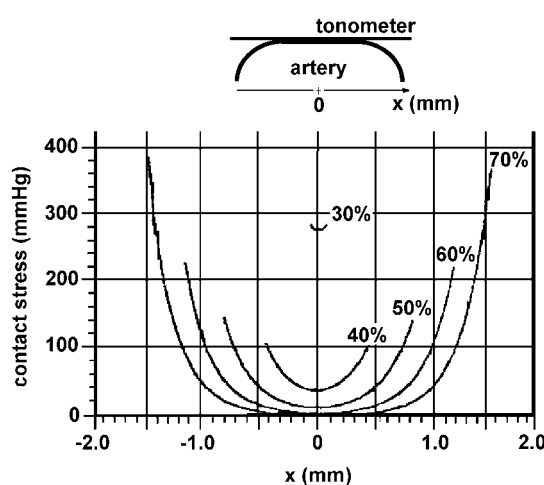


Figure 2–7 Contact stress distribution curves as calculated by G.M. Drzewiecki with his theoretical model. (modified with permission from (Drzewiecki, Melbin et al. 1983))

When the contact stress is zero, the tonometer should measure only the internal blood pressure and no extra deformational stresses. Figure 2–7 shows that the transducer has to be placed very near the centre line, and a sufficient HDP has to be applied so that a deflection degree is reached where deformational stresses become negligible, and the correct blood pressure is measured. It is worth noting that the ‘difference’ between a good and a bad measurement is within fractions of millimetres. This would explain the problems reported in earlier experiments. (Pressman and Newgard 1963; Okino 1964; Stein and Blick 1971) Basically, this second and more refined theoretical model yielded the same conclusions as before: accurate positioning and miniaturization was the key to measuring correctly, while the calibration problem still remained unsolved. The model was however of great importance to the development of arterial tonometers, as it was the first to analyze the evolution and distribution of stress and strain during a tonometer measurement.

Few years later, the first prototypes of the tonometers that are currently commercialized were developed. In 1989 the high-fidelity Millar[®] pen-probe tonometer was developed and validated by R. Kelly et al. together with H. Millar (Millar[®] Instruments, Inc., Houston, TX) and D. Winter (Southwest Research Institute, San Antonio, TX). (Kelly, Hayward et al. 1989a) The latter was together with J.S. Eckerle from SRI International also involved in the development of more sophisticated “self-positioning” devices, e.g. the Colin[®] tonometers (Colin[®] Medical Instruments Corp., San Antonio, TX) as described by O. Kemmotsu et al. in 1991. (Kemmotsu, Ueda et al. 1991a)


3 Discussion and conclusion

To our knowledge, today Millar[®] Instruments Inc. (Houston, TX), Colin[®] Medical Instruments Corp. (San Antonio, TX) and Hypertension Diagnostics[™] Inc. (Eagan, MN) are the only players on the commercial tonometer market (Figure 2–8). They provide three basic products going from a hand-held manual pen-probe (Millar[®], left), to a complete automatic multiple array sensor (Colin[®], right), and a variation in between, where a single sensor is mounted in a fixation mechanism (Hypertension Diagnostics[™], middle).



Figure 2–8 Current commercially available tonometers: Millar[®] Instruments pen-probe (left), Hypertension Diagnostics[™] wrist-probe (middle), Colin[®] Medical Instruments Corp. automated probe (right).

Although the available tonometers are nowadays very accurate and of sufficiently small dimensions, the 3 basic problems as been set out 40 years ago still exist today: (i) positioning has to be very precise and only the Colin[®] devices do this in an automatic way, (ii) motion artefacts are still a problem and that is also why almost no studies have been done with tonometry during exercise conditions, and (iii) the calibration still has to be done with an external measurement which is most often a brachial cuff, thus introducing not only the inherent limitations of a discrete cuff-measurement but also a consistent error due to the difference between brachial (cuff) and radial (tonometric) pressure. Especially when aiming for a complete non-invasive haemodynamic description of the heart and the arterial tree, the combination with other signals (e.g. blood flow wave morphology) needs to be taken into account, as pulse waveforms alone cannot provide for this. Combination of non-invasive pressure and flow was already used by e.g. R. Kelly et al. (Kelly and Fitchett 1992) and R.H. Marcus et al. (Marcus, Korcarz et al. 1994) and will allow to extend some pioneering invasive studies from the 1960s and 1970s (O'Rourke and Taylor 1967; Mills, Gabe et al. 1970; Nichols, Conti et al. 1977; Murgo, Westerhof et al. 1980) to larger populations and with less load for the patient.



3 Arterial tonometry as an alternative for long-term intra-arterial pressure monitoring*

* The content of this chapter has been submitted to the British Journal of Anaesthesia (Br J Anaesth, march 2004):

Barriers to the introduction of applanation tonometry as an alternative for intra-arterial pressure monitoring

Koen Matthys, Alain Kalmar, Patrick Segers, Pascal Verdonck, Michel Struys, Eric Mortier

Abstract

Arterial cannulation with continuous pressure transduction and waveform display remains the accepted standard for blood pressure monitoring in, for instance, the operating theatre during surgery or the intensive care unit. Several peripheral arteries are available for percutaneous cannulation, but radial artery pressure monitoring is most common in anaesthesia and critical care. Arterial tonometry is a non-invasive technique that allows continuous registration of the arterial pressure waveform with only a small load for the patient compared to an interventional pressure measurement. The technique can be applied on any superficial artery supported by bone structure but is most often performed at the radial site.

In this patient study, an invasive (IBP) and non-invasive tonometric (TBP) pressure monitoring were performed on the left and right radial artery in 3 patients undergoing major neurosurgical operation. A total of 5.7 hours of combined TBP and IBP were recorded. In a subsequent off-line analysis, TBP data were compared to IBP both in a qualitative way and by calculation of root mean square differences (RMS). A manual tonometer probe was used to better investigate the different error-introducing aspects. Specific problems of tonometric fixation, positioning, calibration and recalibration are discussed, as well as the potential and limitations of automated tonometry devices. It is shown that physiological alterations at the site of TBP measurement are an important source of artefacts.

Although TBP performed fairly well as an alternative for IBP in steady state scenarios, it was not able to detect relevant pressure variations at all times and in these cases a rather high degree of unpredictability was present. One must conclude that at this point arterial tonometry remains a too unreliable technique for long-term use during a delicate operative procedure.

1 Introduction

In anaesthesia and critical care, arterial cannulation with continuous pressure transduction and waveform display remains the accepted standard for long-term blood pressure monitoring. Most commonly, radial artery pressure is registered because it is easy to perform and rarely associated with complications.(Mandel and Dauchot 1977; Slogoff, Keats et al. 1983) Several techniques are used for placing an arterial catheter, but arterial cannulation using an integrated needle-guidewire-catheter assembly is routinely performed. Despite the qualities of this technique, it remains an invasive technique with a substantial load for the patient.

A non-invasive method with potential to be used for pressure monitoring is arterial applanation tonometry (Pressman and Newgard 1963; Drzewiecki, Melbin et al. 1983). Known clinical applications use the tonometer for short term recordings of a few cardiac cycles (Armentano, Graf et al. 1998; Bank, Kaiser et al. 1999; Tanaka, Dinunno et al. 2000) but the potential of long-term non-invasive monitoring has not yet been fully explored. The ability to continuously and non-invasively monitor blood pressure in the operating room may be advantageous in a number of situations (Kemmons, Ueda et al. 1991a; Kemmons, Ueda et al. 1991b), for example during surgical procedures where beat-to-beat measurements are essential but no blood samples are needed. Its indications could be expanded to any procedure where actually only discrete cuff-monitoring is used. In a previous study by Steiner and colleagues, tonometric continuous blood pressure monitoring was evaluated in an intensive care setting. They concluded that their tonometric device was not accurate enough for replacing invasive blood pressure monitoring, though the causes of the inaccuracy were not examined.(Steiner, Johnston et al. 2003)

The purpose of this study was therefore to acquire combined invasive blood pressure (IBP) and non-invasive tonometric (TBP) recordings during major neurosurgical operation with a manual tonometer sensor (i) to look at different error-introducing aspects of fixation, positioning, calibration and recalibration which are difficult to assess with fully automated devices and (ii) to evaluate whether tonometric assessment of the radial artery pressure waveform can be an alternative for invasive blood pressure measurement via radial artery cannulation.

2 Methods

2.1 Setup and protocol

A total of 2.058.000 paired datapoints were obtained over a period of 343 minutes in 3 patients, consecutively scheduled for major neurosurgical surgery. Written informed consent and institutional approval were obtained. Exclusion criteria were subclavian stenosis and pre-existing radial artery cannulation. Routine continuous monitoring in the operating room included electrocardiography, pulse oxymetry, capnography, blood pressure recording and rectal temperature assessment. All patients remained in supine position. Patients were kept normothermic by a forced-air warming system.

General anaesthesia was induced by intravenous propofol 2 mg/kg. Sis-atracurium 0.1 mg/kg was used for muscle relaxation. General anaesthesia was maintained by continuous infusion of propofol 6 mg/kg/h, remifentanyl 0,1 µg/kg/h and sis-atracurium 0,15 mg/kg/h. Patients were intubated orally and ventilated mechanically to achieve end-tidal CO₂ and O₂ saturation within normal limits. After anaesthesia induction, a 20F 8 cm PE catheter (Laeder Cath, Laboratoires pharmaceutiques, Ecouen, France) was inserted percutaneously into the left radial artery, 1 cm proximal to the wrist. The catheter was connected via 150 cm long (1.5 mm internal diameter) rigid pressure tubing, filled with saline to a continuous flush pressure-transducer system (PMSET 1DT-XX Becton Dickinson Critical Care Systems Pte Ltd, Singapore). The system was calibrated against atmospheric pressure. The midaxillary line was used as the zero-reference point.

At the contralateral arm, an arterial applanation tonometer (model SSD-936, Millar® Instruments Inc., Houston, TX) was placed over the right radial artery, about 1 cm proximal to the wrist. Correct positioning was determined by palpation and waveform evaluation on the anaesthesia monitor. After locating the appropriate position, the sensor was immobilized by means of a Tegaderm™ patch (3M Health Care, Borken, Germany). HDP was then adjusted by means of a custom made bracelet with screw until optimal waveforms with maximal amplitude were obtained (Figure 3–1). During the rest of the procedure, these tonometer settings remained unchanged.

It is common practice to calibrate the tonometer with diastolic and mean pressure values from an oscillometric cuff.(Matthys and Verdonck 2002) However, it has been shown that an oscillometric recording can have a substantial error margin compared to direct invasive recordings.(Nystrom, Reid et al. 1985; Gravlee, Bauer et al. 1989) Since in this study an invasive recording was performed concurrently with the tonometer recording, it was decided to investigate the potential of applanation tonometry in the hypothetical case of having perfect calibration values available. The added effects of an oscillometric cuff are discussed afterwards. This approach has also been applied in other work on tonometry.(Chen, Nevo et al. 1997) In order to investigate the effect of external forces such as an inflating and deflating cuff on the recorded signal, an oscillometric brachial cuff was applied at the same arm as the tonometer during several (randomly chosen) time intervals, recording systolic and diastolic blood pressure values every 3 or 5 min.

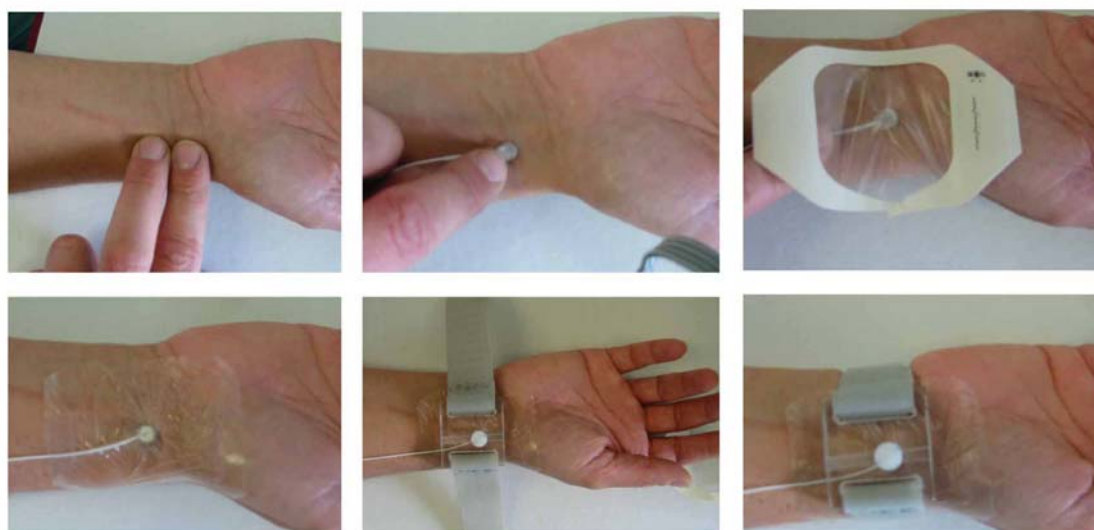


Figure 3–1 Positioning and fixation of the Millar® SSD-936 arterial tonometer.

All monitoring equipment was connected to a Datex AS/3 monitor (Datex-Ohmeda Inc., Madison, WI). Because the Datex AS/3 monitoring system has no standard connection for tonometric sensors, a custom connection was made for this study. Collecting all data via only one integrated monitoring and computing system, has significant advantages (perfect synchronization of multiple signals, maximal patient-safety with minimal use of equipment). All data from the monitor were sampled via the Datex-Ohmeda Collect Software® package for subsequent off-line analysis. IBP and TBP waveforms were sampled at 100 S/s. In the

event that an ECG trigger signal was acquired (fixed sample rate of 300 S/s), the software package ‘oversampled’ the pressure signals (300 S/s, by taking 3 times the sample value at 100 S/s) for synchronization purposes. Data were analyzed per acquisition window of 10000 samples (equal to a 33 s time interval @ 300 S/s, or a 100 s time interval @ 100 S/s). Total acquisition length for patient 1 was 63min, for patient 2 170 min and for patient 3 110 min.

2.2 Evaluation of normalized signals

The trend behaviour of TBP and IBP recordings were investigated per acquisition window, without the confounding influence of TBP calibration errors. This was done by normalizing both IBP and TBP signals to their respective first complete heart cycle in the acquisition window and subsequently differentiating the windows into 4 possible categories as distinguished by an experienced observer (Figure 3–2): (i) IBP and TBP can vary/change in the same direction (case C1-AGR, top); (ii) IBP and TBP can deviate in an opposite direction, or one signal deviates while the other stays in steady state (case C2-DISAGR, top middle); (iii) both signals can be in steady state (case C3-SS, bottom middle); and (iv) poor TBP signal quality, no assessment of a trend possible (case C4-ERR, bottom).

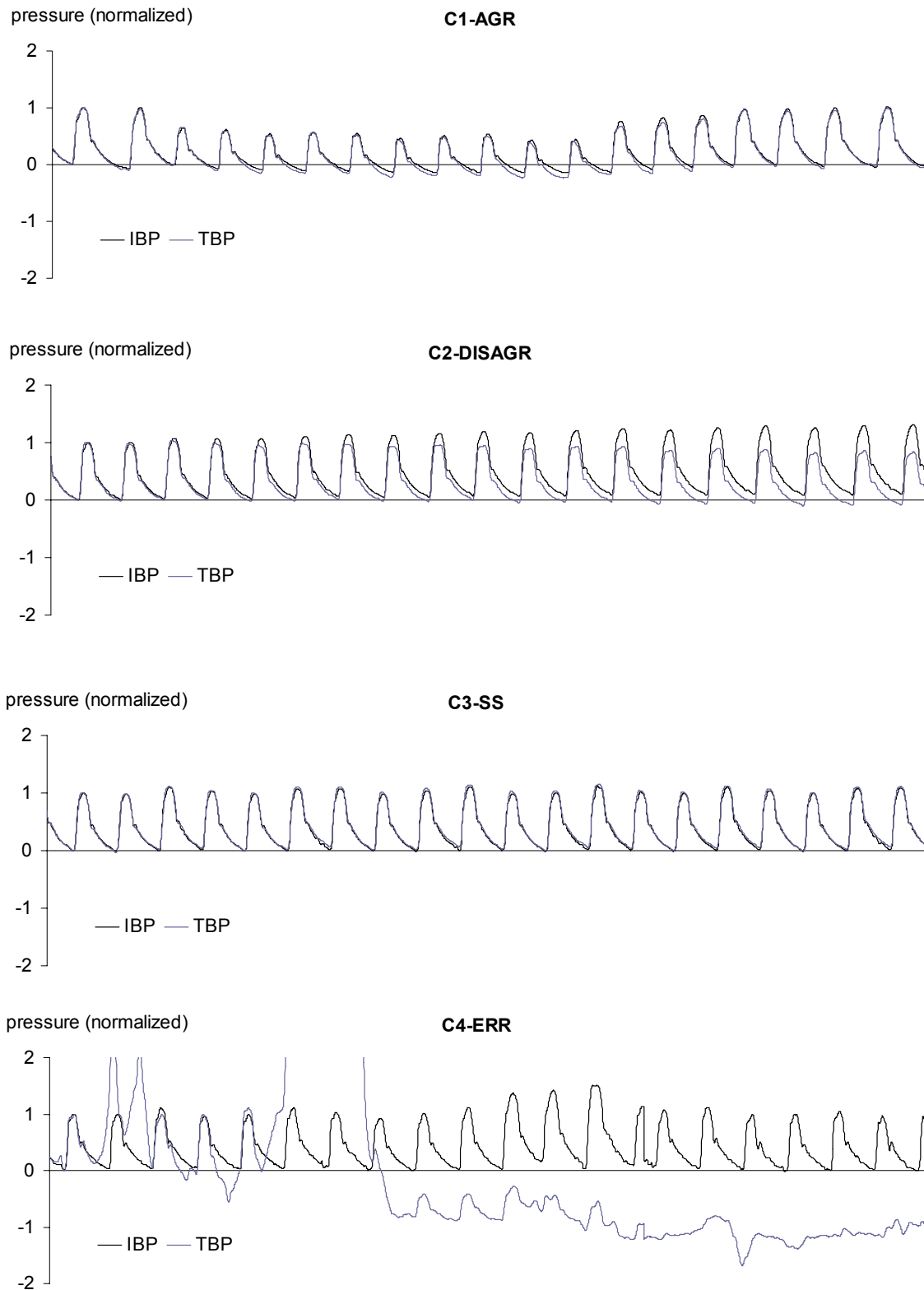


Figure 3–2 The 4 categories investigated: IBP (black) and TBP (grey) signal deviate in the same direction (C1-AGR, top); IBP and TBP signal deviate in an opposite direction, or one signal deviates while the other stays in steady state (C2-DISAGR, top middle); both signals in steady state (C3-SS, bottom middle); and finally, poor signal quality, no assessment of a trend possible (C4-ERR, bottom). Note that only a 20 s time interval of a complete acquisition window is shown here.

2.3 Evaluation of calibrated signals

Following, the reliability of a calibration over time (Figure 3–3) was investigated. In order to do this, the acquisition windows were processed in pairs, with a first and subsequent window. A selected set of cycles with no obvious artefacts available were chosen in the beginning of each first acquisition window and averaged by the observer. Calibration offset and gain for TBP were assessed from this first averaged heart cycle using DBP and MAP pressure values from IBP as a reference. These calibration parameters were then applied on both the first window as well as on the subsequent window. At the end of the subsequent window, a second set of cycles was chosen and averaged. For this second averaged heart cycle, the ratios between DBP, SBP and PP values of TBP and IBP were assessed, as well as the RMS (RMS, root of the sum of the squared differences, normalized to the number of samples) of their respective differences. As such, the calibration spans a double time interval (2×10000 samples) as compared to the qualitative analysis; recalibration is done every other acquisition window, and the stability of the calibration procedure is assessed 66 s (300 S/s) or 200 s (100 S/s) after the calibration.

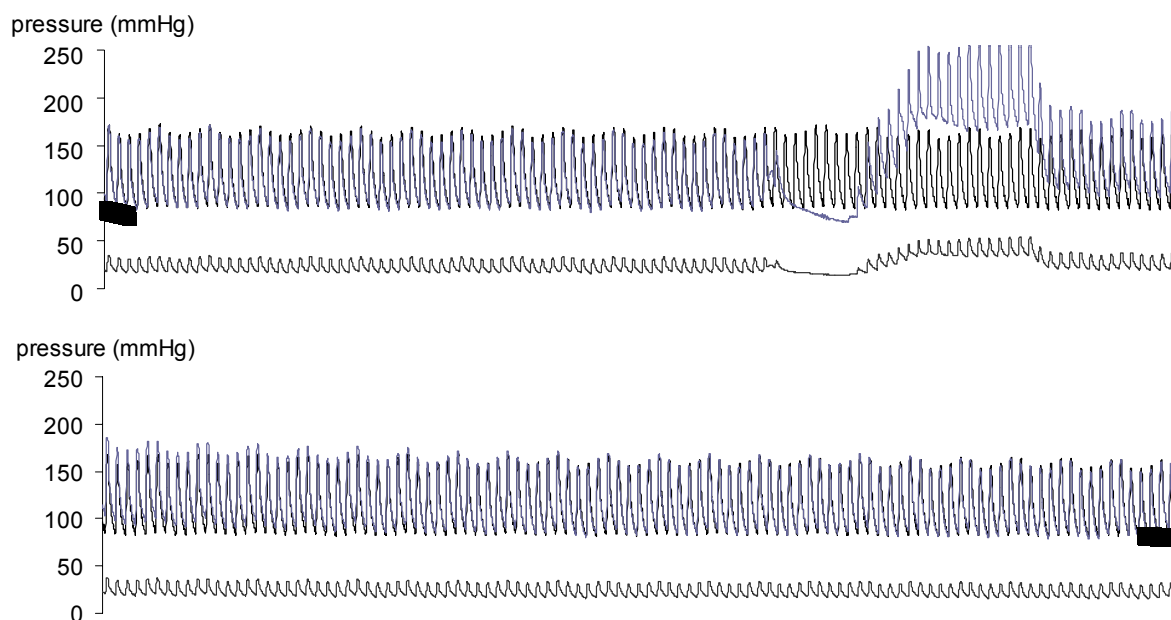


Figure 3–3 Reliability of calibration over time. Signals shown are TBP (dark grey), calibrated TBP (light grey) and IBP (black). Upper panel: Horizontal marker denotes the set of cycles at the beginning of the first acquisition window where calibration parameters are determined. Bottom panel: Horizontal marker denotes the set of cycles at the end of the subsequent acquisition window where the deviation between calibrated TBP and IBP is assessed.

3 Results

3.1 Evaluation of normalized signals

Table 3–1 shows the total number of acquisition windows investigated per patient (P1-P3) and per category (C1-AGR; C2-DISAGR; C3-SS; C4-ERR, Total T: C1+C2+C3+C4). For every patient the steady-state situation C3-SS occurs most (96% for P1, 79% for P2 and 61% for P3). Considering the data of all patients together, 81% of the recordings were steady state scenarios and in this case TBP and IBP always had a very good correspondence. Further, 4% of all recordings showed poor signal quality of TBP. Considering specifically the windows in which pressure variations occurred (C1-AGR; C2-DISAGR, Total T_v : C1+C2), TBP followed IBP only in 56% of the cases.

# AWin (%) (%) ²	ALL	P1	P2	P3
C1-AGR	23 (8) (56) ²	0 (0) (0) ²	5 (5) (33) ²	18 (27) (86) ²
C2-DISAGR	18 (6) (44) ²	5 (4) (100) ²	10 (10) (67) ²	3 (5) (14) ²
C3-SS	229 (81)	108 (96)	81 (79)	40 (61)
C4-ERR	12 (4)	0 (0)	7 (7)	5 (8)
$T(C1+C2+C3+C4)$	282	113	103	66
$T_v(C1+C2)$	41	5	15	21

with (%) = C_x/T and (%)² = C_x/T_v

Table 3–1 Qualitative evaluation of TBP compared to IBP by organizing the acquisition windows (AWin) into four different categories (C1-AGR; C2-DISAGR; C3-SS; C4-ERR), and this for all patients together (ALL) as well as per patient (P1-P3). T: all categories= C1+C2+C3+ C4; T_v : all categories with variations = C1+C2; (%) = C_x/T and (%)² = C_x/T_v .

3.2 Evaluation of calibrated signals

Investigating pressure variations in further detail, it appeared in all the subjects that small variations (e.g. caused by patient ventilation) were adequately followed by TBP (Figure 3–4 A). Very fast changes such as an extra-systolic event are also nicely monitored with sufficient adequacy (Figure 3–4 B and C). However, the more the pressure change is longer in time or

higher in amplitude, TBP monitoring tends to stay invariant to the pressure changes (Figure 3–4 D).

Next, calibration of TBP was performed with recalibration at the beginning of each pair of acquisition windows as explained in the methods. Results of the analysis of differences (precision) between TBP and IBP monitoring are shown in Table 3–2. Overall agreement (point-by-point) yielded an average RMS value of 31.3 ± 12.1 mmHg, while the averaged RMS for SBP, DBP and PP resulted in 18.3 ± 9.3 mmHg, 12.1 ± 4.4 mmHg and 11.0 ± 5.6 mmHg respectively. Using the data of all patients together, an RMS of 34.3 mmHg was found for overall agreement and an RMS of 20.8 mmHg for SBP, 13.2 mmHg for DBP and 12.2 mmHg for PP.

<i>RMS mmHg</i>	<i>ALL</i>	<i>P1</i>	<i>P2</i>	<i>P3</i>	<i>AVG ± SD</i>
<i>Overall</i>	34.3	36.0	40.4	17.5	31.3 ± 12.1
<i>SBP</i>	20.8	21.9	25.2	7.7	18.3 ± 9.3
<i>DBP</i>	13.2	16.1	12.6	7.4	12.1 ± 4.4
<i>PP</i>	12.2	9.8	17.1	6.1	11.0 ± 5.6

with Total # pairs AWin for ALL = 139; P1 = 57; P2 = 48; P3 = 34

Table 3–2 Root mean square (RMS) differences between calibrated TBP and IBP monitoring for all patients together (ALL) and per patient (P1-P3), as well as averaged (AVG ± SD) values. Total number of investigated pairs of acquisition windows is given (Total # pairs AWin).

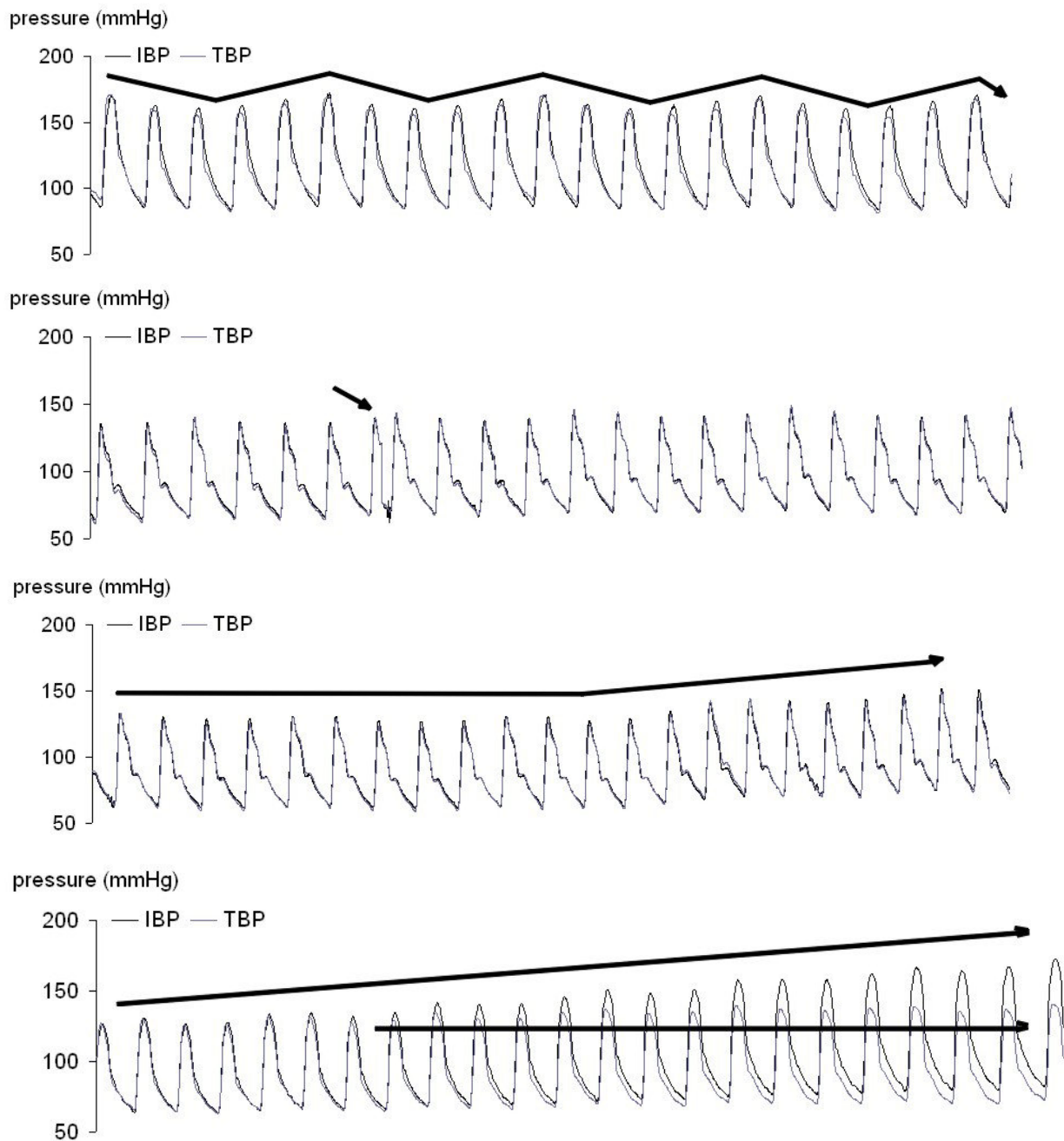


Figure 3–4 Illustrations are named A, B, C, D top to bottom. Time intervals of 20 s are shown. A: C3-SS. Calibrated TBP adequately reproduces ventilatory variations in IBP. B: C3-SS. Calibrated TBP reproduces the extra-systolic curve in IBP. C: C1-AGR. Calibrated TBP follows small IBP rise. D: C2-DISAGR. Calibrated TBP doesn't follow larger IBP rise. Initially, calibrated TBP follows IBP pattern adequately, but when pressure continues to rise, a manifest discrepancy emerges.

The ratios of SBP, DBP and PP of the two recordings are represented in Table 3–3 and Figure 3–5. A value of 110% means that IBP value is 10% higher than TBP value, or that TBP underestimates IBP by 10%. From these data it is clear that when looking at the three patients together, 38.8% of SBP values, 30.9% of DBP values and 32.4% of PP values from calibrated TBP are within $\pm 5\%$ of IBP. Also, 63.3% of SBP, 55.4% of DBP and 53.2% of PP values lie within the $\pm 10\%$ discrepancy interval. Given the fairly equal distributions in Figure 3–5 around 100%, there is no evidence of a consistent over- or underestimating (bias) by TBP recordings. However, considering only the very large deviations (more than $\pm 25\%$), more cases of underestimation ($IBP/TBP > 125\%$) than overestimation ($IBP/TBP < 75\%$) by TBP were noted, and this for SBP as well as for DBP and PP.

# pairs AWin (%)	ALL	P1	P2	P3
Total # pairs AWin	139 (100)	57 (100)	48(100)	34 (100)
	<i>TBP < IBP +5%</i>			
SBP	54 (38.8)	16 (28.1)	20 (41.7)	18 (52.9)
DBP	43 (30.9)	7 (12.3)	16 (33.3)	20 (58.8)
PP	45 (32.4)	17 (29.8)	13 (27.1)	15 (44.1)
	<i>TBP < IBP +-10%</i>			
SBP	88 (63.3)	32 (56.1)	27 (56.3)	29 (85.3)
DBP	77 (55.4)	22 (38.6)	27 (56.3)	28 (82.4)
PP	74 (53.2)	27 (47.4)	24 (50.0)	23 (67.6)

Table 3–3 Number of pairs of acquisition windows (# pairs AWin) for which SBP, DBP and PP from calibrated TBP lie within the 5% and 10% discrepancy intervals of the respective SBP, DBP and PP from IBP, and this for all patients together (ALL) and per patient (P1-P3).

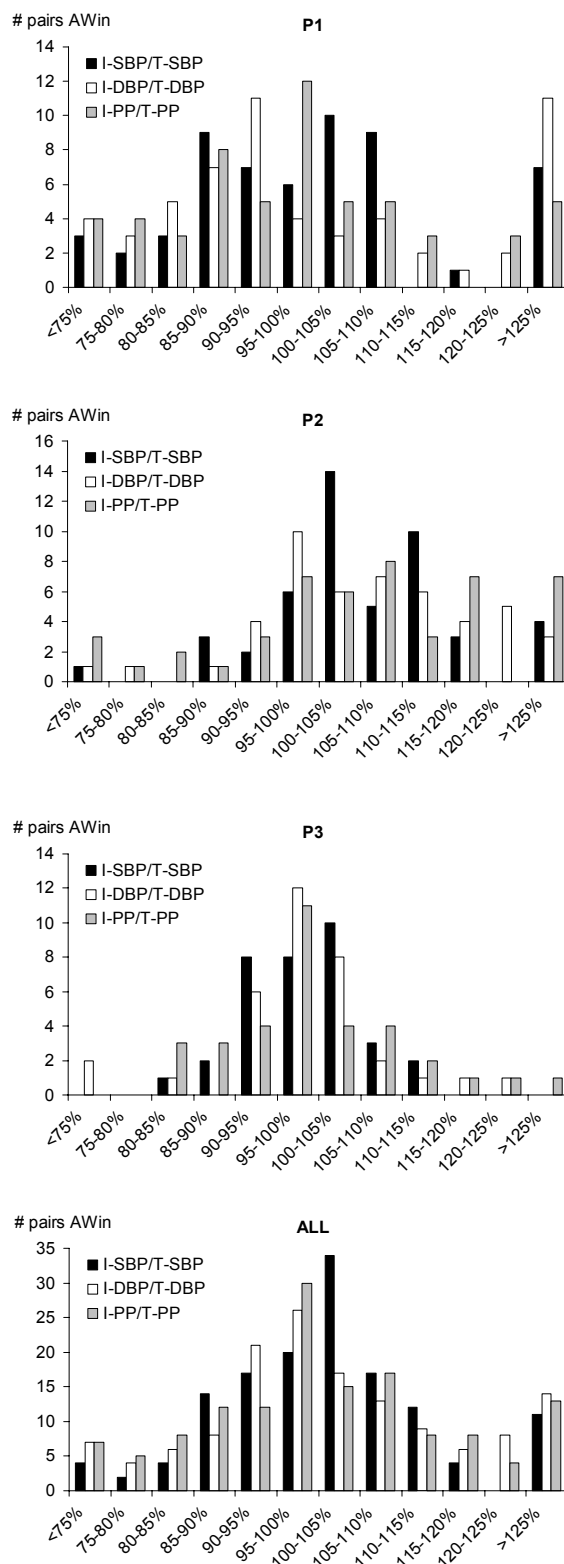


Figure 3–5 Number of pairs of acquisition windows (# pairs AWin) vs. ratio (%) of SBP, DBP and PP values from IBP (I-SBP; I-DBP; I-PP) and the respective values from calibrated TBP (T-SBP; T-DBP; T-PP) per patient (P1-P3) and for all patients together (ALL). Note that the # pairs AWin in e.g. a 5% discrepancy interval (as mentioned in Table 3–3) are found on these plots by adding the bars in both the 95-100% (minus 5%) and 100-105% (plus 5%) interval.

4 Discussion

In this study, 5.7 hours of combined IBP and TBP recordings during neurosurgery were analyzed. The qualitative findings showed that calibrated TBP mirrored IBP adequately in all steady state conditions (81% of the recordings) and that minute variations of blood pressure e.g. due to patient ventilation or very short variations such as an extra-systolic wave were well detected. However, these kind of variations are usually of no clinical relevance unless in specific studies. For pressure variations longer in time and with high amplitude, there was a rather high degree of unpredictability: TBP varied with IBP in the same direction only in 56% of the cases. In 44% of the investigated acquisition windows TBP either deviated in the opposite way or was only adequate in the first seconds after a pressure change and then untruly returned to its initial values suggesting a steady state, while IBP continued to rise or fall.

The TBP inability to monitor slow or long-term pressure variations adequately all the time can be a result of physiological changes in the wrist-tonometer setting. This phenomenon of vessel adaptation to an applied tonometer stress and HDP was also proposed by Steiner et al. when validating an automated tonometry device for monitoring in a neuro-intensive care unit. (Steiner, Johnston et al. 2003) To demonstrate this hypothesis, a varying external force was applied on the arm by means of a brachial cuff, thus artificially inducing a clear and reproducible physiological blood pressure change. The pattern of the uncalibrated TBP during inflating and releasing of the cuff was analyzed, as would occur when the tonometer calibration cuff would be positioned at the same arm as the tonometer sensor instead of at the contralateral arm.

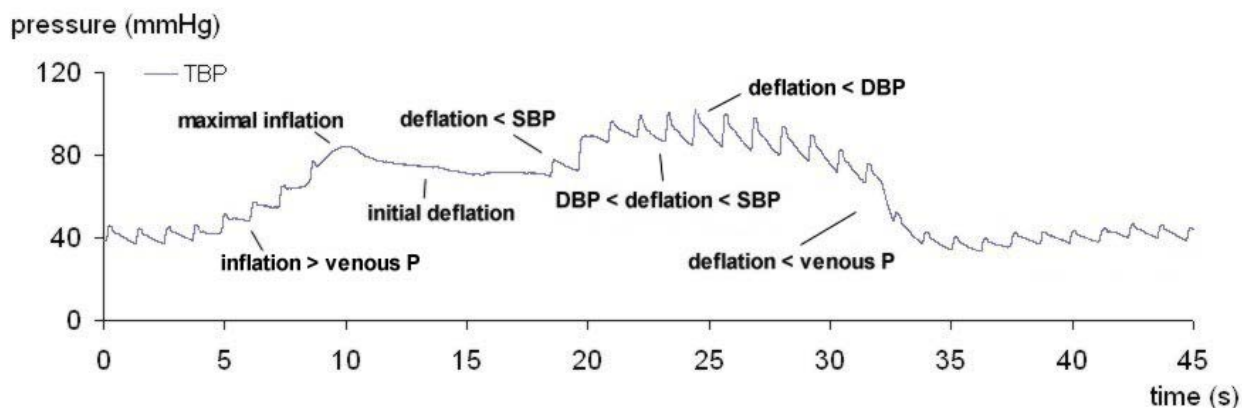


Figure 3–6 Pattern of uncalibrated TBP during cuff inflation and deflation.

When taking a close look at TBP waveforms during cuff inflation (Figure 3–6), one can distinguish different events which could be induced by the following: after the initial cuff inflation, venous pressure starts to rise, while arterial pressure distally to the cuff doesn't change a lot. Since venous stasis also causes increased pressure on the tonometer, it senses increased pressure. One can observe that mean TBP rises very significantly, while the amplitude diminishes only modestly. This can at least partially be explained by the fact that the rigid bracelet has a large contact-area with the wrist-surface, while the sensor has a small contact with the wrist. So a small pressure rise against the bracelet can deliver a significant increase of force onto the small sensor. Once the cuff is inflated to the maximum level, one can see that TBP amplitude drops to zero, while the mean value stagnates. This is logical since total occlusion of the artery and veins implicates that no blood can flow in or out. After this, the cuff is deflated slowly in order to detect SBP and DBP by means of oscillometry. Once the cuff is deflated below SBP, one can see mean and amplitude of the TBP signal rising quickly to a new plateau. This plateau might correspond to maximal venous stasis when venous pressure approximates arterial pressure. Also, since the cuff inflation caused an ischaemic stimulus to the smooth muscle cells in the distal arterial vessel walls, the vessels may dilate and increase the force onto the tonometer. At this point, cuff pressure is between SBP and DBP. Once the cuff pressure is further released and drops below the venous pressure, TBP returns to its normal values remarkably fast, which suggests a predominantly intravascular cause of the artefact.

From a mere technological point of view, the modern electronic tonometric devices are sensitive enough to detect arterial pulsations with a high enough precision for clinical decision making, even in such circumstances as a surgical operation. Also the supporting hardware is capable of reproducing signals at an adequate sampling rate and with sufficient precision. Yet the non-invasive alternative to arterial cannulation finds its way to the clinical practice only hesitatingly, even with tonometric devices on the market for over 20 years now. This is rather remarkable considering the advantages of non-invasive continuous blood pressure measurement compared with invasive monitoring.

Which factors are responsible for the fact that the transfer from basic technology to clinical practice is so hard to take for these devices? In the first place the procedure for the positioning of a manual sensor-type as used in this study is labour-intensive, operator-dependent and in some cases almost impossible. It is indispensable that the position of the sensor together with

the direction and amount of the HDP are not changed after the sensor has been fixed. During the study it became clear that the slightest displacement of the sensor or the fastening mechanism could make the signal of the measurement useless. In an operative setting where after positioning, the patient is covered with sterile linen, this is a substantial disadvantage. Fully automated tonometer devices will surely give better results in terms of fixation and positioning and thus comparison with intra-arterial measurements (Zorn, Wilson et al. 1997) but whether they can fulfill the strict requirements for an operating room should still be further investigated.

So far, the comparison of automated tonometry devices with intra-arterial pressure measurements has only been done on a few cycles or on short-term recordings (10-20min). At the advent of automated tonometry devices in the early 1990s, promising reports of automated tonometry as a replacement for invasive long-term monitoring were published (Kemmons, Ueda et al. 1991a; Kemmons, Ueda et al. 1991b), but later research work questioned these findings. (Siegel, Brock-Utne et al. 1994) Limitations of automated tonometry devices and especially during fast transient changes have been reported (Sato, Nishinaga et al. 1993) what was also found for the manual probe in this study. Though automated devices continuously improve their performance and field of applicability (Kemmons, Ohno et al. 1994) and some commercially devices score better than others (Searle, Perrault et al. 1993; De Jong, Ros et al. 1995; Steiner, Johnston et al. 2003), it can be concluded that for now there is no strict agreement in literature. Specific to this application, Weiss et al. showed from short-term recordings that automated radial arterial tonometry was not suitable at the time of writing to replace invasive monitoring during major surgical procedures. (Weiss, Spahn et al. 1996)

The recent work of Steiner et al. on 15 patients in a neuro-intensive care setting did use long-term recordings (60 min) to validate an automated tonometry device. (Steiner, Johnston et al. 2003) The device was not found suitable due to the significant number of inaccurate measurements and downward signal drift. A disagreement of more than 10 mmHg between mean TBP and IBP occurred in 34% of the recordings (13.1h of remaining data after removal of 19% of sequences with artefacts), and the median differences between TBP and IBP for SBP (-11.0 mmHg) and DBP (3.6 mmHg) showed considerable variability. Steiner et al. also found a tendency of TBP to overestimate high blood pressure and underestimate low pressures.

In this study with the manual tonometer, these consistent problems of drift were not encountered and only 4% of total recordings (5.7 h) were confounded by artefacts. The calculated RMS differences for overall waveform agreement were large (34.3 mmHg) as well as RMS values for SBP (20.8 mmHg), DBP (13.2 mmHg) and PP (12.2 mmHg). Note that SBP values have a bigger deviation than DBP in both studies. By calculating the respective ratios of SBP, DBP and PP of the two recordings, high discrepancy percentages were found with 36.7% of SBP, 44.6% of DBP and 46.8% of PP values measured with TBP lying outside the corresponding IBP $\pm 10\%$.


No evidence was found of a consistent over- or underestimating (bias) by TBP recordings, except for the very large deviations (more than $\pm 25\%$) where more cases of underestimation than overestimation were noted, and this for SBP as well as for DBP and PP.

Apart from movement artefacts, positioning and fixation, the problems are mainly due to the dependence of the tonometer from an external calibration device. Calibration of the tonometric signal is done by an external method, usually a brachial cuff-measurement, based on oscillometry. Using these systems, the intrinsic restrictions of the calibration method have their repercussions on the tonometric signal accuracy. (Gravlee and Brockschmidt 1990)

Finally, the experimental results showed that a regular automatic recalibration of the sensor is required. In the used setting, the stability of the calibration procedure was assessed every 66 s (300 S/s) or 200 s (100 S/s), which corresponds to the fastest commercially available cuff-devices able to recalibrate every minute up to every 3 minutes. Most conventional cuff-devices cannot do more than one calibration every 3 minutes due to the inherent time necessary to inflate and deflate the bracelet. Moreover, one cannot put a continuous load on the arm so that the time interval between calibrations has to be finite anyway. Automated devices do have intelligent technology aboard to notify when a recalibration is needed, but the cuff dependence in terms of inflation time and oscillometric accuracy remains. Moreover, depending on the setting it can be unsuitable to inflate the cuff even at the conventional rate of every 3 to 5 min. Although Steiner et al. used an automated tonometry device that could perform a rapid recalibration, they used a 10 min recalibration time as shorter intervals were unsuitable at the intensive care setting. (Steiner, Johnston et al. 2003)

5 Conclusion

A manual probe was used to control and investigate the different error-introducing aspects (positioning, fixation, calibration and recalibration) better than possible with an automated device. Long-term recordings were analyzed in three patients undergoing neurosurgery. One must conclude that, in this patient-case and the tested setting, the tonometer was not able to detect the relevant pressure changes at all times and a rather high degree of unpredictability was present. By using the invasive recording, an accuracy of calibration and a frequency of recalibration in post-processing was applied that cannot be obtained with any cuff device, and most certainly not in a surgical clinical setting. Therefore, these results represent a ‘best case scenario’ and they readily appear not to be satisfying. As shown, physiological alterations at the site of TBP measurement are an important source of artefacts. Since compensation for these errors is imperative for reliable assessment of the blood pressure, further study of the source of these artefacts is essential before even fully automated tonometry can replace invasive monitoring in non-steady state long-term recording conditions.



4 An acquisition tool for synchronized monitoring of a Doppler spectrogram, an electrocardiogram and arterial tonometry*

* The content of this chapter has been published in the Proceedings of the 25th Annual International Conference of the IEEE Engineering in Medicine and Biology Society (IEEE EMBC 2003, Cancún, Mexico)

Hemolab: a custom built diagnostic tool for non-invasive, synchronized recording and real-time monitoring of a Doppler spectrogram, an electrocardiogram and arterial tonometry

K Matthys, P Segers, D Vanhercke, S G Carlier, P R Verdonck

Abstract

In clinical diagnostic practice, various medical devices are designed for specific investigations and have no margin for adding other input signals or profound post-processing. Although information obtained from these signals separately is useful, using them in a combined way allows for a more profound analysis of the cardiovascular system. The aim was to build an affordable, compact and easy-to-use instrument enabling a synchronized acquisition of arterial pressure and flow waveforms, combined with an electrocardiogram (ECG), all in non-invasive way and to be used in a routine diagnostic setting without prolonging testing protocols or adding discomfort to the patient. The combination of the beat-to-beat pressure and velocity information allows to calculate haemodynamic parameters that can quantify mechanical characteristics of the arterial system such as compliance and resistance. In this study, an applanation tonometer, an ECG recorder and an ultrasound device were used. A handy acquisition tool (Hemolab, ©K Matthys) was built that can combine the output of several stand-alone medical monitoring devices. A synchronized acquisition of a Doppler spectrogram, an electrocardiogram and a continuous pressure signal could already be acquired non-invasively, monitored in real-time and saved for later processing. This study contributes to obtain diagnostic information from non-invasive haemodynamic parameter analysis.

1 Introduction

In clinical cardiovascular practice, various medical devices are used from many different companies. Apart from a few complex and specialized exceptions such as e.g. anaesthetic monitoring equipment in an operating room, devices for routine diagnostic examination are usually built for single and specific investigations e.g. blood pressure measurement by means of a cuff manometer, heart rate and heart rate variability measurement with an electrocardiogram (ECG) recorder, blood velocity through heart valves with ultrasound devices... They usually have little margin for adding other input signals or doing post-processing on the monitored parameters and waveforms. Although the information obtained from these signals separately is useful and important as such, using them in a combined way opens the way to a more profound analysis of the cardiovascular system.

The aim was to build an instrument that enables a synchronized acquisition and real-time monitoring of arterial pressure and flow waveforms, combined with an electrocardiogram, all in a continuous and non-invasive way. Using the ECG as a trigger function, individual heart cycles can then be isolated and/or averaged. The combination of the beat-to-beat pressure and velocity (or flow) information allows to immediately calculate haemodynamic parameters that can quantify the compliance of the arterial system, peripheral resistance etc. The tool had to be affordable, compact, easy-to-use in a routine examination or during a stress test and not solely applicable to the specific types and brands of medical devices used for this study. In the present study, an applanation tonometer, an ECG recorder and an ultrasound device were connected (Figure 4–1).

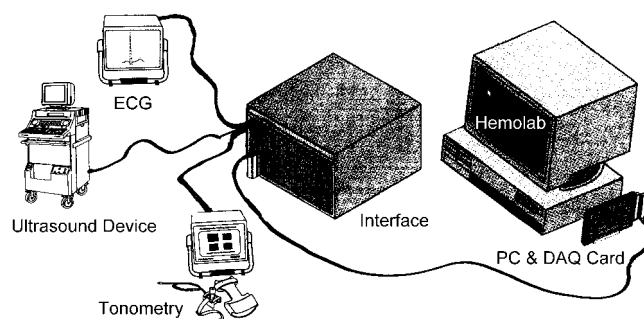


Figure 4–1 Several medical devices (left) linked via a custom hardware interface (middle) to the computer containing the data-acquisition card and the custom-written acquisition software (right).

2 Methods

An applanation tonometer is a non-invasive sensor applied on the skin at the location of a superficial artery, supported by underlying bone. The sensor works by means of a conventional Wheatstone bridge with strain gauges at the sensor tip, transforming pressure (mmHg) into an analogue electric signal (V). It monitors the pressure waveform in the artery in a continuous way but produces only waveforms, not reliable absolute values. In practice, calibration of the pressure waveform is mandatory e.g. by means of a conventional cuff-device giving diastolic, mean and systolic pressures at discrete time intervals.(Matthys and Verdonck 2002)

The electrocardiogram is a representation of the electrical activity of the heart. The output from the ECG recorder is already an analogue electric signal (V). In the specific case of the ultrasound signal, a general way of extracting the data was a priority, since the different ultrasound device manufacturers tend to have little standardization when it comes to signal output. In an ultrasound device, the Doppler principle is used to acquire blood velocities by detecting the change in frequency (Doppler shift) that occurs when an emitted ultrasound beam reflects on a moving particle (e.g. a red blood cell) and is received again.

In between the originally acquired Doppler shift and the final frequency spectrogram (Hz) with the corresponding velocity scale (m/s) shown on the screen, lays some brand-specific signal processing circuitry that is unavailable for the end-user. To solve this black-box problem, the signal available on the audio-output was extracted, which is available on every device since diagnostic procedures are commonly not only done on sight, but also on hearing. This signal is directly related to the Doppler shift. A function was then implemented in the program that allows generating a frequency spectrogram from the audio signal. This was done by means of a sliding window technique and Fast Fourier analysis. As such, no frame-grabbing technique was used to access the images generated by the ultrasound device, but the spectrogram was reconstructed from the obtained Doppler shift information in the audio signal.

An SSD-936 arterial tonometer (Millar[®] Instruments Inc., Houston, TX) and an 800CFM ultrasound device (GE Vingmed Ultrasound AS, Horten, Norway) was used as a pressure and

flow device. Acquisition was done by means of a low-cost E-Series Multifunction data-acquisition (DAQ) card (type NI6023E, National Instruments Corporation, Austin, TX) and custom-written acquisition software (Hemolab, ©K Matthys), developed in Matlab 6® environment (The Mathworks Inc., Natick, MA).

3 Results

Signals from the medical monitoring devices are led to the DAQ-card by means of a in-house built hardware interface with a BNC connector front panel. Provisions have been made in the interface for amplifier and filter circuits, together with output possibilities for appropriate sensor excitation voltages by means of batteries (patient safety).

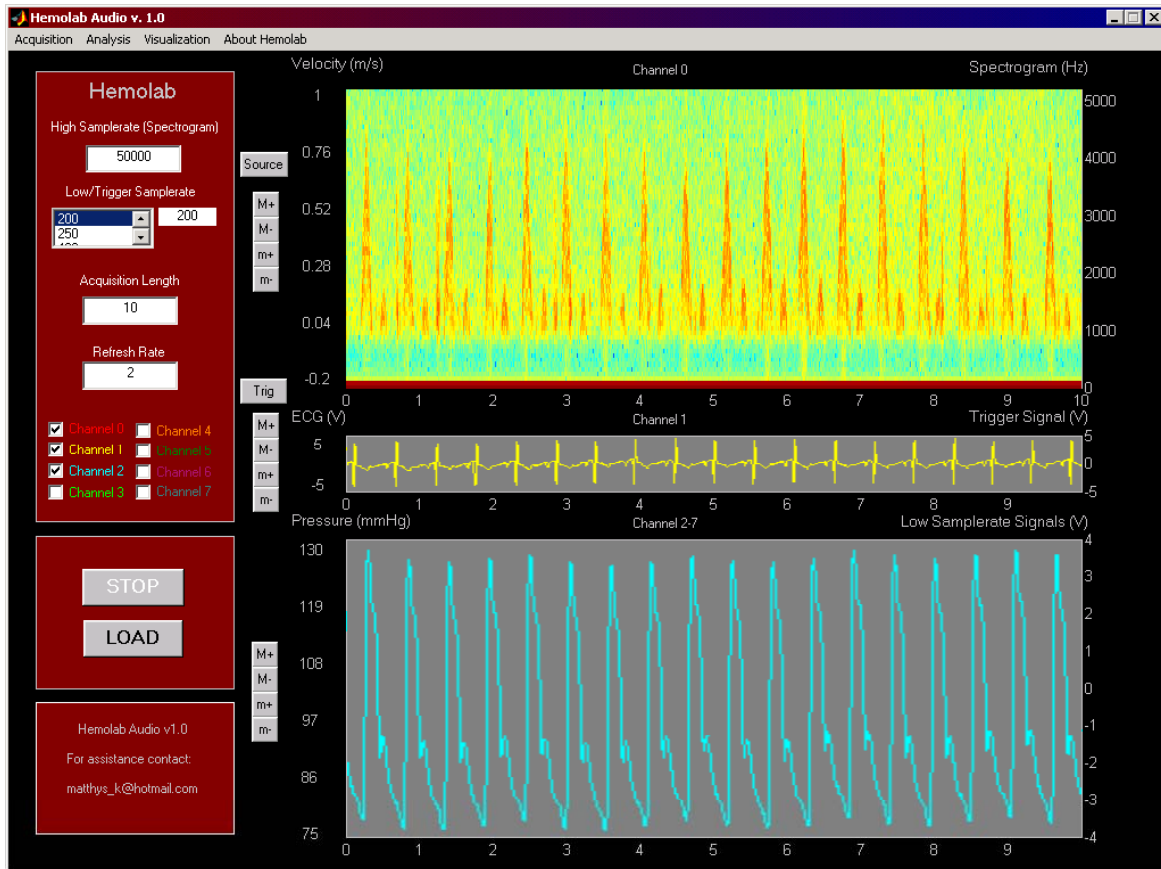


Figure 4–2 GUI front panel: data-acquisition settings and function buttons are on the left, while the signals are shown on the right: velocity (m/s), ECG (V) and pressure (mmHg). There is a menu bar for advanced settings of acquisition, analysis and visualization parameters.

The acquisition software is operated by means of a GUI. The number of channels is limited to 1 high sample rate channel (e.g. Doppler audio) and 7 low sample rate channels (e.g. 1 for ECG, 6 for pressure). As shown in Figure 4–2, checkboxes are available on the GUI front panel to choose the desired configuration.

Values for high and low sample rate, as well as these for the refresh rate (defined as the length of a data block that is taken from the acquisition buffer and shown on screen), and the acquisition length (size of data buffer which can be saved to disk) are all user defined. These settings, along with the start/stop and save/load buttons are available in a frame on the left-hand side of the GUI.

On the right-hand side, there are three different charts. The top right panel contains the spectrogram of the high sample rate signal; the middle panel contains the ECG or trigger signal, while the lower panel is reserved for the rest of the low sample rate channels. The high sample rate signal itself is available by pressing a toggle button next to its spectrogram, thus enabling a new pop-up chart (Figure 4–3, red circle).



Figure 4–3 The new pop-up chart containing the high sample rate signal is enabled by pressing a toggle button (red circle) to the left of its spectrogram. Four push buttons (white circle) allow adjusting the scale to the left of the charts.

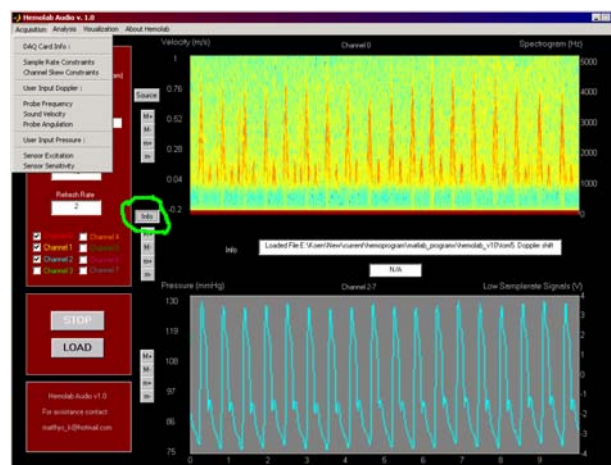


Figure 4–4 Example of a pull down menu in the menu bar, and the toggle button (green circle) that enables to switch between middle chart panel and info line.

Apart from the frequency (Hz) and voltage (V) scales on the right of the charts, which are adjusted automatically, one can also calibrate the signals by adjusting and labelling the scales on the left. This is done by the four push buttons to the left of the charts (Figure 4–3, white circle), used for changing the maximum (M+/M- buttons) and minimum (m+/m- buttons) values on the scale. The scale resolution, labels and dimensions are set in the Visualization menu on the menu bar.

Further, the middle chart panel can be switched with an Information Edit line and Input box by pushing the toggle button to the left (Figure 4–4, green circle). They will also pop up automatically when an item from the menu bar is chosen which requires input or gives back information to the user.

Other pull down menus available on the menu bar -apart from the Visualization menu- are advanced settings in the menu Acquisition concerning information on the DAQ-card, the Doppler probe and pressure sensors, etc. and analysis settings in the menu Analysis covering e.g. spectral window size and overlap. Data are saved in an ASCII-file, containing the signal sampling data along with some generic information on acquisition settings. Previously saved data can be loaded at any time later to review the acquisition, by utilizing the Load push button.

4 Discussion

Aiming to have a real-time, synchronized visualization of all captured signals, as much computing power as possible was left to bringing the signals on screen. Moreover, the solution should stay cost-effective.

Therefore, it was desirable to only sample the Doppler audio at high sample rates (order of 5-10 kS/s), while the sampling of ECG and pressure signals could suffice with a much lower sample rate (typical 200 S/s). Since the low-cost DAQ-card only allowed to sample every input at the same rate, an algorithm was programmed making use of virtual channels and the channel skew property of the DAQ-card (this is the time gap in between switching of channels during acquisition) to establish one channel sampled at high rate (up to 40 kS/s), and all the others at the same low sample rate. The drawback of this algorithm is that the high and low sample rate is not independent from each other. The low sample rate should be a common divider of the high sample rate. In practice however, this is not a big problem, since this requirement can be easily met for most applications.

Further, the faster the data should be visualized, the smaller the data blocks should be that are sent to the screen with a rate determined by the user-defined refresh rate parameter. But this in its turn restricts the sample rate and number of channels acquired. The larger the data blocks, the more visualization tends to be step-wise and not fluently. In conclusion, the user will have to make a trade-off between real-time visualization on one hand and high sample rate and/or high channel number on the other hand.

Finally, buffer space has been limited to one screen only. This means that the chart length of a window (thus total time of the acquisition) is resizable by the user, but only the last completed window is stored and saved to a file at the end of the acquisition. This speeds up the working of the program as far less buffer capacity is needed, and also restricts the amount of data to what is necessary for further post-processing.

5 Conclusion

Although general data-acquisition software is already commercially available, there was a need to build a more specific easy-to-use instrument for haemodynamic analysis. The kind that is self-explanatory and with a minimum of hardware so it can be used in virtually any routine diagnostic setting (e.g. a stress test) without prolonging testing protocols or additional discomfort for a patient.

An acquisition instrument was built and presented here that combines the output of several stand-alone medical monitoring devices. Taking into account some restrictions, a synchronized acquisition of a Doppler spectrogram, an electrocardiogram and a continuous pressure signal could already be acquired non-invasively, monitored in real-time and saved for later processing. When the necessary electrical circuitry for patient safety issues is implemented in the hardware interface, this setup could already be used in a clinical environment. This should lead to continuous further optimization and enhancements of specific features to be applied in future versions. In this way, this study contributes to obtain diagnostic information in a fast and easy way for non-invasive haemodynamic parameter analysis.

IV Vascular haemodynamics during physical exercise and drug-induced stress

In this fourth part, first the practical implications of diagnostic exercise testing and drug induced stress testing are explained (Chapter 1). In the next chapter the feasibility of acquiring vascular haemodynamic parameters during exercise tests is tested on a small subject group during a standing and supine bicycle test (Chapter 2). In the last chapter, this knowledge was applied on a larger clinical study with physical treadmill exercise and drug-induced (dobutamine) stress in order to look at arterial compliance and its relation to myocardial ischaemia (Chapter 3).



1 Background: Exercise and Dobutamine

1 Diagnostic exercise testing

1.1 Review and methodology

During clinical exercise tests, patients are undergoing an imposed load on a treadmill or cycle-ergometer, which is being augmented gradually until the functional limitations of the patient are reached. Exercise tests give a more accurate view on the 'fitness' and cardiovascular condition of a patient than a supine diagnostic examination in rest, as they are a better simulation of the normal daily activity pattern.

The choice of the loading device is important, especially with children and adolescents.(Tomassoni 1993; Paridon 1998) A treadmill can be useful with obese subjects as the intensity of the workout is being controlled by the treadmill velocity, whereas with a cycle-ergometer the patient controls his own cycle frequency. The bicycle test allows a greater stability of thorax and upper limbs, and is less noisy. Searching for Korotkoff sounds and acquiring parameters that require a stable measuring site (e.g. blood pressure) is thus facilitated on the bicycle.

Apart from the device, the stress protocol is equally important.(Rowland 1993) A lot of protocols are available, each having advantages and disadvantages. A good basic rule is to choose a protocol that is adapted to the examined subject in terms of duration and incremental increase in resistance. For example, the duration of one incremental step has no effect on the maximal heart rate or oxygen intake (Zhang, Johnson et al. 1991), but does come into play in reaching a steady state condition while recording submaximal physiological values, allowing for discrete measurements to take place (e.g. cuff inflation needs a finite time), and avoiding loss of motivation for the subject which is imperative to obtain a state of maximal exercise. In this respect, the role of assisting staff and an agreeable environment cannot be undervalued.

1.2 Practical implications

1.2.1 Preliminary aspects

An appropriate choice of measuring devices is imperative when performing acquisitions on a patient in motion. In this thesis, both the manual tonometric probes of Millar[®] Instruments (pen-probe SPT-301 and button-probe SSD-936, Millar[®] Instruments Inc., Houston, TX) have been used during exercise tests on a radial site with an oscillometric cuff calibration for the non-invasive pressure measurements (Figure 1–1 and Figure 1–4). As for the non-invasive flow measurement, the GE Vingmed 800CFM ultrasound device was used (GE Vingmed Ultrasound AS, Horten, Norway) to determine the LVOT (left ventricular outflow tract or cross-sectional area of the aortic valve) and central aortic blood velocity. Both a standing and supine bicycle test were looked upon. In Europe the supine bicycle is less frequently used (compared to the USA) in cardiac diagnosis, unless in special cases such as e.g. athlete monitoring.

1.2.2 Standing bicycle

To reduce the movement noise in pressure recordings at high levels of exercise, adaptations had to be made for appropriate support of the arm and hyperextension of the wrist. Further, it appeared important that the subject had a gripbar to hold on to, but placed in such a way that no complete fist could be made as the contraction of the arm muscles would then impede the tonometric recording on the radial artery (Figure 1–1). On the standing bicycle the suprasternal position for the Doppler probe appeared the most feasible from a mere practical point of view, as it was the easiest position to reach for the operator.

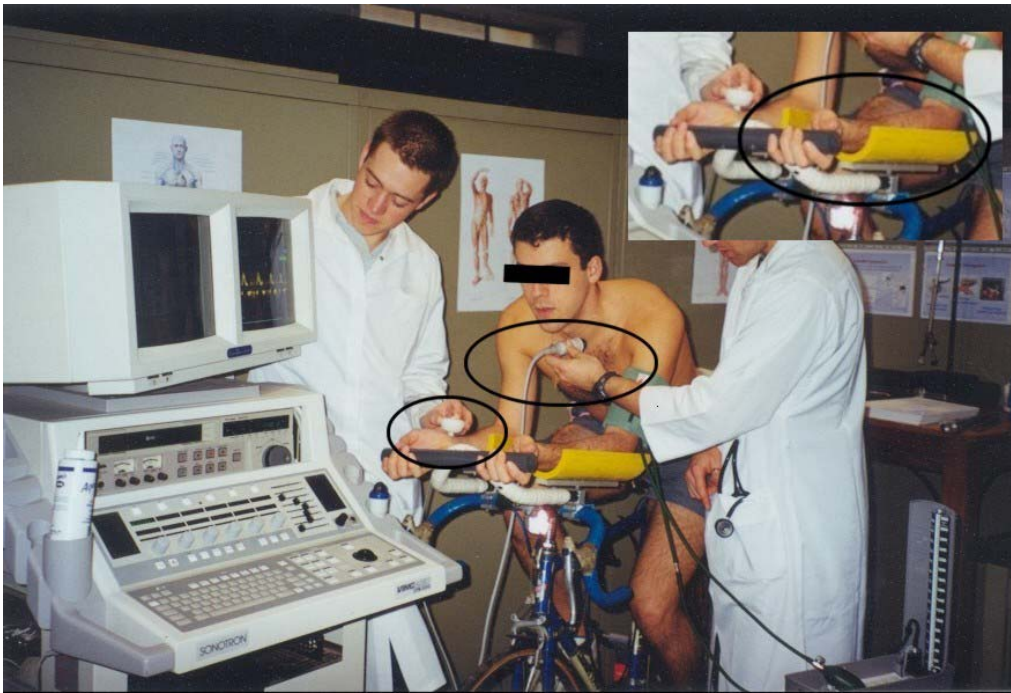


Figure 1–1 Radial pressure measurement (here testing the ‘volume pulse method’, but an identical setting for tonometry is used) in combination with suprasternal Doppler ultrasound velocity recording. Inset: Forearm support and finger grip.

1.2.3 *Supine bicycle*

As thorax and upper limbs are more stable during supine bicycle testing, pressure recordings were more accurate. Forearm support was used. The supine position allowed to investigate different Doppler probe positions (transthoracic, suprasternal) and Doppler modes (continuous, pulsed) (Figure 1–3). At high exercise levels, image quality is being disturbed by the breathing pattern and patient movement, especially for pulsed Doppler. Transthoracic Doppler required an extra 30° side tilt (heart apposed against thorax due to gravity) to obtain better signal quality. Although feasible in practice, it is certainly less comfortable for the patient.

A transthoracic position is a more established technique (in rest), but the continuous wave Doppler from a suprasternal position (aligning Doppler beam to aortic valve) appeared most robust at all exercise levels. Thus, in further experiments the transthoracic position was chosen for LVOT determination at baseline (rest) level, while the velocity measurement was continued in suprasternal position during the exercise test (Figure 1–2).

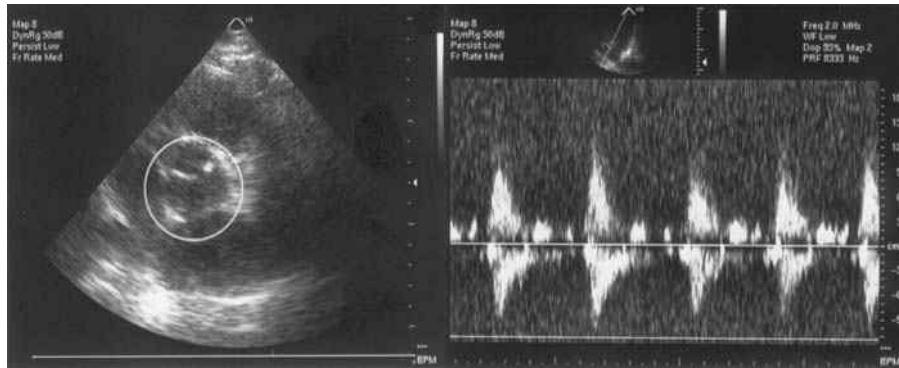


Figure 1-2 Left: Aortic valve image to determine LVOT. Right: Velocity acquisition at the aortic valve. Velocity times LVOT gives blood flow.

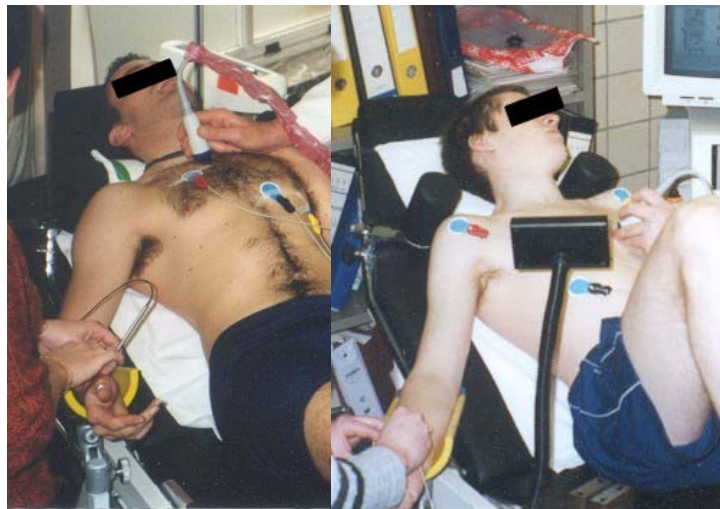


Figure 1-3 Supine bicycle test with radial tonometry (pressure) and suprasternal Doppler ultrasound (velocity). Left: Millar® SPT-301 tonometric pen-probe and suprasternal Doppler probe position. Right: Millar® SSD-936 tonometric button-probe and transthoracic Doppler probe position.



Figure 1-4 Supine cycle-ergometry: complete setup.

2 Dobutamine stress echocardiography

2.1 Review and methodology

Echocardiography is probably the single-most important non-invasive clinical tool for the assessment of left ventricular function. It does not however, reveal any information about myocardial ischaemia or coronary artery disease (CAD) at rest in patients without resting wall motion abnormalities. It is therefore been combined with (drug induced) cardiac stress testing for the diagnosis and prognostication of CAD.(Cohen, Ottenweller et al. 1993; Marwick, Willemart et al. 1993; Hennessy, Codd et al. 1997)

Dobutamine stress echocardiography permits cardiac evaluation of patients who cannot adequately perform a physical exercise test or in whom a controlled test is required. Dobutamine is a synthetic catecholamine which acts in the same manner as adrenaline with an inotropic response at low doses and both inotropic and chronotropic responses at high doses.(Ruffolo, Spradlin et al. 1981)

Overall, dobutamine stress echocardiography is a sensitive and accurate test for the detection and prognostication of CAD although there is some variation between single- and multi-vessel CAD and between patients with normal resting wall motion and those without.(Sawada, Segar et al. 1991; Marwick, Willemart et al. 1993) Most studies show that the sensitivity of detecting multi-vessel disease is in the range of 85-90% and that of detecting single-vessel disease is in the range of 75-80% with specificities of about 80% and 65% respectively.(Sawada, Segar et al. 1991; Marwick, Willemart et al. 1993) Overall sensitivity and specificity in validation studies shows the range in sensitivity of 70-96% (mean 84%) and for specificity of 60-97% (mean 84%).(Hennessy, Codd et al. 1997) Combining results from most studies gives a mean overall accuracy for dobutamine stress echo of about 80%.(Sawada, Segar et al. 1991; Marwick, Willemart et al. 1993; Senior, Basu et al. 1996)

2.2 Practical implications

The standard dobutamine protocol, involving infusion starting at a rate of 5 $\mu\text{g/kg/min}$ and increased every three minutes to the doses of 10, 20, 30 and 40 $\mu\text{g/kg/min}$ (Sawada, Segar et al. 1991) is empiric, and steady state is not attained at each dose increment. Echocardiographic images of the heart are digitally acquired at baseline, low dose (following 5 $\mu\text{g/kg/min}$), pre-peak and peak in the parasternal long-axis, parasternal short-axis, apical 2- and 4-chamber views, and apical long axis view (Figure 1–5).

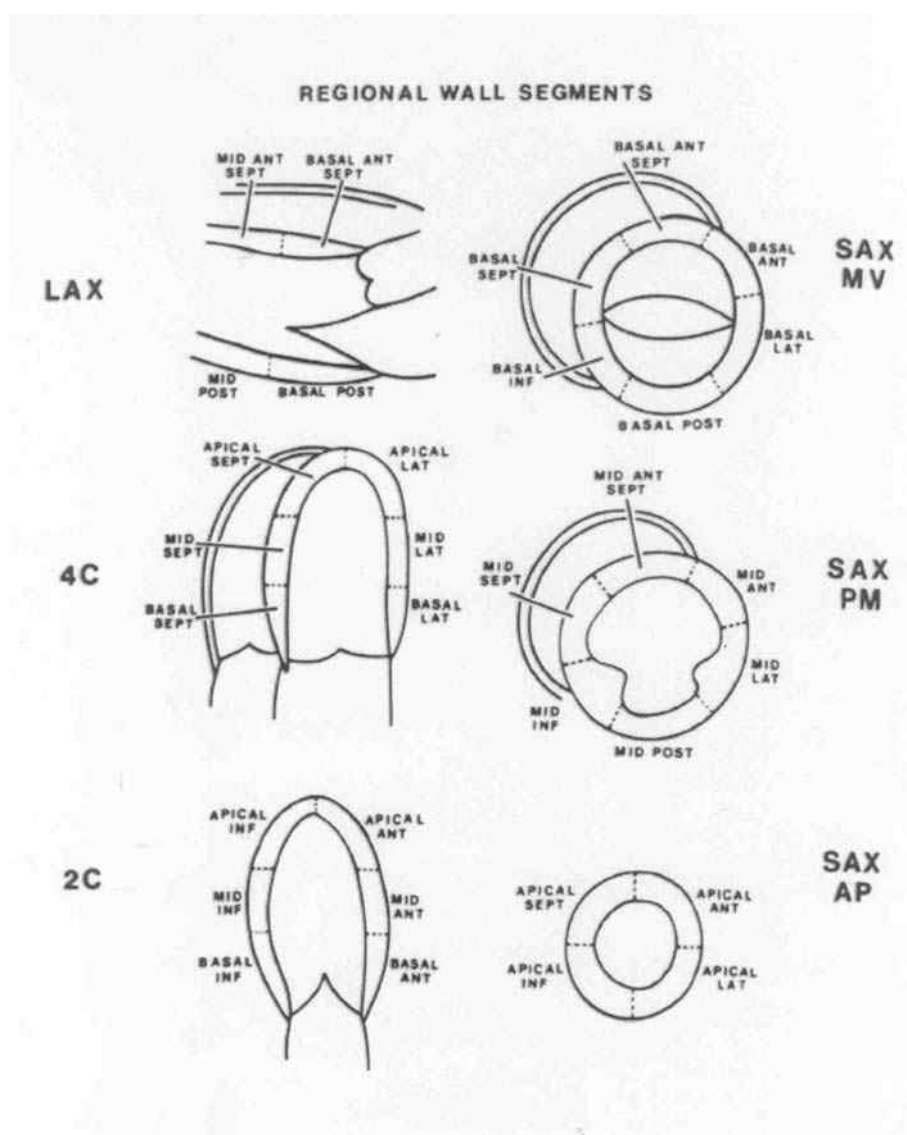


Figure 1–5 Echocardiographic images of the heart acquired in the parasternal long-axis (LAX), short-axis (SAX, at mitral valve MV, in the middle PM and at apex AP), 2- and 4-chamber views (2C and 4C). (Cerqueira, Weissman et al. 2002)

Image analysis is done qualitatively in a quad-screen format by view and scored according to the American Society of Echocardiography's 16-segment model (Figure 1–6). The wall motion score index (WMSI) is defined as the sum of individual segment scores, divided by the total number of segments, with the individual scores determined as either 1) normal, 2a) mildly hypokinetic, 2b) severely hypokinetic, 3) akinetic, 4) dyskinetic or 5) aneurysmal.(Sawada, Segar et al. 1991; Cohen, Ottenweller et al. 1993; Olmos, Dakik et al. 1998)

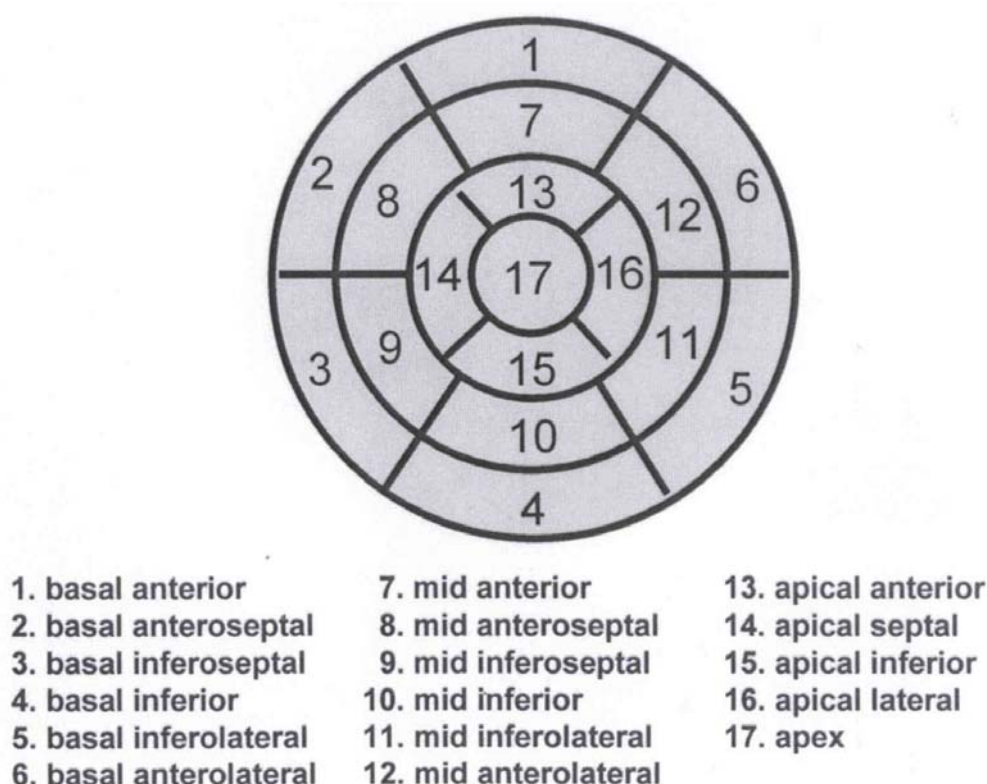



Figure 1–6 Left ventricular segmentation.(Cerqueira, Weissman et al. 2002)

Blood pressure, ECG and symptoms are recorded every three minutes during the test and endpoints are the end of the protocol with adequate heart rate ($> 85\%$ maximal predicted heart rate, MPHR), significant wall abnormalities on echocardiography, significant (> 2 mm) ST-segment depression on ECG, severe symptoms or arrhythmias.(Sawada, Segar et al. 1991) Dobutamine stress echocardiography in the hands of an examiner with correct training in the field is feasible with diagnostic images in $> 95\%$ of patients.

Summary

The clinical relevance of measuring vascular parameters and particularly arterial compliance during exercise has been addressed. The attention in this thesis lies on the technological aspect of assessing haemodynamic parameters during stress conditions. Nevertheless, the following chapters will encapsulate this engineering aspect into clinical studies on the derivation of compliance measurements in normals and diabetes, and the relation of arterial compliance with the extent of ischaemia. Both physical exercise tests (supine and standing bicycle tests) and dobutamine induced stress tests have been described here in terms of methodology and practical implications to adequately perform the necessary simultaneous pressure and flow acquisitions.



2 Haemodynamic assessment in adolescents during a standing and supine bicycle stress test*

* The content of this chapter has been published in the Proceedings of Computers in Cardiology (CinC 2002, Memphis, TN)

Non-invasive assessment of hemodynamics in adolescents with arterial tonometry and Doppler ultrasound during a conventional stress test

K Matthys, D Vanhercke, S Van Aken, K De Groote, I Coomans, P Verdonck

Abstract

Aiming to improve early diagnosis of people at cardiovascular risk, a custom setup is being developed to allow an adequate haemodynamic analysis of heart function and arterial circulation properties, based on non-invasive acquisition of pressure (arterial tonometry) and flow (Doppler ultrasound techniques) waveforms. In an experimental setting 15 healthy volunteers were examined on a custom made supine bicycle. Able to record usable data throughout the bicycle test and automatically analyze derived haemodynamic parameters such as compliance, peripheral resistance, etc., the setup was also applied in a real clinical environment. This research contributes to a more complete cardiovascular examination without significant additional discomfort for the patient or prolongation of the test protocol.

1 Introduction

Aiming to improve an early diagnosis, a setup for the adequate haemodynamic analysis of heart function and arterial circulation properties is being developed by using arterial tonometry and Doppler ultrasound techniques, not only for use in rest conditions but also during stress tests. These non-invasive techniques are comfortable for the examined subjects and allow routine application.

Quantifying the properties of heart and blood vessels is possible by the assessment of haemodynamic parameters such as peripheral resistance, arterial compliance, etc. Calculation of these parameters can be done in real-time provided that three signals are simultaneously available: heart rate, blood pressure and blood flow waveforms. The specific goal was to build an experimental diagnostic setup for use with physical exercise that allows acquiring these three non-invasively measured signals in a synchronized way from separate medical devices. Haemodynamic parameters can then be calculated automatically to investigate the effect of incremental physical stress.

2 Methods

2.1 Experimental setting

To examine the feasibility of acquiring signals continuously while the subject is performing a stress test, 15 healthy volunteers (10 male, age 23.2 ± 3.7) were asked to cycle on a in-house made supine bicycle in an experimental setting (Hydraulics Laboratory, Civil Eng. Dept, Ghent University, Belgium).



Figure 2-1 Supine stress test on a custom made bicycle.

Tonometric pressure data was recorded on the right radial artery, with a cuff calibration on the opposite arm, and Doppler flow recordings done in a suprasternal position (Figure 2-1). The load level was augmented every 3 minutes (step protocol, with a maximum of 8 levels), while cycling was done at a constant speed of 20 km/h. During exercise, an ECG recording, the pressure signal of a tonometric pen-probe (SPT-301, Millar[®] Instruments Inc., Houston, TX) placed on the radial artery and the Doppler spectrogram, automatically derived by the setup from the audio signal of a Doppler device (800CFM, GE Vingmed SA, Horten, Norway), were simultaneously acquired from the separate devices and visualized in real-time on one computer, and then processed with an in-house program (SAM, [©]S Carlier), already used for previous studies in resting conditions (Figure 2-2). The tonometric probe as well as the Doppler probe were held manually in position during the readings.

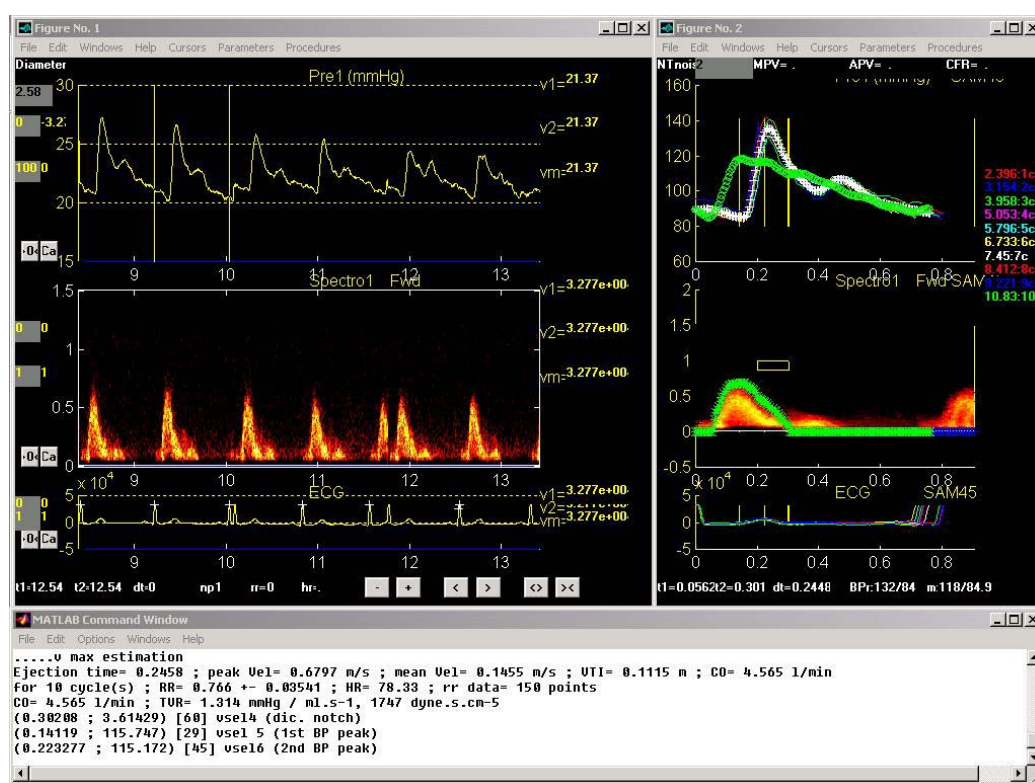


Figure 2–2 Screen print of the data analysis program (SAM, ©S Carlier). Tonometric pressure data, Doppler flow recordings and ECG are shown on the left. The same signals averaged over 1 heart cycle are shown on the right.

As a tonometer only gives information on the *waveform*, and does not provide absolute values, a calibration for the pressure waveform is necessary. This was obtained by an automatic cuff-device for domestic use (Nais Blood Pressure Watch®, Matsushita Electric Works Ltd, Osaka, Japan), applied at the opposite radial artery. A calibration measurement was done at the beginning of each load level, thus providing systolic and diastolic blood pressure values.

Pressure and flow waveforms are required at the very beginning of the vascular tree (i.e. at the site of the aortic valve). As pressure cannot be acquired non-invasively at this site (flow can by the Doppler technique), transformation of a peripheral blood pressure waveform (non-invasively measured with the tonometer) to a central aortic pressure waveform was (automatically) done by use of a generalized transfer function.(Chen, Nevo et al. 1997) With this information, parameters such as arterial compliance, peripheral resistance, aortic impedance, stroke volume, cardiac output etc. were finally calculated.

2.2 Clinical setting

The above setup was subsequently applied in a clinical environment on 9 adolescent patients (8 male, age 15.4 ± 4.4), who were scheduled for a diagnostic stress test (Figure 2–3) as part of a study protocol in which the therapeutic effect of lisinopril (ACE inhibitor) and the early symptoms of kidney damage in juvenile diabetics were investigated.



Figure 2–3 Clinical setting on a standing bicycle (Paediatric Cardiology Department, Ghent University Hospital, Belgium).

The clinical study was already on-going before the here presented feasibility study was added and as such it was imperative to adapt to the existing protocol, involving a standing (instead of supine) bicycle test with a ramp protocol (start: 0 Watt, slope: subject weight in kg/4 = W/min: e.g. 60 kg = 15 W/min). A more specialized cuff calibration device on the brachial artery intended for stress tests (inflating again every 3 minutes) could be used instead of the cuff-device for domestic use in the experimental setting. Breath-by-breath gas analysis was also to be performed to calculate peak oxygen uptake ($\text{VO}_2 \text{ max}$).

3 Results

3.1 Experimental setting

The test was completed (load level 8, 21 min) by 9 of 15 subjects and the second last level (load level 7, 18 min) was still completed by 14 of 15 subjects. One subject only reached level 6, 15 min. The number of subjects for which the calibration values could be obtained as higher load levels were reached, drops fairly quick from 11 subjects at 9 minutes of exercise (load level 4) to only 2 subjects at load level 8, due to instable readings from the cuff calibration device (Table 2–1, Cuff). Therefore, it was decided only to investigate the signals measured during the first three load levels, thus looking solely at moderate stress activity.

As signal quality from the tonometric pen-probe is very sensitive to motion artefacts, it became less feasible with higher load levels to find and stabilize a correct position for the probe on the radial artery and record a sufficient amount (i.e. 10 to 15) of heart cycles within the 3 minute timeframe of one load level. At load level 3 (6 minutes of cycling), calibration and signal quality of blood pressure, flow and ECG, were still good in 8 of 15 subjects (Table 2–1, Cycles).

<i>Load level</i>	<i>L0</i>	<i>L3</i>	<i>L6</i>	<i>L9</i>	<i>L12</i>	<i>L15</i>	<i>L18</i>	<i>L21</i>
	<i>1</i>	<i>2</i>	<i>3</i>	<i>4</i>	<i>5</i>	<i>6</i>	<i>7</i>	<i>8</i>
<i>Cuff</i>	15	14	14	11	10	7	5	2
<i>Cycles</i>	13	11	8					
<i>Female</i>	3	2	1					
<i>Male</i>	10	9	7					

Table 2–1 Number of subjects (from a total of 10 male and 5 female) for whom calibration (Cuff) and signal quality (Cycles) were still good for a specific load level (Lx).

For these 8 subjects haemodynamic parameters were calculated off line, with an emphasis on resistance and compliance values. Results are shown in Figure 2–4 and Figure 2–5.

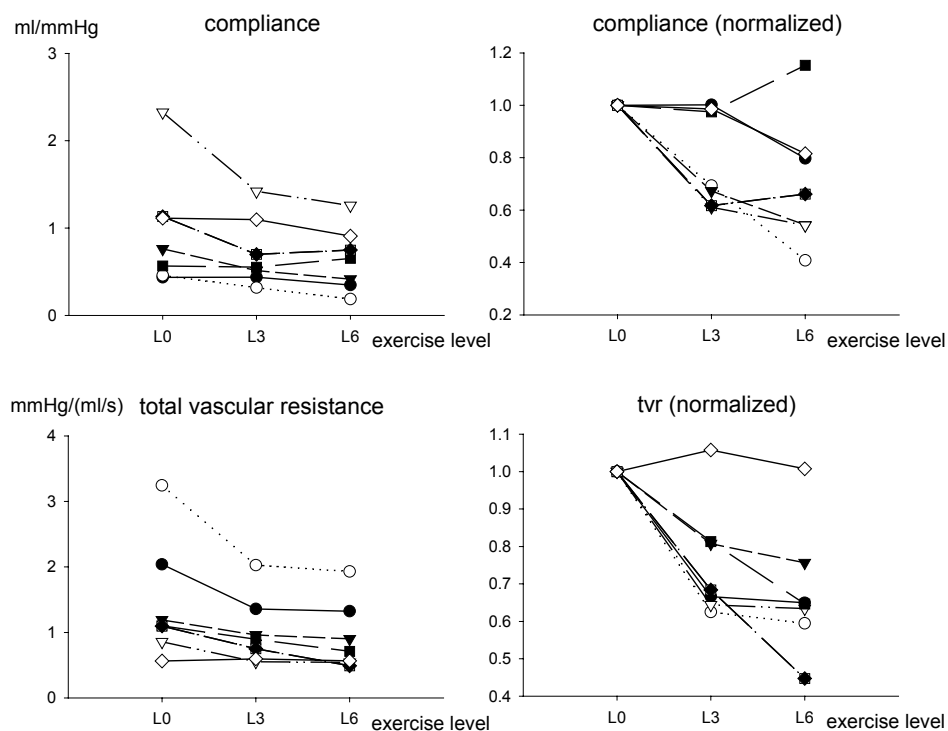


Figure 2-4 Compliance and total vascular resistance (left) also normalized to their value at load level L0 (right).

As the values for total vascular resistance and compliance varied quite a lot amongst different subjects, they were also normalized to their value at load level L0. A measure for maximal compliance is estimated by using the ratio of stroke volume to pulse pressure (difference between systolic and diastolic pressure), and a measure for the amount of damping that waveforms undergo in the vascular tree is given by a time constant τ , defined as resistance times compliance (Figure 2-5).

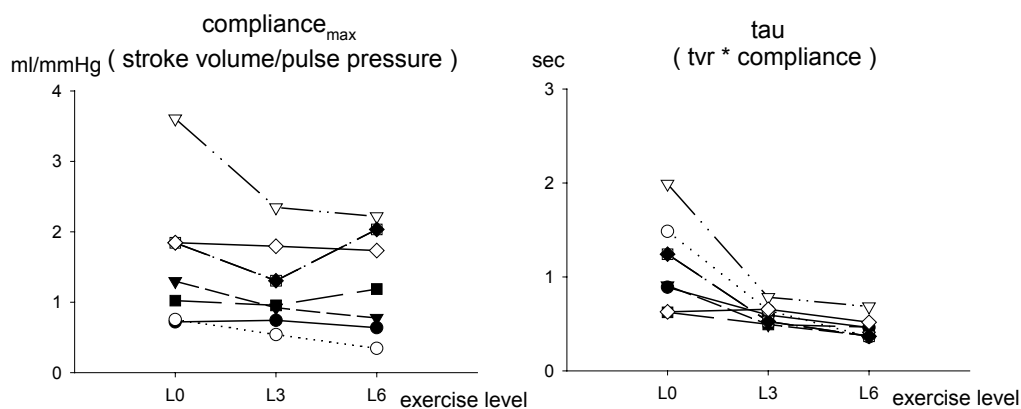


Figure 2-5 Values for compliance_{max} defined as the ratio of stroke volume to pulse pressure (left), with time constant τ defined as resistance times compliance (right).

As far as real quantification is concerned these results are definitely limited, because of the small number of subjects and the practical drawbacks, which occurred concerning calibration and raw signal quality. Nevertheless, already a fairly good indication of the change of these examined haemodynamic parameters during stress activity was obtained in a fast and non-invasive way, clearly demonstrating the potential for such a setup and protocol in a real clinical environment.

3.2 Clinical setting

A standing bicycle generates more motion artefacts to the sensitive tonometer probe and the upright cycling position is less optimal for Doppler image assessment. Another learning curve was necessary before acquiring pressure and flow waveforms every 3 minutes throughout the whole exercise test was achieved for the last 2 (of 9) patients. Reasons for failure in other 7 (of 9) cases were at first shortcomings of the diagnostic setup in the new, clinical environment (hardware failure (2), data loss (1)), external factors (patient illness (1), no show (1), unavailability of supervising physician (1)) and finally measurement factors (inability to detect radial pulse with tonometer (1)). An illustration of the outcome of a successful diagnostic test is given in Figure 2–6 to Figure 2–8 (peak exercise at 15 min, max power: 240 Watt, heart rate: 204 bpm, max SBP/DBP: 223/35 mmHg, VO_2 max: 42.1 ml/kg.min).

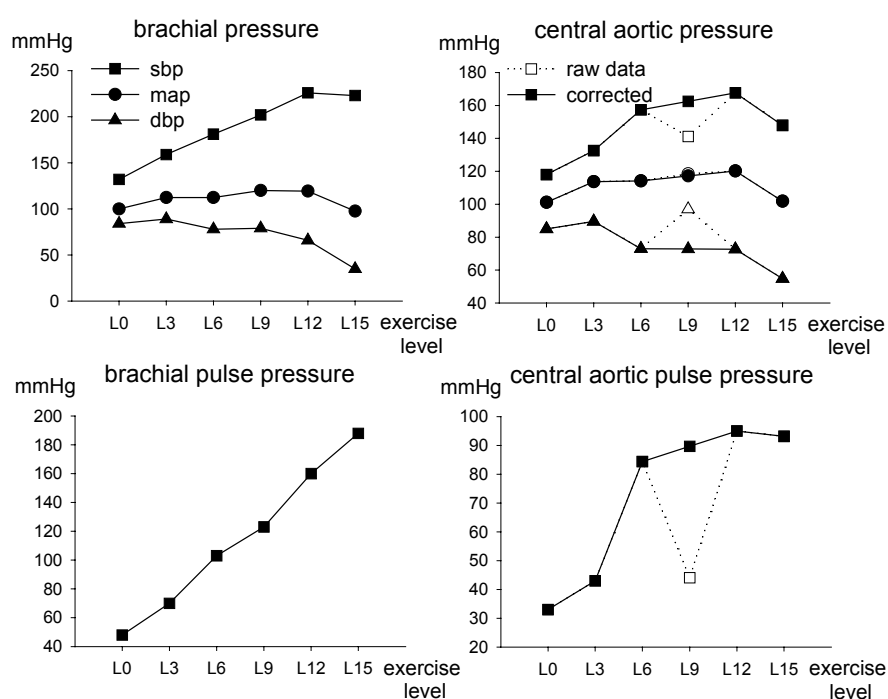


Figure 2–6 Measured peripheral (left) and calculated central aortic (right) pressure.

Figure 2–6 shows the calibration values for blood pressure. Haemodynamic calculation requires the use of the central aortic pressure; therefore it is derived with a mathematical transformation from pressure at a peripheral site. As derived aortic values showed an extreme outline value at load level L9, which after examination was due to the poor quality of the tonometer pressure data at that level, all parameters at level L9 were replaced by an average value of level L6 and level L12 (raw data vs. corrected, Figure 2–6 and Figure 2–8).

Both measured as derived pressures show an increasing systolic blood pressure and slightly decreasing diastolic pressure, thus an increase of pulse pressure during exercise. While Figure 2–7 shows the expected increasing slope of blood flow and cardiac output with exercise, the main focus lied on resistance and compliance parameters (Figure 2–8). Compliance was measured in three different ways: the pulse pressure method (Stergiopulos, Meister et al. 1995) and the area method (Liu, Brin et al. 1986), for which again two variations were used (differing by the fact that integration during calculation is done over a different part in time of the heart cycle: ‘area end’ uses the ‘dicrotic notch to end diastole’ interval, while ‘area all’ uses the whole cardiac cycle). The formulae and protocol for these compliance calculations are described in Figure 1–23 and Eqn. 1.77 to Eqn. 1.79 of Part II, Chapter 1.

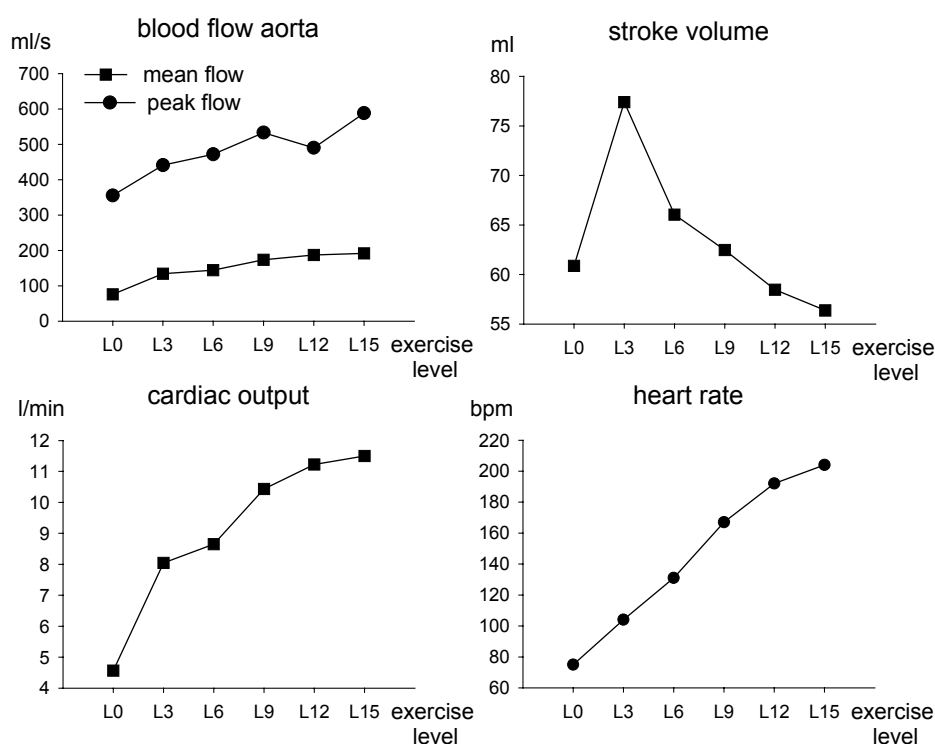


Figure 2–7 Blood flow and cardiac output values, together with heart rate and stroke volume.

For the examined subject, peripheral resistance (Figure 2–8, upper left) showed a clear decline in an almost linear way (from 1.33 mmHg.s/ml in rest to 0.53 mmHg.s/ml at peak exercise) with an average drop of 0.16 mmHg.s/ml every 3 min. Arterial compliance with pulse pressure method (Figure 2–8, lower left) seemed to drop in more of an exponential way (from 1.19 ml/mmHg in rest to 0.34 ml/mmHg at peak exercise). Compliance at maximum exercise appeared 4 times lower than in rest. The results also showed that use of the area method is less appropriate than the pulse pressure method, because it appeared more sensitive to artefacts introduced by the mathematical transformation of pressure (with transfer function) or to poor quality of the raw signals data. This is clear by the extreme outline values shown on Figure 2–8.

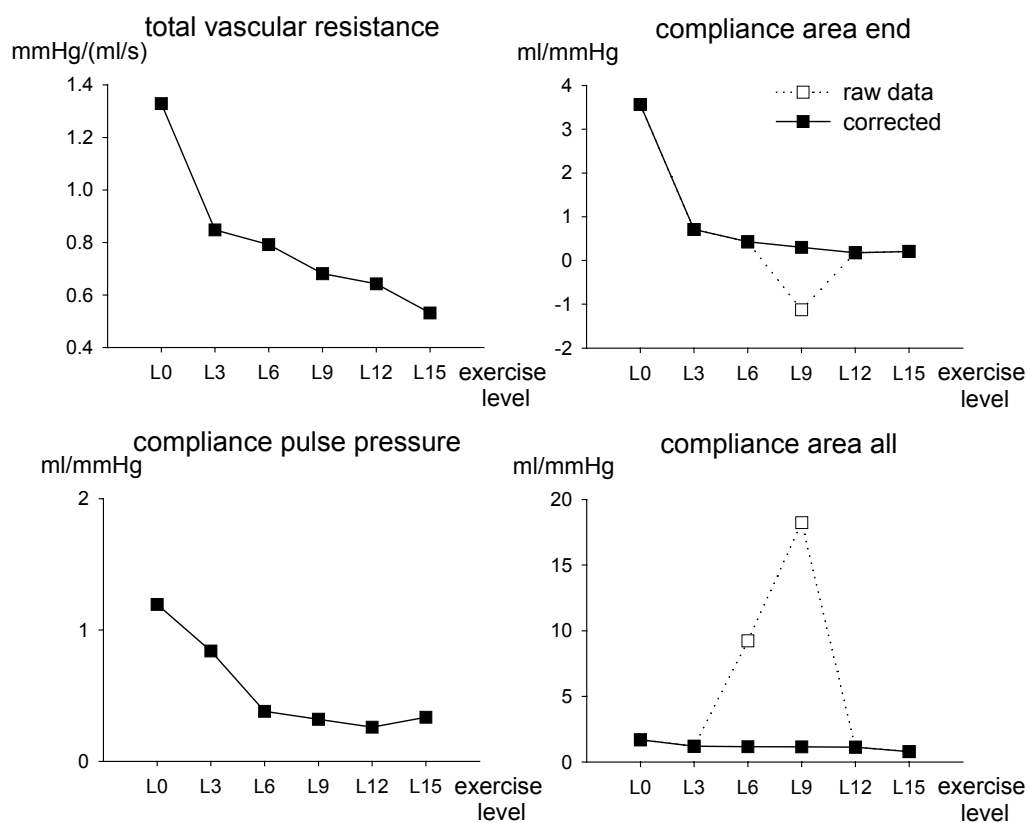



Figure 2–8 Total vascular resistance and total arterial compliance.

4 Discussion and Conclusion

First, these experiments have taught that an experienced operator is necessary for handling the tonometric and Doppler probes. Second, it became obvious that despite preparations in an experimental setting the level of difficulty increases significantly again when going to an existing clinical setting and a learning curve is always present for each specific study protocol. In this case, the standing bicycle setup, added gas-analysis equipment, and adversary effects of patients vs. healthy volunteers (e.g. illness during exercise) posed additional difficulties to be overcome. Especially the non-invasive pressure measurement requires a lot of attention. Perhaps a hands-free tonometer using a wrist fixation - e.g. an automated Colin[®] device (Colin[®] Medical Instruments Corp., San Antonio, TX) - could be an improvement, but it is also far more expensive. Also, a very reliable calibration device is imperative.

Looking more at the computational point of view, more efforts are necessary on the level of the mathematical transformation from peripheral to central aortic pressure and its validity during exercise, which is a difficult thing to assess as such an investigation requires invasive data during exercise which most likely no ethical committee would approve to. Another issue to be investigated is whether during exercise it is still valid to use 'simple' definitions of resistance, compliance etc. Maybe pressure-dependent formulae could be more appropriate in fast changing haemodynamic conditions such as during exercise. (Langewouters, Wesseling et al. 1985; Li, Cui et al. 1990)

The quantitative results of this study are certainly limited. Nevertheless, it has demonstrated the feasibility of adding extra haemodynamic information to a routine diagnostic investigation by the combination of simple non-invasive techniques such as an ECG, Doppler and tonometer device, and this both in an experimental as well as real clinical exercise test environment. The knowledge obtained in this study can contribute to a more complete cardiovascular examination without significant additional discomfort for the examined subject or prolongation of the test protocol.



3 Haemodynamic assessment in adults during dobutamine stress or a treadmill exercise test*

* Part of the content of this chapter has been published in the Supplement to the JACC, Volume 39, Number 9 (Supplement B) May 1, 2002, Page 5B

Total Arterial Compliance as a Predictor of Ischemia at Stress Echocardiography

Brian A Haluska, Koen Matthys, Rodel Leano, Stephane G Carlier, Thomas H Marwick

The content of this chapter has been submitted to the Journal of the American College of Cardiology (JACC, march 2004)

Influence of Arterial Compliance on Extent of Ischemia during Stress Echocardiography

Koen S Matthys, Brian A Haluska, Robert Fathi, Stephane G Carlier, Thomas H Marwick

Abstract

The objective was to identify an association between total arterial compliance (TAC) and extent of ischaemia at stress echocardiography (SE). The extent of ischaemia at SE is ascribed to the balance between cardiac workload and coronary perfusion. However, the status of the arterial tree may play a role because reduced total arterial compliance (TAC) poses an increased workload on the heart at the same time as potentially worsening coronary perfusion. In this study, 255 consecutive patients (147 men; age 59 ± 9), who presented for SE for clinical indications, were examined. Ischaemia was defined by an inducible or worsening wall motion abnormality, and wall motion score (WMSI) was calculated by the ASE standard. Peak WMSI was indicative of ischaemia and/or scar and delta WMSI was indicative of extent of ischaemia. TAC was assessed by simultaneous radial applanation tonometry and pulsed wave Doppler at rest in all patients. Ischaemia was identified by SE in 65 patients (25%). Total arterial compliance was 1.08 ± 0.42 ml/mmHg in the normal group and 1.17 ± 0.51 ml/mmHg for the abnormal group ($p = \text{NS}$). However, peak WMSI was predicted by age, blood pressure, TAC, risk factors and use of a β -blocker. Moreover the change in WMSI with stress was determined by TAC, risk factors and use of a β -blocker. While traditional cardiovascular risk factors are strong predictors of ischaemia on SE, TAC is an independent predictor of extent of ischaemia.

1 Introduction

Total arterial compliance (TAC) reflects the properties of the vessel wall and distal vasculature, and is a determinant of arterial pressure and flow. Arterial compliance is reduced with age, vascular disease and hypertension (Safar and London 1987; London, Pannier et al. 1994; McVeigh, Bratteli et al. 1999), and is linked with the sequellae of these disorders. Reduction of vessel elasticity leads to an increment of afterload on the heart (as lower arterial compliance is closely related to increased pulse pressure), which in turn leads to left ventricular hypertrophy.(Rajkumar, Cameron et al. 1997) Increased pulse pressure is a determinant of cardiovascular risk and mortality.(Benetos, Safar et al. 1997; Franklin, Khan et al. 1999; Kannel, Vasan et al. 2003) A stiffer vascular system also leads to lower diastolic pressure (Randall, Van Den Bos et al. 1984), resulting in a decreased coronary perfusion pressure.(Kass, Saeki et al. 1996)

Since decreased arterial compliance increases cardiac load and decreases coronary driving pressure, it might be anticipated that this aspect of vascular function would be a determinant of ischaemia in patients with coronary artery disease (CAD).(Gatzka, Cameron et al. 1998) Although limited data support an association with reduced exercise capacity and the presence of a lower ischaemic threshold (Kingwell 2002; Kingwell, Waddell et al. 2002), the relation between compliance and the extent of ischaemia is undefined. Potentially, TAC may determine the degree of positivity of SE. This study sought whether arterial compliance was a determinant of ischaemic burden, using an imaging test to measure the extent of ischaemia.

2 Methods

2.1 Patient selection

Presenting for SE for clinical indications, 255 consecutive patients (147 men; age 59 ± 8 years) were studied - 65 dobutamine echo (DSE) and 190 exercise echo (ExSE). TAC was assessed by simultaneous radial applanation tonometry and pulsed wave Doppler at rest in all patients. Coronary angiograms were performed at the discretion of the treating cardiologist in 26 (10%) patients.

2.2 Clinical evaluation

Cardiovascular risk factors that were designated include smoking, hypertension (HTN; blood pressure $> 140/90$), diabetes (DM; fasting blood glucose > 6.7 mmol/l) and hypercholesterolaemia (CHOL; total cholesterol > 5.2 mmol/l), previous myocardial infarction (PREV MI) and previous cardiac intervention (PREV CI). Most patients and the relevant control subjects were receiving one or more of the following medical therapies: β -blockers, angiotensin-converting enzyme inhibitors (ACE inhibitors), calcium antagonists, long acting nitrates or a statin.

2.3 Stress echocardiography

Stress echocardiography was performed in all patients – either DSE or ExSE, based on anticipated functional capacity. After preparing patients for standard 12-lead ECG monitoring, and obtaining resting blood pressure, resting echocardiographic images (5 views) were digitally acquired as cine-loops consisting of one cardiac cycle. For ExSE, patients underwent a maximal treadmill test using a Bruce protocol; for DSE, dobutamine was then infused at a rate of 5, 10, 20, 30 and 40 $\mu\text{g/kg/min}$ in three-minute stages. Echocardiographic images were obtained at each stage on videotape and digitally acquired at rest, low dose (5 or 10 $\mu\text{g/kg/min}$), pre-peak and peak infusion. Blood pressure, heart rate, ECG changes and symptoms were also monitored at each stage. Standard endpoints were used to terminate the

test. A diagnostic test was defined as reaching $> 85\%$ maximal predicted heart rate (MPHR), and patients were excluded if they did not reach $> 85\%$ MPHR.

The digital SE images were stored on magneto-optical disk and analyzed off-line by an expert observer. The American Society of Echocardiography's 16-segment wall motion scoring was used with a positive test (ischaemia) defined by an inducible or worsening wall motion abnormality and wall motion score index (WMSI) calculated by the method described earlier in the first chapter of this part.(Olmos, Dakik et al. 1998) Peak WMSI was considered to be reflective of total ischaemic burden (ie. ischaemia and/or scar) and change in WMSI was used to represent the extent of ischaemia.

2.4 Total arterial compliance

Total arterial compliance was calculated by the pulse pressure method (PPM, see section 6.3.3, Part II, Chapter 1) by simultaneously acquiring applanation tonometry and pulsed wave Doppler of the left ventricular outflow. 2D echocardiographic images and pulsed Doppler were acquired using a Vingmed System 5 ultrasound system (GE Vingmed Ultrasound SA, Horten, Norway) with a 1.7 MHz harmonic imaging probe. Radial applanation tonometry was performed using a Millar[®] SPT-301 Mikro-Tip[®] transducer (Millar[®] Instruments Inc., Houston, TX). Blood pressure was taken using a standard sphygmomanometer in the arm that the tonometry was being performed on after the patient had been allowed to rest 5-10 minutes. Tonometric pulse, pulsed Doppler (obtained from the audio output of the echo machine), and ECG were all acquired simultaneously with specialized software using an A/D board (WaveBook 512, IOtech Inc., Cleveland, OH) and transferred to a laptop PC and stored as binary files. Measurements were taken after 5-10 minutes of rest. First, the patient's blood pressure was taken and entered into the acquisition program to calibrate the tonometric pulse signal. With the patient in a left lateral decubitus position, standard resting echocardiographic images (5 views) were acquired and stored digitally for off-line analysis. Tonometry was performed on the left arm in all patients. The radial artery was located and when optimal Doppler and tonometry signals were found, three sets of gated data (ECG, tonometry, Doppler) were acquired and stored. Depending on heart rate, this was usually 20-30 cardiac cycles per patient.

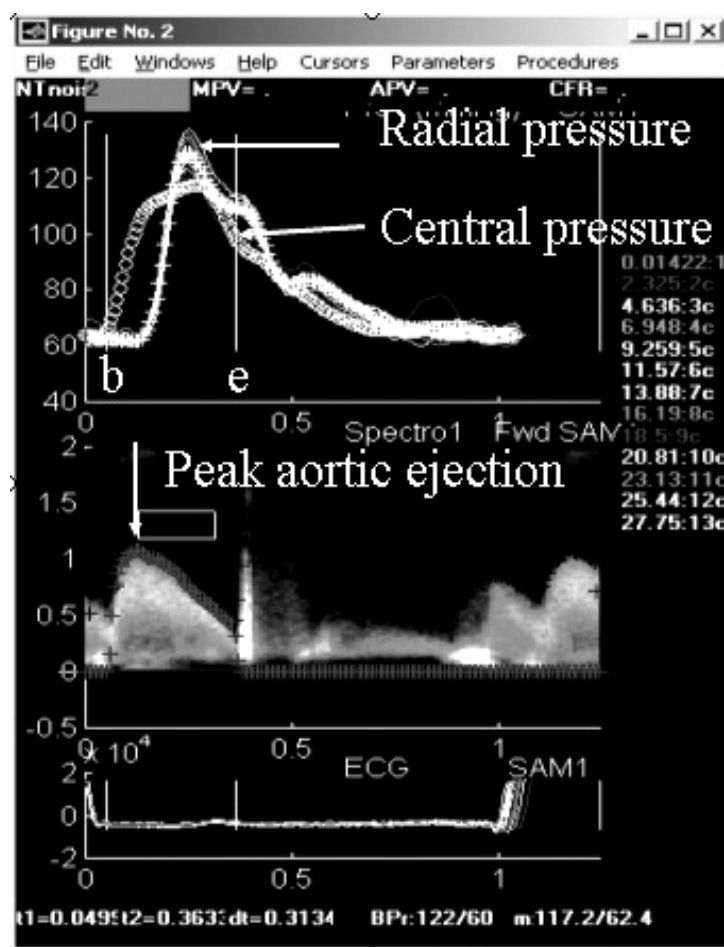


Figure 3–1 An in-house data analysis program (SAM, ©S Carlier) was used to determine mean values for pressure and flow and calculate a mean aortic pressure waveform using a transfer function model.

The binary files were processed and analyzed using an in-house analysis program (SAM, ©S Carlier) written in MatLab 4 environment (The Mathworks, Inc., Natick, MA). The left ventricular outflow tract diameter (LVOT) was measured off-line from the digitally stored parasternal long axis view and entered into the analysis program. Calibration of the tonometry was performed using mean and diastolic brachial cuff pressure. Specific cardiac cycles of tonometry and Doppler were chosen from the raw dataset based on data quality and averaged for analysis - depending on data quality this amounted from 4 to 15 cycles. After identifying the Doppler signal, beginning and end ejection and peak ejection on both Doppler and pressure signals, the analysis program determined mean values for pressure and flow and calculated a mean aortic pressure wave using the transfer function (Figure 3–1). (Chen, Nevo et al. 1997) Mathematical algorithms in the analysis program are used to derive values for compliance and other haemodynamic indices from the pressure and flow data.

2.5 Statistical analysis

Statistical analysis was undertaken using commercially available software (SPSS v9.0, SPSS Inc., Chicago, IL). Continuous data was represented as mean \pm SD. Independent samples t-test was performed to compare the positive and negative SE groups. The level of significance was set at a p-value of 0.05. General linear univariate and multivariate models were performed to determine predictors of peak WMSI (ischaemia) and delta WMSI (extent of ischaemia).

3 Results

Clinical characteristics of the group are shown in Table 3–1. The SE test was positive for ischaemia (abnormal SE) in 65 patients (25%). A t-test for equality of means revealed that patients with abnormal SE were more likely to be older, male and taking medication. Further, there were significant differences in diastolic blood pressure (78 ± 10 mmHg vs 71 ± 12 mmHg; $p < 0.0001$), cardiac output (4.7 ± 1.2 l/min vs 5.2 ± 1.6 l/min; $p = 0.007$), and total vascular resistance (1.32 ± 0.39 mmHg/(ml/s) vs 1.12 ± 0.38 mmHg/(ml/s); $p = 0.001$) between the normal and abnormal SE groups. However, TAC was 1.08 ± 0.42 ml/mmHg for the group without ischaemia and 1.17 ± 0.51 ml/mmHg for the ischaemic group ($p = \text{NS}$). Of the patients with abnormal SE there were 39 (60%) with ischaemia (with or without scar), 35 (53%) with scar only and 22 (34%) with viability. WMSI was 1.6 ± 0.5 at rest, 1.7 ± 0.5 at peak, and delta WMSI was 0.1 ± 0.3 .

<i>Patient clinical characteristics</i>			
	<i>All (N = 255)</i>	<i>- SE (N = 190)</i>	<i>+ SE (N = 65)</i>
Age	59 ± 9	58 ± 8	62 ± 10
Male	147 (77%)	100 (53%)	47 (72%)
Smoker	94 (42%)	56 (32%)	38 (73%)
Hypertension	166 (70%)	127 (69%)	39 (75%)
Diabetes mellitus	114 (47%)	99 (52%)	15 (29%)
Hypercholesterolaemia	119 (47%)	84 (47%)	35 (67%)
β-blocker therapy	58 (25%)	27 (15%)	31 (60%)
ACE inhibitor therapy	83 (36%)	65 (36%)	18 (37%)
Ca ⁺⁺ antagonist therapy	81 (35%)	57 (31%)	24 (51%)
Nitrate	19 (9%)	3 (2%)	16 (44%)
Statin	85 (37%)	61 (34%)	24 (46%)

Table 3–1 Patient clinical characteristics: all (N = 255); normals group (- SE, N = 190); abnormals group (+ SE, N = 65). Numbers give frequency of occurrence in each specific group. Percentages are modified for missing values.

General linear (univariate and multivariate) models were constructed to determine predictors for peak WMSI (total extent of abnormal function), and delta WMSI (extent of ischaemia).

Variables entered into the model were cardiovascular risk factors, medications and pressure and flow characteristics. Variables with significance levels are depicted in Table 3–2 and Table 3–3. The independent correlates of peak WMS were age, pressure, TAC, risk factors and β -blocker use, while the correlates of delta WMS were TAC, risk factors and β -blocker use.

<i>Univariate</i>			<i>Multivariate</i>		
<i>Variable</i>	<i>R²</i>	<i>p</i>	<i>Variable</i>	<i>R²</i>	<i>p</i>
Age	0.232	0.003	Age	0.198	0.02
SBP	0.201	0.03	SBP	0.206	0.01
DBP	0.246	0.001	DBP	0.211	0.01
CO	0.194	0.04	PP	0.209	0.01
TAC	0.260	<0.0001	TAC	0.231	0.003
Smoking	0.413	<0.0001	Smoking	0.460	<0.0001
DM	0.420	<0.0001	DM	0.426	<0.0001
β -Blocker	0.336	<0.0001	β -Blocker	0.346	<0.0001

Table 3–2 Univariate and multivariate linear models for predictors of peak WMSI. Pressures are peripheral measurements. SBP = Systolic blood pressure; DBP = diastolic blood pressure; PP = pulse pressure; CO = cardiac output; TAC = total arterial compliance; DM = diabetes.

<i>Univariate</i>			<i>Multivariate</i>		
<i>Variable</i>	<i>R²</i>	<i>p</i>	<i>Variable</i>	<i>R²</i>	<i>p</i>
Age	0.158	0.05			
SBP	0.230	<0.0001	SBP	0.209	<0.0001
PP	0.237	<0.0001	PP	0.236	<0.0001
CO	0.210	0.001	CO	0.157	0.01
TAC	0.194	0.003	TAC	0.153	0.02
Smoking	0.297	<0.0001	Smoking	0.312	<0.0001
DM	0.367	<0.0001	DM	0.411	<0.0001
β -Blocker	0.244	<0.0001	β -Blocker	0.259	<0.0001

Table 3–3 Univariate and multivariate linear models for predictors of delta WMSI. Pressures are peripheral measurements. SBP = systolic blood pressure; DBP = diastolic blood pressure; PP = pulse pressure; CO = cardiac output; TAC= total arterial compliance; DM = diabetes.

4 Discussion and Conclusion

This study confirms the association of reduced arterial compliance with more extensive ischaemia. These findings reinforce the importance of vascular function to not only cardiac function but also the results of stress echocardiography.

Compliance was investigated as a possible determinant of CAD. Aortic stiffness and left ventricular mass are increased in subjects having CAD.(Gatzka, Cameron et al. 1998) However, the understanding of how these entities interact is still limited. As wave reflections are stronger in a stiffer vascular system, resulting in a higher augmentation index, it has been shown that increased augmentation index, and hence decreased compliance is associated with an increased risk of coronary artery disease.(Hayashi, Nakayama et al. 2002) Total arterial compliance is probably a predictor of CAD, but not a strong one, especially when traditional risk factors are also accounted for (as shown in the univariate and multivariate general linear models). The lack of difference in total arterial compliance between the groups of patients with a normal and abnormal stress echocardiogram in this study does not contradict the role of compliance in ischaemia. This can probably be accounted for by the number of diabetics and hypertensives in the group with normal stress echocardiograms, who likely had reduced compliance due to their underlying disease and cardiovascular risk factors.

Also the interaction of arterial compliance with ischaemia has been looked upon. The extent of ischaemia reflects an interplay between supply and demand, and both are influenced by compliance. On one hand, ejecting into a stiffer systemic tree will increase cardiac load and myocardial oxygen consumption (increased demand).(Kelly, Tunin et al. 1992) On the other hand, a loss of compliance induces an increase in pulse pressure, resulting from an increase in systolic and a decrease in diastolic pressure.(Randall, Van Den Bos et al. 1984) The systolic pressure increase contributes to the increased cardiac load (Kelly, Tunin et al. 1992), while the decrease in diastolic pressure reduces coronary perfusion (decreased supply).(Watanabe, Ohtsuka et al. 1993; Kass, Saeki et al. 1996) Previous work has shown an association of compliance with exercise capacity and ischaemic threshold.(Kingwell 2002; Kingwell, Waddell et al. 2002) Kingwell et al. have shown that in healthy individuals exercise capacity is related to maximum cardiac output, which may be influenced by systemic compliance.(Kingwell 2002) Indeed, Cameron et al. already showed a correlation between


lower arterial stiffness and higher levels of aerobic fitness.(Cameron and Dart 1994; Cameron, Rajkumar et al. 1999)

However, in CAD patients exercise capacity is related to myocardial ischaemia, the threshold of which is mainly determined by coronary perfusion and cardiac workload, or thus the interaction between supply and demand. Kingwell et al. hypothesized in a study of 96 CAD patients that a stiffer systemic tree would lower ischaemic threshold.(Kingwell, Waddell et al. 2002) Myocardial ischaemia was not assessed with an imaging technique as was done in this manuscript, but by means of evaluating the ST-segment depression on the ECG during a treadmill test. These investigators found that various different measures of arterial stiffness (arterial compliance TAC, pulse wave velocity PWV, augmentation index Aix) inversely correlated with time to ischaemia, independent of potential confounding factors such as gender, age or mean arterial pressure. In this study, it was found from the stress echo test that total arterial compliance was not only a predictor of peak WMSI (ischaemia and resting dysfunction) but also of delta WMSI (extent of ischaemia) in the multivariate model.

In conclusion, while traditional cardiovascular risk factors such as age, hypertension, diabetes etc. are strong predictors of ischaemia on stress echocardiography, reduction of TAC potentiates the extent of ischaemia on stress echocardiography.

V Vascular haemodynamics during coronary intervention

This final part looks at the diagnostic value of haemodynamic indices derived from pressure and flow, measured with minimally invasive techniques, during coronary intervention. The first chapter elaborates on the technique of coronary stenting, the commonly used quantification techniques during an intervention (QCA and IVUS) and functional indices derived from pressure and flow, especially the fractional flow reserve index (FFR). In a second chapter, QCA, IVUS and FFR are compared for the assessment of optimal stent deployment, while the third chapter digs deeper into the impact of the so-called ‘waterfall’ effect present in the myocardial coronaries on the derivation of the FFR index.

A decorative vertical bar on the left side of the page, consisting of a thin grey line and a thicker black line.

1 Background: Stents, QCA, IVUS & FFR

1 Coronary stenting

1.1 Overview

In case a patient with coronary vessel disease cannot be helped with the administration of drugs, an intervention will be imperative. One of the most common techniques used to alleviate the effects of atherosclerosis (lumen narrowing due to plaque deposits) is coronary stenting. A coronary stent is a tubelike, endovascular prosthesis that is put at the height of the lesion in a coronary artery to enlarge the cross-sectional area and further maintain the new lumen size.

Today, dozens of stenttypes are commercially available and are marketed by numerous companies. Stents have to comply with various demands in terms of strength, durability, flexibility and biocompatibility. An excellent review on the market of coronary stents can be found in the books of P.W. Serruys and co-workers.(Serruys and Rensing 2002)

The stents used in this thesis are ACS Multi-Link™ stents (Guidant/Advanced Cardiovascular Systems, Santa Clara, CA). They are balloon-expandable (see further in this chapter), highly flexible, stainless steel stents with a profile built of rings interconnected with several bridges (Figure 1–1). The clinical use of this stent started in 1993, and FDA⁶ approval was obtained for it in 1997.(Kutryk and Serruys 1999)

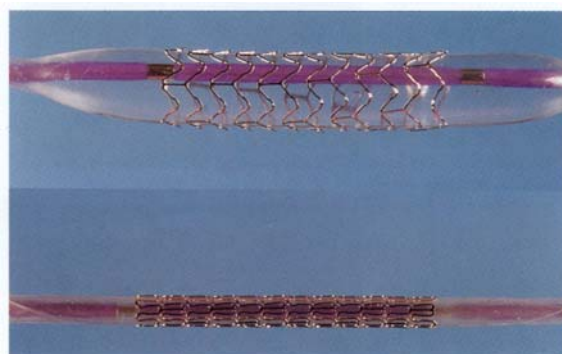


Figure 1–1 ACS Multi-Link™ stent (Guidant/Advanced Cardiovascular Systems, Santa Clara, CA).(Serruys and Kutryk 1998)

⁶ U.S. Food and Drug Administration, highest control and regulation body of the Dept. of Health and Human Services in the U.S. More information: <http://www.fda.gov/>

1.2 Technique

Stents are being inserted in the body via a catheter. A guiding catheter is being inserted from the femoral artery up to the ostia of the epicardial coronaries. It is used to inject contrast dye for visualization (see section 2 of this chapter) and “guide” another catheter that has the stent at its tip. Inside the stent-carrying catheter a guidewire is present that allows to control catheter motion and positioning (Figure 1–2).

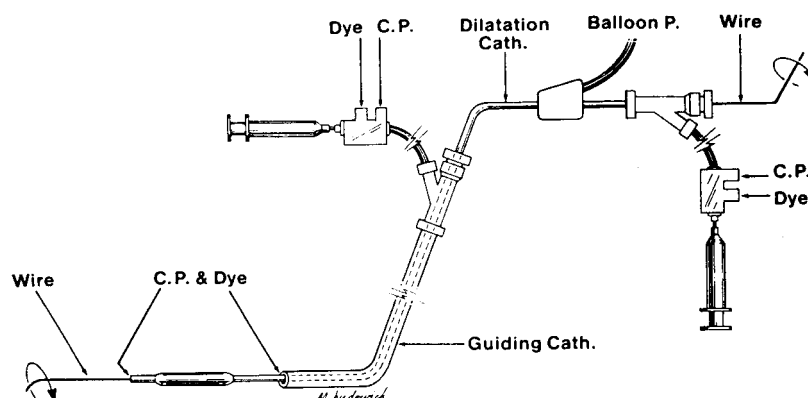


Figure 1–2 Stent delivery system for balloon expandable stents.(Schlant and Alexander 1994)

Self expandable stents are elastic springs that, once put in the correct position, are being unfolded to their uncompressed size by removing a protective shield. Balloon expandable stents are more common. They are plastic deformable and are being delivered in a compressed state on a deflated balloon. At the correct site, the balloon is inflated and the stent is expanded. When the positioning has been successful, the balloon is deflated and withdrawn, while the stent in its expanded shape maintains the new lumen opening⁷ (Figure 1–3).

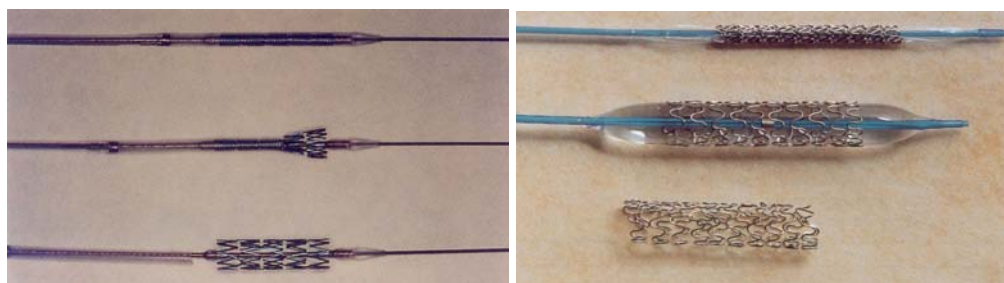


Figure 1–3 Left: Self expandable stents. Right: Balloon expandable stents.(Serruys and Kutryk 1998)

⁷ This procedure has in fact evolved from the technique of percutaneous coronary transluminal angioplasty (PTCA), where a vessel is expanded by means of a balloon catheter but no stent is left behind.

1.3 Complications

Apart from casual incidents such as vessel damage, occlusion of side branches, rupture of the delivery balloon etc., two major complications are to be addressed here: restenosis and thrombosis.

1.3.1 Restenosis

In-stent restenosis is the reoccurrence of narrowing in a treated section (Figure 1–4, left). The restenosis mechanism is complex and still not fully understood. Implanting a stent induces a healing response from the body, which is the so-called ‘neointimal scar tissue’ proliferation. A too strong tissue proliferation (‘intimal hyperplasia’) can cause in-growth in the new stent lumen and is often mentioned as a primary cause for restenosis. Restenosis is being reduced by optimizing the post-interventional therapy, and special coatings on the stent struts. (White and Ramee 1991; Serruys, Foley et al. 1993; Topol 2002)



Figure 1–4 Left: Cross-sectional area of a restenosed stent. The black dots are the stent struts, and new deposits are narrowing the lumen again. (Serruys and Kutryk 1998) Right: Example of a thrombosis growth three days after stent implantation into a venous graft, together with intrusion of the vessel wall through the stent profile. (Serruys 1997)

1.3.2 Thrombosis

Thrombosis is the formation of a blood clot (thrombus) which attaches to the stent struts and subsequently induces an occlusion (Figure 1–4, right). Subacute thrombosis can occur up to one month after intervention. A stent is per definition a thrombogenic device. Important players that can affect thrombogenicity are the interaction of blood components and stent struts, and the correct positioning or contact with the vessel wall. During an intervention it is

therefore important that an appropriate stent is chosen corresponding to the lesion in terms of length and diameter, and that an adequate inflation pressure is being applied so that no loose struts occur. To avoid thrombotic occlusions after a successful procedure, the patient is being treated immediately with antiplatelet agents (substances that impede blood clotting).

1.4 Drug-eluting stents

In the 1990s antithrombotic stentcoatings were developed to reduce the thrombogenicity of the metallic stent struts and moreover to provide for a very localized treatment. The pharmacological agents (e.g. Heparin) were for instance inserted in a polymer substance that was applied as a stentcoating by using high-tech production methods (e.g. PE CVD or Plasma-Enhanced Chemical Vapor Deposition). (Harder, Rzany et al. 1999) Together with the upcoming use of antiplatelet agents and optimal high-pressure stent deployment, subacute thrombotic incidence has now dropped to about 0.5%. (Sousa, Serruys et al. 2003a)

These Heparin-coated stents paved the way for the drug-eluting stents, conceived to attack the second and more persistent problem of restenosis. Current-generation commercially available stents have been used to apply a drug-carrier coating that allows elution of the drug with a controlled kinetic profile. A lot of research is on-going for optimization of drug-eluting stent strut geometry. Both synthetic polymers and biological materials are investigated as coating materials with potential, and the research for the appropriate drug or even multi-drug insert is also very hot topic. (O'Neill and Leon 2003; Sousa, Serruys et al. 2003a; Sousa, Serruys et al. 2003b) Although the long-term reliability and the cost-benefit relation (price for an uncoated stent is about 500 €, for a drug-stent 2400 €) should still be defined (Fattori and Piva 2003), the outcome of recent large-scale, multi-center patient studies such as SIRIUS (1100 patients) and RAVEL (238 patients) is definitely impressive. The RAVEL study group reports that, considering an in-stent restenosis of 50% or more of the luminal diameter after 6 months, there was a 26.6% occurrence in the standard-stent group and no occurrence at all in the drug-stent group. (Morice, Serruys et al. 2002) Thus has the question definitely become valid whether at the advent of drug-eluting stents vascular radiation therapy will become obsolete in the fight against neointimal proliferation and restenosis. (Teirstein and King 2003)

2 Quantitative coronary angiography (QCA)

2.1 Overview

Angiography is the gold standard for visualization of a coronary intervention. The history of angiography runs parallel with that of cardiac catheterization. In the early days of cardiac catheterization (Forssmann, 1929) a radiopaque contrast medium was being injected in the bloodstream that could be visualized by X-rays (fluoroscopy). Later on, the technique of percutaneous insertion of catheters advanced, and dye was usually injected with a catheter right above the aortic valve. Further in 1958, this non-selective technique was replaced by visualizing only the desired coronary artery by Sones and co-workers. The preshaped catheters that are specific for every coronary ostium, thought of by Judkins in 1968, advanced this method a lot. Still, determination of percentage stenosis with coronary angiography remained very dependent on the interpretation of the operator. It was the work of Gensini and later Brown in the 1970s to finally replace the mere 'eyeballing' method by a quantitative approach by projecting the angiogram onto an X-Y coordinate system. Nowadays, quantitative coronary angiography (QCA) is a high-tech visualization method fully using modern technology in terms of digital imaging processing, automatically delineation of vessel walls etc. (Forssmann 1929; Verel and Grainger 1978; Cohn 1979; Grossman 1980; Schroeder 1985; Pijls and De Bruyne 1997)

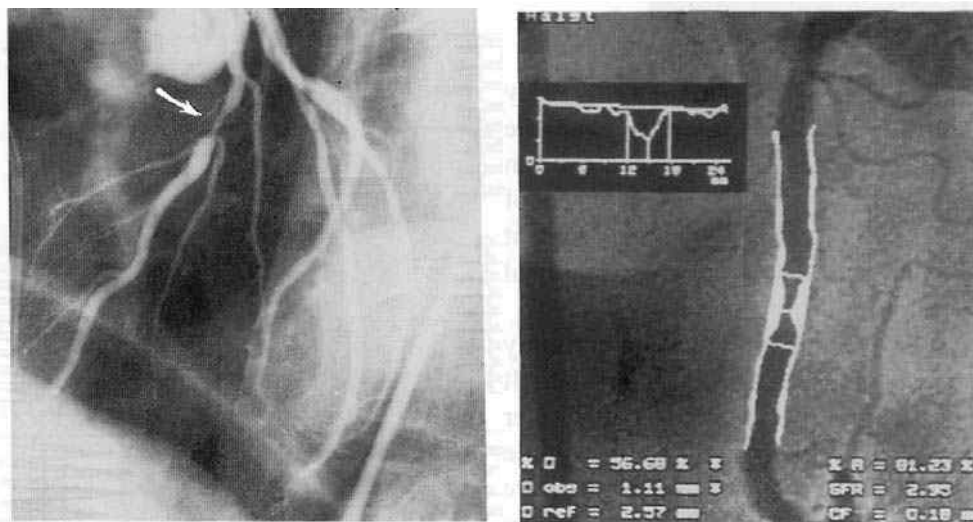


Figure 1–5 Left: Classical angiography, showing a lesion quantified by the operator ('eyeballing'). Right: Quantitative coronary angiography (QCA), showing a delineated lesion of which the size is being assessed in an X-Y coordinate system.

2.2 Technique

Classic X-ray machines have one beam, but advanced devices with two beams are available to perform a ‘biplane’ angiography. In any case, visualization has to be done from several different angles as the coronaries have a tortuous 3D structure. As a result, vessels can overlap each other in one specific view or a stenosis can be placed in a eccentric way, etc. Projections are combinations of LAO (‘Left Anterior Oblique View’) and RAO (‘Right Anterior Oblique View’), with cranial and caudal directions (Figure 1–6).(Schlant and Alexander 1994)

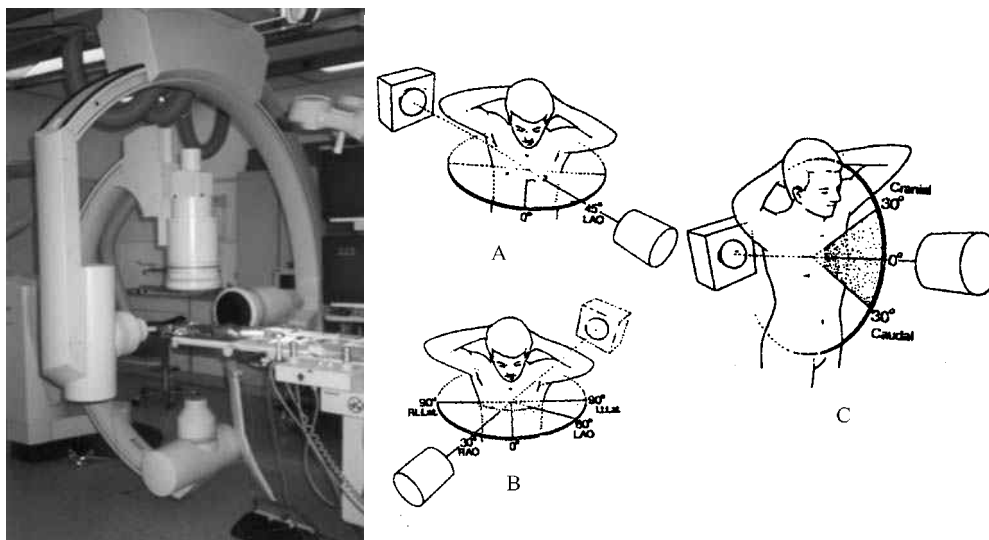


Figure 1–6 Left: Biplane angiography. Right: A: Left anterior oblique view (LAO), B: Right anterior oblique view (RAO) , C: Cranial and caudal.

Based on the quantitative information from the QCA, cut-off values can be determined to assess the severity of a stenosis. The minimal lumen diameter (MLD) of the stenosed area is being compared with a proximal, healthy considered segment with reference diameter (RD), so that the diameter stenosis percentage (DS) can be calculated with:

$$DS = 100 \cdot \frac{RD - MLD}{RD} \quad \text{Eqn. 1.1}$$

Looking specifically at deployment of stents, a DS smaller than 10% is generally considered to be an adequate indication for an optimal stent placement (all struts well apposed against the vessel wall).(Kutryk and Serruys 1999)

2.3 Pros and cons

QCA is very reproducible, fairly cheap, fast and safe. Hence the reasons why it is still the gold standard for invasive diagnostic visualization. Apart from the fact that several projections in different angles are necessary to get a complete and reliable view, there is a more profound drawback. QCA only determines lumen size and not vessel size at the height of the stenosis and as mentioned a proximal, healthy considered segment is used as a reference. When the effect of atherosclerosis is spread out (e.g. multi vessel disease), there is a risk of mistakenly comparing the lesion with an affected segment. Since the lumen size of the latter will be smaller than that of a healthy segment, underestimation of the stenosis percentage will occur. This is also why the presence of light residual stenosis ($< 20\%$) is often not detected on a QCA.(Pijls and De Bruyne 1997)

3 Intravascular ultrasound (IVUS)

3.1 Overview

Research in intraluminal ultrasound started around the 1960s when Cieszynski mounted a piezo-electric crystal on a cathetertip for the investigation of inner ventricle walls and coronaries via the crystal induced ultrasound.(Cieszynski 1960) The mounted transducer elements were gradually improved over the years and expanded in number, but it took some twenty years before a general interest in intravascular ultrasonography came about.

As ultrasound can penetrate the vessel wall, it seemed a handy tool to study plaque-morphology and composition. The technical challenge was the reduction of transducers and cathetersize to navigate with ease and with control through the coronary arteries. Rapid development of micro-electronics and piezo-electric technology reduced cathetersizes down to about 3F (0.9 mm) in 1994 already, small enough to gain access in the bigger part of lesions being treated with catheterization (Figure 1–7).(Yock, Fitzgerald et al. 1995; Giuliani, Gersch et al. 1996; Uren 1996)

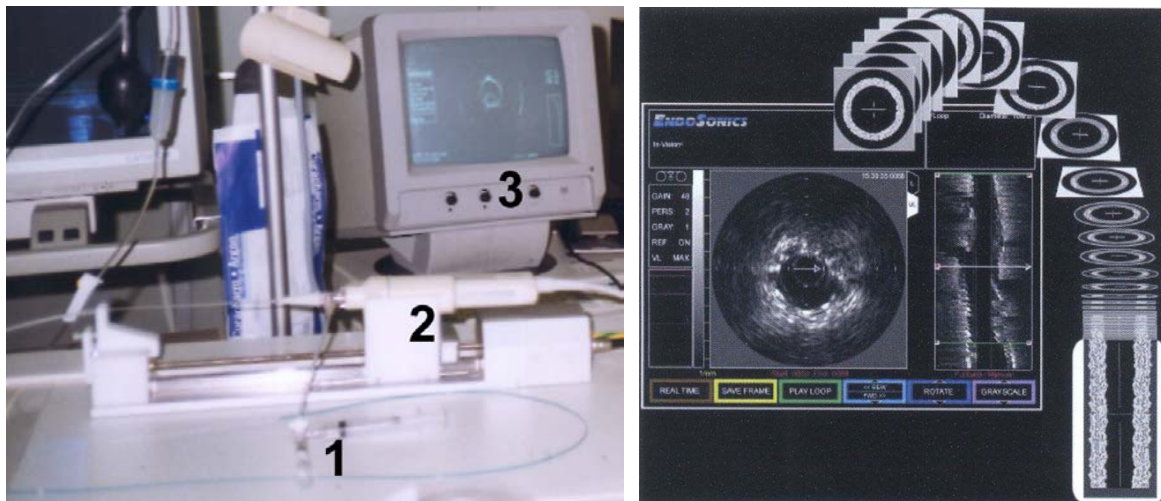


Figure 1–7 Left: Intravascular ultrasound (IVUS) catheter (1), catheter pull-back mechanism (2) and IVUS image (3). Right: 2D IVUS image with cross-sectional information (left) and composition of longitudinal vessel wall information (right) by putting all the 2D slices one after another.

3.2 Technique

As with conventional ultrasound, the basic principle of IVUS or intravascular ultrasound is the conversion of electrical energy into ultrasound waves by means of piezo-electric crystals, and the detection of the reflected waves (echoes) with a transducer. The transducer converts the acoustic energy of the ultrasound wave back into electrical energy, which is then amplified and filtered to create a graphical image, representing a cross-sectional area of the vessel and vessel wall at the position of the transducer.

Older mechanical scan systems used one transducer which was being rotated, but modern electronical systems, also called 'solid state' scan systems, use multiple (32 to 64) transducers mounted concentrically on the cathetertip. IVUS transducers are positioned very close to the vessel wall so that a very high image resolution can be obtained (axial $< 100 \mu\text{m}$, lateral $< 250 \mu\text{m}$) when using high frequencies (20 to 50 MHz). The high resolution will limit the tissue penetration depth (about 5 mm at 20 MHz down to 3 mm at 40 MHz). Ultrasound catheters are being inserted into the vascular system with the same techniques as for an interventional treatment (use of a guidewire and fluoroscopy). Image acquisition is being done by manually or automatically pulling back the IVUS catheter (Figure 1–7, left) from distal to proximal through the stenosis so that subsequent cross-sectional slices can be made (10 tot 30 frames/s, Figure 1–7, right). In post-processing, even 3D reconstructions can then be made (Figure 1–8, right). (White and Ramee 1991; Schlant and Alexander 1994; Giuliani, Gersch et al. 1996)

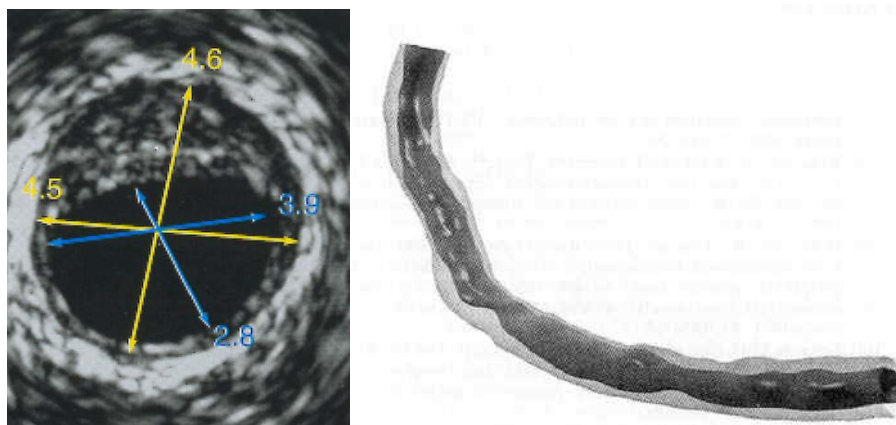


Figure 1–8 Left: Quantification of geometrical parameters of a stenosed coronary segment on one IVUS image.(Uren 1996) Right: Many IVUS images put one after another to generate a 3D reconstruction.(Thoraxcentre, Rotterdam, The Netherlands)

3.3 Applications

IVUS technology can be used in a multiple of vascular investigations. IVUS images allow to look at vessel wall structure beyond the endothelial layer. The composition of plaque can also be distinguished (soft or fatty plaque, fibrous plaque, calcification) by the contrast differences on the image. It is further an accurate tool for quantification of geometrical vessel parameters (Figure 1–8, left). Common indices measured are the Lumen Symmetry Index (LSI) and the Plaque Eccentricity Index (PEI) (Uren 1996; Di Mario, Gorge et al. 1998) but they will not be discussed further here.

In terms of guiding with intervention, IVUS can be used to assess the reference segment (pre-interventional) or look at dissections and formation of thrombosis (post-interventional). More specific to this thesis, an excellent IVUS application is assessing the expansion and correct positioning of a stent implant (Yock, Fitzgerald et al. 1995; Uren 1996; Di Mario, Gorge et al. 1998), as shown on Figure 1–9 and further elaborated in the following chapter.

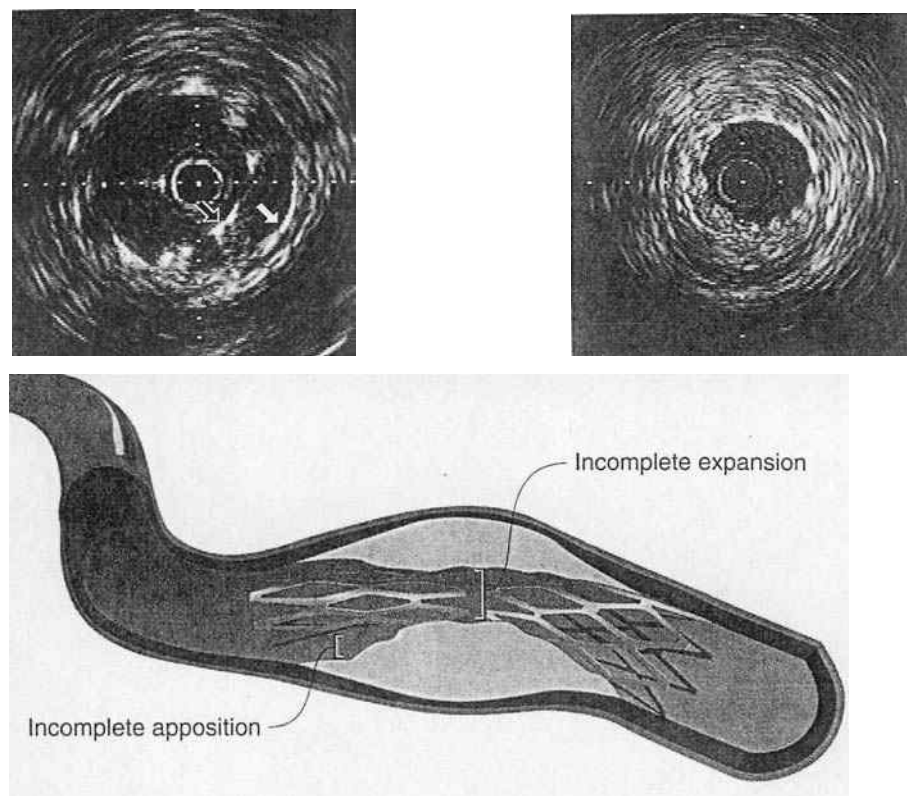


Figure 1–9 Upper left: incomplete stent apposition (black arrow is the stent strut, white arrow shows the vessel wall). Upper right: incomplete stent expansion (compare lumen size with upper left image). Bottom: Suboptimally deployed stent.(Yock, Fitzgerald et al. 1995)

4 Functional pressure and flow indices

4.1 Overview

In recent years, a lot of attention has been paid to the assessment of functional indices in the cathlab that are derived from minimally invasive pressure and/or flow measurements. These indices are easily measured and can provide additional diagnostic information next to angiography or ultrasound.(Fischer, Samady et al. 2002)

In the 1980s, Grüntzig⁸ already tried to relate functional significance of a stenosis with pressure measurements, but the results were not satisfying. At that point in time, the catheters used were still not small enough with respect to the coronary lumen. Further, it was not yet recognized that only measurements in hyperaemia and not in rest are relevant, and also that it is not the transstenotic pressure gradient as such, but the absolute distal pressure which determines myocardial perfusion.

A variety of indices exist. Velocity-based indices comprise e.g. the ‘coronary flow reserve’ (CFR), the ‘diastolic to systolic velocity ratio’, the ‘proximal to distal velocity ratio’, etc. Indices such as the ‘instantaneous hyperaemic diastolic flow pressure slope index’ (IHDFPS), use both pressure and flow. Thinking of a clear discriminating power between significant and non-significant stenoses and the potential for assessing stent deployment, the ‘Fractional Flow Reserve’ (FFR) index was chosen in this thesis to be investigated further.(De Bruyne, Bartunek et al. 1996; Pijls, De Bruyne et al. 1996; Pijls and De Bruyne 1997; Kern 2000; Meuwissen, Chamuleau et al. 2001)

4.2 Fractional Flow Reserve (FFR)

The myocardial fractional flow reserve FFR assesses the limitation of heart muscle perfusion by the presence of an epicardial stenosis.(Carrier, Van Langenhove et al. 1999; Kern 2000) Fractional flow reserve (FFR) is defined as the ratio of myocardial flow in a stenosed coronary segment during hyperaemia (Q) to hyperaemic flow through the same segment in

⁸ Andreas Grüntzig, 1939-1985. German physician working at University Hospital Zurich, Switzerland. Performed first balloon angioplasty in 1977 as an alternative to coronary artery bypass grafting.

the hypothetical case that there is no stenosis present (Q_N). Pijls et al. (Pijls, van Son et al. 1993) and De Bruyne et al. (De Bruyne, Baudhuin et al. 1994) have shown that FFR can be obtained from pressure measurements proximal and distal to the stenosis only and that it assesses the physiologic significance of a coronary stenosis (Pijls, De Bruyne et al. 1996). The pressure-based FFR is easily measured during transluminal interventions and normal and cut-off values have unequivocally been determined (Pijls and De Bruyne 1997; Pijls, Kern et al. 2000), as explained in section 4.3 of this chapter.

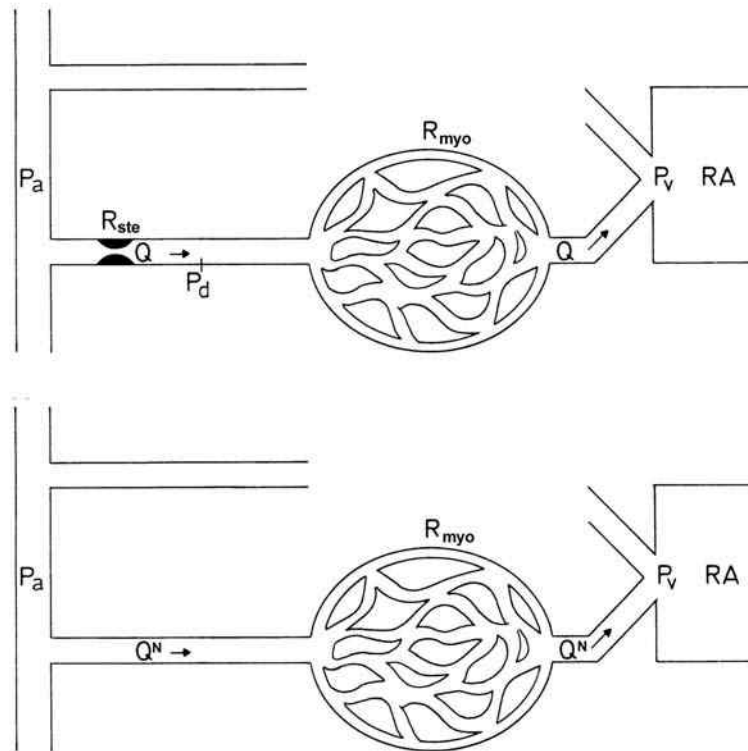


Figure 1–10 The simplified model of the coronary circulation as proposed by Pijls and De Bruyne, consisting of a resistance representing the stenosis (R_{ste}) in series with the myocardial resistance (R_{myo}). P_a : aortic pressure; P_d : pressure distal to the stenosis; P_v : venous pressure; Q : flow ($Q_N = Q$ when $R_{ste} = 0$); RA: right atrium. (modified with permission from (Pijls and De Bruyne 1997))

The simplified model of the coronary circulation as proposed by Pijls and De Bruyne consists of a resistance representing the stenosis (R_{ste}) placed in series with the myocardial resistance R_{myo} (Figure 1–10, upper panel). Pressure drops along these resistances are defined as:

$$\Delta P_{ste} = P_a - P_d \quad \text{Eqn. 1.2}$$

$$\Delta P_{myo} = P_d - P_v \quad \text{Eqn. 1.3}$$

In the above formulae, P_a stands for mean aortic pressure, P_d for mean distal coronary pressure and P_v for mean central venous pressure. P_a , P_d and P_v need to be measured during maximal coronary hyperaemia when myocardial resistance is minimal and assumed to be constant (Pijls and De Bruyne 1997). This condition is imperative for the calculation of flow in the model of Pijls-De Bruyne as, in the case of constant myocardial resistance, flow is directly proportional to the pressure drop causing the flow movement. Maximal myocardial flow (Q) can then be written as:

$$Q = \frac{\Delta P_{myo}}{R_{myo}} = \frac{P_d - P_v}{R_{myo}} \quad \text{Eqn. 1.4}$$

In absence of a stenosis, R_{ste} equals zero and P_d would approximate P_a (Figure 1–10, lower panel). In this hypothetical case, flow (Q_N) is given as:

$$Q_N = \frac{P_a - P_v}{R_{myo}} \quad \text{Eqn. 1.5}$$

FFR can thus be expressed as:

$$FFR = \frac{Q}{Q_N} = \frac{(P_d - P_v) \cdot R}{(P_a - P_v) \cdot R} = \frac{(P_d - P_v)}{(P_a - P_v)} \approx \frac{P_d}{P_a} \quad \text{Eqn. 1.6}$$

In the latter equation, the assumption was made that the central venous pressure P_v is negligible. There is a controversy about the exact pressure to be used distal to the myocardial resistance for the calculation of FFR. This is addressed extensively in the last chapter. Formulae that separate the influence of the coronary arteries and the collaterals have also been derived, as well as formulae for multiple stenoses, but this will not be discussed further here. (De Bruyne, Pijls et al. 2000)

4.3 Practical use

FFR can be determined quickly and simply. The average aortic pressure P_a is measured with a catheter and the distal pressure P_d can be recorded with an ultrathin pressure wire. (Pijls, De

Bruyne et al. 1996) A healthy coronary will have an FFR equal to 1, independent of patient, artery or myocardial distribution. The cut-off value of 0.75 has a 95 % accuracy to distinguish between significant and non-significant stenosis (Figure 1–11).(De Bruyne, Bartunek et al. 1995; Pijls, Van Gelder et al. 1995; Pijls and De Bruyne 1997) Collateral flow is being accounted for and it can be used with multi-vessel disease as no healthy reference segment is necessary.

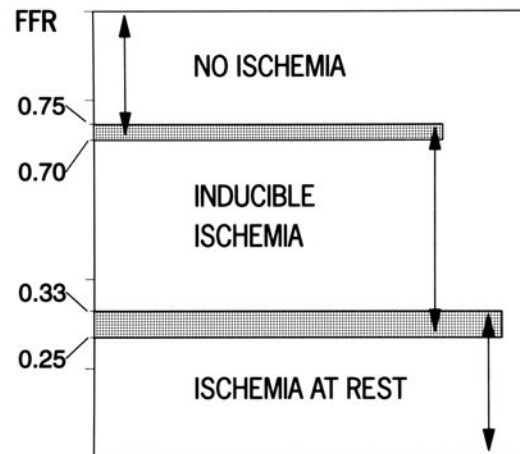


Figure 1–11 FFR cut-off boundaries for ischaemia.

Recently, cut-off values for FFR to assess the deployment of coronary stents have also been proposed in literature. Hanekamp et al. defined an FFR larger than 0.94 as an indication for optimal stent deployment.(Hanekamp, Koolen et al. 1999) However, these FFR cut-off values for stent deployment are not established yet and are the subject of discussion, as will be shown in the next chapter.(Fearon, Luna et al. 2001; Matthys, Carlier et al. 2001)

Summary

In this chapter the technique of coronary stenting has been explained. The stent delivery system was addressed and the attention was put on two important complications: restenosis and thrombosis. While the mechanism of the first is still not fully understood, the latter can be induced by an obstruction in the bloodstream such as a badly apposed or incomplete deployed stent implant. State-of-the-art technology in terms of drug-eluting stents that drastically reduce these complications have been described.

The basic principles have been described of two diagnostic imaging techniques that visualize the interventional procedure and quantify the outcome. Quantitative coronary angiography is the gold standard technique making use of contrastfluid and X-ray. It is fast and well reproducible, but it can underestimate a stenosis in certain cases. Intravascular ultrasound is a more expensive technique that allows imaging of a cross-sectional area, including information on wall and plaque morphology and composition.

Finally, the functional index of Fractional Flow Reserve has been explained. It is an index derived from pressure measurements that can easily be performed during the intervention and that allows to have additional diagnostic information. However, some controversy on the exact derivation of the formula does exist. It will be addressed in the last chapter of this part.

A sharp cut-off value for FFR (0.75) to evaluate whether a stenosis is significant and is to be treated or not, has been well established in literature. A second cut-off value for optimal stent deployment (0.94) has also been derived, but still deserves some investigation. It will be dealt with in the following chapter.



2 Evaluation of the FFR Index for the Assessment of Stent Deployment*

* The content of this chapter has been published in Cathet Cardiovasc Intervent 54:363-375 (2001)

In vitro study of FFR, QCA and IVUS for the assessment of optimal stent deployment
K Matthys, S Carlier, P Segers, J Ligthart, G Sianos, P Serrano, P Verdonck, PW Serruys

Abstract

Evaluation tests were done to assess whether the fractional flow reserve (FFR) index discriminates between suboptimally and optimally deployed stents. Latex tubes ($\varnothing = 4\text{mm}$) with diameter stenosis 40% ($n = 3$), 50% ($n = 3$) and 60% ($n = 3$) were tested in a pulsatile flow system using water. Measurements were done at baseline ($n = 9$; FFR/QCA) and after suboptimal (SOD; 3 mm balloon at 8 atm) and optimal (OD; 4 mm balloon at 16 atm) deployment of a 35 mm stent ($n = 6$; FFR/QCA/IVUS). Varying Q from 150 to 50 ml/min increased FFR by 2-7%. Conversely, at 100 ml/min, FFR increased by only 0.8% from SOD to OD ($P < 0.05$). Extrapolating data to blood flow, the gain in FFR from SOD to OD is less than 5% for $Q = 100\text{ ml/min}$, while FFR may increase by 15 to 20% by changes in blood flow from 50 to 150 ml/min. One must conclude that IVUS and QCA are more appropriate for the assessment of optimal stent deployment.

1 Introduction

The availability of ultrathin pressure wires, allowing accurate pre- and poststenotic pressure measurements, has increased the use of fractional flow reserve (FFR) in clinical practice. FFR has, nevertheless, some important limitations due to the fact that FFR is determined by the pressure drop over the lesion. First, this pressure drop is function of flow. FFR is thus by definition sensitive to the flow level in the coronary artery. Myocardial infarction may have a large impact on maximally recruitable flow during hyperaemia and, consequently, on the calculated values of FFR. Second, FFR has been proposed as a valuable tool to assess optimal stent deployment during intervention (Hanekamp, Koolen et al. 1999). This implies that the difference in pressure drop over a sub- and optimally deployed stent is large enough to allow discrimination between both situations.

In this study, an in vitro setup will be used to address both raised concerns regarding FFR to (i) test the flow dependency of FFR, and (ii) investigate whether FFR is able to discriminate between suboptimally and optimally deployed stents.

2 Methods

2.1 In vitro setup

The experimental setup comprises a cardiovascular simulator to generate physiologic aortic pressures in a closed hydraulic circuit, using water as test fluid. Water viscosity is roughly three times lower than blood viscosity. In order to fulfil the requirements of fluid dynamic similarity between the experimental model (water) and the real (blood) flow in the coronary circulation, experiments are performed at low water flows (range: 50 to 200 ml/min), corresponding to blood flows of 150 to 600 ml/min, hereby largely covering the normal physiological range of hyperaemic coronary blood flow. The conversion is further addressed in detail in the discussion and in Appendix A. Stenosed latex tubes, representing diseased epicardial coronary segments with different degree of stenosis severity, were inserted in this circuit. 9 latex tubes ($\varnothing = 4$ mm) were tested with stenosis length of 15 mm and target diameter stenosis (DS) of 40 % ($n = 3$), 50 % ($n = 3$) and 60 % ($n = 3$).

2.1.1 *The cardiovascular simulator*

The cardiovascular simulator was described in earlier work (Verdonck, Kleven et al. 1992; Segers, Dubois et al. 1998; Segers, Fostier et al. 1999), and is not discussed in detail. Figure 2–1 shows a schematical drawing of the setup of heart (a) and coronaries. To simulate the tortuous pattern of the coronary tree in an anatomical correct way, the latex coronary artery phantoms were mounted on a 3D shape of a human heart, a thin-walled latex “epicardial surface” (b). The aortic outlet of the original simulated heart was connected to the inlet of this latex epicardium. The normal flow-path of blood within the heart was by-passed by a V-shaped PVC-tube (c). To have coronary inflow immediately distal to the aortic valve, a bileaflet aortic prosthetic valve (d) (St. Jude Medical Inc., St. Paul, MN) was placed at the V-tube outlet. Intra-arterial pressure measurements show realistic aortic pressure wave contours distal to the aortic valve at the outlet (Figure 2–4, lower panel), which justifies this intervention in the afterload of the simulator.

At the aortic outlet, a latex aorta model (e) and two epicardial coronary vessels can be connected (f, g). In this study only the connection in the LAD position (g) was used to mount one of nine latex coronary artery phantoms (h). The epicardial segment is connected downstream to a computer-controlled time-varying resistance (i) which impedes coronary flow in systole, representing the myocardial resistance vessels. This myocardial resistance is then, in turn, connected to a passive resistance element (j), modelling the capillaries of the myocardium.

2.1.2 The coronary artery phantoms

The stenotic epicardial coronary segments were modelled as latex tubes moulded in several layers on three tubular moulds ($\varnothing = 4$ mm), with different narrowing sizes in the middle according to the desired stenosis severity (DS = 40 %, 50 % and 60 %). In previous attempts to dilate 100 % latex tubes by means of a balloon catheter, the stenosed segment returned completely to its original dimensions due to elastic recoil. Therefore, a plastic substance was introduced at the site of the narrowing, and the elastic latex compound was used solely for the healthy part of the coronary segment (Figure 2–2). The elastic-plastic model thus obtained suited the purpose of the tests of which the results are commented below. One can also refer to the discussion for further details on the coronary artery phantoms.

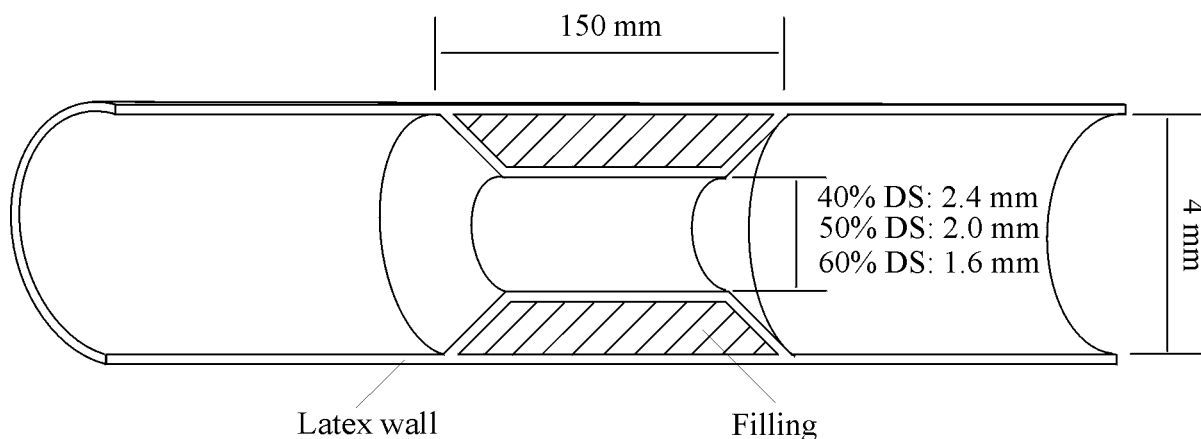


Figure 2–2 Drawing of the coronary artery phantom. A plastic substance is introduced at the site of the narrowing (filling) . The elastic latex compound is used solely for the healthy part of the coronary segment. Depending on the degree of diameter stenosis (resp. 40, 50 and 60% DS), different inner diameters (resp. 2.4, 2.0, 1.6 mm) had to be accounted for.

2.1.3 Passive and active myocardial resistance

The passive resistance element is composed of 29 capillaries captured in a water-filled reservoir (Figure 2–3, right side)(Segers, Fostier et al. 1999). The resistance can be changed by increasing the pressure in the water reservoir and thus occluding the capillaries. Coronary flow, however, is inhibited during systole due to the mechanical contraction of the heart muscle, and myocardial blood delivery is maximal during relaxation (Mates, Gupta et al. 1978; Pijls and De Bruyne 1997). The passive resistance was therefore connected in series with a time-varying resistance, which impedes the flow during systole, and is minimal during diastole. A 10 ml syringe is used as an air-filled reservoir, with one latex tube (representing a myocardial resistance vessel) on the inside (Figure 2–3, left side).

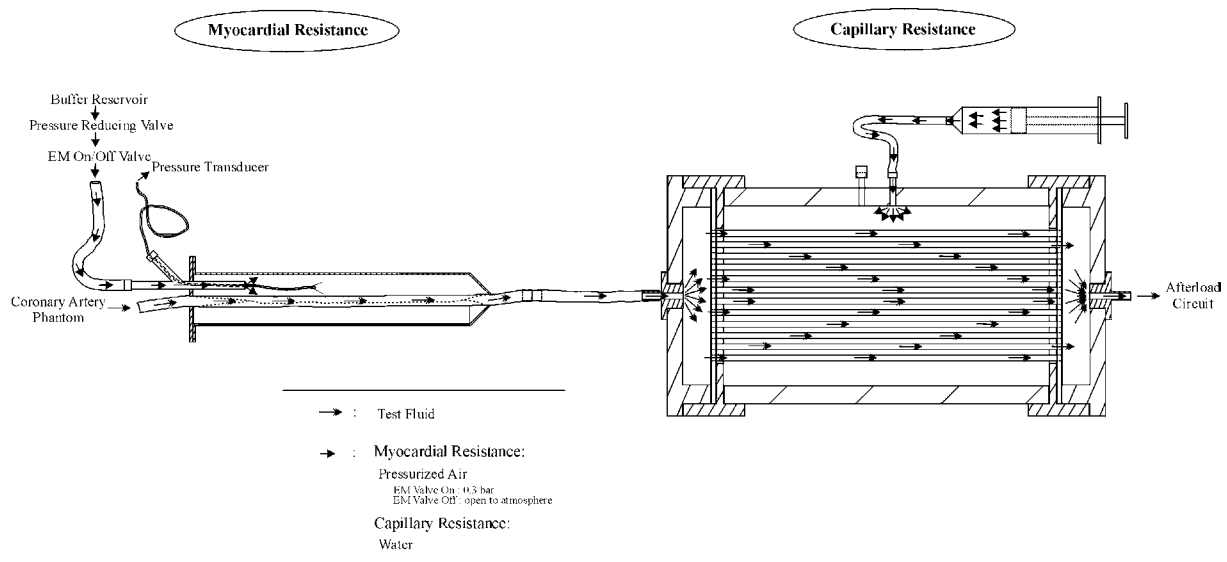


Figure 2–3 The capillaries of skeletal muscles, tissue and organs are modeled as a passive resistance element (right side). The contraction of the myocardial muscle is simulated by a time-varying resistance (left side). When an electromagnetic (EM) on/off valve closes, the time-varying resistance becomes inactive, and flow passes through the latex tube, enclosed in the syringe (full line contour). When the time-varying resistance is activated, pressure is delivered from a buffer reservoir through the opened on/off valve into the syringe and the latex tube collapses (dotted line contour).

The air-filled reservoir of the resistance is connected via an electromagnetic on/off valve to a buffer reservoir in the pneumatic circuit of the cardiovascular simulator. This way, the latex tube is collapsed - and myocardial flow impeded - in phase with myocardial contraction. Figure 2–4 (upper left) clearly shows that without the myocardial resistance, maximal flow is

delivered during systole, which is not physiologically correct. Maximal blood delivery shifts to diastole when the resistance is activated (Figure 2–4, upper right).

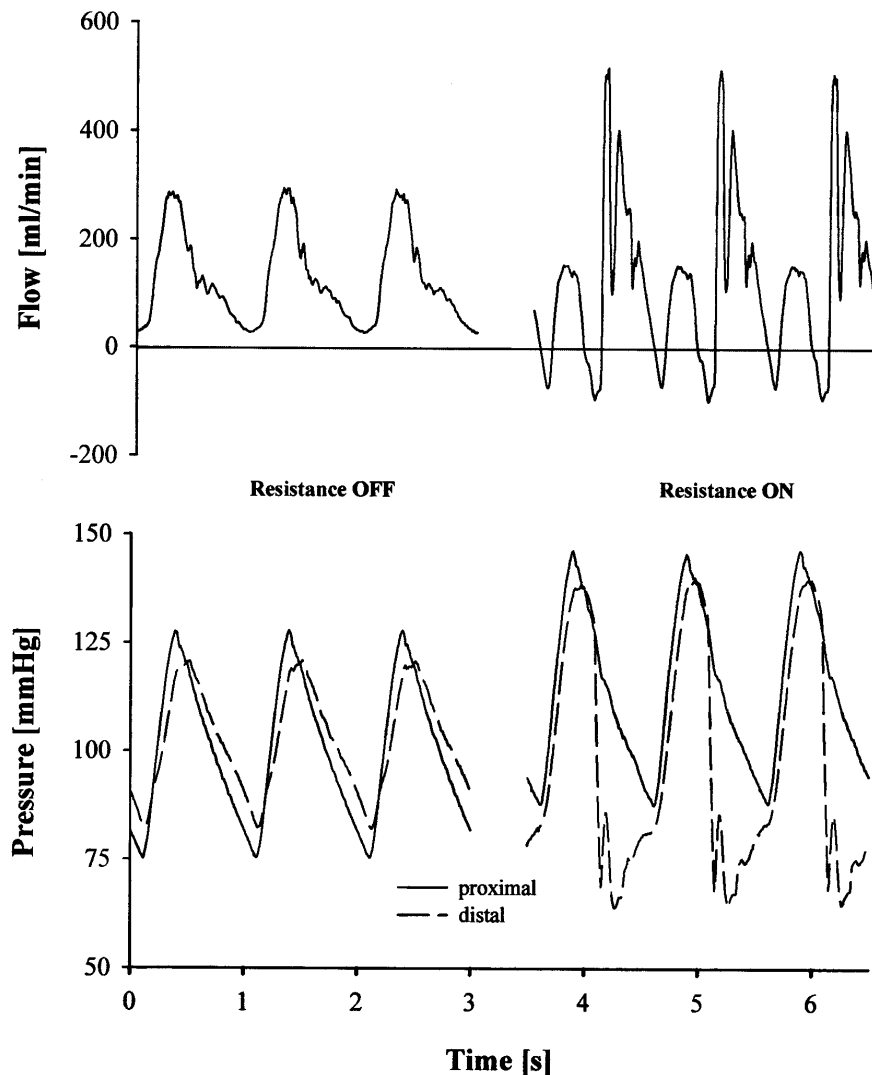


Figure 2–4 Intra-arterial pressure and flow waves, measured distal to the aortic valve (see Figure 2–1, (d)). Without the time-varying resistance (on/off valve closed), maximal flow is delivered during systole (upper left panel). Maximal blood supply shifts to diastole when the resistance is activated (upper right panel).

2.2 Measurement protocol

Intra-arterial pressure was measured proximal (P_a) and distal (P_d) to the stenosis at a sampling rate of 200 S/s, using epidural catheters directly connected to piezo-electric pressure transducers (Becton, Dickinson and Company, Franklin Lakes, NJ). The pressure catheters do not cross the stenosis. Flow was measured proximal to the stenosis by means of a two-channel

ultrasonic flowmeter (Transonic Systems Inc., Ithaca, NY). A second flow probe was mounted distal to the capillary resistance as control. Heart rate was set to 60 bpm and initial mean aortic blood pressure to 100 mmHg. Throughout a single experiment, flow was varied stepwise from 50 ml/min to about 200 ml/min by changing the capillary resistance value.

First, baseline (BL) measurements were done in all 9 stenotic latex tubes ($\varnothing = 4$ mm). A 35 mm ACS Multilink™ stent (Guidant/ACS®, Santa Clara, CA) was deployed in 6 tubes, with a 3 mm balloon at 8 atm. This allowed to simulate conditions of suboptimal stent deployment (SOD). After tests in the hydraulic bench, the tubes were taken to the cathlab for IVUS and biplane QCA, with the tubes tested under static pressure conditions at 100 mmHg. Stents were then further optimally deployed (OD) under angiographic guidance using a 4 mm balloon at 16 atm. QCA and IVUS were repeated, and the OD tubes were taken back to the hydraulic bench for flow measurement and assessment of FFR.

2.3 Data analysis

2.3.1 FFR

Intra-arterial pressure measurements P_a and P_d were averaged over 5 heart cycles. FFR was calculated for each tube as P_d/P_a . Values were averaged over 3 tubes per target stenosis severity and are given as mean \pm SD.

2.3.2 QCA

The reference diameter (RD) measured in frontal and lateral view with the biplane QCA was averaged, as well as the frontal and lateral minimal lumen diameter (MLD). Diameter stenosis percentages (DS) were then calculated by means of Eqn. 1.1.

2.3.3 IVUS

The IVUS images were used in a qualitative way to verify whether or not the coronary stent was well apposed to the vessel wall. IVUS procedures were done following clinical guidelines as published by Di Mario et al. (Di Mario, Grge et al. 1998).

Data were analyzed using 2-way repeated measurements ANOVA to study the effect of flow and stenosis level on pressure-flow relations and FFR. QCA data were analyzed using 1-way repeated measurements ANOVA. The Bonferroni t-test was used as post-hoc test if significance was reached ($p < 0.05$). FFR data were analyzed at 100 ml/min, pooling data from all 9 tubes. Differences between BL, SOD and OD were assessed using paired t-tests.

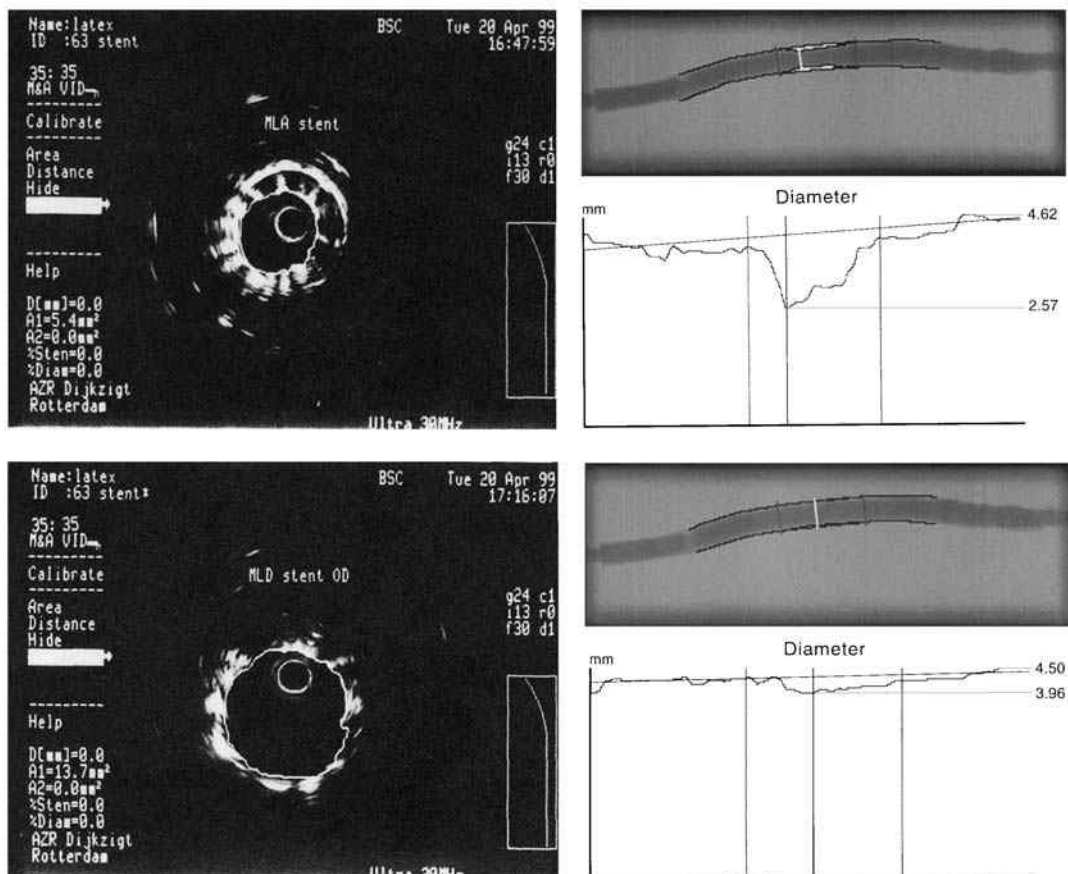


Figure 2–5 Upper panels show IVUS and QCA images for a suboptimally deployed (SOD) stent. The minimal lumen diameter is clearly detected via the QCA analysis, and IVUS shows the loose struts of the malapposed stent. Lower panels show IVUS and QCA for the same stent after optimal deployment (OD). There is a minor residual stenosis and IVUS shows stent struts which are well apposed against the coronary artery wall.

3 Results

Baseline QCA yielded effective DS values of 40%, 54% and 59% respectively (Table 2–1). There was significant residual stenosis after SOD as confirmed by IVUS and QCA ($DS = 35 \pm 3\%$, $32 \pm 1\%$ and $39 \pm 2\%$, respectively). OD reduced DS values down to $13 \pm 4\%$, $10 \pm 2\%$ and $10 \pm 2\%$, respectively, and IVUS images confirmed overall contact of the stent with the vessel wall (Figure 2–5). The differences between BL, SOD, and OD were significant (1-way ANOVA) when assessed by means of QCA and IVUS, except for 40% DS (no difference between BL and SOD).

<i>Target DS (%)</i>	<i>Tube #</i>	<i>BL</i>			<i>SOD</i>			<i>OD</i>		
		<i>RD (mm)</i>	<i>MLD (mm)</i>	<i>DS (%)</i>	<i>RD (mm)</i>	<i>MLD (mm)</i>	<i>DS (%)</i>	<i>RD (mm)</i>	<i>MLD (mm)</i>	<i>DS (%)</i>
40	1				3.9	2.6	33	4.2	3.5	15
	2	3.2	1.9	40						
	3				4.2	2.6	37	4.3	3.9	10
50	4				3.9	2.6	33	4.1	3.6	11
	5	3.3	1.5	54						
	6				4.2	2.9	31	4.1	3.8	9
60	7				4.1	2.5	38	4.2	3.8	9
	8	4.0	1.6	59						
	9				4.2	2.5	41	4.2	3.7	11

Table 2–1 QCA analysis results. Reference diameter (RD), minimal lumen diameter (MLD) and diameter stenosis percentages (DS) are shown for baseline conditions (BL), suboptimally deployed (SOD) and optimally deployed (OD) stents.

At BL, for $Q = 100$ ml/min, FFR was 0.964 ± 0.005 , 0.947 ± 0.004 and 0.923 ± 0.012 for 40%, 50% and 60% DS, respectively. FFR varied inversely with Q ($p < 0.001$, 2-way RM ANOVA) at BL, SOD and OD (Figure 2–6). At BL, varying Q from 150 to 50 ml/min increased FFR by 2-7%. For OD, variation is less than 5%. Pooling all data at 100 ml/min, FFR increased from 0.955 ± 0.009 after SOD to 0.963 ± 0.005 after OD. ($+ 0.8\%$; $p < 0.05$; paired t-test).

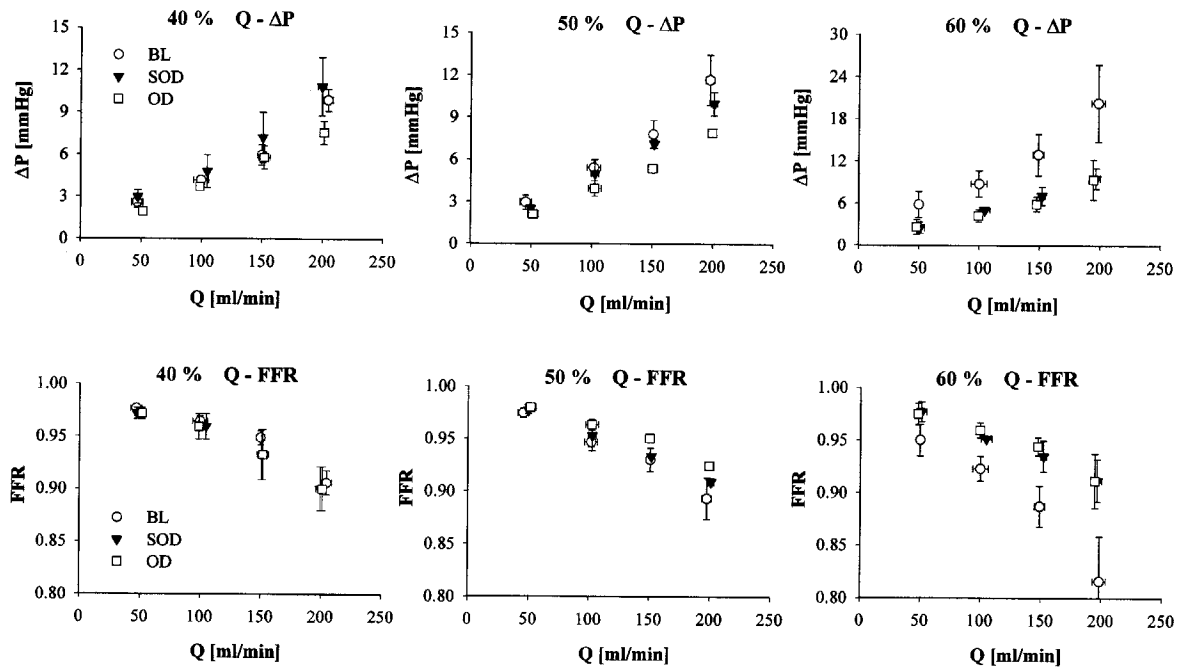


Figure 2-6 Upper panels show the measured flow values (Q) and pressure drops (ΔP) for baseline (BL), suboptimal (SOD) and optimal (OD) deployment conditions. Values are shown for each of the target diameter stenosis percentages separately (resp. 40%, 50% and 60%). From this data, the Q-FFR relationships were derived as shown in the lower panels. These data clearly demonstrate the flow dependency of FFR.

4 Discussion and Conclusion

In this study, a hydraulic coronary artery model was used to address some limitations of FFR in clinical practice. Its flow dependency was demonstrated, and its (in)sensitivity to optimal stent deployment assessed.

From a hydraulic point of view, the flow dependency of FFR is easily demonstrated if P_d is replaced in the formula for FFR by its equivalent: $P_d = P_a - \Delta P$ with ΔP the pressure drop over the stenosis. FFR then becomes:

$$FFR = \frac{P_d}{P_a} = \frac{P_a - \Delta P(Q)}{P_a} = 1 - \frac{\Delta P(Q)}{P_a} = FFR(Q) \quad \text{Eqn. 2.1}$$

ΔP is always function of flow. In case of laminar, Poiseuille flow, there is a linear relation between Q and ΔP . Over a stenosis, this relation is quadratic (Young and Tsai 1973). P_a is often taken the (mean) central aortic pressure and it is relatively insensitive to the flow level in the investigated coronary artery. Note that ΔP is also function of blood viscosity. For the same flow, ΔP is higher if viscosity is higher and the haematocrit or fibrinogen concentration may therefore modulate FFR. A solution to enhance the flow independence of FFR might be to measure pressure proximal to the stenosis P_p and not in the aorta ($FFR = P_d/P_p$ instead of P_d/P_a). One should also realize that in clinical practice, catheters cross the stenosis, disturbing the flow pattern and contributing to ΔP . Even for ultrathin wires commonly used, their influence is not always negligible. (De Bruyne, Pijls et al. 1993; Krams, Wentzel et al. 1999)

In clinical practice, FFR is useful to assess the severity of a coronary stenosis and to decide whether or not to do an intervention. A threshold value of 0.75 is used. This value was assessed in patients with stable angina (Pijls, De Bruyne et al. 1996; Pijls and De Bruyne 1998). In patients with post-myocardial reperfusion or unstable angina, maximal hyperaemic flow could be lower than in stable angina patients. As FFR is function of flow, the 0.75 threshold might not hold in these patients. This has been recently shown by Jeremias et al. (Jeremias, Filardo et al. 2000) who demonstrated that the FFR measured post-balloon occlusion was lower than post-adenosine hyperaemia (0.58 ± 0.2 vs. 0.63 ± 0.23 , $p < 0.001$).

This difference was related to a higher hyperaemic flow obtained after balloon occlusion than after intracoronary administration of adenosine.

This study shows little discriminating power of FFR between suboptimally (SOD) and optimally deployed (OD) stent. Given the definition of FFR, this means that the pressure drop over the tested stenosed latex tube does not differ significantly between SOD and OD (at the same flow level). In hydraulic terms, the pressure drop over an SOD stent may arise from (i) pressure losses due to the higher residual stenosis, or (ii) pressure losses due to flow turbulence around the loose struts in the flow. Little effect was found of the difference in residual DS ($11 \pm 2\%$ for OD, $35 \pm 4\%$ for SOD) on the pressure drop and FFR. This is not surprising, and confirms other studies showing effects of stenosis on pressure drops only for high stenosis values (Young and Tsai 1973). More remarkable is the observation that the pressure losses due to loose stent struts are not significant either. Some interesting studies on flow turbulence due to the positioning of the stent struts were performed by Peacock et al., and Berry et al. (Peacock, Hankins et al. 1995; Berry, Moore Jr et al. 1997). Unfortunately, these studies emphasized mainly on flow visualization and characterization, rather than the quantification of pressure losses.

In recent work, Hanekamp et al. (Hanekamp, Koolen et al. 1999) tested the feasibility of FFR for the assessment of optimal stent deployment. A cut-off value of 0.94 was proposed, with $\text{FFR} \geq 0.94$ indicating optimal deployment. The agreement between an $\text{FFR} > 0.94$ and optimal stent expansion by IVUS was 91% (optimal expansion assessed by IVUS as (i) complete apposition of all struts, (ii) a symmetry index, being the ratio of minimal to maximal in-stent luminal diameter > 0.7 and (iii) an in-stent minimal cross sectional area $> 90\%$ of the reference area). They concluded that IVUS and FFR were of similar value to assess optimal stent deployment, and that for this purpose, coronary pressure measurement can be used as a cheap and rapid alternative for IVUS. Although the mean reference diameter (RD) in the study by Hanekamp et al. is not given, it is expected that it was around 3.0 mm, which is the most common size of stented coronary vessels (Serruys, Foley et al. 1993; Serruys, de Jaegere et al. 1994). In these conditions, a suboptimal stent expansion with a suboptimal residual diameter stenosis (DS) of 30% gives a minimal lumen diameter (MLD) of 2 mm, whereas an optimally expanded stent with a residual DS of 10% is associated to an MLD of 2.7 mm. In the in vitro experiments performed here with latex tubes presenting a mean RD of 4 mm, SOD stents, with a mean residual DS of 36%, had a MLD of 2.6 mm, and the OD with a mean

DS of 11% had a MLD of 3.6 mm. This may explain the discrepancy between these results demonstrating minimal change of the FFR between SOD and OD stent expansion and the clinical data of Hanekamp et al. However, the IVUS pullbacks in this study demonstrated that although a sufficient MLD was restored to give an FFR value > 0.9 , still, large segments of stents were malapposed and were not detected by abnormal FFR values. These extensive segments would have surely had clinical implications such as (sub)acute thrombosis in a clinical setting.

In previous configurations of the cardiovascular simulator, the arteries were mounted in a horizontal plane, neglecting the 3D component of the peripheral vascular bed. The coronary arteries, however, are particularly tortuous. In order to respect their 3D anatomical shape, they were mounted on a latex epicardial surface as shown in Figure 2–1. This setup better resembles coronary anatomy, but is still a merely static supporting structure. A dynamically moving structure, would further decrease model limitations.

For the latex coronary artery phantoms, a feasibility study was performed comparing phantom fills of 100% latex with various types of plastic substances. A PTCA procedure was simulated, as well as the deployment of ‘home made’ stents (De Scheerder, Wang et al. 1997). As a criterion, the residual stenosis percentage of the stenosed segment was used and compared to that what is usually observed in clinical practice immediately after PTCA or (optimal) stent deployment. Experiments led to the currently used configuration. Nevertheless, optimal stent deployment still yielded average residual DS $\geq 10\%$, which, in clinical practice, is an upper limit for OD deployment (de Jaegere, Mudra et al. 1998). Thus, further and more elaborate investigation of an appropriate stenosed coronary artery phantom may be required.

With the time-varying resistance more realistic flow patterns were obtained, realizing flow impediment during systole. There are, however, still some limitations leading to perturbations during activation of the myocardial resistance (Figure 2–4). Replacing the simple on/off valve with a regulating actuator would probably smoothen out the flow wave. Furthermore, only one coronary artery with no side branches was simulated. In vivo, the heart is irrigated by a dense network of arteries, arterioles and capillaries. Extending the latex model into greater detail, i.e., more epicardial branches and more myocardial resistance vessels, would also improve the physiological relevancy of the simulated coronary flow pattern.

QCA and IVUS test were done in the cathlab, while the hydraulic tests were performed in the hydraulic lab. It was impossible, for practical and technical reasons, to use the cardiovascular simulator in the cathlab. Therefore, a 2D static setup was used in the cathlab, in which the coronary phantom was inserted after previous testing in the hydraulic bench. There was no 3D supporting structure, nor a pulsatile flow regime during QCA and IVUS. The coronary artery phantoms were however filled with water and contrast agent and then pressurized to 100 mmHg, similar to mean aortic pressure (P_a) in the hydraulic tests with the cardiovascular simulator.

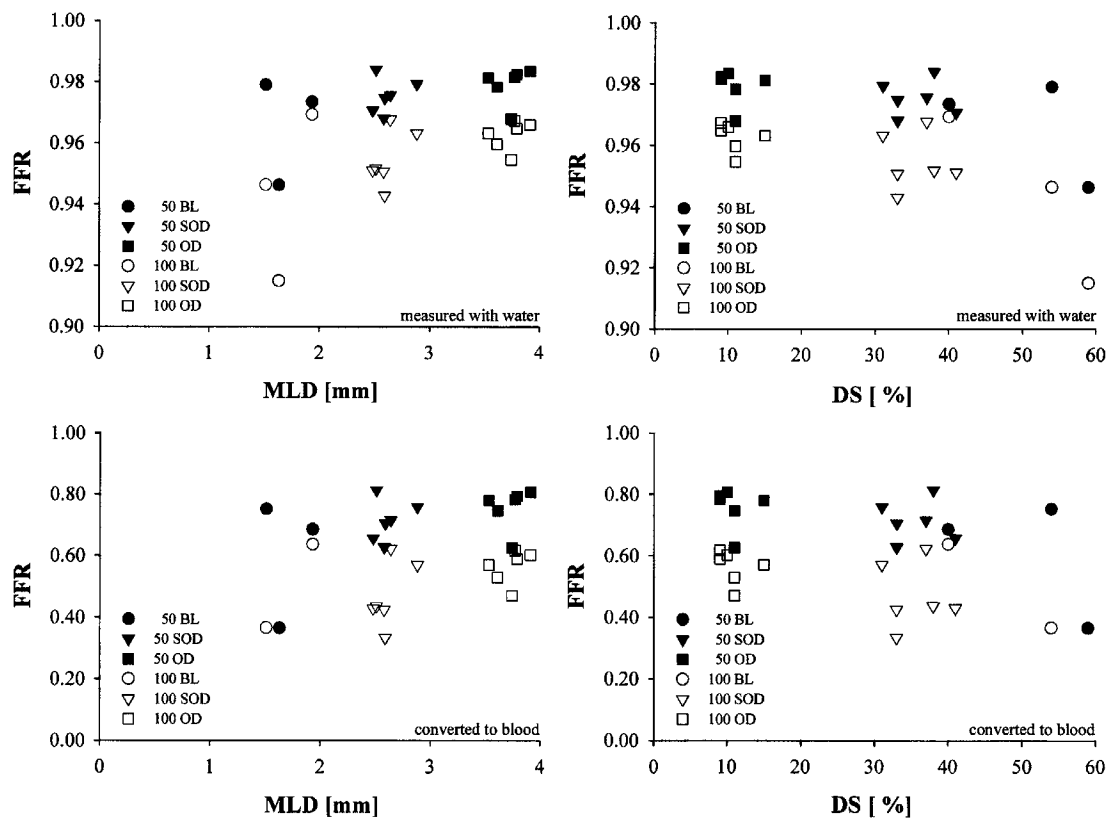


Figure 2-7 Relationship between FFR and minimal lumen diameter (MLD) (left panels) and between FFR and diameter stenosis percentage (DS) (right panels). Data is shown for baseline (BL), suboptimal (SOD) and optimal (OD) deployment conditions at two different flow (Q) levels (50 and 100 ml/min). Upper panels show the measured values with water, while lower panels show the same data but with values converted to blood.

Another limitation is the use of water for test fluid. Being Newtonian, water has no shear-thinning effects but this aspect is less important as the dimensions of the coronary phantoms largely exceed those of blood particles, and velocity and shear rate are high enough to neglect non-Newtonian effects. More important is the fact that the viscosity of water is 3 to 4 times

lower than blood. Consequently, pressure drops are 3 to 4 times lower as well, and calculated FFR values are higher than the values for blood at the same flow level. Nevertheless, the results can be converted to blood flow using dimensionless numbers and the theory of dynamic similarity (Streeter 1961). For each FFR value at a certain flow level with water experiments, there is a corresponding lower FFR value for blood at a (higher) blood flow level. A detailed outline of such a conversion is given in Appendix A. As an example, for a coronary artery phantom with target diameter stenosis of 60%, it was found that after optimal stent deployment (OD), $FFR_{\text{water}} = 0.98$ for $Q_{\text{water}} = 50.54$ ml/min. These values correspond to a blood flow (Q_{blood}) of 168.47 ml/min, and $FFR_{\text{blood}} = 0.81$ (see Appendix A). The water experiments, covering a range of 50-200 ml/min, cover a blood range of 150 to 600 ml/min. As an illustration, Figure 2–7 shows FFR values for water (upper panels) and the converted values for blood (lower panels) for BL, SOD and OD as a function of MLD and DS. Note that changes in flow have a much larger effect on FFR than going from SOD to OD.

In conclusion, it was demonstrated that FFR is confounded by the blood flow level and the blood viscosity. Further, only small differences were found in FFR between a suboptimally and an optimally deployed stent assessed by IVUS (complete stent apposition). Anatomical parameters post-percutaneous coronary intervention remain strong predictors of e.g. restenosis and assessing optimal stent deployment is more dependent on anatomical measures than measures of functional perfusion. IVUS and QCA are thus more appropriate for the assessment of optimal stent deployment than FFR when a minimal lumen diameter has been reached, normalizing the $FFR > 0.9$. In clinical conditions such as unstable angina/post-myocardial infarction reperfusion, cautious interpretation of FFR measurements should be based on potential low flow conditions.



3 A Corrected FFR Index to Account for the Myocardial Waterfall Effect*

* The content of this chapter has been accepted for publication in Biomechanics and Modeling in Mechanobiology (BMMB, march 2004)

Influence of Zero-Flow Pressure on Fractional Flow Reserve

Tom E Claessens, Paul L Van Herck, Koen S Matthys, Patrick Segers, Christiaan J Vrints, Pascal R Verdonck

Abstract

Fractional Flow Reserve (FFR) is conventionally calculated as the ratio of the pressure distal (P_d) and proximal (P_a) to the stenosis ($FFR = P_d/P_a$). It is hypothesized that the presence of a 'zero-flow' pressure (P_{zf}) requires a modification of this equation. Using a dynamic hydraulic bench model of the coronary circulation that allows to incorporate an adjustable P_{zf} , the relation was studied between pressure-derived $FFR = P_d/P_a$, flow-derived true $FFR_Q = Q/Q_N$ (= ratio of flow through a stenosed vessel to flow through a normal vessel), and the corrected pressure-derived $FFR_C = (P_d - P_{zf}) / (P_a - P_{zf})$ under physiological aortic pressures (70, 90 and 110 mmHg). Imposed P_{zf} values varied between 0 and 30 mmHg. FFR_C was in good agreement with FFR_Q , whereas FFR consistently overestimated FFR_Q . This overestimation increased when P_{zf} increased or when P_a decreased and could be as high as 56% ($P_{zf} = 30$ mmHg and $P_a = 70$ mmHg). According to this experimental study, calculating the corrected FFR_C instead of FFR if P_{zf} is known, provides a physiologically more accurate evaluation of the functional severity of a coronary artery stenosis.

1 Introduction

To assess the severity and extent of coronary artery disease, patients are often referred for coronary angiography. Since the visual appreciation of intermediate coronary lesions does not always reflect their physiological significance, an additional measurement of functional indices is often mandatory to assess the physiological relevancy of the stenosis. One such index that gained widespread clinical application in the past few years is Fractional Flow Reserve (FFR), which is in clinical practice commonly calculated as $FFR \approx P_d/P_a$. In this formula, P_d is the myocardial perfusion pressure distal to the stenosis, while P_a is the aortic pressure.

In fact, the perfusion of the myocardium does not only depend on the upstream pressure, but also on the pressure acting on the downstream side (P_v). This was accounted for by Pijls and De Bruyne who generally defined FFR as $(P_d - P_v)/(P_a - P_v)$ (Pijls and De Bruyne 1997), but in clinical practice, P_v is assumed to be low and is commonly neglected. However, it is still controversial which pressure should be taken for P_v in the FFR formula. Pijls and De Bruyne defined it as the venous pressure, but it was shown by Bellamy that coronary flow actually stops at a pressure above venous pressure (Bellamy 1978), a pressure termed ‘zero-flow’ pressure (P_{zf}), which is obtained as the pressure-axis intercept of the coronary pressure-flow relation. Since P_{zf} is the actual back pressure in the coronary circulation, it should be included in the formula for FFR instead of venous pressure. In literature, several mechanisms have been proposed to explain P_{zf} , the most important being the waterfall theory and the intramyocardial capacitance. (Permut and Riley 1963; Klocke, Mates et al. 1985; Spaan 1985) Irrespective of its origin, Siebes et al. recently demonstrated in a parametric analysis in a lumped model of the coronary circulation that neglecting P_{zf} may overestimate FFR, and hence underestimate the functional severity of the stenosis. (Siebes, Chamuleau et al. 2002)

In recent years, a validated hydraulic bench model of the epicardial coronary vessels was used to study (epicardial) coronary haemodynamics in general and FFR in particular. This type of model was first applied to validate the concept of FFR (Segers, Fostier et al. 1999), and next to demonstrate the insensitivity of FFR in detecting suboptimal stent deployment (Matthys, Carlier et al. 2001), a finding that was later confirmed in a clinical study (Fearon, Luna et al. 2001). Although the latter model incorporated the biphasic character of coronary blood flow

(perfusion in diastole), the myocardial resistance model was still simple and the measured epicardial pressure-flow relationships did not take into account the existence of a zero-flow pressure (P_{zf}), a critical pressure level that needs to be overcome in order to perfuse the myocardium.

In this paper, first a modification of the hydraulic bench resistance model is presented that allows to incorporate a non-zero and adjustable P_{zf} , yielding coronary pressure-flow relations better matching coronary physiology. To achieve this, the concept of the waterfall model will be applied. Secondly, in analogy with Siebes et al., it is studied to what extent neglecting P_{zf} overestimates P_d/P_a and how this relates to the level of aortic pressure.

2 Methods

2.1 Model of the microcirculation

2.1.1 The waterfall concept

The coronary bed is usually schematized as shown in Figure 3–1A, with the constant myocardial resistance given by R_{myo} and the stenosis resistance given by R_{ste} . Aortic pressure is represented by P_a , whereas P_d is pressure distal to the stenosis and P_v is pressure distal to the myocardial bed.

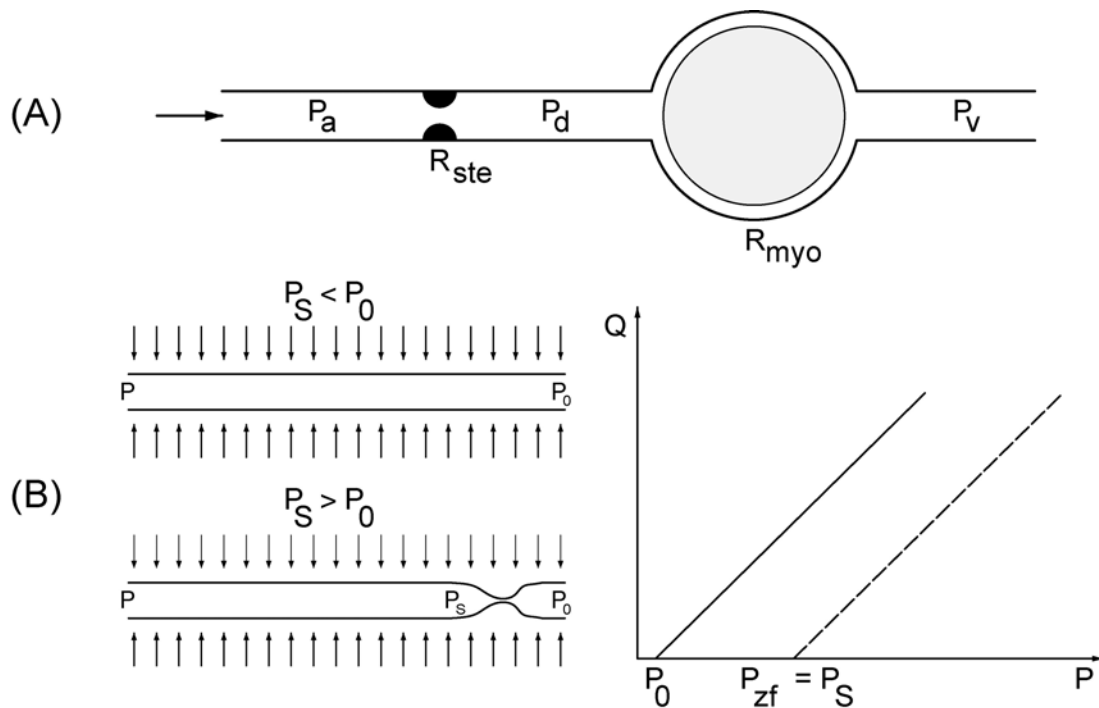


Figure 3–1 (A) Schematic representation of the coronary circulation, with indication of proximal (aortic) (P_a), distal (P_d) and venous (P_v) pressure, and the myocardial (R_{myo}) and stenosis resistance (R_{ste}). **(B)** Schematic representation of a collapsible tube with upstream pressure (P) and outflow pressure (P_0), surrounded with pressure P_s . If $P_s < P_0$, the tube remains patent along its entire length. No waterfall is created. Back pressure in the linear pressure-flow relation equals P_0 (solid line). If $P_s > P_0$, a partial collapse occurs at the outflow end of the tube. The linear pressure-flow relation shifts to the right but has the same slope. Back pressure is now P_s ($= P_{zf}$), because a waterfall is created (dashed line).

If no stenosis is present, and a linear pressure-flow relation is assumed, then coronary flow can be written as $Q_N = (P_a - P_v)/R_{\text{myo}}$. (Pijls and De Bruyne 1997) In the presence of a stenosis, P_d becomes the myocardial inflow pressure instead of P_a . As the myocardial resistance has not

changed, one can state that $Q = (P_d - P_v)/R_{myo}$. Therefore, FFR, which is defined as Q/Q_N , also equals $(P_d - P_v)/(P_a - P_v) \approx P_d/P_a$ if P_v is small enough.

Bellamy has shown, however, that the pressure-flow relation in the coronary bed is more complex than presented above, as coronary flow ceases even if inflow pressure is higher than venous pressure.(Bellamy 1978) The existence of such a zero-flow pressure P_{zf} can be explained by a model introduced by Burton.(Burton 1954) Closure of vessels by smooth muscle tone would cause cessation of flow when outflow pressure is below a 'critical closing pressure'. This idea was further refined by Permutt and Riley, who stated that a partial collapse of vessels by vascular tone and extravascular compression will occur rather than complete vessel closure.(Permutt and Riley 1963) This partial collapse can also be modelled in a collapsible tube upon which a surrounding pressure (P_s) is exerted, as shown in Figure 3–1B. Under these circumstances, flow is determined by the properties of the tube (length and internal diameter), the fluid viscosity and the pressure difference between the inflow pressure (P) and the surrounding pressure (P_s), instead of the outflow pressure (P_v). Pressure changes distal to the point of collapse have no influence on flow. Because of these properties, one speaks of a 'vascular waterfall' (see also Appendix B). Consequently, P_{zf} , which equals P_s in this application (Figure 3–1B), should be accounted for since it causes a rightward shift of the pressure-flow relation. Therefore one may conclude that coronary flow $Q = (P_a - P_v)/R$ if $P_{zf} < P_v$ and $Q = (P_a - P_{zf})/R$ if $P_{zf} \geq P_v$. The correct expression for a pressure-derived FFR then becomes $FFR_C = (P_d - P_{zf})/(P_a - P_{zf})$.

2.1.2 Application in the hydraulic bench model

The constructed model of the myocardial resistance (Figure 3–2A) represents a vessel path in an average layer of the myocardial wall. Basically, it is made of a silicon tube ($\varnothing = 2$ mm, total length of 45 cm) embedded in a plexiglas chamber containing 4 separate compartments. All compartments are sealed and connected to external watercolumns generating surrounding pressures to mimic extravascular pressures in the myocardium. The myocardial resistance model (c) is supplied from an upstream reservoir (a) at a constant, but adjustable level (range 0-70 mmHg) to generate different flow levels (Figure 3–2B). The outflow pressure is atmospheric pressure (d). In each compartment, different surrounding pressures are applied, further referred to as P_{S1} to P_{S4} . Note that the model reflects hyperemic conditions, as FFR is

always measured during hyperemia. As such, the model does not contain the autoregulating properties of the coronary circulation.

2.1.3 Experimental validation of the myocardial resistance model

Ten different external pressure configurations (C1-C10) are studied (Table 3–1). In the first configuration there are no surrounding pressures. In configurations 2 to 4, a homogeneous P_S over the whole vessel path is assumed. The water level in each of the watercolumns is therefore identical. Configurations C5 to C7 are similar to the previous 3 configurations, except for the most downstream region, where no surrounding pressure is used. In the last three configurations (C8-C10) a low P_{S4} is used in the most downstream region. P_{S1} , P_{S2} and P_{S3} are chosen arbitrarily.

	P_S	P_{S2}	P_{S3}	P_{S4}	Physiological explanation
	(mmHg)				
C1	0	0	0	0	no extravascular pressure
C2	18	18	18	18	homogeneous low extravascular pressure
C3	37	37	37	37	homogeneous average extravascular pressure
C4	55	55	55	55	homogeneous high extravascular pressure
C5	18	18	18	0	similar to C2, but no extravascular venous pressure
C6	37	37	37	0	similar to C3, but no extravascular venous pressure
C7	55	55	55	0	similar to C4, but no extravascular venous pressure
C8	18	37	37	18	low extravascular venous pressure
C9	37	37	37	18	low extravascular venous pressure
C10	18	37	55	18	low extravascular venous pressure

Table 3–1 Surrounding pressure configurations. P_{S1} to P_{S4} are the surrounding pressures in the respective compartments (mmHg). Configurations are referred to as C1 to C10.

Pressures are measured 3 cm proximal (P_a) to the myocardial resistance model using epidural catheters (e) directly connected to a piezo-electric transducer (Datex-Ohmeda™, Helsinki, Finland). The signal is sampled at 200 S/s during 5 seconds using a custom-written acquisition program in Labview (National Instruments™, Austin, TX). Flow is measured in a

volumetric way at the distal end of the system (d). For these experiments, the generated flow conditions are steady state.

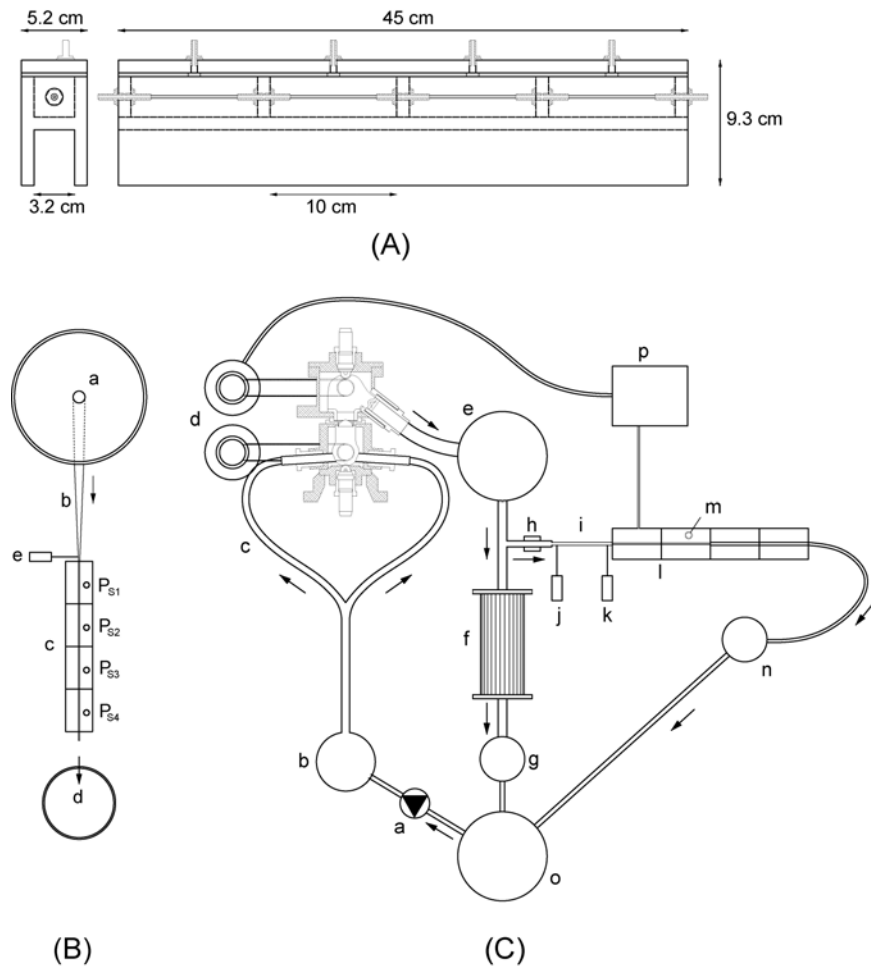


Figure 3–2 (A) Myocardial resistance model representing an average layer in the myocardial wall. The model exists of 4 small ($\varnothing = 2$ mm) silicon tubes embedded in 4 different perspex compartments, in which surrounding pressures can be created by means of external watercolumns (not shown in figure). (B) Schematic representation of the first experimental setup to assess the hydraulic characteristics of the myocardial resistance model (c). The model is supplied with water originating from a reservoir at a constant pressure level (a) by means of a tube (b). Outflow pressure is atmospheric pressure (d). Driving pressure is measured proximal to the model with a pressure sensor (e). Ten different surrounding pressure configurations were tested. A configuration is a specific combination of four pressures P_{S1} to P_{S4} imposed by means of watercolumns connected to the four compartments of the resistance model. (C) Schematic representation of the main hydraulic setup. The myocardial resistance model (l) and the peripheral resistance (f) are perfused by a water-glycerine mixture (70%/30%) under physiological pressures generated by a cardiovascular simulator (d), fed by 2 (instead of 4) pulmonary veins (c). The compliance of the aorta is adjusted by a Windkessel (e). Zero-flow pressures in the coronary resistance are controlled by an external adjustable watercolumn (m). The effect of a systolic compression is simulated by a pneumatic unit (p). Pressure is measured proximal (j) and distal (k) from the coronary artery (i). Flow is measured proximal from the coronary artery (h). Pump (a) brings the test fluid from reservoirs (n), (g) and (o) to a reservoir on preload level (b), in order to close the hydraulic loop.

2.2 FFR in a hydraulic bench model of the coronary circulation

The aim of these experiments is to assess the influence of a non-zero P_{zf} and aortic pressure on FFR in an integrated pulsatile hydraulic bench model of the left heart and epicardial coronary circulation (Figure 3–2C). The waterfall myocardial resistance model, as elaborated above, is therefore connected to the epicardial coronary vessel and different values for P_{zf} are obtained by changing the surrounding pressure in the myocardial resistance model.

2.2.1 *Experimental setup description*

Pulsatile flow is generated by a model of the human left heart (d), which basically consists of 2 (instead of 4) pulmonary veins (c), the left atrium and ventricle and the aortic arch.(Verdonck, Kleven et al. 1992) The elastic properties of the aorta are simulated by installing an air chamber (Windkessel element) (e). Distal to the Windkessel, most of the test fluid (30% glycerine and 70% water; density 1060 kg/m^3 and dynamic viscosity 3.5 mPa.s at room temperature, thus comparable to blood) flows towards the global systemic resistance (f), while only a smaller quantity (coronary flow) perfuses the myocardial resistance model (l). Distal to the resistance model an overflow reservoir (n) is installed to avoid air being sucked into the tubes at any time. Another reservoir (o) receives flow from the peripheral resistance and the overflow reservoir. The test fluid is then again elevated to the preload level (b) using a pump (a).

Compared to the myocardial resistance model validation experiments, the model was modified in 3 ways. First, the 1st compartment was connected to the pneumatic unit (p) also actuating the model of the left ventricle. This way, the 1st compartment is compressed in phase with the LV contraction, simulating the effect of LV contraction on systolic flow (systolic flow impediment).(Matthys, Carlier et al. 2001) Secondly, to allow for a simple control of P_{zf} , a (constant) external pressure was applied only on the 2nd compartment. Thirdly, in order to realize coronary flow values within a physiological range (300 ml/min in hyperemic conditions), tubes with a larger diameter ($\varnothing = 3.5 \text{ mm}$) were used in compartments 3 and 4. As such, the first two compartments of the model include all ‘active’ resistance components, i.e. the systolic flow impediment and non-zero P_{zf} . This active part was then further connected to a passive peripheral resistance element (f), composed of a porous

material embedded in a water-filled reservoir, of which the resistance level is changed by increasing the pressure in the water reservoir and thus compressing the porous material inside. This passive resistance was controlled to an appropriate value and kept constant throughout the whole experiment.

2.2.2 Experimental protocol

Flow is measured proximal (h) to the epicardial coronary artery using an ultrasonic flow meter (Transonic, Ithaca, NY). Pressures are registered in the proximal (j) and distal (k) part of the coronary artery. Mean aortic pressure is set to 70, 90 and 110 mmHg by adjusting the pneumatic actuating pressure (enhancing cardiac contractility). For each level of aortic pressure, P_{zf} is varied between 0 and 30 mmHg in steps of 5 mmHg. Data are recorded during 5 seconds, and time averaged to obtain P_a , P_d and Q . Experiments are first done using either a healthy (control) silicon phantom ($\varnothing = 3$ mm, length 10 cm) of the Left Anterior Descending (LAD) and then repeated using a phantom with a 75% diameter stenosis (89% area stenosis) (i). They are mounted proximal to the model of the microcirculation.

2.2.3 Data Analysis

The analysis consists of comparing the following three formulae for Fractional Flow Reserve: (1) conventional pressure-derived $FFR = P_d/P_a$; (2) flow-derived $FFR_Q = Q/Q_N$; (3) corrected pressure-derived $FFR_C = (P_d - P_{zf})/(P_a - P_{zf})$.

The different methods for calculating Fractional Flow Reserve are compared by a Bland-Altman analysis (Bland and Altman 1986), using FFR_Q as the gold standard. Analysis of variance (ANOVA) with a post hoc Scheffé test is used to assess the difference between the methods. The level of significance is set at a p-value of 0.05. All values are expressed as mean \pm SD. Statistics are performed using Statview 5 (SAS Institute Inc., Cary, NC).

3 Results

3.1 Model of the microcirculation

The pressure-flow relations measured in the myocardial resistance model (in steady state conditions) are displayed in Figure 3–3. The curves are linear in a large interval, but the resistance starts to decrease at relatively low flows. For all conditions, the intercept with the pressure-axis or P_{zf} approximates the highest surrounding pressure in the compartments. Measured P_{zf} values for the 10 combinations are shown in Table 3–1. This negligible difference between the pressure intercept (P_{zf}) and the value of the surrounding pressure can be explained by the fact that the used silicone tubes have a minimal stiffness which sustains a possible collapse in case of a minor positive transmural pressure. Given the observation that P_{zf} is only determined by the absolute value of the highest external pressure applied - and not by the position where this pressure was exerted - it is justified to only use one compartment for mimicking the extravascular pressures for the second part of the study. The second compartment will be used for this purpose. Also, in order to reduce the resistance distal to the waterfall site (and to allow to simulate realistic flow levels for normal aortic pressure levels), the diameter of the silicone tube in compartments 3 and 4 is increased to 3.5 mm.

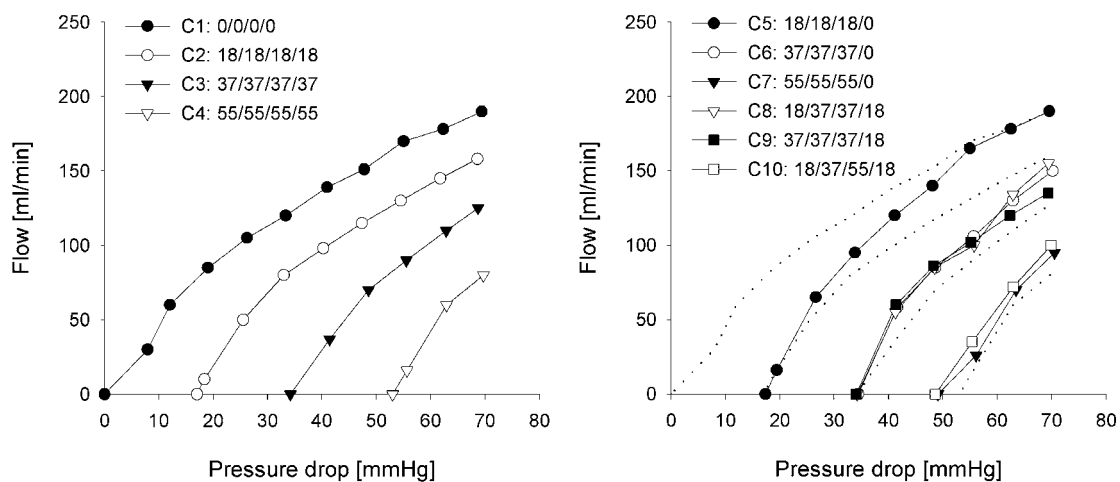


Figure 3–3 Left: Measured myocardial pressure-flow relations under surrounding pressure configurations C1 to C4. Zero-flow pressures are nearly identical to the applied surrounding pressure. Resistance of the model is not constant, but increases with flow. Right: Pressure-flow relations for configurations C5 to C10. C1 to C4 are shown as dotted lines. Zero-flow pressures are now determined by the greatest surrounding pressure in one of the compartments.

3.2 FFR in a hydraulic bench model of the coronary circulation

The effect of various levels of P_{zf} and aortic pressure on FFR, FFR_C and FFR_Q (reference method) is shown in Figure 3–4 for the 75% diameter stenosis. A good agreement was found between FFR_Q and FFR_C for each value of surrounding pressure, except for $P_s = 0$ mmHg, where FFR is equal to FFR_C and both overestimate FFR_Q .

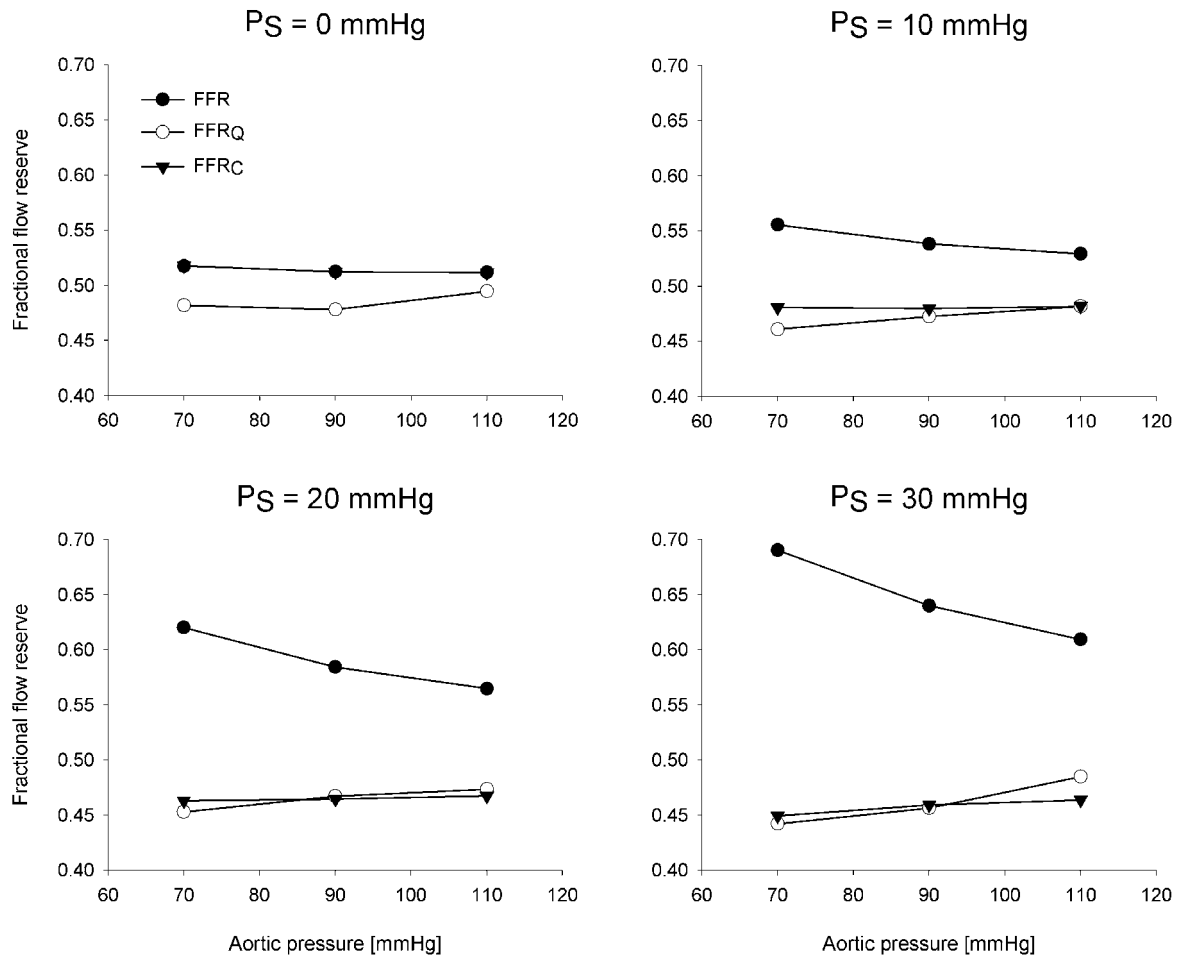


Figure 3–4 Relation between pressure-derived $FFR = P_d/P_a$, corrected pressure-derived $FFR_C = (P_d - P_{zf})/(P_a - P_{zf})$ and flow-derived $FFR_Q = Q/Q_N$ for various surrounding (P_s) and aortic pressures. FFR_Q and FFR_C correlate well. FFR consistently overestimates FFR_Q and FFR_C , except if $P_s = 0$ mmHg.

The mean difference between FFR_Q and FFR is -0.101 ± 0.067 ($p < 0.0001$), while the mean difference between FFR_Q and FFR_C is -0.011 ± 0.011 ($p < 0.05$) (Figure 3–5A). It also follows from the Bland-Altman analysis that FFR consistently overestimates FFR_Q , the degree of overestimation being dependent on aortic pressure and P_{zf} . This is summarized in Figure 3–5B where FFR is presented as a percent value of FFR_Q . The overestimation varies between 2.84% (for $P_s = 5$ mmHg and $P_a = 110$ mmHg) and 56.18% (for $P_s = 30$ mmHg and $P_a = 70$ mmHg).

The degree to which FFR overestimates FFR_Q increases with decreasing aortic pressure and increasing surrounding pressure.

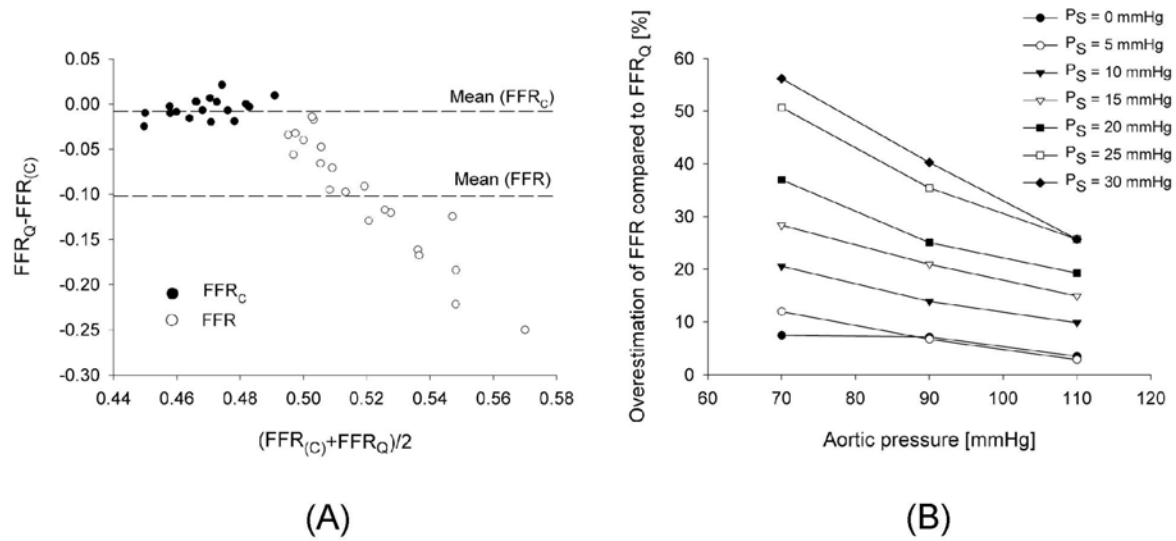


Figure 3–5 (A) Bland-Altman description of the relation between FFR_Q and FFR_C . FFR clearly overestimates FFR_Q , while FFR_C matches FFR_Q very well. (B) Overestimation of pressure-derived FFR compared to flow-derived FFR_Q increases with increasing surrounding pressure and decreasing aortic pressure. Maximum overestimation is 56.18% (for $P_S = 30$ mmHg and $P_a = 70$ mmHg).

4 Discussion and Conclusion

This study shows that applying the waterfall principle to a hydraulic myocardial resistance model yields an experimental setup that allows to generate epicardial coronary pressure and flow data incorporating biphasic flow patterns and easily controllable zero-flow pressure levels. This experimental setup further enabled to demonstrate that the pressure based Fractional Flow Reserve corrected for a zero-flow pressure (FFR_C) agrees well with the flow based FFR_Q , while the conventional FFR overestimates FFR_Q . The degree of overestimation is directly related to P_{zf} . As a consequence, it may be physiologically more accurate to assess the severity of a stenosis with a corrected FFR_C . Currently, this back pressure to coronary flow is neglected and FFR is calculated as a ratio of distal to aortic pressure P_d/P_a .

Segers et al. previously made use of a hydraulic bench model of the coronary artery and microcirculation to validate the basic concept of FFR.(Segers, Fostier et al. 1999) Later, Matthys et al. further elaborated this model by implementing the effect of ventricular contraction during systole on flow.(Matthys, Carlier et al. 2001) In this paper, coronary pressure-flow relations were simulated in a more physiological way with the incorporation of an (adjustable) zero-flow pressure. This was achieved by directly simulating the waterfall principle via compression of a collapsible tube.

The hydrodynamic properties of the myocardial resistance model were assessed in a first series of experiments. In the absence of an external pressure, the pressure-flow relation is virtually linear and passes through the origin. The pressure-flow relation shifts to the right when increasing the surrounding pressure, resulting in a positive zero-flow pressure. Various explanations have been given for the physics behind P_{zf} , including the waterfall concept and the effect of intramyocardial compliance.(Klocke, Mates et al. 1985; Spaan 1985; Hoffman and Spaan 1990) To the best of our knowledge, however, an exact clarification has not been given up to date. The main objective with the hydraulic bench model was to design a myocardial resistance model that allows to generate appropriate pressure-flow curves showing a positive zero-flow pressure in the integrated hydraulic bench model. The applied waterfall model fulfills this criterion, demonstrated by the steady state measurements on the resistance model itself. Note, however, that the presented model is no attempt to model the coronary microcirculation as such. To do so, it is more realistic to use multiple parallel tubes to mimic

several parallel layers in the myocardium, each of them being subjected to a different P_{zf} with the highest extravascular pressure exerted near the endocardial layer. An electrical analogue of such a model has been developed by Downey and Kirk for the systolic waterfall.(Downey and Kirk 1975)

Subsequently, the effect of variable aortic and surrounding pressures on FFR was assessed in the model. The data show that FFR overestimates the 'reference' FFR_Q , while FFR corrected for P_{zf} (FFR_C) is an excellent estimate for FFR_Q . The overestimation increases with increasing P_{zf} and decreasing aortic pressure and may amount to more than 50% according to the present study (if $P_a = 70$ mmHg and $P_{zf} = 30$ mmHg). As some patients may have high zero-flow pressures, FFR could therefore be a too optimistic evaluation of the stenosis severity. This issue was recently also addressed by Siebes et al. (Siebes, Chamuleau et al. 2002) in a theoretical parametric study, in which the effects of elevated back pressures and variable aortic pressures were investigated. They showed that the pressure-derived FFR equals FFR_Q when P_{zf} is included in the formula and that FFR exceeds FFR_Q when P_{zf} is not accounted for. These hydraulic bench study results are thus in perfect agreement with their theoretical considerations.

Although it is clear that neglecting P_{zf} (or P_v) in FFR overestimates FFR_Q (the reference value), the question remains whether this consideration is relevant in a clinical setting, especially given the difficulties in estimating P_{zf} . In humans, P_{zf} is usually determined by extrapolation of the pressure-flow relation to the pressure-axis during diastole. Using this method, some studies indeed have shown rather high values for P_{zf} in humans during hyperemia ($P_{zf} = 37.9 \pm 9.8$ mmHg according to Dole et al. (Dole, Richards et al. 1984), $P_{zf} = 36.9 \pm 16$ mmHg according to Meneveau et al. (Meneveau, Di Mario et al. 1993)). Recently Tanaka showed that the P_{zf} is higher in patients with an old myocardial infarction in comparison with patients with angina pectoris.(Tanaka, Takazawa et al. 2003) If this measured P_{zf} represents a correct estimate of the back pressure in the coronary circulation, FFR can be overestimated by as much as 40% for an average aortic pressure of 90 mmHg and a 75% diameter stenosis (Figure 3–5B). Based on these findings, it is recommended to modify the traditional formulation FFR and to incorporate P_{zf} in the formula.

On the other hand, the conventionally calculated FFR has shown to be very valuable in clinical practice and has been proven to correlate well with non-invasive studies.(De Bruyne,

Bartunek et al. 1995; Pijls, Van Gelder et al. 1995; Pijls, De Bruyne et al. 1996) According to these studies, mainly performed in selected patients (no prior MI, single vessel disease), a cut off value of $FFR < 0.75$ showed a sensitivity of 88% and specificity of 100% for scintigraphic evidence of myocardial ischaemia.(Pijls, De Bruyne et al. 1996) More recently, a similar study was carried out in a heterogeneous group of consecutive patients, but still resulted in high sensitivity and specificity values of 79% and 73%, respectively.(Yanagisawa, Chikamori et al. 2002) Correcting FFR for P_{zf} will not lead to major changes for a stenosis with an FFR in the threshold region of 0.75 or higher. The effect will mainly be apparent for stenoses in the lower FFR range, where the haemodynamic severity of the stenosis is obvious. Nevertheless, from a conceptual point of view, measuring P_{zf} and implementing it in the expression for FFR_C , is a more accurate way of assessing coronary stenosis severity.

While this study concentrated on P_{zf} in the microcirculation, others have been focusing on the importance of the interplay between the resistance of the microcirculation and the assessment of the severity of coronary stenoses.(Meuwissen, Chamuleau et al. 2001; Chamuleau, Siebes et al. 2003) A novel promising index for the assessment of coronary stenosis has recently been presented that is based on pressure and flow measurements.(Meuwissen, Siebes et al. 2002) This hyperaemic stenosis resistance index, defined as the ratio of hyperaemic stenosis pressure gradient and hyperaemic average peak-flow velocity is likely to be a more powerful indicator for stenosis severity than the conventional FFR.(Siebes, Verhoeff et al. 2004)

This hydraulic bench study has some inherent limitations. In nature, the pressure compressing the coronary bed is dynamic, i.e., it is high during systole (systolic flow impediment) and low during diastole (generating P_{zf}). In the model, systolic flow impediment and P_{zf} generation are uncoupled. Systolic flow impediment is generated by applying pneumatic pressure compressing the ventricular chamber to the first compartment of the myocardial resistance model, while P_{zf} is created by applying a constant external pressure on the second compartment. Furthermore, the obtained pressure-flow relations are slightly non-linear, probably due to turbulences near the connections between the different compartments. Also, collateral flow was not accounted for. Collateral flow has the same effect on FFR as an increased zero-flow pressure: both result in a an overestimation of the FFR in comparison with the flow ratio in the real coronary circulation.(Pijls, van Son et al. 1993; Siebes, Chamuleau et al. 2002) Absence of collateral circulation in the model does not influence the validity of the results, since the aim was to investigate the effect of P_{zf} only. Finally, the

experiments were performed for only one stenosis of intermediate severity. The relation between stenosis severity and percentage overestimation has not been studied. The general nature of the findings, however, warrants applicability for other stenosis levels.

In conclusion, in a hydraulic model of the coronary circulation, it was shown that the presence of a zero-flow pressure requires a modification of the formula of FFR. Since the P_{zf} will mainly affect FFR values that, even after correction, leave no doubt about the indication for treatment, this finding may not have a large impact on clinical policy. Still, the used model is a better representation of the current understanding of coronary haemodynamics.

General Discussion and Conclusion

Scientific results

The study of arterial function has gained wide interest in the past decade. With this thesis, the aim was to contribute to the field of the assessment of vascular haemodynamics and arterial function. In particular, the goal was to investigate non-invasive and minimally invasive methods for the assessment of vascular function at rest and during cardiovascular challenge. In the past, simultaneous pressure and flow measurements were invasive and difficult to obtain in clinical practice. This thesis strives to show the potential (and limitations) of combined non-invasive pressure and flow measurement technology to enhance routine haemodynamic arterial diagnostics under different load conditions. Following an introduction (Part I) on the basic principles of the cardiovascular system and the outline of this thesis, the results were organized in two categories: methodological aspects (Part II and III) and (clinical) applications (Part IV and V).

Methodological aspects

In a first methodological section (Part II), the focus lied on the theoretical aspects related to haemodynamic assessment. Specific interests included vascular biomechanics (haemodynamic properties), system identification (arterial transfer function) and system modelling (arterial network).

- First, wall elasticity, vascular resistance, compliance and wave travel in the arterial circulation were addressed to provide a sound basis of vascular haemodynamics.
- Second a comparison was made between different approaches for the determination of the radial-aortic transfer function (TFF). The parametrically derived TFF based on the ARX model was found to be more suitable than the non-parametric TFF method based on spectral analysis. Subsequently two different parametric approaches were compared for accuracy and noise-sensitivity. A time-shifted approach appeared better than the inversion of TFF in the physiological direction.

- Last, an arterial network model from previous studies was adapted and enhanced (i) in structure and (ii) in functionality to predict the degree of vascular unloading necessary (by respective changes of diameter D and elastic modulus E) to reduce increased pulse pressure - a cardiovascular risk factor - to a desired normal value.

The second methodological section (Part III) focused on how to assess pressure and flow, and hence arterial haemodynamics, in practice.

- First, an overview of non-invasive and minimally invasive pressure and flow devices was given, to motivate and clarify the choice for arterial tonometry and Doppler-echocardiography for pressure and flow measurements, respectively.
- Second, a review was given about tonometry technology and modelling. Although the available tonometers are nowadays very accurate and of sufficiently small dimensions, there are still 3 basic problems (i) difficult positioning, (ii) sensitivity to motion artefacts and (iii) (external) calibration.
- Third, the potential of tonometry as a long-term monitoring device was investigated. Based on a comparison with an intra-arterial measurement during neuro-surgery, it must be concluded that arterial tonometry remains a too unreliable technique for use during a delicate operative procedure at this point.
- Last, an in-house diagnostic acquisition program was developed that is able to combine the output of several stand-alone medical monitoring devices and that, in particular, allows the synchronized acquisition of a Doppler spectrogram, an electrocardiogram and a continuous pressure signal.

(Clinical) Applications

A first section (Part IV) covered the non-invasive haemodynamic analysis during rest and stress conditions. Specific interest included derivation of total arterial compliance during physical stress and drug-induced stress, and its relation with myocardial ischaemia.

- First, an introductory chapter explained the basics of non-invasive haemodynamic acquisitions during physical and drug-induced stress testing.
- Second, the feasibility was demonstrated of simultaneous measurement of ECG, Doppler and tonometer in a small-scale in vivo study during physical exercise on a supine and standing bicycle. It was shown that extra haemodynamic information can be added to a routine diagnostic investigation by the combination of simple non-invasive techniques, without significant additional discomfort for the examined subject or prolongation of the test protocol.
- Third, as a demonstration of the clinical relevancy, the correlation of compliance with extent of myocardial ischaemia was studied in a larger-scale in vivo study during dobutamine induced stress. It was found that while traditional cardiovascular risk factors such as age, hypertension, diabetes etc. are strong predictors of ischaemia on stress echo, total arterial compliance (TAC) predicts not only ischaemia but also the extent of ischaemia with stress echocardiography during a drug-induced test.

The second applications section (Part V) covered the minimally invasive haemodynamic analysis during interventional procedures. Specific interest included quantification of coronary stenting and the use of pressure and/or flow derived haemodynamic indices.

- First, an overview on coronary stenting and diagnostic imaging tools was presented, together with the introduction of pressure and/or flow derived haemodynamic indices, and especially the Fractional Flow Reserve (FFR) index.
- Second, in a first in vitro study, it was demonstrated that FFR is confounded by the blood flow level and the blood viscosity. FFR was applied to assess optimal stent deployment and only small differences in FFR were found between a suboptimally and an optimally deployed stent. It was concluded that imaging techniques such as IVUS and QCA are more appropriate for the assessment of optimal stent deployment than FFR.

- Last, in a second in vitro study, the effect of myocardial resistance on the derivation of FFR was analyzed and a corrected FFR_C index was proposed to incorporate the impact of the so-called ‘waterfall’ effect induced by surrounding pressures imposed on the myocardial coronaries.

Future work

It has become clear in recent literature that generalized transfer functions are inadequate for the reconstruction of *all* details of the central pressure wave from radial measurements. In order to merely address global characteristics of the waveform, such a function can be sufficient but when striving towards more clinical benefit from pressure waveform synthesis and analysis by investigating (differences in) derived parameters (such as for instance compliance indices), further elaboration on arterial transfer functions is mandatory. As was presented on last year’s Annual Scientific Session of the American College of Cardiology (ACC) by a collaborating research group (Haluska, Short et al. 2003), estimates of arterial compliance calculated using the generalized radial transfer function and direct carotid waveforms showed 5-10 % differences in women and older patients. Specific transfer functions should indeed be considered for specific subgroups and loading conditions. However, obtaining such a load- and subject-dependent method is not an easy task in practice (hence the popularity of the generalized approach). On one hand, efforts are necessary on the theoretical level of system identification. Besides the simple linear methods used today and illustrated in this work, more advanced (non-linear) modelling techniques should be evaluated on their potential for characterizing the vascular tree. On the other hand and maybe more important, more clinical validation data is to be acquired. And this is a difficult task as invasive data is hard to come by when not investigating pathological cases that require catheterization. For instance during exercise it is quite impossible to acquire invasive data for the transfer function estimation in a healthy subject along the different load levels of a bicycle protocol, as it is unlikely that an ethical committee would ever agree to such an approach. Maybe pharmacologically induced exercise could be considered here, but this is also not a routine diagnostic procedure applicable for every patient. For patients who require catheterization, one could think of deriving a patient-specific transfer function upon catheterization, and subsequently use this transfer function in combination with non-invasive recordings for future blood pressure assessment. A follow-up per patient on how this transfer

function evolves with age and pathological disorders could be very valuable, but it is clear that seen the invasive aspect this can never lead to a more global routine. There will always be the trade-off between the added value of a patient-specific approach and the amount of conclusions that also apply to a larger population, and vice versa. In theory, the best transfer function remains no transfer function at all, which is only possible for measurements exactly at the desired location. In practice however, this location is just not always reachable. Besides improving the generalized approach by deriving corrections for certain groups with an already designated social importance (women, elderly, hypertensives, etc.), one could also try to get away from the radial measurement site and measure closer to the heart, thus reducing the impact of the mathematical transformation in the whole processing, for instance by making use of carotid instead of radial pressure waveforms.

The arterial model presented here allowed to investigate the relation between pulse pressure and changing diameter and modulus of elasticity. It would be interesting to expand the potential of the model by visualizing relations between other haemodynamic parameters (e.g. compliance) and physical properties (e.g. wall thickness) as well. Since this information is in fact already available in the model, the implementation of these extra features could be easily done. Moreover, limited results of in vitro experiments have been compared with the arterial model but more experimental data is certainly necessary, which is currently being acquired by a collaborating research group (A. Avolio, personal communication). Since the data involves large reduction of the modulus of elasticity, it is imperative to question the validity of the (linear) model approach under these conditions, although in vitro data-points acquired so far showed good agreement. It might be appropriate to reinvestigate the model from a computational point-of-view. A comparison between linear and non-linear distributed network models has been given by Segers and colleagues (Segers, Stergiopoulos et al. 1997), in which also the augmented pulse pressure amplification due to a purely resistive terminal impedance (used in this model) was addressed. It could be interesting to analyze the presented model with more complex terminal impedance models. Finally, it would be valuable to include the interaction of the arterial system with the heart, but seen the initial engagement with this model did not include this idea, it might become cumbersome to combine the current frequency-based approach with for instance an impulse response and elastance model for the ventricular interaction, and as such it would be better to consider an entirely new implementation of the model to include this complex feature as well.

Arterial tonometry has been in the centre of attention throughout this work. Besides its potential, limitations in terms of fixation, positioning techniques and most of all calibration methods have been addressed. In this thesis the construction of transfer functions was done by means of invasive data, which is the proper approach, but often invasive peripheral data is not available and when tonometry is used in this case, one must be aware that the wrist-tonometer system with skin and underlying tissue is also modelled in the transfer function. Seen the fact that the last theoretical model on the wrist-tonometer system is 20 years old (Drzewiecki, Melbin et al. 1983) and simplifications were made for instance on the visco-elastic tissue behaviour to reduce the complexity of the calculations, it could be interesting to quantify this again with nowadays available computing power. In this work, it has been shown that tonometry as yet is not suitable for long-term monitoring. The TegadermTM patch fixation (3M Health Care, Borken, Germany) of the manual tonometer used in this thesis appeared to be very useful and this could also be applied in future setups during exercise where it was found that a good fixation is imperative to get quantitative results for the pressure waveform. In routine practice the radial tonometer signal is often calibrated by means of a brachial cuff, but this already introduces a substantial error and on-going studies show that the variation between an estimated and measured aortic waveform is half due to the applied transfer function and half due to the brachial calibration of the radial tonometer (Luc Van Bortel, personal communication). Where possible a radial cuff-device was used in this thesis, but these devices appeared to perform poorly during exercise. As a future suggestion for calibration during exercise, one might consider to investigate the new device Vasotrac[®] from Medwave (Medwave Inc., Danvers, MA) that appears to work on tonometric principles to generate SBP, DBP and MAP values every 15 heartbeats, or even an ambulatory (continuous) device like the Finapres[®] (FMS Finapres Medical Systems, Arnhem, NL) to extract beat-to-beat radial SBP, DBP and MAP values as a calibration for the tonometer. Last, besides comparison between manual and automatic tonometry devices during exercise, one should also keep exploring the alternatives for arterial tonometry such as the promising results from echo-track studies in which pressure is derived from wall distensibility curves. (Van Bortel, Balkestein et al. 2001)

Commercial software packages are available for *general* signal processing and have been looked upon in an initial stage in this thesis, but there was a need for *specific* haemodynamic tools such as the in-house acquisition instrument presented here. For future applications, the

in-house analysis software for post-processing might be coupled with this acquisition tool to become a fully featured signal processing package. Seen the modular approach of the acquisition tool implementation, the adding of existing programs written in Matlab[®] environment (The Mathworks, Inc., Natick, MA) is feasible. Meanwhile commercial efforts should not be ignored, as with the growth of the biomedical engineering field more and more specialized tools become available. Dominant players on the industrial engineering market for automation and control are developing ever better tools for biomedical research, such as for instance National Instruments (National Instruments Corporation, Austin, TX) with the Biobench[™] technology, a product for data acquisition and analysis in life sciences. Other, originally biomedical research oriented, small initiatives or spin-off companies are expanding fast, and even away from the pure biomedical field towards more general industrial acquisition and signal processing, such as for instance Notocord[®] (Notocord Systems, Croissy, FR). As for the hardware devices of pressure and flow measurement, there is less cross-over between the different companies, although commercial players specifically on the tonometer and ultrasound market are definitely aware of the value of combining efforts and it can be foreseen that collaborations will come of this in the future.

Finally when considering the interventional applications discussed in this thesis, it was found that a cautious use of FFR for stent deployment assessment is required and that the introduction of a zero-flow pressure in the formula of FFR is a better representation of coronary haemodynamics. The latest developments in the field of functional indices for the assessment of coronary intervention (53rd 2004 ACC Annual Scientific Session, New Orleans, LA) is the development of non-hyperaemic indices such as the pulse transmission coefficient (PTC) and the Lesion Severity Index (LSI), which have been shown to be highly correlated with FFR and thus may represent a simple, less expensive method for the assessment of functional stenosis severity, without administration of vasodilative agents.(Brosh, Higano et al. 2004a; Brosh, Higano et al. 2004b)

Appendix

Appendix A

Converting flow and pressure measurements for water to results for blood requires two steps. First, extra parameters have to be calculated for water in order to derive two non-dimensional numbers: Reynolds (Re_{water}) and Euler (ξ_{water}). Second, applying the theory of dynamic similarity, one can express that Re_{water} equals Re_{blood} and ξ_{water} equals ξ_{blood} . From these two equations, it is then possible to obtain flow and pressure values for blood, as demonstrated below.

Step 1: Re_{water} and ξ_{water}

Internal diameter of the coronary artery phantom, as well as the physical properties of water is given in Table A1. Cross-sectional area A is calculated with: $A = \pi D^2/4$, while water velocity V_{water} is derived from the measured flow Q_{water} ($= 50.54 \text{ ml/min}$) with $V = Q/A$. Pressure drop ΔP_{water} and FFR_{water} are derived from the measured proximal and distal stenosis pressures with: $\Delta P = P_p - P_d$ and $FFR = P_d/P_p$, resulting in $\Delta P_{\text{water}} = 1.76 \text{ mmHg}$ and $FFR_{\text{water}} = 0.98$. Finally, the Reynolds and Euler number (Re_{water} , ξ_{water}) are calculated using:

$$Re = \frac{V \cdot D \cdot \rho}{\mu} \quad \text{Eqn. A1}$$

$$\xi = \frac{\Delta P}{\rho \cdot V^2} \quad \text{Eqn. A2}$$

resulting in $Re_{\text{water}} = 268$, and $\xi_{\text{water}} = 52$.

Step 2: Q_{blood} and FFR_{blood}

Calculations are to be done in an ‘inverse’ way, starting from Re and ξ . Necessary physical properties for blood are given in Table A2. Blood velocity (V_{blood}) is calculated using: V_{blood}

$=Re_{\text{blood}}\mu_{\text{blood}}/D\rho_{\text{blood}}$, with $Re_{\text{blood}} = Re_{\text{water}} = 268$. Blood flow (Q_{blood}) is then obtained via $Q = VA$, resulting in $Q_{\text{blood}} = 168.47$ ml/min.

As ξ_{water} equals ξ_{blood} , it is possible to derive ΔP_{blood} with: $\Delta P_{\text{blood}} = \xi_{\text{blood}}\rho_{\text{blood}}V_{\text{blood}}^2$, giving 20.58 mmHg. Finally, stating that $P_{\text{p blood}}$ equals $P_{\text{p water}}$, $P_{\text{d blood}}$ can be found ($P_{\text{d}} = P_{\text{p}} - \Delta P$) and also FFR_{blood} ($FFR = P_{\text{d}}/P_{\text{p}}$), yielding a value of 0.81.

Conclusion

Having performed the above calculations, one can conclude that $FFR_{\text{water}} = 0.98$, at a flow level of $Q_{\text{water}} = 50.54$ ml/min, corresponds to $FFR_{\text{blood}} = 0.81$ for $Q_{\text{blood}} = 168.47$ ml/min.

<i>Parameter</i>	<i>Symbol (units)</i>	<i>Formula</i>	<i>Value</i>
internal diameter	D (m)		0.004
cross-sectional area	A (mm ²)	$A = \frac{\pi D^2}{4}$	12.6
water density	ρ_{water} (kg/m ³)		1000
water viscosity	μ_{water} (Pa.s)		0.001
water velocity	V_{water} (m/s)	$V = \frac{Q}{A}$	0.067
water flow	Q_{water} (ml/min)		50.54
proximal stenosis pressure	$P_{\text{p water}}$ (mmHg)		106.55
distal stenosis pressure	$P_{\text{d water}}$ (mmHg)		104.79
pressure drop	ΔP_{water} (mmHg)	$\Delta P = P_{\text{p}} - P_{\text{d}}$	1.76
FFR_{water} (OD)	FFR_{water}	$FFR = \frac{P_{\text{d}}}{P_{\text{p}}}$	0.98
Reynolds _{water}	Re_{water}	$Re = \frac{VD\rho}{\mu}$	268
Euler _{water}	ξ_{water}	$\xi = \frac{\Delta P}{\rho V^2}$	52

Table A1 Measured and derived parameters for water.

<i>Parameter</i>	<i>Symbol (units)</i>	<i>Formula</i>	<i>Value</i>
Reynolds _{blood}	Re _{blood}	$Re_{blood} = Re_{water}$	268
internal diameter	D (m)		0.004
blood density	ρ_{blood} (kg/m ³)		1050
blood viscosity	μ_{blood} (Pa.s)		0.0035
blood velocity	V _{blood} (m/s)	$V_{blood} = Re_{blood} \frac{\mu_{blood}}{D\rho_{blood}}$	0.22
cross-sectional area	A (mm ²)	$A = \frac{\pi D^2}{4}$	12.6
blood flow	Q _{blood} (ml/min)	$Q = VA$	168.47
Euler _{blood}	ξ_{blood}	$\xi_{blood} = \xi_{water}$	52
pressure drop	ΔP_{blood} (mmHg)	$\Delta P_{blood} = \xi_{blood} \rho_{blood} V_{blood}^2$	20.58
proximal stenosis pressure	P _{p blood} (mmHg)	$P_{p blood} = P_{p water}$	106.55
distal stenosis pressure	P _{d blood} (mmHg)	$P_d = P_p - \Delta P$	85.97
FFR _{blood} (OD)	FFR _{blood}	$FFR = \frac{P_d}{P_p}$	0.81

Table A2 Corresponding parameters for blood.

Appendix B

The waterfall theory is explained stepwise by means of an example in which two waterfalls are created (Figure B1). The example demonstrates how pressure-flow curves are calculated.

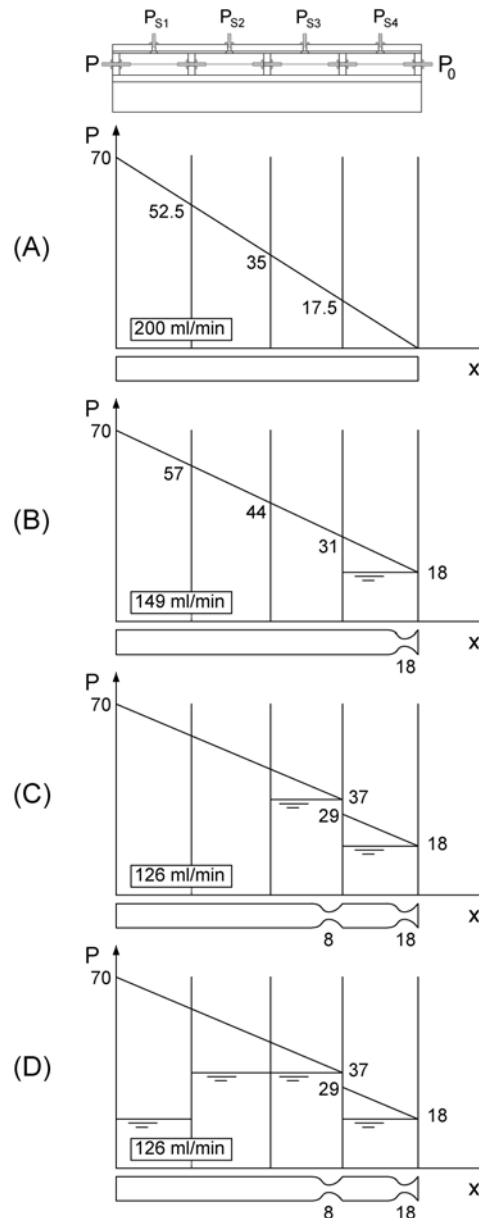


Figure B1 Example of a theoretical resistance model with hydraulic waterfalls. Inflow pressure $P = 70$ mmHg. Outflow pressure $P_0 = 0$ mmHg. Possible waterfalls are shown under each graph. With $P_S = 0$ pressure decreases from 70 to 0 mmHg and no waterfall exists (A). If $P_{S4} > 0$, a waterfall is created at the distal end of the model. $P_{zf} = P_{S4}$ becomes the back pressure causing a flow reduction (B). A second waterfall is created in the third compartment because P_{S3} is higher than the internal pressure in the third compartment. P_{zf} increases to P_{S3} and resistance decreases to $\frac{3}{4}$ of its original value. Flow decreases as a result (C). Surrounding pressure in compartments 1 and 2 have no influence on pressure and flow as long as they are lower than internal pressure (D).

Initially a configuration without surrounding pressures is assumed. In this condition, it means that the pressure-flow relations are determined by Poiseuille's Law: $Q = \Delta P/R$. For simplicity, consider $Q = 200$ ml/min and $\Delta P = 70$ mmHg, such that total resistance equals $70 \text{ mmHg}/200 \text{ ml/min} = 0.35 \text{ mmHg/ml/min}$. Outflow pressure P_0 is kept constant at 0 mmHg. If the inflow pressure P is 70 mmHg, then, according to Poiseuille's Law, pressures inside the tubes at the end of each chamber are 52.5 mmHg, 35 mmHg, 17.5 mmHg and 0 mmHg respectively (Figure B1, A).

In the following 3 steps, it is explained how to obtain pressures and flow in the vessel, when applying surrounding pressures as in configuration C8 (18/37/37/18). First, raise P_{S4} to 18 mmHg (Figure B1, B). Because this pressure is above the outflow pressure, one could think that the vessel collapses due to the positive transmural pressure and flow will stop. Yet, if flow stops, there is no pressure gradient between the inflow pressure and the pressure in the last compartment, which means that pressure in the last compartment would increase to 70 mmHg (hydrostatic situation) and the vessel reopens. What actually happens, is that the vessel partially collapses at the end of the fourth compartment, thereby creating a local pressure drop, called a hydraulic waterfall. Under these circumstances, there is a perfect equilibrium between the inner and surrounding pressure. The magnitude of this pressure drop will be exactly 18 mmHg. Hence, pressure proximal to this narrowing must be 18 mmHg too since outflow pressure was assumed 0 mmHg. Because the inflow pressure is 70 mmHg and the outflow pressure is 18 mmHg, the driving pressure is only 52 mmHg instead of 70 mmHg. As a result, flow will decrease to $Q = (70-18)/0.35 = 149$ ml/min.

If in addition P_{S3} is augmented to 37 mmHg, another waterfall will originate because the internal pressure at the end of the third compartment (31 mmHg) is lower than 37 mmHg. Driving pressure is only $70-37 = 33$ mmHg now, while the resistance is reduced to $\frac{3}{4}$ of its initial value ($70 \text{ mmHg}/200 \text{ ml/min}$). Flow is now $33/(\frac{3}{4} \cdot 0.35) = 126$ ml/min. As flow is constant along the vessel path, pressure at the proximal end of the last compartment is $18 + 126 \cdot (\frac{1}{4}) \cdot 0.35 = 29$ mmHg. The magnitude of the second waterfall is then $37-29 = 8$ mmHg (Figure B1, C).

When increasing P_{S1} and P_{S2} to 18 and 37 mmHg respectively, no waterfall will be added because the internal pressure is greater than surrounding pressures (Figure B1, D). Pressure and flow are identical to the previous situation.

In this theoretical example it has been made clear how 2 waterfalls are created: the first one at the end of compartment 4 and the second one between compartment 3 and 4. For every inflow pressure and surrounding pressure configuration, flow can be calculated in an analogous way.

Nomenclature

Abbreviations

2C	two chamber view
2D	two dimensional
2WK	two element Windkessel
3D	three dimensional
3WK	three element Windkessel
4C	four chamber view
A/D	analog to digital
AAMI	American Association for the Advancement of Medical Instrumentation
ACC	American College of Cardiology
ACE	angiotensin-converting enzyme
ADO IC	adenosine injection
AGR	agreement
AM	area method
ANOVA	analysis of variance
AoI	aortic signal input
AoO	aortic signal output
Ao-R	aorta to radial artery
ARX	AutoRegressive eXogenous model
AS	arterial network segment
ASE	American Society of Echocardiography
AV	atrioventricular
AWin	acquisition window
BL	baseline
BNC	Bayonet Neill Concelman
CAD	coronary artery disease
CFR	coronary flow reserve
CHOL	hypercholesterolaemia
CI	cardiac intervention
CO	cardiac output
CWD	continuous wave Doppler
DAQ	data acquisition

DBP	diastolic blood pressure
DFT	discrete Fourier transform
DISAGR	disagreement
DM	diabetes mellitus
DS	diameter stenosis percentage
DSE	dobutamine SE
ECG	electrocardiogram
EDV	end-diastolic volume
EF	ejection fraction
ERR	error
ESBP	end-systolic blood pressure
ESV	end-systolic volume
ExSE	physical exercise SE
FDA	Food and Drug Administration
FFR	fractional flow reserve
FFT	fast Fourier transform
GUI	graphical user interface
HDP	hold down pressure
HR	heart rate
HTN	hypertension
IBP	invasive blood pressure
IHDFPS	instantaneous hyperaemic diastolic flow pressure slope index
IOP	intraocular pressure
IV4	method of Instrumental Variables
IVUS	intravascular ultrasound
LA	left atrium
LAD	left anterior descending coronary branch
LAX	long-axis view
LCA	left coronary artery
LCX	left circumflex coronary branch
LS	least squares
LSI	lumen symmetry index
LSI	lesion severity index

LV	left ventricle
LVDT	Linear Variable Displacement Transducer
LVOT	left ventricular outflow tract
MAP	mean arterial pressure
MI	myocardial infarction
MLD	minimal lumen diameter
MPHR	maximal predicted heart rate
MR	myocardial resistance
MV	mitral valve
NIBP	non-invasive blood pressure devices
NS	not significant
OD	optimal deployment
PEI	plaque eccentricity index
PM	papillary muscle
PP	pulse pressure
PPM	pulse pressure method
PREV	previous
PRF	pulse repetition frequency
PTC	pulse transmission coefficient
PTCA	percutaneous coronary transluminal angioplasty
PWD	pulsed wave Doppler
PWV	pulse wave velocity
QCA	quantitative coronary angiography
RA	right atrium
R-Ao	radial artery to aorta
RCA	right coronary artery
RD	reference diameter
RI	radial signal input
RM	repeated measures
RMB	right marginal coronary branch
RMS	root mean square
RO	radial signal output
RPD	right posterior descending coronary branch

RV	right ventricle
SA	sinoatrial node
SAX	short-axis view
SBP	systolic blood pressure
SD	standard deviation
SE	stress echocardiography
SOD	suboptimal deployment
SPA	spectral analysis
SS	steady state
STFT	short-time Fourier transform
SV	stroke volume
TAC	total arterial compliance
TBP	tonometric blood pressure
TD	time delay
TDM	time decay method
TFF	transfer function
TVR	total vascular resistance
WMSI	wall motion score index

Symbols

a	parameter
b	parameter
c	speed of sound
c_0	pulse wave velocity
d	time-shift
$e(t)$	residual error
f	frequency
$f(t)$	function in time-domain
h	wall thickness
i	index
k	index
k	spring constant
k_t	taperfactor
l	length
n_a	parameter estimation order
n_b	parameter estimation order
$n(t)$	noise signal
p	pressure
p	chance
q	flow
$q(x)$	load function
q^{-1}	shift operator
r	radius
r	correlation coefficient
r_t	target range
s	index
t	time
$u(t)$	input signal
v	velocity
v_l	volume
w	width

$w(t)$	Hanning window function
$x(t)$	time-domain function
$y(t)$	output signal
$z(t)$	complex Doppler signal
A	area
A	Fourier coefficient
A	amplitude
$A(q^{-1})$	polynomial in q^{-1}
A_0	Fourier coefficient
A_{ix}	augmentation index
A_K	Fourier coefficient
B	Fourier coefficient
$B(q^{-1})$	polynomial in q^{-1}
B_K	Fourier coefficient
C	compliance
C	category
C	configuration
CC	compliance coefficient
$C_{uy}(\omega)$	co-spectrum
D	diameter
DC	distensibility coefficient
E	Young's modulus of elasticity
E'	Hardung's complex visco-elastic modulus
F	force
$F(K)$	frequency-domain function
F_{10}	Womersley parameter
$H(e^{j\omega})$	frequency-response function
Hb	haemoglobin
Hct	haematocrit
$I(t)$	quadrature component
J	Bessel function
K	index

L	length value
L	level
M	amplitude
M'_{10}	Womersley parameter
N	amount
P	pressure value
Q	flow value
$Q(t)$	quadrature component
$Q_{uy}(\omega)$	quad-spectrum
R	radius value
R	resistance
Re	Reynolds number
R_s	vascular resistance
$R_{uu}(\tau)$	auto-correlation function
$R_{uy}(\tau)$	cross-correlation function
$S_{uu}(j\omega)$	auto-spectrum
$S_{uy}(j\omega)$	cross-spectrum
T	period
T	total
T_w	wall tension
$U(k)$	DFT of $u(t)$
V	velocity value
$V(e)$	cost function
V_l	volume value
$VO_{2\max}$	peak oxygen uptake
V_r	reaction force
$X(t)$	vector
$Y(k)$	DFT of $y(t)$
Z_0	characteristic impedance
Z_i	input impedance
Z_L	longitudinal impedance
Z_T	terminal impedance

Greek Symbols

μ	dynamic fluid viscosity
η	wall viscosity
σ	stress
ρ	fluid density
ε	strain
ν	kinematic fluid viscosity ($\nu = \mu/\rho$)
ϕ	phase angle
ω	angular frequency ($\omega = 2\pi f$)
λ	parameter ($\lambda = h/R_0$)
π	the number Pi ($\pi = 3.141592\dots$)
α	Womersley parameter ($\alpha^2 = R^2\omega/\nu$)
γ	complex propagation constant
τ	timeconstant ($\tau = R_s C$)
τ	time-shift
θ	angle
θ	vector
δ	displacement
ξ	Euler number
Γ^*	complex reflection coefficient
ν_p	Poisson's ratio
ε'_{10}	Womersley parameter

Subscripts

0	upstream
0	source
100	100%, control
a	arterial
a	aortic
avg	average
b	backward
blood	blood
c	complex
c	chamber
c	contact
C	corrected
C	compliance
d	diastole
D	Doppler
d	demodulated
d	distal
d	derived
dyn	dynamic
es	end systolic
f	forward
fund	fundamental
H	Hanning
i	inflection
i	inner
i	in
i	initial
inc	incremental
m	measured
m	mean
max	maximal

myo	myocardial
N	normal
Nyq	Nyquist
o	outer
o	out
o	ocular
o	outflow
p	pressure
p	proximal
Q	flow
r	reflected
R	receiver
R	resistance
rest	rest
S	surrounding
s	sample
stat	static
ste	stenosis
t	transmural
t	transducer
v	venous
v	vascular
water	water
ys	yield stress
zf	zero-flow

Operators

Δ	difference
Σ	summation
\int	integral operator
e^x	Euler's constant ($e=2.7183$)
$\partial/\partial x$	partial derivative with respect to variable x
d/dx	derivative with respect to the variable x
\bar{x}	average value
\hat{x}	estimated value
\angle	phase
$ $	amplitude or absolute value
$*$	complex conjugate
j	complex number ($j^2 = -1$)
Re	real part
Im	imaginary part
\sin	sine
\cos	cosine
\tan	tangent
\arctan	arc-tangent
X^T	transposed matrix
∞	infinite
\varnothing	diameter

Units

m	[L]	meter	
cm	[L]	centimeter	10^{-2} m
mm	[L]	millimeter	10^{-3} m
μm	[L]	micrometer	10^{-6} m
km	[L]	kilometer	10^3 m
F	[L]	French	1F = 1/3 mm
mmHg	[L]	mm Mercury	1 mmHg = 133.3 Pa
s	[T]	second	
ms	[T]	milliseconds	10^{-3} s
min	[T]	minute	60 s
h	[T]	hour	3600 s
g	[M]	gram	
kg	[M]	kilogram	10^3 g
l	[L ³]	liter	10^{-3} m ³
ml	[L ³]	milliliter	10^{-3} l
N	[ML/T ²]	Newton	
Pa	[M/T ² /L]	Pascal	
atm	[M/T ² /L]	atmosphere	101325 Pa
Hz	[1/T]	Hertz	
kHz	[1/T]	kiloHertz	10^3 Hz
MHz	[1/T]	MegaHertz	10^6 Hz
V		Volt	
A		Ampère	
Ω		Ohm = V/A	
W		Watt	
dB		decibel	
rad		radians	
°		angular degrees	
°C		degrees Celsius	
bpm		beats per minute	
S/s		samples per second	

References

- Allbutt, T. (1921). Greek medicine in Rome. London, Macmillan.
- Armentano, R., Graf, S., Barra, J., Velikovsky, G., Baglivo, H., Sanchez, R., Simon, A., Pichel, R. and Levenson, J. (1998). "Carotid wall viscosity increase is related to intima-media thickening in hypertensive patients." *Hypertension* 31(1 Pt 2)(Jan): 534-9.
- Asmar, R., Rudnichi, A., Blacher, J., London, G. and Safar, M. (2001). "Pulse pressure and aortic pulse wave are markers of cardiovascular risk in hypertensive population." *Am J Hypertens* 14: 91-97.
- Association for the Advancement of Medical Instrumentation (1992). Electronic or automated sphygmomanometers. Arlington, VA, AAMI.
- Avolio, A. (1980). "Multi-branched model of the human arterial system." *Med Biol Eng Comput* 18: 709-718.
- Avolio, A. (1995). "Genetic and environmental factors in the function and structure of the arterial wall." *Hypertension* 26: 34-37.
- Avolio, A., Fa-Quan, D., Wei-Qiang, L., Yao-Fei, L., Zhen-Dong, H., Lian-Fen, X. and M., O. R. (1985). "Effects of aging on arterial distensibility in populations with high and low prevalence of hypertension : comparison between urban and rural communities in China." *Circulation* 71: 202-210.
- Bahr, D., Dhupar, K., Petzke, J. and Ziemann, E. (1977). A microprocessor-based arterial tonometer. 1st Ann Symp Comp Appl Med Care, Washington DC.
- Bahr, D. and Petzke, J. (1973). The automatic arterial tonometer. 26th ACEMB: 259.
- Bahr, D. and Petzke, J. (1980). Continuous arterial tonometry. Essential noninvasive monitoring in anesthesia. J. S. Gravenstein, R. S. Newbower, A. K. Ream, N. Ty Smith and J. Barden. New York, Grune & Stratton, Inc.: 25-36.
- Baker, D. (1978). Principles of Doppler. Ultrasound, its applications in medicine and biology. M. Fry. New York, Elsevier.

REFERENCES

- Balkestein, E. J., van Aggel-Leijssen, D. P., van Baak, M. A., Struijker-Boudier, H. A. and Van Bortel, L. M. (1999). "The effect of weight loss with or without exercise training on large artery compliance in healthy obese men." *J Hypertens* 17: 1831-5.
- Bank, A. J., Kaiser, D. R., Rajala, S. and Cheng, A. (1999). "In vivo human brachial artery elastic mechanics: effects of smooth muscle relaxation." *Circulation* 100: 41-7.
- Bellamy, R. F. (1978). "Diastolic coronary artery pressure-flow relations in the dog." *Circ Res* 43(1): 92-101.
- Benetos, A., Safar, M., Rudnichi, A., Smulyan, H., Richard, J.-L., Ducimetière, P. and Guize, L. (1997). "Pulse pressure: a predictor of long-term cardiovascular mortality in a French male population." *Hypertension* 30: 1410-15.
- Berenson, G. (2002). "Childhood risk factors predict adult risk associated with subclinical cardiovascular disease. The Bogalusa Heart Study." *Am J Cardiol* 90(10C): 3L-7L.
- Bergel, D. H. (1961a). "The dynamic elastic properties of the arterial wall." *J Physiol* 156: 458-469.
- Bergel, D. H. (1961b). "The static elastic properties of the arterial wall." *J Physiol* 156: 445-457.
- Berne, R. M., Sperelakis, N. and Geiger, S. R., Eds. (1979). *Handbook of Physiology, Section 2 The Cardiovascular System, Vol1 The Heart*, American Physiological Society.
- Berry, J. L., Moore Jr, J. E., Newman, V. S. and Routh, W. D. (1997). "In vitro flow visualization in stented arterial segments." *J Vasc Invest* 3(2): 63-68.
- Bettman, O. (1979). *A pictorial history of medicine*. Springfield, Ill., Charles C. Thomas.
- Birch, A. A. and Morris, S. L. (2003). "Do the Finapres and Colin radial artery tonometer measure the same blood pressure changes following deflation of thigh cuffs?" *Physiol Meas* 24(3): 653-660.
- Blacher, J., Pannier, B., Guerin, A., Marchais, S., Safar, M. and London, G. (1998). "Carotid arterial stiffness as a predictor of cardiovascular and all-cause mortality in end-stage renal disease." *Hypertension* 32(3)(Sep): 570-4.

- Bland, M. and Altman, D. (1986). "Statistical methods for assessing agreement between two methods of clinical measurement." *Lancet* 1: 307-310.
- Bos, W., van Goudoever, J., van Montfrans, G., van den Meiracker, A. and Wesseling, K. (1996). "Reconstruction of brachial artery pressure from noninvasive finger pressure measurements." *Circulation* 94: 1870-75.
- Bos, W. J. W. (1995). Measurement of finger and brachial artery pressure. PhD Thesis. Amsterdam, Universiteit van Amsterdam.
- Bramwell, C. J. and Hill, A. (1922). "The velocity of the pulse wave in man." *Proc R Soc Lond [Biol]* 93: 298-306.
- Brandenburg, R. O., Fuster, V., Giuliani, E. R. and McGoon, D. C., Eds. (1987). *Cardiology: Fundamentals and Practice*. Chicago, Year Book Medical Publishers, Inc.
- Brooks, D. E., Goodwin, T. W. and Seaman, G. V. F. (1970). "Interactions among erythrocytes under shear." *J Appl Physiol* 28: 172-7.
- Brosh, D., Higano, S. T., Kern, M. J., Lennon, R. J., Holmes, D. R. J. and Lerman, A. (2004a). "Pulse transmission coefficient: a nonhyperemic index for physiologic assessment of procedural success following percutaneous coronary interventions." *Catheter Cardiovasc Interv* 61(1): 95-102.
- Brosh, D., Higano, S. T., Lennon, R. J., Carlier, S. G., Kern, M. J., Beyar, R., Gruberg, L. and Lerman, A. (2004b). Lesion Severity Index, a new nonhyperemic physiologic parameter for the assessment of coronary artery stenosis: a comparison to fractional flow reserve. ACC 2004 53rd Annual Scientific Session, New Orleans, LA.
- Burrus, C. S., McClellan, J. H., Oppenheim, A. V., Parks, T. W., Schafer, R. W. and Schuessler, H. W. (1994). *Computer-based exercises for signal processing using Matlab*. Englewood Cliffs, NJ, Prentice-Hall, Inc.
- Burton, A. C. (1954). "Relation of Structure to Function of Walls of Bloods Vessels." *Physiology Review* 34: 619-52.

- Cameron, J. and Dart, A. (1994). "Exercise training increases total systemic arterial compliance in humans." *Am J Physiol* 266(2 Pt 2)(Feb): H693-701.
- Cameron, J., McGrath, B. and Dart, A. (1998). "Use of radial artery applanation tonometry and a generalized transfer function to determine aortic pressure augmentation in subjects with treated hypertension." *J Am Coll Cardiol* 32: 1214-1220.
- Cameron, J. D., Rajkumar, C., Kingwell, B. A., Jennings, G. L. and Dart, A. M. (1999). "Higher systemic arterial compliance is associated with greater exercise time and lower blood pressure in a young older population." *J Am Geriatr Soc* 47(6): 653-6.
- Canty, J. M., Klocke, F. S. and Mates, R. E. (1985). "Pressure and tone dependence of coronary diastolic input impedance and capacitance." *Am J Physiol* 248: H700-11.
- Carlier, S. G., Van Langenhove, G., Lupotti, F., Albertal, M., Mastik, F., Bom, K. and Serruys, P. W. (1999). "Coronary flow reserve versus geometric measurements of coronary dimensions: advantages and limitations of the functional stenosis assessment." *J Intervent Cardiol* 12: 411-424.
- Caro, C., Lever, M., Parker, K. and Fish, P. (1987). "Effect of cigarette smoking on the pattern of arterial blood flow: Possible insight into mechanisms underlying the development of atherosclerosis." *Lancet* 2: 11-13.
- Caro, C. G., Pedley, J. G., Schroter, R. C. and Seed, W. A. (1978). *The mechanics of the circulation*. New York, Oxford University Press.
- Cerqueira, M. D., Weissman, N. J., Dilsizian, V., Jacobs, A. K., Kaul, S., Laskey, W. K., Pennell, D. J., Rumberger, J. A., Ryan, T. and Verani, M. S. (2002). "Standardized myocardial segmentation and nomenclature for tomographic imaging of the heart. A statement for healthcare professionals from the Cardiac Imaging Committee of the Council on Clinical Cardiology of the American Heart Association." *Circulation* 105: 539-542.
- Chamuleau, S. A., Siebes, M., Meuwissen, M., Koch, K. T., Spaan, J. A. and Piek, J. J. (2003). "Association between coronary lesion severity and distal microvascular resistance in patients with coronary artery disease." *Am J Physiol Heart Circ Physiol* 285: H2194-200.

- Chen, C.-H., Nevo, E., Fetters, B., Pak, P. H., Yin, F. C. P., Maughan, W. L. and Kass, D. A. (1997). "Estimation of central aortic pressure waveform by mathematical transformation of radial tonometry pressure. Validation of generalized transfer function." *Circulation* 95: 1827-1836.
- Cieszynski, T. (1960). "Intracardiac method for the investigation of structure of the heart with aid of ultrasonics." *Arch Immun Ter Dosw* 8: 551.
- Cohen, J., Ottenweller, J., George, A. and Duvvuri, S. (1993). "Comparison of Dobutamine and exercise echocardiography for detecting coronary artery disease." *Am J Cardiol* 72: 1226-31.
- Cohn, P. F. (1979). *Diagnosis and therapy of coronary artery disease*. Boston, Little, Brown and Co.
- Cooke, P. H. and Fay, F. S. (1972). "Correlation between fiber length ultrastructure, and the length-tension relationship of mammalian smooth muscle." *J Cell Biol* 52: 105-116.
- Cournand, A. and Ranges, H. A. (1941). "Catheterisation of the right atrium in man." *Proc Soc Exp Biol Med* 46: 462-6.
- Cox, R. (1969). "Comparison of linearized wave propagation models for arterial blood flow analysis." *J Biomech* 2: 251-265.
- Cox, R. H. (1968). "Wave propagation through a Newtonian fluid contained within a thick-walled, viscoelastic tube." *Biophys J* 8: 691-709.
- Danesh, J., Collins, R., Peto, R. and Lowe, G. D. O. (2000). "Haematocrit, viscosity, erythrocyte sedimentation rate: meta-analyses of prospective studies of coronary heart disease." *Eur Heart J* 21: 515-520.
- Davis, R. F. (1985). "Clinical comparison of automated auscultatory and oscillometric and catheter-transducer measurements of arterial pressure." *J Clin Monit* 1(2): 114-9.
- De Backer, T. L., De Buyzere, M., Segers, P., Carlier, S., De Sutter, J., Van de Wiele, C. and De Backer, G. (2002). "The role of whole blood viscosity in premature coronary artery disease in women." *Atherosclerosis* 165(2): 367-73.

- De Bruyne, B., Bartunek, J., Sys, S. U. and Heyndrickx, G. R. (1995). "Relation between myocardial fractional flow reserve calculated from coronary pressure measurements and exercise-induced myocardial ischemia." *Circulation* 92(1): 39-46.
- De Bruyne, B., Bartunek, J., Sys, S. U., Pijls, N. H. J., Heyndrickx, G. R. and Wijns, W. (1996). "Simultaneous coronary pressure and flow velocity measurements in humans. Feasibility, reproducibility, and hemodynamic dependence of coronary flow reserve, hyperemic flow versus pressure slope index, and fractional flow reserve." *Circulation* 94(8): 1842-9.
- De Bruyne, B., Baudhuin, T., Melin, J. A., Pijls, N. H. J., Heyndrickx, G. R. and Wijns, W. (1994). "Coronary flow reserve calculated from pressure measurements in man: validation with positron emission tomography." *Circulation* 89: 1013-1022.
- De Bruyne, B., Pijls, N. H. J., Heyndrickx, G. R., Hodeige, D., Kirkeeide, R. L. and Gould, K. L. (2000). "Pressure-derived fractional flow reserve to assess serial epicardial stenosis: theoretical basis and animal validation." *Circulation* 101(15): 1840-7.
- De Bruyne, B., Pijls, N. H. J., Paulus, W. J., Vantrimpont, P. J., Sys, S. U. and Heyndrickx, G. R. (1993). "Transstenotic coronary pressure gradient measurement in humans: in vitro and in vivo evaluation of a new pressure monitoring angioplasty guide wire." *J Am Coll Cardiol* 22: 119-126.
- de Jaegere, P., Mudra, H., Figulla, H., Almagor, Y., Doucet, S., Penn, I., Colombo, A., Hamm, C., Bartorelli, A., Rothman, M., Nobuyoshi, M., Yamaguchi, T., Voudris, V., Di Mario, C., Makovski, S., Hausmann, D., Rowe, S., Rabinovich, S., Sunamura, M. and van Es, G. A. (1998). "Intravascular ultrasound-guided optimized stent deployment. Immediate and 6 months clinical and angiographic results from the Multicenter Ultrasound Stenting In Coronaries Study (MUSIC Study)." *Eur Heart J* 19: 1214-1223.
- De Jong, J. R., Ros, H. H. and De Lange, J. J. (1995). "Noninvasive continuous blood pressure measurement during anaesthesia: a clinical evaluation of a method commonly used in measuring devices." *Int J Clin Monit Comput* 12(1)(Feb): 1-10.
- De Mey, S. (2002). *Diastology. Insights from model studies and clinical observations using color M-mode Doppler echocardiography*. PhD Thesis. Faculty of Applied Sciences. Ghent, Ghent University.

- De Scheerder, I. K., Wang, K., Kerdsinchai, P., Desmet, W., Dens, J., Supanantarook, C. and Piessens, J. H. (1997). "Clinical and angiographic outcome after implantation of a home-made stent for complicated coronary angioplasty." *Cathet Cardiovasc Diagn* 42(3): 339-347.
- Deswysen, B., Charlier, A. and Gevers, M. (1980). "Quantitative evaluation of the systemic arterial bed by parameter estimation of a simple model." *Med Biol Eng Comput* 18: 153-166.
- Di Mario, C., Gorge, G., Peters, R., Kearney, P., Pinto, F., Hausmann, D., von Birgelen, C., Colombo, A., Mudra, H., Roelandt, J. and Erbel, R. (1998). "Clinical application and image interpretation in intracoronary ultrasound. Study group on intracoronary imaging of the working group of coronary circulation and of the subgroup on intravascular ultrasound of the working group of echocardiography of the European Society of Cardiology." *Eur Heart J* 19: 207-229.
- Dobson, J. (1927). "Erasistratus." *Proc Roy Soc Med* 20: 825.
- Dole, W. P., Richards, K. L., Hartley, C. J., Alexander, G. M., Campbell, A. B. and Bishop, V. S. (1984). "Diastolic coronary artery pressure-flow velocity relationships in conscious man." *Cardiovasc Res* 18(9): 548-54.
- Downey, J. M. and Kirk, E. S. (1975). "Inhibition of coronary blood flow by a vascular waterfall mechanism." *Circ Res* 36(6): 753-60.
- Drzewiecki, G. M. (1979). Arterial tonometry. MSc Thesis. Philadelphia, MA, University of Pennsylvania.
- Drzewiecki, G. M., Melbin, J. and Noordergraaf, A. (1983). "Arterial tonometry: review and analysis." *J Biomech* 16(2): 141-52.
- Drzewiecki, G. M., Melbin, J. and Noordergraaf, A. (1989). "The Korotkoff sound." *Ann Biomed Eng* 17: 325-359.
- Drzewiecki, G. M. and Noordergraaf, A. (1979). Arterial tonometry: basic requirements. 32nd Annual Conference on Engineering in Medicine and Biology, Denver, CO: 58.
- Duke-Elder, S. and Gloster, J. (1968). Physiology of the eye. The intra-ocular pressure. System of Ophthalmology. S. Duke-Elder. London, Henry Kimpton. IV.

REFERENCES

- Dwight, H. B. (1961). *Mathematical tables*. New York, Dover.
- Eckerle, J. and Newgard, P. (1976). A noninvasive transducer for the continuous measurement of arterial blood pressure. 29th ACEMB, Boston, MA.
- Evans, D., McDicken, W., Skidmore, R and Woodcock, J. (1989). *Doppler ultrasound: physics, instrumentation and clinical applications*. New York, Wiley & Sons.
- Fahraeus, R. and Lindqvist, T. (1931). "Viscosity of blood in narrow capillary tubes." *Am J Physiol* 96: 562-8.
- Fattori, R. and Piva, T. (2003). "Drug-eluting stents in vascular intervention." *The Lancet* 361: 247-9.
- Fearon, W. F., Luna, J., Samady, H., Powers, E. R., Feldman, T., Dib, N., Tuzcu, E. M., Cleman, M. W., Chou, T. M., Cohen, D. J., Ragosta, M., Takagi, A., Jeremias, A., Fitzgerald, P. J., Yeung, A. C., Kern, M. J. and Yock, P. G. (2001). "Fractional flow reserve compared with intravascular ultrasound guidance for optimizing stent deployment." *Circulation* 104(16): 1917-22.
- Fetics, B., Nevo, E., Chen, C.-H. and Kass, D. A. (1999). "Parametric model derivation of transfer function for noninvasive estimation of aortic pressure by radial tonometry." *IEEE Transactions on Biomedical Engineering* 46(6): 698-706.
- Fischer, J. J., Samady, H., McPherson, J. A., Sarembock, I. J., Powers, E. R., Gimple, L. W. and Ragosta, M. (2002). "Comparison between visual assessment and quantitative angiography versus fractional flow reserve for native coronary narrowings of moderate severity." *Am J Cardiol* 90(3): 210-5.
- Foreman, R. and Kirk, E. S. (1980). "Comparative effects of vasodilator drugs on large and small coronary resistance vessels in the dog." *Cardiovasc Res* 14: 601-6.
- Forssmann, W. (1929). "Die Sondierung des rechten Herzens." *Klin Wochenschr* 8: 2085-96.
- Frank, O. (1899). "Die Grundform des arteriellen Pulses. Erste Abhandlung. Mathematische Analyse." *Z Biol* 37: 483-526.
- Frank, O. (1903). "Kritik der Elasticchen Manometer." *Z Biol* 44: 445-613.

- Franklin, D. L., Baker, D. W. and Rushmer, R. F. (1962). "Ultrasonic transittime flowmeter." IRE Trans Biomed Eng 9: 44-49.
- Franklin, P. (1949). An introduction to Fourier methods and the Laplace transformation. New York, Dover Publications.
- Franklin, S., Khan, S., Wong, N., Larson, M. and Levy, D. (1999). "Is pulse pressure useful in predicting risk of coronary heart disease? The Framingham Heart Study." Circulation 100: 354-360.
- Frisch-Fay, R. (1962). Section 4.9. Flexible Bars. London, Butterworths.
- Fry, D. L., Griggs, D. M. and Greenfield, J. C. (1963). In vivo studies on pulsatile blood flow. Pulsatile blood flow. E. O. Attinger. New York, McGraw-Hill.
- Fung, Y. C. (1981). Biomechanics: Mechanical properties of living tissues. New York, Springer-Verlag.
- Gagnon, D. R., Zhang, T. J., Brand, F. N. and Kannel, W. B. (1994). "Hematocrit and the risk of cardiovascular disease-the Framingham study: a 34-year follow-up." Am Heart J 127(3): 674-82.
- Garcia, M. J., Thomas, J. D. and Klein, A. L. (1998). "New Doppler echocardiographic applications for the study of diastolic function." J Am Coll Cardiol 32(4): 865-75.
- Gatzka, C. D., Cameron, J. D., Kingwell, B. A. and Dart, A. M. (1998). "Relation between coronary artery disease, aortic stiffness and left ventricular structure in a population sample." Hypertension 32: 575-578.
- Geddes, L. A. (1984). Cardiovascular devices and their applications. New York, John Wiley.
- Giuliani, E. R., Gersch, B. J., McGoon, M. D., Hayes, D. L. and Schaff, H. V. (1996). Mayo Clinic Practice of Cardiology. St Louis, Mosby.
- Gizdulich, P. and Wesseling, K. H. (1990). Reconstruction of brachial arterial pulsation from finger arterial pressure. 12th Int Conf IEEE Eng Med Biol Soc 12: 1046-1047.

REFERENCES

- Goldmann, H. and Schmidt, T. H. (1957). "Uber applanations-tonometrie." *Ophthalmologica* 134: 221-242.
- Goldstein, S. and Killip, T. (1962). "Comparison of direct and indirect arterial pressures in aortic regurgitation." *N Engl J Med* 267: 1121-1124.
- Goldwyn, R. and Watt, T. J. (1967). "Arterial pressure pulse contour analysis via a mathematical model for the clinical qualification of human vascular properties." *IEEE Trans Bio-Med Eng* 14: 11-17.
- Gorback, M. S. (1988). Considerations in the interpretation of systemic pressure monitoring. Complications in critical care medicine. P. D. Lumb and C. W. Bryan-Brown. Chicago, Year Book Medical Publishers: 296.
- Gow, B. S. and Taylor, M. G. (1968). "Measurement of viscoelastic properties of arteries in the living dog." *Circ Res* 23: 111-122.
- Gravenstein, J. S., Paulus, D. A., Feldman, J. and McLaughlin, G. (1985). "Tissue hypoxia distal to a Penaz finger blood pressure cuff." *J Clin Monit* 1(2): 120-5.
- Gravlee, G., Bauer, S., O'Rourke, M. and Avolio, A. (1989). "A comparison of brachial, femoral and aortic intraarterial pressures before and after cardiopulmonary bypass." *Anaesth. Intensive Care* 17: 305-311.
- Gravlee, G. and Brockschmidt, J. K. (1990). "Accuracy of four indirect methods of blood pressure measurements, with hemodynamic correlations." *J Clin Monit* 6(4): 284-98.
- Gregg, D. E. (1940). "Registration and interpretation of normal phasic inflow into a left coronary artery by an improved differential manometer method." *Am J Physiol* 130: 114-25.
- Gregg, D. E. and Shipley, R. E. (1944). "Augmentation of left coronary inflow with elevation of left ventricular pressure, and observations on the mechanism for increased coronary inflow with increased cardiac load." *Am J Physiol* 142: 44-51.
- Grossman, W. (1980). Cardiac catheterization and angiography. Philadelphia, Lea & Febiger.

- Guillaume, M., Lapidus, L., Beckers, F., Lambert, A. and Bjorntorp, P. (1996). "Cardiovascular risk factors in children from the Belgian province of Luxembourg. The Belgian Luxembourg Child Study." *Am J Epidemiol* 144(9): 867-80.
- Guyton, A. C. (1963). *Circulatory Physiology: cardiac output and its regulation*. Philadelphia, Saunders.
- Guyton, A. C. and Hall, J. E. (2000). *Textbook of medical physiology*. Philadelphia, W.B. Saunders.
- Hales, S. (1733). *Statical essays: containing Haemastaticks*. London, Innys, Manby & Woodward.
- Haluska, B. A., Short, L., Mottram, P., Carlier, S. G. and Marwick, T. H. (2003). Is a radial-aortic transfer function for total arterial compliance robust in women and the elderly? ACC 2003 52nd Annual Scientific Session, Chicago, IL, *J Am Coll Cardiol* 41(6 Suppl 1): 298-299.
- Hamilton, W. F. and Dow, P. (1939). "An experimental study of the standing waves in the pulse propagated through the aorta." *Am J Physiol* 125: 48-59.
- Hanekamp, C. E. E., Koolen, J. J., Pijls, N. H. J., Michels, H. R. and Bonnier, H. J. R. M. (1999). "Comparison of quantitative coronary angiography, intravascular ultrasound, and coronary pressure measurement to assess optimum stent deployment." *Circulation* 99: 1015-1021.
- Hanevold, C., Waller, J., Daniels, S., Portman, R. and Sorof, J. (2004). "The effects of obesity, gender, and ethnic group on left ventricular hypertrophy and geometry in hypertensive children: a collaborative study of the International Pediatric Hypertension Association." *Pediatrics* 113(2): 328-33.
- Harder, C., Rzany, A. and Schaldach, M. (1999). "Coating of vascular stents with antithrombogenic amorphous Silicon Carbide." *Progress in Biomedical Research* 4(1): 71-7.
- Hardung, V. (1952). "Über eine Methode zur Messung der dynamischen Elastizität und Viskosität kautschukähnlicher Körper, insbesondere von Blutgefäßen und anderen elastischen Gewebteilen." *Helv Physiol Pharmacol Acta* 10: 482-498.
- Hatle, L. and Angelsen, B. (1990). *Doppler ultrasound in cardiology: physical principles and clinical applications*. Philadelphia, Lea & Febiger.

- Hayashi, T., Nakayama, Y., Tsumura, K., Yoshimaru, K. and Ueda, H. (2002). "Reflection in the arterial system and the risk of coronary heart disease." *Am J Hypertens* 15: 405-409.
- Haynes, R. H. (1961). "Physical basis of the dependence of blood viscosity on tube radius." *Am J Physiol* 198: 1193-8.
- Hennessy, T. G., Codd, M. B., Kane, G., McCarthy, C., McCann, H. A. and Sugrue, D. D. (1997). "Dobutamine stress echocardiography in the detection of coronary artery disease: importance of the pretest likelihood of disease." *Am Heart J* 134(4): 685-92.
- Hirai, T., Sasayama, S., Kawasaki, T. and Yagi, S. (1989). "Stiffness of systemic arteries in patients with myocardial infarction: a noninvasive method to predict severity of coronary atherosclerosis." *Circulation* 80: 78-86.
- Hoffman, J. I. and Spaan, J. A. (1990). "Pressure-flow relations in coronary circulation." *Physiol Rev* 70(2): 331-90.
- Hoffman, J. I. E. (1984). "Maximal coronary flow and the concept of coronary vascular reserve." *Circulation* 70: 153-9.
- Hope, S. A., Meredith, I. T. and Cameron, J. D. (2003). "Is there any advantage to using an arterial transfer function." *Hypertension* 42(3): e6-7.
- Hope, S. A., Tay, D. B., Meredith, I. T. and Cameron, J. D. (2002). "Comparison of generalized and gender-specific transfer functions for the derivation of aortic waveforms." *Am J Physiol Heart Circ Physiol* 283(3): H1150-6.
- Hope, S. A., Tay, D. B., Meredith, I. T. and Cameron, J. D. (2003). "Use of arterial transfer functions for the derivation of aortic waveform characteristics." *J Hypertens* 21: 1299-1305.
- Hope, S. A., Tay, D. B., Meredith, I. T. and Cameron, J. D. (2004). "Use of arterial transfer functions for the derivation of central aortic waveform characteristics in subjects with type 2 diabetes and cardiovascular disease." *Diabetes Care* 27(3): 746-51.
- Ioannou, C. V., Stergiopoulos, N., Katsamouris, A. N., Startchik, I., Kalangos, A., Licker, M. J., Westerhof, N. and Morel, D. R. (2003). "Hemodynamics induced after acute reduction of proximal thoracic aorta compliance." *Eur J Vasc Endovasc Surg* 26: 195-204.

- Isaaz, K., Thompson, A., Ethevenot, G., Cloez, J., Brembilla, B. and Pernot, C. (1989). "Doppler echocardiographic measurement of low velocity motion of the left ventricular posterior wall." *Am J Cardiol* 66-75.
- James, M., Watt, P., Potter, J., Thurston, H. and Swales, J. (1995). "Pulse pressure and resistance artery structure in the elderly." *Hypertension* 26: 301-306.
- Jeremias, A., Filardo, S. D., Whitbourn, R. J., Kernoff, R. S., Yeung, A. C., Fitzgerald, P. J. and Yock, P. G. (2000). "Effects of intravenous and intracoronary adenosine 5'-triphosphate as compared with adenosine on coronary flow and pressure dynamics." *Circulation* 101: 318-323.
- Jeremy, R. W., Huang, H., Hwa, J., McCarron, H., Hughes, C. F. and Richards, J. G. (1994). "Relation between age, arterial distensibility, and aortic dilatation in the Marfan syndrome." *Am J Cardiol* 74: 369-373.
- Kahle, W., Leonhardt, H. and Platzer, W., Eds. (1992). *Sesam atlas van de anatomie, deel 2 inwendige organen*. Baarn, The Netherlands, Bosch & Keuning NV.
- Kannel, W. B., Vasan, R. S. and Levy, D. (2003). "Is the relation of systolic blood pressure to risk of cardiovascular disease continuous and graded, or are there critical values?" *Hypertension* 42(4): 453-6.
- Kapoor, A. S., Ed. (1989). *Interventional cardiology*. New York, Springer-Verlag Inc.
- Karamanoglu, M., Avolio, A. and O'Rourke, M. (1990). "Real-time estimation of aortic pressure wave contour from non-invasive measurements of the peripheral pulse in the upper limb." *Aust J Cardiol* 10: 329-330.
- Karamanoglu, M. and Fenely, M. P. (1996). "Derivation of the ascending aorta-carotid pressure transfer function with an arterial model." *Am J Physiol* 271: H2399-H2404.
- Karamanoglu, M., Gallagher, D. E., Avolio, A. P. and O'Rourke, M. F. (1995). "Pressure wave propagation in a multibranched model of the human upper limb." *Am J Physiol* 269: H1363-H1369.

- Karamanoglu, M., O'Rourke, M. F., Avolio, A. P. and Kelly, R. (1993). "An analysis of the relationship between central aortic and peripheral upper limb pressure waves in man." *Eur Heart J* 14: 160-167.
- Kass, D. A., Saeki, A., Tunin, R. S. and Recchia, F. A. (1996). "Adverse influence of systemic vascular stiffening on cardiac dysfunction and adaptation to acute coronary occlusion." *Circulation* 93: 1533-41.
- Kelly, R. and Fitchett, D. (1992). "Noninvasive determination of aortic input impedance and external left ventricular power output: a validation and reproducibility study of a new technique." *J Am Coll Cardiol* 20: 952-63.
- Kelly, R., Hayward, C., Ganis, J., Daley, J., Avolio, A. and O'Rourke, M. (1989a). "Noninvasive registration of the arterial pressure pulse waveform using high-fidelity applanation tonometry." *Journal of Vascular Medicine and Biology* 1(3): 142-149.
- Kelly, R., Hayward, C., Ganis, J., Daley, J., Avolio, A. and O'Rourke, M. (1989b). "Noninvasive registration of the arterial pressure pulse waveform using high-fidelity applanation tonometry." *J Vasc Med Biol* 1(3): 142-149.
- Kelly, R. P., Tunin, R. and Kass, D. A. (1992). "Effect of reduced aortic compliance on cardiac efficiency and contractile function of in situ canine left ventricle." *Circ Res* 71: 490-502.
- Kemmotsu, O., Ohno, M., Takita, K., Sugimoto, H., Otsuka, H., Morimoto, Y. and Mayumi, T. (1994). "Noninvasive, continuous blood pressure measurement by arterial tonometry during anesthesia in children." *Anesthesiology* 81(5)(Nov): 1162-8.
- Kemmotsu, O., Ueda, M., Otsuka, H., Yamamura, T., Okamura, A., Ishikawa, T., Winter, D. and Eckerle, J. (1991a). "Blood pressure measurement by arterial tonometry in controlled hypotension." *Anesth Analg* 73(1)(Jul): 54-8.
- Kemmotsu, O., Ueda, M., Otsuka, H., Yamamura, T., Winter, D. and Eckerle, J. (1991b). "Arterial tonometry for noninvasive, continuous blood pressure monitoring during anesthesia." *Anesthesiology* 75(2)(Aug): 333-40.
- Kenner, T. (1967). "Neue Gesichtspunkte und Experimente zur Beschreibung und Messung der Arterienelastizität." *Arch Kreislaufforsch* 54: 68-139.

- Kern, M. J. (2000). "Coronary physiology revisited: practical insights from the cardiac catheterization laboratory." *Circulation* 101: 1344-1351.
- Kern, M. J. (2001). "Curriculum in interventional cardiology: coronary pressure and flow measurements in the cardiac catheterization laboratory." *Cathet Cardiovasc Interv* 54(3): 378-400.
- Khoury, E. M. and Gregg, D. E. (1963). "Miniature electromagnetic flowmeter applicable to coronary arteries." *J Appl Physiol* 18: 224-7.
- Kim, S. (2002). A study of non-Newtonian viscosity and yield stress of blood in a scanning capillary - tube rheometer. PhD Thesis. Faculty of Engineering. Philadelphia, Drexel University.
- Kingwell, B. A. (2002). "Large artery stiffness: implications for exercise capacity and cardiovascular risk." *Clin Exp Pharmacol Physiol* 29: 214-217.
- Kingwell, B. A., Waddell, T. K., Medley, T. L., Cameron, J. D. and Dart, A. M. (2002). "Large artery stiffness predicts ischemic threshold in patients with coronary artery disease." *J Am Coll Cardiol* 40(4): 773-9.
- Kleinman, B., Powell, S., Kumar, P. and Gardner, R. M. (1992). "The fast flush test measures the dynamic response of the entire blood pressure monitoring system." *Anesthesiology* 77(6): 1215-20.
- Klocke, F. J., Mates, R. E., Canty, J. M., Jr. and Ellis, A. K. (1985). "Coronary pressure-flow relationships. Controversial issues and probable implications." *Circ Res* 56(3): 310-23.
- Kobayashi, S., Yano, M., Kohno, M., Obayashi, M., Hisamatsu, Y., Ryoike, T., Ohkusa, T., Yamakawa, K. and Matsuzaki, M. (1996). "Influence of aortic impedance on the development of pressure-overload left ventricle hypertrophy in rats." *Circulation* 94: 3362-3368.
- Kolin, A. (1936). "An electromagnetic flowmeter: principles of the method and its application to blood flow measurements." *Proc Soc Exp Biol Med* 35: 53-56.
- Korotkoff, N. C. (1905). "On the subject of methods of determining blood pressure." *Wien med Wschr* 11: 365.

- Korteweg, D. J. (1878). "Über die Fortpflanzungsgeschwindigkeit des Schalles in elastischen Röhren." *Ann Phys Chem (NS)* 5: 525-37.
- Krafka, J. (1939). "Comparative studies of the histophysics of the aorta." *Am J Physiol* 125: 1-14.
- Krams, R., Wentzel, J. J., Céspedes, I., Carlier, S. G., van der Steen, A. F. W., Lancée, C. T. and Slager, C. J. (1999). "Effect of catheter placement on 3-D velocity profiles in curved tubes resembling the human coronary system." *Ultrasound Med Biol* 25(5): 803-810.
- Ku, D. D. (1982). "Coronary vascular reactivity after acute myocardial ischemia." *Science* 218: 576-8.
- Kutryk, M. J. B. and Serruys, P. W. (1999). *Coronary stenting: Current perspectives. A companion to the Handbook of coronary stents*. London, Martin Dunitz Ltd.
- Laird, J. D. (1980). "Thomas Young M.D. (1773-1829)." *Am Heart J* 100: 1-8.
- Langewouters, G., Wesseling, K. and Goedhard, W. (1984). "The static elastic properties of 45 human thoracic and 20 abdominal aortas in vitro and the parameters of a new model." *J Biomech* 17: 425-435.
- Langewouters, G., Wesseling, K. and Goedhard, W. (1985). "The pressure dependent dynamic elasticity of 35 thoracic and 16 abdominal human aortas in vitro described by a 5 component model." *J Biomech* 18: 613-620.
- Laskey, W. K., Parker, H. G., Ferrari, V. and Kussmaul, W. G. (1990). "Estimation of total systemic arterial compliance in humans." *Am J Physiol* 69: 112-119.
- Latham, R. D., Westerhof, N., Sipkema, P., Rubal, B. J., Reuderink, P. and Murgo, J. P. (1985). "Regional wave travel and reflections along the human aorta: a study with six simultaneous micromanometric pressures." *Circulation* 72: 1257-1269.
- Lehmann, E., Gosling, R., Fatemi-Langroudi, B. and Taylor, M. (1992). "Non-invasive Doppler ultrasound technique for the in vivo assessment of aortic compliance." *J Biomed Eng* 14: 250-256.
- Li, J. (1986). "Time domain resolution of forward and reflected waves in the aorta." *IEEE Trans Biomed Eng* 33: 783-785.

- Li, J., Cui, T. and Drzewiecki, G. (1990). "A nonlinear model of the arterial system incorporating a pressure-dependent compliance." *IEEE Trans Biomed Eng* 37: 673-678.
- Li, J. K. J. (1987). *Arterial System Dynamics*. New York, New York University Press.
- Li, J. K.-J. (1996). *Comparative cardiovascular dynamics of mammals*. New York, CRC Press.
- Li, J. K.-J. (2000). *The arterial circulation. Physical principles and clinical applications*. Totowa, New Jersey, Humana Press Inc.
- Li, J. K.-J., Melbin, J. and Noordergraaf, A. (1984). Optimality of pulse transmission at vascular branching junctions. *6th Int Conf Cardiovasc Syst Dynamics*: 228-230.
- Linford, R. G. and Ryan, N. W. (1965). "Pulsatile flow in rigid tubes." *J Appl Physiol* 20: 1078-82.
- Liu, Z., Brin, K. and Yin, F. (1986). "Estimation of total arterial compliance : an improved method and evaluation of current methods." *Am J Physiol* 251: H588-H600.
- Ljung, L. (1987). *System identification: theory for the user*. Englewood Cliffs, Prentice Hall.
- London, G., Pannier, B., Guerin, A., Marchais, S., Safar, M. and Cuche, J. (1994). "Cardiac hypertrophy, aortic compliance, peripheral resistance, and wave reflection in end-stage renal disease. Comparative effects of ACE inhibition and calcium channel blockade." *Circulation* 90(6)(Dec): 2786-96.
- MacKay, R. S. (1960). "Fast, automatic, ocular pressure measurement based on an exact theory." *IRE Trans on Medical Electronics ME-7*: 61-67.
- Mackay, R. S., Marg, E. and Oechsli, R. (1960). "Automatic tonometer with exact theory: various biological applications." *Science* 131: 1668-1669.
- Madhavan, S., Ooi, W., Cohen, H. and Alderman, M. (1994). "Relation of pulse pressure and blood pressure reduction to the incidence of myocardial infarction." *Hypertension* 23: 395-401.
- Maeta, H. and Hori, M. (1985). "Effects of a lack of Aortic Windkessel properties on the left ventricle." *Jpn Circ J* 49: 232-237.

- Mahomed, F. (1872). "The physiology and clinical use of the sphygmograph." *Medical Times and Gazette* 1: 62-65.
- Mandel, M. and Dauchot, P. (1977). "Radial artery cannulation in 1000 patients: precautions and complications." *J Hand Surg* 2 2(6): 482-5.
- Marcus, R. H., Korcarz, C., McCray, G., Neumann, A., Murphy, M., Borow, K., Weinert, L., Bednarz, J., Gretler, D. D., Spencer, K. T., Sareli, P. and Lang, R. M. (1994). "Noninvasive method for determination of arterial compliance using Doppler echocardiography and subclavian pulse tracings." *Circulation* 89: 2688-2699.
- Marey, E. J. (1860). *Recherches sur le pouls au moyen d'un nouvel appareil enregistreur: le sphygmographe*. Paris, E Thunot et Cie.
- Marwick, T. H., Willemart, B., D'Hondt, A. M., Baudhuin, T., Wijns, W., Detry, J. M. and Melin, J. (1993). "Selection of the optimal non-exercise stress for the evaluation of ischemic regional myocardial dysfunction and malperfusion: comparison of Dobutamine and Adenosine using echocardiography and 99mTc-MIBI single photon emission computed tomography." *Circulation* 87(2): 345-54.
- Mates, R. E., Gupta, R. L., Bell, A. C. and Klocke, F. J. (1978). "Fluid dynamics of coronary artery stenosis." *Circ Res* 42: 152-162.
- Matthys, D., Craen, M., De Wolf, D., Vande Walle, J. and Verhaaren, H. (1996). "Reduced decrease of peripheral vascular resistance during exercise in young type I diabetic patients." *Diabetes Care* 19(11): 1286-1288.
- Matthys, K. and Verdonck, P. (2002). "Development and modelling of arterial applanation tonometry: a review." *Technology and Health Care* 10(1): 65-76.
- Matthys, K. S., Carlier, S. G., Segers, P., Ligthart, J., Sianos, G., Serrano, P., Verdonck, P. R. and Serruys, P. W. (2001). "In vitro study of FFR, QCA and IVUS for the assessment of optimal stent deployment." *Catheter Cardiovasc Interv* 54: 363-375.
- McCarthy, M. (2001). "Heart disease prevention should start with the young, studies suggest." *The Lancet* 357(9260): 939.

- McDonald, D. (1955). "The relationship of pulsatile pressure to flow in arteries." *J Physiol* 127: 533-552.
- McDonald, D. A. (1960). *Blood flow in arteries*. London, Edward Arnold.
- McVeigh, G. (1996). "Arterial compliance in hypertension and diabetes mellitus." *Am J Nephrol* 16(3): 217-22.
- McVeigh, G. E., Bratteli, C. W., Morgan, D. J., Alinder, C. M., Glasser, S. P., Finkelstein, S. M. and Cohn, J. N. (1999). "Age-related abnormalities in arterial compliance identified by pressure pulse contour analysis: aging and arterial compliance." *Hypertension* 33: 1392-8.
- Meneveau, N., Di Mario, C., Gil, R., de Jaegere, P., de Feyter, P. J., Roelandt, J. and Serruys, P. W. (1993). "Instantaneous pressure-velocity relationship of the coronary flow, alternative to coronary reserve measurement: a feasibility study and reproducibility of the method." *Arch Mal Coeur Vaiss* 86(7): 975-85.
- Merril, E. W., Benis, A. M., Gilliland, E. R., Sherwood, T. K. and Salzman, E. W. (1965). "Pressure-flow relations of human blood in hollow fibres at low flow rates." *J Appl Physiol* 20: 954-67.
- Meuwissen, M., Chamuleau, S. A., Siebes, M., Schotborgh, C. E., Koch, K. T., de Winter, R. J., Bax, M., de Jong, A., Spaan, J. A. and Piek, J. J. (2001). "Role of variability in microvascular resistance on fractional flow reserve and coronary blood flow velocity reserve in intermediate coronary lesions." *Circulation* 103(2): 184-187.
- Meuwissen, M., Siebes, M., Chamuleau, S. A., van Eck-Smit, B. L., Koch, K. T., de Winter, R. J., Tijssen, J. G., Spaan, J. A. and Piek, J. J. (2002). "Hyperemic stenosis resistance index for evaluation of functional coronary lesion severity." *Circulation* 106: 441-6.
- Millasseau, S. C., Patel, S. J., Redwood, S. R., Ritter, J. M. and Chowienzyk, P. J. (2003). "Pressure wave reflection assessed from the peripheral pulse. Is a transfer function necessary?" *Hypertension* 41: 1016-1020.
- Millasseau, S. C., Ritter, J. M. and Chowienzyk, P. J. (2003). "Clinical assessment of wave reflection. Response: Augmentation index and the radial-to-aortic transfer function." *Hypertension* 42(5): e15-6.

REFERENCES

- Millen, B., Quatromoni, P., Nam, B., O'horo, C., Polak, J., Wolf, P. and D'agostino, R. (2004). "Dietary patterns, smoking, and subclinical heart disease in women: Opportunities for primary prevention from the Framingham nutrition studies." *J Am Diet Assoc* 104(2): 208-14.
- Mills, C. J., Gabe, I. T., Gault, J. H., Mason, D. T., Ross, J. J., Braunwald, E. and Shillingford, J. P. (1970). "Pressure-flow relationships and vascular impedance in man." *Cardiovascular Res* 4: 405-417.
- Mills, C. J. and Shillingford, J. P. (1967). "A catheter tip electromagnetic velocity probe and its evaluation." *Cardiovasc Res* 1: 263-73.
- Milnor, W. R. (1972). *Pulmonary hemodynamics. Cardiovascular Fluid Dynamics.* D. H. Bergel. London, Academic Press. 2.
- Milnor, W. R. (1989). *Hemodynamics.* Baltimore, Maryland, Williams & Wilkins.
- Moens, A. I. (1878). *Die Pulskurve.* Leiden, E. J. Brill.
- Mohan, D. and Melvin, J. W. (1982). "Failure properties of passive human aortic tissue. I-uniaxial tension tests." *J Biomech* 1: 887-902.
- Morice, M. C., Serruys, P. W., Sousa, J. E., Fajadet, J., Ban Hayashi, E., Perin, M., Colombo, A., Schuler, G., Barragan, P., Guagliumi, G., Molnar, F., Falotico, R. and Group., F. t. R. S. (2002). "A randomized comparison of a sirolimus-eluting stent with a standard stent for coronary revascularization." *N Engl J Med* 346(23): 1773-80.
- Morita, S., Asou, T., Kuboyama, I., Harasawa, Y., Sunagawa, K. and Yasui, H. (2002). "Inelastic vascular prosthesis for proximal aorta increases pulsatile arterial load and causes left ventricular hypertrophy in dogs." *J Thorac Cardiovasc Surg* 124(4): 768-774.
- Morita, S., Kuboyama, I., Asou, T., Tokunaga, K., Nose, Y., Nakamura, M., Harasawa, Y. and Sunagawa, K. (1991). "The effect of extraanatomic bypass on aortic input impedance studied in open chest dogs. Should the vascular prosthesis be compliant to unload the left ventricle?" *J Thorac Cardiovasc Surg* 102(5): 774-83.
- Morris, C. L., Smith 2d, C. M. and Blackshear Jr, P. L. (1987). "A new method for measuring the yield stress in thin layers of sedimenting blood." *Biophys J* 52: 229-240.

- Murgo, J. P. and Millar, H. (1972). "A new cardiac catheter for high fidelity differential pressure recordings." *Proc Ann Conf Engng Med Biol* 14: 303-304.
- Murgo, J. P., Westerhof, N., Giolma, J. P. and Altobelli, S. A. (1980). "Aortic input impedance in normal man: relationship to pressure wave forms." *Circulation* 62(1): 105-116.
- Nakagawara, M. and Yamakoshi, K. (2000). "A portable instrument for non-invasive monitoring of beat-by-beat cardiovascular haemodynamic parameters based on the volume-compensation and electrical-admittance method." *Med Biol Eng Comput* 38: 17-25.
- Naqvi, N. H. and Blaufox, M. D. (1998). *Blood pressure measurement. An illustrated history.* New York, The Parthenon Publishing Group Inc.
- Nelesen, R. A. and Dimsdale, J. E. (2002). "Use of radial arterial tonometric continuous blood pressure measurement in cardiovascular reactivity studies." *Blood Press Monit* 7(5): 259-63.
- Nelles, O. (2001). *Nonlinear system identification. From classical approaches to neural networks and fuzzy models.* Berlin Heidelberg, Springer-Verlag.
- Nichols, W. W., Conti, C. R., Walker, W. E. and Milnor, W. R. (1977). "Input impedance of the systemic circulation in man." *Circ Res* 40: 451-458.
- Nichols, W. W. and McDonald, D. A. (1972). "Wave velocity in the proximal aorta." *Med Biol Eng* 10: 327-335.
- Nichols, W. W. and O'Rourke, M. F. (1990). *Mc Donald's blood flow in arteries. Theoretical, experimental and clinical principles.* London, Edward Arnolds.
- Nichols, W. W., O'Rourke, M. F., Avolio, A. P., Yaginuma, T., Murgo, J. P., Pepine, C. J. and Conti, C. R. (1985). "Effects of age on ventricular/vascular coupling." *Am J Cardiol* 55: 1179-84.
- Nichols, W. W., O'Rourke, M. F., Avolio, A. P., Yaginuma, T., Murgo, J. P., Pepine, C. J. and Conti, C. R. (1987). Age related changes in left ventricular/arterial coupling. *Ventricular/vascular coupling.* F. C. P. Yin. New York, Springer-Verlag: 79-114.
- Nieman, D. C. (1995). *Fitness and sports medicine. A health-related approach.* Mountain View, CA, Mayfield Publishing Company.

- Noordergraaf, A. (1969). Hemodynamics. Bioengineering. H. Schwann. New York, McGraw-Hill.
- Noordergraaf, A., Verdouw, P. D. and Boom, H. B. C. (1963). "The use of an analog computer in a circulation model." *Prog Cardiovasc Dis* 5: 419-39.
- Nystrom, E., Reid, K. H., Bennett, R., Couture, L. and Edmonds, H. L. J. (1985). "A comparison of two automated indirect arterial blood pressure meters: with recordings from a radial arterial catheter in anesthetized surgical patients." *Anesthesiology* 62(4): 526-30.
- Ogle, B. M. and Mooradian, D. L. (2002). "Manipulation of remodelling pathways to enhance the mechanical properties of a tissue engineered blood vessel." *J Biomed Eng* 124: 724-33.
- Okamoto, R. J., Wagenseil, J. E., DeLong, W. R., Peterson, S. J., Kouchoukos, N. T. and Sundt III, T. M. (2002). "Mechanical properties of dilated human ascending aorta." *Ann Biomed Eng* 30(5): 624-635.
- Okino, H. (1964). "Measurement of intraluminal pressure from external pressure with strain transducers." *J Appl Physiol* 19: 545-549.
- Olmos, L. I., Dakik, H., Gordon, R., Dunn, J. K., Verani, M. S., Quinones, M. A. and Zoghbi, W. A. (1998). "Long-term prognostic value of exercise echocardiography compared with exercise 201Tl, ECG, and clinical variables in patients evaluated for coronary artery disease." *Circulation* 98(24): 2679-86.
- Olson, R. A. and Burger, R. (1987). "Metabolic control of coronary blood flow." *Prog Cardiovasc Dis* 29: 369-87.
- Olson, R. A. and Gregg, D. E. (1965). "Myocardial reactive hyperemia in the unanesthetized dog." *Am J Physiol* 208: 224-30.
- O'Neill, W. W. and Leon, M. B. (2003). "Drug-eluting stents. Costs versus clinical benefit." *Circulation* 107: 3008-3011.
- O'Rourke, M. and Taylor, M. (1967). "Input impedance of the systemic circulation." *Circ Res* 20: 365.
- O'Rourke, M. F. (1971). "Pressure and flow waves in systemic arteries and the anatomical design of the arterial system." *J Appl Physiol* 23: 139-149.

- O'Rourke, M. F., Avolio, A. and Qasem, A. (2003). "Clinical assessment of wave reflection." *Hypertension* 42(5): e15-6.
- O'Rourke, M. F., Kim, M., Adji, A., Nichols, W. W. and Avolio, A. (2004). "Use of arterial transfer function for the derivation of aortic waveform characteristics." *J Hypertens* 22: 431-434.
- Paridon, S. M. (1998). *Exercise Testing. The science and practice of pediatric cardiology.* J. W. J. Pine. Baltimore, Williams & Wilkins.
- Pauca, A. L., O'Rourke, M. F. and Kon, N. D. (2001). "Prospective evaluation of a method for estimating ascending aortic pressure from the radial artery pressure waveform." *Hypertension* 38: 932-937.
- Peacock, J., Hankins, S., Jones, T. and Lutz, R. (1995). "Flow instabilities induced by coronary artery stents: assessment with an in vitro pulse duplicator." *J Biomechanics* 28(1): 17-26.
- Penaz, J. (1973). *Photoelectric measurement of blood pressure, volume and flow in the finger.* Digest of the 10th International Conference on Medical Engineering, Dresden, Germany.
- Permut, S. and Riley, R. L. (1963). "Hemodynamics of Collapsible Vessels With Tone: the Vascular Waterfall." *J Appl Physiol* 18: 924-32.
- Peronneau, P. (1970). "Vélocimetre sanguin par effet Doppler a émission ultrasonore pulsée." *Onde Electrique* 50: 369.
- Peterson, L. H., Jensen, R. E. and Parnell, J. (1960). "Mechanical properties of arteries in vivo." *Circ Res* 8: 622-639.
- Pijls, N. H. J. and De Bruyne, B. (1997). *Coronary pressure.* Dordrecht, Kluwer Academic Publishers.
- Pijls, N. H. J. and De Bruyne, B. (1998). "Coronary pressure measurement and fractional flow reserve." *Heart* 80: 539-542.
- Pijls, N. H. J., De Bruyne, B., Peels, K., Van der Voort, P., Bonnier, H. J. R. M., Bartunek, J. and Koolen, J. J. (1996). "Measurement of fractional flow reserve to assess the functional severity of coronary artery stenoses." *N Engl J Med* 334: 1703-1708.

- Pijls, N. H. J., Kern, M. J., Yock, P. G. and De Bruyne, B. (2000). "Practice and potential pitfalls of coronary pressure measurement." *Cathet Cardiovasc Interv* 49: 1-16.
- Pijls, N. H. J., Van Gelder, B., Van der Voort, P., Peels, K., Bracke, F. A. L. E., Bonnier, H. J. R. M. and el Gamal, M. I. H. (1995). "Fractional flow reserve. A useful index to evaluate the influence of an epicardial coronary stenosis on myocardial blood flow." *Circulation* 92: 3183-3193.
- Pijls, N. H. J., van Son, J. A. M., Kirkeeide, R. L., De Bruyne, B. and Gould, K. L. (1993). "Experimental basis of determining maximum coronary, myocardial and collateral blood flow by pressure measurements for assessing functional stenosis severity before and after percutaneous transluminal coronary angioplasty." *Circulation* 87: 1354-1367.
- Pipes, L. A. (1958). *Applied mathematics for engineers and physicists*. New York, McGraw-Hill.
- Poiseuille, J. L. M. (1840). "Recherches expérimentales sur le mouvement des liquides dans les tubes de très-petits diamètres." *Comptes rendus hebdomadaires des séances de l'Académie des sciences* 11(961-967): 1041-48.
- Posey, J. A., Geddes, L. A., Williams, H. and Moore, A. G. (1969). "The meaning of the point of maximum oscillations in cuff pressure in the indirect measurement of blood pressure. 1." *Cardiovasc Res Cent Bull* 8(1): 15-25.
- Pressman, G. L. and Newgard, P. M. (1963). "A transducer for the continuous external measurement of arterial blood pressure." *IEEE Trans Bio-Med Electron* 10: 73-81.
- Pressman, G. L. and Newgard, P. M. (1965). *Development of a blood-pressure transducer for the temporal artery*, SRI, Menlo Park CA.
- Price, S. and Wilson, L. (1992). *Pathophysiology, clinical concepts of disease processes*. Philadelphia, Mosby-Year Book Inc.
- Putz, R. and Pabst, R., Eds. (1994a). *Sobotta. Atlas of human anatomy*. Munich, Germany, Urban & Schwarzenberg.
- Putz, R. and Pabst, R., Eds. (1994b). *Sobotta. Atlas of human anatomy*. Munich, Germany, Urban & Schwarzenberg.

- Rajkumar, C., Cameron, J., Christophidis, N., Jennings, G. and Dart, A. (1997). "Reduced systemic arterial compliance is associated with left ventricular hypertrophy and diastolic dysfunction in older people." *J Am Geriatr Soc* 45(7)(Jul): 803-8.
- Ramsey, M. 3rd. (1991). "Blood pressure monitoring: automated oscillometric devices." *J Clin Monit* 7(1): 56-67.
- Randall, J. E. (1958). "Statistical properties of pulsatile pressure and flow in the femoral artery of the dog." *Circ Res* 6: 689-698.
- Randall, O. S., Van Den Bos, G. C. and Westerhof, N. (1984). "Systemic compliance: Does it play a role in the genesis of essential hypertension?" *Cardiovasc Res* 18: 455-462.
- Reneman, R. S., Hoeks, A. P. G. and Westerhof, N. (1996). "Non-invasive assessment of artery wall properties in humans - methods and interpretation." *J Vascular Investigation* 2: 53-64.
- Riva-Rocci, S. (1896). "Un nuovo sfigmomanometro." *Gazz Med Ital, Torino* 47: 981.
- Rowland, T. W. (1993). *Aerobic exercise testing protocols. Pediatric laboratory exercise testing. Clinical guidelines.* T. W. Rowland. Champaign, Human Kinetics Publishers: 195.
- Ruffolo, R. R. J., Spradlin, T. A., Pollock, G. D., Waddell, J. E. and Murphy, P. J. (1981). "Alpha and beta adrenergic effects of the stereoisomers of dobutamine." *J Pharm Exp Therap* 219(2): 447-52.
- Rushmer, R. F. (1972). *Structure and function of the cardiovascular system.* Philadelphia, Saunders.
- Safar, M. E. and London, G. M. (1987). "Arterial and venous compliance in sustained essential hypertension." *Hypertension* 10: 133-139.
- Sato, T., Nishinaga, M., Kawamoto, A., Ozawa, T. and Takatsuji, H. (1993). "Accuracy of a continuous blood pressure monitor based on arterial tonometry." *Hypertension* 21: 866-874.
- Sawada, S. G., Segar, D. S., Ryan, T., Brown, S. E., Dohan, A. M., Williams, R., Fineberg, N. S., Armstrong, W. F. and Feigenbaum, H. (1991). "Echocardiographic detection of coronary artery disease during Dobutamine infusion." *Circulation* 83(5): 1605-14.

- Scheie, H. G. and Albert, D. M. (1977). Textbook of ophthalmology. London, W.B. Saunders Company.
- Schlant, R. C. and Alexander, R. W., Eds. (1994). Hurst's the heart: arteries and veins. New York, McGraw-Hill.
- Schmidt, R. and Thews, G. (1989). Human physiology, Springer-Verlag.
- Schroeder, J. S., Ed. (1985). Invasive cardiology. Philadelphia, F. A. Davis Company.
- Searle, N., Perrault, J., Ste-Marie, H. and Dupont, C. (1993). "Assessment of the arterial tonometer (N-CAT) for the continuous blood pressure measurement in rapid atrial fibrillation." Canadian Journal of Anaesthesia 40: 388-393.
- Segers, P. (1997). Biomechanische modellering van het arterieel systeem voor de niet-invasieve bepaling van de arteriële compliantie. PhD Thesis. Faculty of Applied Sciences. Ghent, Ghent University.
- Segers, P., Carlier, S., Pasquet, A., Rabben, S., Hellevik, L., Remme, E., De Backer, T., De Sutter, J., Thomas, J. and Verdonck, P. (2000). "Individualizing the aorto-radial pressure transfer function: feasibility of a model-based approach." Am J Physiol Heart Circ Physiol 279: 542-549.
- Segers, P., Dubois, F., De Wachter, D. and Verdonck, P. (1998). "Role and relevancy of a cardiovascular simulator." J Cardiovascular Engineering 3(1): 48-56.
- Segers, P., Fostier, G., Neckebroek, J. and Verdonck, P. (1999). "Assessing coronary artery stenosis severity: in vitro validation of the concept of fractional flow reserve." Cathet Cardiovasc Interv 46: 375-379.
- Segers, P., Stergiopoulos, N., Verdonck, P. and Verhoeven, R. (1997). "Assessment of distributed arterial network models." Med Biol Eng Comput 35(6): 729-36.
- Senior, R., Basu, S., Handler, C., Raftery, E. B. and Lahiri, A. (1996). "Diagnostic accuracy of dobutamine stress echocardiography for detection of coronary heart disease in hypertensive patients." Eur Heart J 17(2): 289-95.

- Serruys, P. W., Ed. (1997). Handbook of coronary stents. London, Martin Dunitz Ltd.
- Serruys, P. W., de Jaegere, P., Kiemeneij, F., Macaya, C., Rutsch, W., Heyndrickx, G., Emanuelsson, H., Marco, J., Legrand, V., Materne, P., Belardi, J., Sigwart, U., Colombo, A., Goy, J. J., van den Heuvel, P., Delcan, J. and Morel, M. A. (1994). "A comparison of balloon expandable stent implantation with balloon angioplasty in patients with coronary artery disease." *N Engl J Med* 331: 489-495.
- Serruys, P. W., Foley, D. P., Kirkeeide, R. L. and King, S. r. (1993). "Restenosis revisited: insights provided by quantitative coronary angiography." *Am Heart J* 126: 1243-1267.
- Serruys, P. W. and Kutryk, M. J. B., Eds. (1998). Handbook of coronary stents. London, Martin Dunitz Ltd.
- Serruys, P. W. and Rensing, B. J., Eds. (2002). Handbook of coronary stents. Philadelphia, Taylor & Francis.
- Shercliff, J. A. (1962). The theory of electromagnetic measurement, Cambridge University Press.
- Siebes, M., Chamuleau, S. A., Meuwissen, M., Piek, J. J. and Spaan, J. A. (2002). "Influence of hemodynamic conditions on fractional flow reserve: parametric analysis of underlying model." *Am J Physiol Heart Circ Physiol* 283(4): H1462-70.
- Siebes, M., Verhoeff, B. J., Meuwissen, M., de Winter, R. J., Spaan, J. A. and Piek, J. J. (2004). "Single-wire pressure and flow velocity measurement to quantify coronary stenosis hemodynamics and effects of percutaneous interventions." *Circulation* 109: 756-62.
- Siegel, L., Brock-Utne, J. and Brodsky, J. (1994). "Comparison of arterial tonometry with radial artery catheter measurements of blood pressure in anesthetized patients." *Anesthesiology* 81(3)(Sep): 578-84.
- Simon, A., Safar, L., London, G., Levy, B. and Chau, N. (1979). "An evaluation of large arteries compliance in man." *Am J Physiol* 237: H550-H554.
- Slogoff, S., Keats, A. and Arlund, C. (1983). "On the safety of radial artery cannulation." *Anesthesiology* 59(1): 42-7.

REFERENCES

- Smith, C. R. and Bickley, W. H. (1964). The measurement of blood pressure in the human body, National Aeronautics and Space Administration: 1-34.
- Smith, N., Wesseling, K. and de Wit, B. (1985). "Evaluation of two prototype devices producing noninvasive, pulsatile, calibrated blood pressure measurement from a finger." *J Clin Monit* 1(1): 17-29.
- Söderström, S., Nyberg, G., O'Rourke, M. F., Sellgren, J. and Pontén, J. (2002). "Can a clinically useful aortic pressure wave be derived from a radial pressure wave." *Br J Anaesth* 88: 481-8.
- Sousa, J. E., Serruys, P. W. and Costa, M. A. (2003a). "New frontiers in cardiology. Drug-eluting stents: part I." *Circulation* 107: 2274-2279.
- Sousa, J. E., Serruys, P. W. and Costa, M. A. (2003b). "New frontiers in cardiology. Drug-eluting stents: part II." *Circulation* 107: 2283-2289.
- Spaan, J. A. (1985). "Coronary diastolic pressure-flow relation and zero flow pressure explained on the basis of intramyocardial compliance." *Circ Res* 56(3): 293-309.
- Speiser, D. (1982). "Daniel Bernoulli (1700-1782)." *Helvetica Physica Acta* 55: 504-523.
- Stearns, S. D. and Hush, D. R. (1990). *Digital signal analysis*. Englewood Cliffs, NJ, Prentice-Hall Inc.
- Stearns, S. D. and Ruth, D. A. (1996). *Signal processing algorithms in Matlab*. Upper Saddle River, NJ, Prentice-Hall, Inc.
- Stein, P. and Blick, E. (1971). "Arterial tonometry for the atraumatic measurement of arterial blood pressure." *J Appl Physiol* 30: 593-596.
- Steiner, L. A., Johnston, A. J., Salvador, R., Czosnyka, M. and Menon, D. K. (2003). "Validation of a tonometric noninvasive arterial blood pressure monitor in the intensive care setting." *Anaesthesia* 58: 448-454.
- Stergiopoulos, N., Meister, J. and Westerhof, N. (1994). "Simple and accurate way for estimating total and segmental arterial compliance: the pulse pressure method." *Ann Biomed Eng* 22: 392-397.

- Stergiopoulos, N., Meister, J. J. and Westerhof, N. (1995). "Evaluation of methods for the estimation of total arterial compliance." *Am J Physiol* 268: H1540-H1548.
- Stergiopoulos, N., Segers, P. and Westerhof, N. (1999). "Use of the pulse pressure method for estimating total arterial compliance in vivo." *Am J Physiol* 276(2): H424-H428.
- Stergiopoulos, N., Westerhof, B. E. and Westerhof, N. (1998). "Physical basis of pressure transfer from periphery to aorta: a model-based study." *Am J Physiol* 274: H1386-H1392.
- Stergiopoulos, N., Young, D. and Rogge, T. (1992). "Computer simulation of arterial flow with application to arterial and aortic stenoses." *J Biomech* 25: 1477-1488.
- Stewart, D. J., Pohl, V. and Bassenge, E. (1988). "Free radicals inhibit endothelium-dependent dilation in the coronary resistance bed." *Am J Physiol* 225: H765-9.
- Streeter, V. L. (1961). *Handbook of fluid dynamics*. New York, McGraw-Hill Book Company, Inc.
- Takazawa, K., O'Rourke, M. F., Fujita, M., Tanaka, N., Takeda, K., Kurosu, F. and Ibukiyama, C. (1996). "Estimation of ascending aortic pressure from radial arterial pressure using a generalised transfer function." *Z Kardiol* 85(Suppl 3): 137-139.
- Tanaka, H., Dinunno, F. A., Monahan, K. D., Clevenger, C. M., DeSouza, C. A. and Seals, D. R. (2000). "Aging, habitual exercise, and dynamic arterial compliance." *Circulation* 102(11): 1270-5.
- Tanaka, N., Takazawa, K., Takeda, K., Aikawa, M., Shindo, N., Amaya, K., Kobori, Y. and Yamashina, A. (2003). "Coronary flow-pressure relationship distal to epicardial stenosis." *Circulation Journal* 67(6): 525-529.
- Tanaka, S. and Yamakoshi, K. (1996). "Ambulatory instrument for monitoring indirect beat-to-beat blood pressure in superficial temporal artery using volume-compensation method." *Med Biol Eng Comput* 34: 441-447.
- Tardy, Y., Meister, J., Perret, F., Brunner, H. and Arditi, M. (1991). "Non-invasive estimate of the mechanical properties of peripheral arteries from ultrasonic and photoplethysmographic measurements." *Clin Phys Physiol Meas* 12: 39-54.

REFERENCES

- Taylor, M. G. (1966). "Use of random excitation and spectral analysis in the study of frequency-dependent parameters of the cardiovascular system." *Circ Res* 18: 585-95.
- Teirstein, P. S. and King, S. (2003). "Vascular radiation in a drug-eluting stent world. It's not over till it's over." *Circulation* 108: 384-385.
- Tice, F., Peterson, J., Orsinelli, D., Binkley, P., Cody, R., Guthrie, R. and Pearson, A. (1996). "Vascular hypertrophy is an early finding in essential hypertension and is related to arterial pressure waveform contour." *Am Heart J* 132(3)(Sep): 621-7.
- Tomassoni, T. L. (1993). Conducting the pediatric exercise test. Pediatric laboratory exercise testing. Clinical guidelines. T. W. Rowland. Champaign, Human Kinetic Publishers: 195.
- Topol, E. J., Ed. (2002). Textbook of interventional cardiology. Philadelphia, W. B. Saunders.
- Uren, N. G. (1996). An introduction to intravascular ultrasound. Oxford, Remedica.
- Van Bortel, L. M., Balkestein, E. J., van der Heijden-Spek, J. J., Vanmolkot, F. H., Staessen, J. A., Kragten, J. A., Vredeveld, J. W., Safar, M. E., Struijker-Boudier, H. A. and Hoeks, A. P. (2001). "Non-invasive assessment of local arterial pulse pressure: comparison of applanation tonometry and echo-tracking." *J Hypertens* 19: 1037-1044.
- Van der Hoeven, G. M. A. and Beneken, J. E. W. (1970). A reliable transducer for the recording of the arterial pulse wave. Utrecht, Inst Med Phys, TNO. Progress Report 2.
- Van Nooten, G. (1998). Hartchirurgie - Coronaire chirurgie. Syllabus Algemene Heelkunde. Ghent, Faculty of Medicine. Ghent University.
- Verdonck, P. (1993). Studie van de bloedstroom doorheen de mitraalklep. PhD Thesis. Faculty of Applied Sciences. Ghent, Ghent University.
- Verdonck, P., Kleven, A., Verhoeven, R., Angelsen, B. and Vandenbogaerde, J. (1992). "Computer-controlled in vitro model of the human left heart." *Med Biol Eng Comput* 30: 656-659.
- Verel, D. and Grainger, R. G. (1978). Cardiac catheterization & angiocardiology. New York, Churchill Livingstone.

- Vogel, R. A. and Benitez, M. (2000). "Cardiovascular risk: from Framingham to the future." *Rev Cardiovasc Med* 1(1): 34-42.
- von Recklinghausen, H. (1931). *Neue Wege zur Blutdruckmessung*. Berlin, Springer-Verlag.
- Watanabe, H., Ohtsuka, S., Kakihana, M. and Gugishita, Y. (1993). "Coronary circulation in dogs with an experimental decrease in aortic compliance." *J Am Coll Cardiol* 21: 1497-506.
- Weaver, C. S., Eckerle, J. S., Newgard, P. M., Warnke, C. T., Angell, J. B., Terry, S. C. and Robinson, J. (1978). *A study of noninvasive blood pressure measurement techniques. Noninvasive Cardiovascular Measurements*. Billingham, WA, S.P.I.E. 167.
- Weiss, B., Spahn, D., Rahmig, H., Rohling, R. and Pasch, T. (1996). "Radial artery tonometry: moderately accurate but unpredictable technique of continuous non-invasive arterial pressure measurement." *Br J Anaesth* 76(3)(Mar): 405-11.
- Welch, P. D. (1967). "The use of fast Fourier transform for the estimation of power spectra: a method based on time averaging over short, modified periodograms." *IEEE Transactions on Audio and Electroacoustics* 15(2): 70-73.
- Wells, P. (1977). *Doppler methods. Biomedical Ultrasonics*. P. Wells. New York, Academic Press.
- Wesseling, K. H., Weber, H. and De Wit, B. (1973). "Estimated five component viscoelastic model parameters for human arterial walls." *J Biomech* 6: 13-24.
- Westerhof, N., Bosman, F., De Vries, C. J. and Noordergraaf, A. (1969). "Analog studies of the human systemic arterial tree." *J Biomech* 2: 121-143.
- Westerhof, N. and Noordergraaf, A. (1970). "Arterial viscoelasticity: a generalized model." *J Biomech* 3: 357-379.
- Westerhof, N., Sipkema, P., Van Den Bos, G. and Elzinga, G. (1972). "Forward and backward waves in the arterial system." *Cardiovasc Res* 6: 648-656.
- White, C. J. and Ramee, S. R., Eds. (1991). *Interventional cardiology, clinical application of new technologies*. New York, NY, Raven Press.

REFERENCES

- Wilkinson, I. B., Prasad, K., Hall, I. R., Thomas, A., MacCallum, H., Webb, D. J., Frenneaux, M. P. and Cockcroft, J. R. (2002). "Increased central pulse pressure and augmentation index in subjects with hypercholesterolemia." *J Am Coll Cardiol.* 39(6): 1005-11.
- Wilmore, J. H. and Costill, D. L. (1999). *Physiology of Sport and Exercise*. Champaign, IL, Human Kinetics Publishers.
- Womersley, J. R. (1955a). "Method for the calculation of velocity, rate of flow and viscous drag in arteries when the pressure gradient is known." *J Physiol* 127: 553-63.
- Womersley, J. R. (1955b). "Oscillatory flow in arteries: effect of radial variation in viscosity on rate of flow." *J Physiol* 127: 28-39.
- Womersley, J. R. (1955c). "Oscillatory motion of a viscous liquid in a thin-walled elastic tube. I: The linear approximation for long waves." *Phil Mag* 46: 199-221.
- Womersley, J. R. (1957a). The mathematical analysis of the arterial circulation in a state of oscillatory motion, Wright Air Development Center. Technical Report WADC-TR56-614.
- Womersley, J. R. (1957b). "Oscillatory flow in arteries: the constrained elastic tube as a model of arterial flow and pulse transmission." *Phys Med Biol* 2: 178-87.
- Yanagisawa, H., Chikamori, T., Tanaka, N., Hatano, T., Morishima, T., Hida, S., Iino, H., Amaya, K., Takazawa, K. and Yamashina, A. (2002). "Correlation between thallium-201 myocardial perfusion defects and the functional severity of coronary artery stenosis as assessed by pressure- derived myocardial fractional flow reserve." *Circ J* 66(12): 1105-9.
- Yellin, E. (1995). *The momentum of mass, the momentum of ideas, and diastolic function. Systolic and diastolic function of the heart*. N. B. Ingels, G. Daughters, J. Baan et al. Amsterdam, IOS Press.
- Yock, P., Fitzgerald, P. and Popp, R. (1995). "Intravascular ultrasound." *Scientific American. Science & Medicine* 2(5): 68-77.
- Young, D. F. and Tsai, F. (1973). "Flow characteristics in models of arterial stenoses. II. Unsteady flow." *J Biomechanics* 6: 547-559.

- Young, T. (1808). "Hydraulic investigations, subservient to an intended Croonian lecture on the motion of the blood." *Phil Trans Roy Soc* 98: 164-86.
- Young, T. (1809). "On the functions of the heart and arteries. The Croonian lecture." *Phil Trans Roy Soc* 99: 1-31.
- Zhang, Y. Y., Johnson, M. C., Chow, N. and Wasserman, K. (1991). "Effects of exercise testing protocol on parameters of aerobic function." *Med Sci Sports Exerc* 23: 625-630.
- Zorn, E., Wilson, M., Angel, J., Zanella, J. and Alpert, B. (1997). "Validation of an automated arterial tonometry monitor using Association for the Advancement of Medical Instrumentation standards." *Blood Press Monit* 2(4)(Aug): 185-188.

Acknowledgements

A word of gratitude to all the people who contributed in realizing this thesis. Special thanks to the colleagues and technicians of the Hydraulics Lab in Ghent, to the colleagues of the Cardiac Imaging in Brisbane and of the Samuels Building in Sydney. For contributions to specific parts of this thesis:

Part II, Chapter 2

Jan Poelaert and Jan Heerman for their help in acquiring the necessary invasive data signals at the intensive care unit in the Cardiology Department of the Ghent University Hospital. Mihaela Sbarciog and Robain De Keyser of the Department of Electrical Energy, Systems & Automation of the Ghent University for their valuable feedback on system identification.

Part II, Chapter 3

Alberto Avolio for taking me on board in his Arterial Function Group. Fernando Camacho for the accompaniment at many late night work hours, and all other phd students and colleagues of the 4th and 5th floor in the Samuels Building for the stimulating working environment at the Graduate School for Biomedical Engineering in Sydney.

Part III, Chapter 2

Abraham Noordergraaf and Gary Drzewiecki for helping out with obtaining the old and hard-to-find publications. Graduate students Frédéric Vagenende and Anneleen De Smet for their assistance with the library look-ups and colleague Patrick Segers for his careful reading of the manuscript. This research was funded by a specialization grant of the Institute for the Promotion of Innovation by Science and Technology in Flanders (IWT-991175).

Part III, Chapter 3

J. Van Aken at the Department of Anaesthesia of the Ghent University Hospital for the support in the planning and execution of the data acquisition and help with administration. F. van Thuyne and D. De Guytere for the technical support in the adjustment of the electronic connections and mechanical accessories.

Part III, Chapter 4

Jurgen Deviche for his technical assistance in building the hardware interface, and also colleagues Tom Claessens, Kris Dumont, Stein-Inghe Rabben and Samantha Poli for their valuable feedback on writing and testing of this work.

Part IV, Chapter 2

Stéphane Carlier for the use of his electronic equipment and especially Tine De Backer for her unexpected help in the hospital although in a very pregnant condition.

Part IV, Chapter 3

Stuart Moir for getting me started in the Auslab database, Robert Fathi for the cath scores, Phillip Mottram and Leanne Jeffries for the help with completing and finding patient data reports in the dispersed file cabinets. Special thanks to Tom Marwick for the invitation and offered opportunity in his Cardiac Imaging Group of the Queensland University School of Medicine and Brian Haluska for his valuable help and generous hospitality. Also Beatrijs Moerkerke of the Applied Mathematics and Computer Science Department of the Ghent University for clarifying the statistical problems.

Part V, Chapter 2

Ivo Vanderick and Guidant for supplying the stents. This research was funded by a specialization grant of the Institute for the Promotion of Innovation by Science and Technology in Flanders (IWT-991175), the Special Research Fund of Ghent University and the Belgian National Bank.

Part V, Chapter 3

Martin Van Daele, Marcel Anteunis and Stefaan Bliki for technical assistance during the realization of the hydraulic model of the coronary circulation. This research was funded by specialization grants of the Institute for the Promotion of Innovation by Science and Technology in Flanders (IWT 21228 and IWT 993175), the Antwerp University and a post-doctoral grant from the Fund for Scientific Research in Flanders (FWO-Vlaanderen).

This research has been an example of collaboration in a multidisciplinary field. I had the pleasure of working with the following authors and co-authors for publications in this thesis:

Pascal R Verdonck, Patrick Segers, Tom E Claessens, Frédéric Vagenende, Anneleen De Smet
Hydraulics Laboratory, Department of Civil Engineering, Faculty of Applied Sciences, Ghent University, Ghent, Belgium

Eric P Mortier, Alain Kalmar
Department of Anaesthesia, Ghent University Hospital, Ghent, Belgium

Henri Verhaaren, Sara Van Aken, Katya De Groote, Ilse Coomans
Department of Paediatric Cardiology, Ghent University Hospital, Ghent, Belgium

Paul L Van Herck, Christiaan J Vrints
Department of Cardiology, Antwerp University Hospital, Edegem, Belgium

Daniel Vanhercke
Department of Cardiology, General Hospital St Lucas, Campus H Familie, Ghent, Belgium

Stéphane G Carlier
Lenox Hill Hospital and Cardiovascular Research Foundation, New York, NY, USA

Patrick W Serruys, Jurgen Ligthart, Georges Sianos, Pedro Serrano
Thorax Centre, Rotterdam, The Netherlands

Alberto P Avolio
Graduate School of Biomedical Engineering, Faculty of Engineering, University of New South Wales, Sydney, Australia

Thomas H Marwick, Brian A Haluska, Rodol Leano, Robert Fathi
Cardiac Imaging Group, Southern Clinical Division, School of Medicine, Faculty of Health Sciences, University of Queensland, Brisbane, Australia

For all those still struggling, I can recommend
“Piled Higher and Deeper” by Jorge Cham at www.phdcomics.com.



